Correlations in spin-orbit coupled ultracold quantum gases

Juan Sánchez Baena

ADVERTIMENT La consulta d'aquesta tesi queda condicionada a l'acceptació de les següents condicions d'ús: La difusió d'aquesta tesi per mitjà del repositori institucional UPCommons (http://upcommons.upc.edu/tesis) i el repositori cooperatiu TDX (http://www.tdx.cat/) ha estat autoritzada pels titulars dels drets de propietat intel·lectual **únicament per a usos privats** emmarcats en activitats d'investigació i docència. No s'autoritza la seva reproducció amb finalitats de lucre ni la seva difusió i posada a disposició des d'un lloc aliè al servei UPCommons o TDX. No s'autoritza la presentació del seu contingut en una finestra o marc aliè a UPCommons (*framing*). Aquesta reserva de drets afecta tant al resum de presentació de la tesi com als seus continguts. En la utilització o cita de parts de la tesi és obligat indicar el nom de la persona autora.

ADVERTENCIA La consulta de esta tesis queda condicionada a la aceptación de las siguientes condiciones de uso: La difusión de esta tesis por medio del repositorio institucional UPCommons (http://upcommons.upc.edu/tesis) y el repositorio cooperativo TDR (http://www.tdx.cat/?locale-attribute=es) ha sido autorizada por los titulares de los derechos de propiedad intelectual **únicamente para usos privados enmarcados** en actividades de investigación y docencia. No se autoriza su reproducción con finalidades de lucro ni su difusión y puesta a disposición desde un sitio ajeno al servicio UPCommons No se autoriza la presentación de su contenido en una ventana o marco ajeno a UPCommons (*framing*). Esta reserva de derechos afecta tanto al resumen de presentación de la tesis como a sus contenidos. En la utilización o cita de partes de la tesis es obligado indicar el nombre de la persona autora.

WARNING On having consulted this thesis you're accepting the following use conditions: Spreading this thesis by the institutional repository UPCommons (http://upcommons.upc.edu/tesis) and the cooperative repository TDX (http://www.tdx.cat/?locale- attribute=en) has been authorized by the titular of the intellectual property rights **only for private uses** placed in investigation and teaching activities. Reproduction with lucrative aims is not authorized neither its spreading nor availability from a site foreign to the UPCommons service. Introducing its content in a window or frame foreign to the UPCommons service is not authorized (framing). These rights affect to the presentation summary of the thesis as well as to its contents. In the using or citation of parts of the thesis it's obliged to indicate the name of the author.

Correlations in Spin-Orbit coupled ultracold quantum gases

PhD. Program in Computational and Applied Physics

Juan Sánchez-Baena

Supervisors: Jordi Boronat Medico
Ferran Mazzanti Castrillejo

Department of Physics
Universitat Politècnica de Catalunya

This dissertation is submitted for the degree of
Doctor of Physics

October 2020

Acknowledgements

English: First of all, I would like to thank my supervisors, Jordi Boronat Medico and Ferran Mazzanti Castrillejo, for all their support and for everything I have learnt from them during the last six and a half years. During this time, and under their supervision, I have completed a Bsc. Thesis, an Msc. Thesis and now, this PhD. Thesis. Even since I started working alongside them, when I was just a third year Physics Engineering student, they have treated me with utmost respect and affection, and they have always tried to make sure that my time within the Barcelona Quantum Monte Carlo research group was enjoyable. It has been a pleasure to work with them, and to be able to learn a ton of things from them day by day. I would also like to thank the administrative staff (Ana Calle, Cristina Astier, Montserrat Río, Ana María Ortega, Susana Vera, Trinidad Carneros, Laura Martínez and Samuel Montavez) for all their help when dealing with horrendous bureaucracy. They have made things much easier. I owe also a big thank you to the people in charge of the computer support in the Physics Department, Alfredo Soldevilla and Agustí Emperador, for all their help during this time. I would like to give a very special thank you to my colleagues: Raúl Bombín, Huixia Lu, Grecia Guijarro, Viktor Cikojević, Giulia De Rosi, Grigory Astrakharchik and Pietro Massignan, with whom I have shared hundreds of meals, a few dinners and even a few trips. It has been great to spend all this time with you. I would not like to forget my former office partners: Guillem Ferré, Amani Tahat and Andrés Henao, who made my beginnings in the group easier, nor Adrian Macia, with whom I had the privilege to work with in the first scientific publication I participated in.

Starting, and completing this PhD Thesis is the result of the passion that I feel towards Physics. However, the fact that I enjoy Physics is, in huge part, a consequence of the excellent teachers I had during the Physics Engineering Degree at Universitat Politècnica de Catalunya. Their great dedication, and all the efforts they directed towards providing a good learning experience for us, the students, made me greatly enjoy each one of my undergraduate years, and inspired me to become a professional physicist. Their great job, and the impact it had on me, made me realize that it is as important to become a good teacher as it is to become a good researcher. I would also like to give a big thank you to my high school teachers for their support and for everything they taught me. I would like to specially thank Miguel Sánchez, my

Social Science teacher during my first two years in high school, for his endless trust and support, which had a big impact in me.

Obviously, the greatest thank you goes to my parents, Juan and Rosario, for everything they have done for me since I was born. If I am here now it is because of them. I owe all the big steps forward that I have made in life to them. I owe everything to them. They are the best parents anyone could have. I also want to dedicate some words to my best friends, Julio César and Paula, for always being there when I needed them. And finally, I would like to thank my friends, Adrián Osuna and Adrián Urgell, and the rest of the gang, for all the funny moments we have shared in the last few years. They have been incredibly helpful to deal with the inherent stress of doing a PhD Thesis.

Spanish En primer lugar, me gustaría agradecer a mis directores de tesis, Jordi Boronat Medico y Ferran Mazzanti Castrillejo, todo el apoyo y las muchas enseñanzas que me han brindado estos años. No sólo durante los cuatro años que ha durado esta tesis doctoral, sinó también durante los dos años y medio anteriores, en los que realicé con ellos los Trabajos de Fin de Grado y de Máster. Empecé a trabajar con ambos cuando no era más que un estudiante de tercero del Grado en Ingeniería Física, y desde el primer momento me acogieron, e hicieron todo lo posible para que la estancia en el grupo de investigación fuera lo más cómoda y beneficiosa posible para mí. Ha sido un auténtico placer poder trabajar a su lado, y aprender día a día de ellos. Querría continuar agradeciendo la ayuda del personal administrativo, con especial énfasis a Ana Calle, Cristina Astier, Montserrat Río, Ana María Ortega, Susana Vera, Trinidad Carneros, Laura Martínez y Samuel Montavez. Gracias a ellos me ha sido mucho más fácil lidiar con las horribles gestiones burocráticas que, en ocasiones, he tenido que realizar. Así mismo, he de agradecer a Alfredo Soldevilla y a Agustí Emperador toda su ayuda en lo que a soporte técnico se refiere. Y me gustaría tener una mención especial para mis compañeros investigadores, tanto estudiantes de doctorado, como postdocs y profesores: Raúl Bombín, Huixia Lu, Grecia Guijarro, Viktor Cikojević, Giulia De Rosi, Grigory Astrakharchik y Pietro Massignan. Con ellos he compartido innumerables comidas, algunas cenas, e incluso algún que otro viaje. Gracias por vuestro apoyo, y por los buenos momentos que hemos pasado. No querría olvidarme de mis antiguos compañeros de despacho: Guillem Ferré, Amani Tahat y Andrés Henao, que me hicieron los comienzos más fáciles, ni de Adrián Macia, con quién tuve la suerte de colaborar en la primera publicación científica en la que participé.

Si he llegado a empezar y completar este doctorado, es por la pasión que despierta en mí la Física. No obstante, el hecho de disfrutar de ella debo agradecérselo en gran medida a los excelentes profesores que tuve en el Grado de Ingeniería Física de la Universitat Politècnica de Catalunya. El gran desempeño y dedicación, como docentes, de todos y cada uno de ellos contribuyó a que mi experiencia como estudiante de

Grado fuese muy agradable, y me hizo tener claro que quería dedicar mi vida a hacer carrera dentro del mundo de la Física. Así mismo, me hicieron ver lo importante que es tratar de convertirse en un buen docente, además de tratar de ser un buen investigador. También quiero tener unas palabras para mis profesores de secundaria y bachillerato, a los que les agradezco su dedicación y las enseñanzas que me transmitieron. Me gustaría hacer especial mención a Miguel Sánchez, mi profesor de Ciencias Sociales durante mi primer y segundo año de Educación Secundaria Obligatoria, por toda la confianza que depositó en mí y por cómo fue clave para que creyese plenamente en mí mismo, en términos académicos.

Por supuesto, he de agradecer inmensamente a mis padres, Juan y Rosario, todo el apoyo que me han dado, desde siempre. No estaría aquí si no fuese por ellos, y les debo cada paso importante que he podido dar en mi vida, y todos los que me quedan por dar. Les debo todo. Siento que no podría ser más afortunado en ese aspecto. También quiero acordarme de mis dos mejores amigos, Julio César y Paula, por estar a mi lado, dispuestos a escucharme y apoyarme, siempre que los he necesitado. Para terminar, quiero agradecer a mis amigos Adrián Osuna y Adrián Urgell, así como al resto del grupo, los muchos momentos divertidos que hemos compartido durante los últimos cuatro años. Han sido fundamentales para aliviar el estrés puntual que conlleva la ardua tarea de realizar una tesis.

Table of contents

List of figures

List of tables

Chapter 1

Introduction

The experimental realization of Bose Einstein Condensates (BEC) of rubidium and sodium atoms at ultralow temperatures [6, 7] in 1995 represented a major breakthrough in the research field of ultracold quantum gases. For the first time, the phenomenon of Bose Einstein Condensation, which had been theoretically predicted by Albert Einstein [8] following the ideas of Satyendra Nath Bose, almost 70 years ago, could be observed in a laboratory. From a fundamental perspective, a BEC is a state of matter produced when a bosonic system formed by many particles cools down to sufficiently low temperatures. Under these conditions, and if inter atomic correlations are weak enough, a large fraction of particles occupies the minimum energy state, which we know as the Bose Einstein Condensate, or BEC. This is a phenomenon exclusive to bosons. The realization of the first BEC opened the way for experiments involving exotic interactions such as dipoles [9, 10] and synthetic Spin Orbit Coupling (SOC) systems [1, 2]. While the initially realized BEC had very weak interactions, exploiting Feshbach resonances allowed the modification of the scattering length in a broad range of values [11]. Nowadays, due to the high degree of controllability and tunability of the experimental set-ups, these systems have become a premier platform to study a wide variety of quantum phenomena.

In particular, in this Thesis we focus on systems under the effect of Spin Orbit Coupling (SOC), which denotes the interplay between a particle's linear (or angular) momentum and its spin. SOC has been a subject of interest in the recent years, both theoretically and experimentally. It plays an important role in a wide variety of exotic quantum phenomena, such as topological [12] and Mott [13–15] insulators, topological superconductors [16], Majorana fermions [17] and spintronics [18]. Spin-Orbit Coupling is a relativistic effect and emerges naturally in electronic systems. An electron moving in a static electric field, such as the crystal field of a lattice, experiments a magnetic field on its moving frame, which is proportional to its velocity. This magnetic field then couples to the particle's magnetic momentum, which is proportional to its spin, and gives rise to SOC [1]. The SOC term is of relevance in heavy atomic and molecular systems, specifically when computing bonding and spectral properties [19].

While electronic systems are the natural platform where SOC arises, this kind of interaction can be synthetically engineered in ultracold atom systems [1, 2, 20]. Unlike in electronic systems, where the properties of SOC are largely determined by the specific material, ultracold atoms constitute a much more controllable and tunable platform that enables a precise and detailed study of the properties of SOC [21]. In this Thesis, we focus on the study of SOC in ultracold gases. The synthetic implementation of SOC in a Bose-Einstein Condensate (BEC) was first achieved by Spielman's group [1] via the dressing of two atomic spin states with a pair of lasers in a neutral BEC. Under these circumstances, the resulting SOC interaction features equal Rashba [22] and Dresselhaus [23] strengths, and is known as Raman SOC or one-dimensional SOC, since the momentum-spin coupling involves only one spatial component of the momentum operator, $\hat{\sigma}_z \hat{P}_x$. It is important to remark that there are no conventional spin states in synthetic SOCs, but rather atomic states that are labeled as pseudospins [24], for which the SOC interaction is engineered. Because of this, it is possible to have bosonic systems with pseudospin 1/2, something that does not happen spontaneously in nature. In this sense, a pair of Raman lasers intersecting at 90^o and detuned from resonance creates a momentum dependent coupling between two hyperfine atomic states (the pseudospins) by the simultaneous driving of a spin flip transition and transferring of momentum. This is done for atoms with a Λ-type configuration of internal levels, which contains a pair of ground hyperfine levels suitable to mimic the spin up and down states. This results into the effective Hamiltonian

$$\hat{H} = \frac{\hat{P}^2}{2m} + \frac{\lambda\hbar}{m}\hat{P}_x\hat{\sigma}_z + \frac{\lambda^2\hbar^2}{2m} - \frac{\Omega}{2}\hat{\sigma}_x \tag{1.1}$$

where m is the mass of the atom, λ is the SOC strength and the coupling strength, Ω, is known as the Raman coupling. It must be remarked that the Hamiltonian in Eq. (1.1) is obtained after applying a unitary transformation consisting on a position and time dependent rotation to the Hamiltonian in the reference frame of the laboratory [1, 25]. In the specific case of the experiment of Ref. [1], ^{87}Rb atoms in the continuum (not in a lattice) where employed, while the hyperfine states chosen as pseudospins are $|+1\rangle = |F = 1, m_F = 0\rangle$ and $|-1\rangle = |F = 1, m_F = -1\rangle$. A scheme of the employed states is shown in Fig. 1.1. A bias magnetic field introduces a $\hbar\omega_z$ Zeeman shift between the $|F = 1, m_F = 0\rangle$ and $|F = 1, m_F = -1\rangle$ states, which in turn are detuned by an amount δ from Raman resonance, an effect also caused by the same magnetic field. The state $|F = 1, m_F = +1\rangle$ can be neglected due to the quadratic Zeeman shift $\hbar\omega_q$, which is much larger than the difference in energy between the $|F = 1, m_F = 0\rangle$ and $|F = 1, m_F = -1\rangle$ states. Following this same scheme, Raman SOC has also been realized with ^{87}Rb bosons in a lattice [26, 27], and also with other species: ^{6}Li [28], ^{40}K [29], ^{87}Sr [30], ^{173}Yb [31, 32], and ^{161}Dy [33].

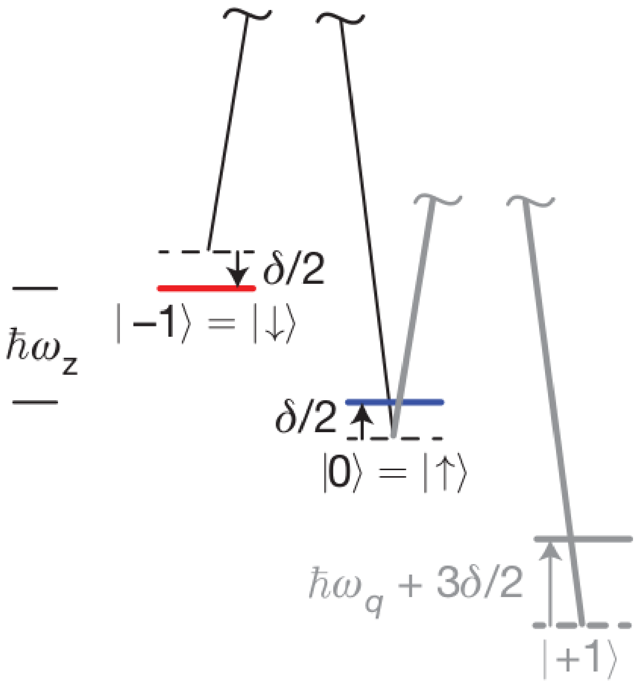

Fig. 1.1 Level diagram of the ^{87}Rb system for which synthetic Raman SOC is engineered in Ref. [1]. The Zeeman shift $\hbar\omega_z$ and the detuning from resonance δ are induced by a bias magnetic field. The quadratic Zeeman shift $\hbar\omega_q$ is such that the state $|F=1,\, m_F=+1\rangle$ can be discarded, leading to an effective two-level Hamiltonian. Taken from Ref. [1].

The aforementioned experimental set-ups for SOC systems are typically realized in the dilute regime, where the BECs used have a very large condensate fraction. This implies that these systems show a low level of inter-atomic correlations and, therefore, they can be accurately described both in quantitative and qualitative terms by mean field theory. Within this formalism, the interaction between particles is modeled as a contact potential (i.e. a zero range interaction) proportional to the scattering length, which can be both measured and tuned in actual experiments. Under these circumstances, the ground state of a BEC can be obtained by solving the Gross-Pitaevskii equation (GPE). The GPE is the most used theoretical tool to describe the current experiments with ultracold atoms in general, although it has limited applicability. On one hand, the quantitative accuracy of the GPE decreases as the *gas parameter*, defined as $x_g = na^3$, with n the density and a the s-wave scattering length, increases. The gas parameter measures the degree of inter-atomic correlations in a many-body system: the higher its value, the more important correlations are [34]. On the other hand, there are many examples of systems with attractive interactions for which the GPE predicts a collapse that is not seen when correlations are introduced. This is the case, for instance, for dipolar systems in three dimensions [9, 10], unstable

Bose-Bose mixtures [35–38] and SOC systems [39], among others. In this context, it is essential to go beyond the standard mean field description.

The limitations of mean field theories can be overcome in several ways. Out of all the possibilities, we focus on two options: quantum Monte Carlo methods and Beyond Mean Field calculations following the Bogoliubov formalism. These approaches are complementary: while quantum Monte Carlo methods can account for inter-atomic correlations at all orders, they are limited in terms of the number of particles that can be simulated, since the computational cost of the calculations grows with this quantity. On top of that, these methods are computationally more expensive than Beyond Mean Field calculations. On the other hand, the Beyond Mean Field approaches account for inter-atomic correlations only at the first order, which means that, for large enough values of the gas parameter, they are still unable to quantitatively describe a quantum many-body system. However, first order correlations are enough to describe most of the experimental systems that involve the instabilities at the mean field level. When SOC is present, the balance between both approaches slightly shifts: while in the absence of SOC quantum Monte Carlo methods are strictly more accurate than Beyond Mean Field calculations, when SOC is incorporated this is not necessarily true, mainly because quantum Monte Carlo algorithms are subject to approximations that are absent in the Bogoliubov formalism.

The application of Quantum Monte Carlo methods to simulate SOC systems is not straight-forward, specially in the case of Diffusion Monte Carlo (DMC), a method able to obtain exact ground state properties of a many-body quantum system. The non-locality of the SOC Hamiltonians, induced by the presence of linear contributions of the momentum operator, hinders the application of the standard DMC formulation. Therefore, the derivation of new DMC algorithms, capable of sampling SOC potentials, is required. On top of that, and in general, the ground state wave function of a SOC Hamiltonian is a complex function, unlike the general case of Bose systems without SOC. Since the DMC algorithm is unable to propagate simultaneously the modulus and the phase of a wave function, one must resort to the fixed phase approximation [40]. Within this approach, one fixes the phase of the wave function and evolves the modulus in imaginary time, obtaining the best possible physical estimates given a phase constraint. As a consequence, the quality of the estimations is directly related to the quality of the phase employed, see for instance the case of the energy, for which only an upper bound to the true ground state energy can be obtained.

Previous DMC calculations with SOC have been carried out in the study of electronic structures [19, 41], quantum dots in semi-conductors [42], and repulsive Fermi gases [43]. A DMC method incorporating the SOC terms that arise in electronic systems has already been developed [19]. In this method, the authors implement the spin-orbit term of the propagator through the use of the T-moves technique [44]. They also use a regularized, continuous representation of the spin degrees of freedom. Since SOC introduces a sign problem in the off-diagonal matrix elements of the propagator, the authors of Ref. [19] define an effective Hamiltonian in such a way that the propagator becomes positive-definite. It can be shown that the energy estimation obtained with this effective Hamiltonian yields an upper bound to the fixed-phase energy [45]. In this Thesis, we adapt the T-moves DMC algorithm of Ref. [19] to the usual, discrete representation of the spin, giving rise to the Discrete Spin T-moves DMC (DTDMC), and show how to treat the synthetic SOC present in ultracold quantum gases. We also introduce a new DMC algorithm for treating the SOC terms of the propagator, where the spin integrated wave function is propagated in imaginary time. In doing so, we avoid almost completely the sign problem induced by SOC terms, meaning that no effective Hamiltonian needs to be defined. We call this new method the Spin Integrated DMC (SIDMC). This method, however, can not sample two-body, spin-dependent potentials.

As mentioned previously, SOC interactions induce the emergence of a wide variety of exotic phenomena. An important example concerning Raman SOC is the appearance of a stripe phase, which presents a density modulation along a privileged direction. Similar spatial periodicity can be found in other ultracold atom systems, like dipoles, where the anisotropy of the two-body interaction leads to the formation of stripes for high enough densities [46, 47]. However, in a Raman SOC system, the driving mechanism for stripe formation is of single particle nature. This implies that stripes can be present in systems with very low densities and gas parameters, thus making them more experimentally accessible. The appearance of a stripe phase in Raman SOC systems can be understood from the single particle picture (see Chapter 2) by looking at the dispersion relation induced by SOC. While in non-SOC systems a quadratic dependence of the energy with respect to the momentum is observed, Raman SOC induces a double well structure (with two minima at opposed momenta) that enables the possibility of stripes. However, at the single particle level, the superposition of states with opposite momenta has the same energy as one of the states separately. This degeneracy is broken by interactions, which favor either the single momentum state or the stripe configuration, depending on the asymmetry of the different spin channels of the interaction. At the mean field level, where interactions are modeled by a contact potential proportional to the scattering length, stripes are favored if $a_{+1,-1} < a_{+1,+1}$, given that $a_{+1,+1} = a_{-1,-1}$, for a given range of values of the Raman coupling. Here, the $+1$, -1 indexes indicate the spin component while $a_{s,s'}$ is the spin-dependent scattering length. Moreover, the greater the difference between $a_{+1,-1}$ and $a_{+1,+1}$, the larger the Raman coupling window for the stripe phase and, as a consequence, the higher the contrast stripes can achieve [25], meaning by contrast the difference between the maxima and minima in the striped density pattern. In the experiment of Ref. [1], the nature of inter- and intra-spin interactions is completely determined by the atomic species employed, ^{87}Rb, which features an almost spin-independent interaction

($a_{+1,+1} \simeq a_{-1,-1} \simeq a_{+1,-1}$, with $\gamma = (a_{+1,+1} - a_{+1,-1})/(a_{+1,+1} + a_{+1,-1}) = 0.0012$ [25]). Because of this, the experimental observation of the stripes induced by Raman SOC remained an open problem, even after SOC was first realized with ultracold atoms. The stripe phase is superfluid [4, 48], and at the same time it breaks continuous spatial symmetry, giving rise to supersolidity. Because of this, Raman SOC stripes are commonly referred in the literature as supersolid stripes, or superstripes.

In 2017, a new scheme for the generation of synthetic Raman SOC was realized by Ketterle's group [2], which enabled the first ever experimental detection of the stripe phase in a Raman SOC system. In contrast to the experiment of Ref. [1], the two lowest eigenstates of an asymmetric double well were used as pseudospin states, instead of employing two different hyperfine states of an atom. SOC was then induced by a couple of Raman beams providing a momentum transfer and a spin flip from one well to the other. This scheme provided two clear advantages in terms of observing the stripe phase: first, since all atoms are in the same hyperfine state, there is no sensitivity to external magnetic fields, and second, and most important, the inter-spin interaction depends on the overlap between the eigenstates of each well, and thus it can be tuned in experiments. This allowed the implementation of highly asymmetric spin-dependent interactions with $a_{+1,+1} \gg a_{+1,-1}$, opening the detection of stripes. In order to increase the signal to noise ratio, a superlattice composed of several coherently coupled asymmetric double wells was employed, with SOC induced in the quasi two-dimensional space orthogonal to the direction of the superlattice, for each double well. This is illustrated in Fig. 1.2. Stripes were detected with Bragg scattering using near-resonant yellow light.

More recently, in 2018, the realization of a SOC interaction involving angular momentum was achieved [49]. Unlike Raman SOC, this interaction contains a term of the form $\hat{L}_z\hat{\sigma}_z$. The implementation of this coupling is achieved by the use of a co-propagating pair of beams which carry different angular momentum, to transfer the relative winding phase to the atoms during a Raman transition [5]. In other words, angular momentum is transferred to the atoms instead of linear momentum. In the pioneer experiment of Ref. [49], SOC is synthetically implemented with ^{87}Rb atoms employing the $|F = 1, m_F = 0\rangle$ and $|F = 1, m_F = -1\rangle$ hyperfine states as pseudospin states. We explore in Chapter 5 this kind of SOC, known as Spin Orbital Angular Coupling (SOAC), both at the mean field level and by using of the Diffusion Monte Carlo method.

In general, SOC is equivalent to a gauge potential coupling to the spin degrees of freedom [50, 51]. Because of this, the implementation of SOC potentials can be achieved by the generation of synthetic gauge potentials. The experiments mentioned above correspond to one-dimensional SOC, which is equivalent to an Abelian gauge potential with zero Berry's curvature, which means it is topologically trivial. However, a higher dimensional SOC is equivalent to a non-Abelian gauge potential with non-zero Berry's

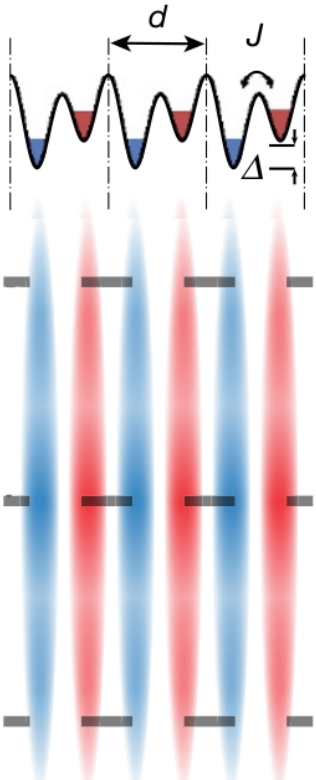

Fig. 1.2 Illustration of the superlattice of double wells employed in the experiment of Ref. [2] to engineer Raman SOC. Here d is the lattice constant of the superlattice, Δ is the well offset and J is the inter-well tunneling. SOC is implemented in the quasi two-dimensional system perpendicular to the direction of the superlattice. The stripe density modulations induced by SOC are represented by the change in brightness of the red and blue densities shown in the Figure. Taken from Ref. [2].

curvature, and thus gives rise to non-trivial topological effects. The experimental realization of higher dimensional SOC interactions has not been achieved until recently. Rashba SOCs has been realized with ^{87}Rb atoms in an optical Raman lattice with double Λ configuration [52, 50] after several theoretical proposals had been made to implement 2D [53–56] and 3D [57, 58] Rashba SOC. In this scheme, two pairs of light beams create a lattice and Raman potentials simultaneously, inducing hopping between sites together with spin flips in two different directions. The relative phase between the two Raman couplings can be tuned experimentally, and as a consequence, the dimensionality of the induced SOC can be changed between 1D and 2D. Rashba SOC was also achieved experimentally for a system of ^{40}K fermions in the continuum, where a tripod scheme consisting of three lasers couples three hyperfine states [59]. Despite the one-dimensional Raman SOC being less rich from the topological point of view, the lower difficulty of its experimental realization has led to the observation of interesting physical phenomena such as the formation of supersolid stripes. Because of this, while two and three-dimensional SOC interactions such as Rashba and Weyl SOC are used to test the Diffusion Monte Carlo methods developed in this Thesis, our study focuses on Raman SOC only, with special attention on the supersolid stripe phase.

Among the previous theoretical works in the field of ultracold atoms with SOC, we believe that the prediction of the phase diagram at the mean field level for a system under Raman SOC [25, 60] is of major relevance. By performing a variational optimization of an ansatz wave function, the authors are able to find three different phases and determine the values of the Raman coupling, density and scattering length at which each phase is energetically favorable. Three different phases arise in the system: the plane wave, single minimum and the stripe phase. The plane wave and single minimum phases correspond to a state of definite momentum (which is non-zero for the plane wave phase and zero for the single minimum phase), while the stripe phase is a superposition of states with opposite momenta. However, as any result obtained in mean field, its validity is restricted to situations where inter-atomic correlations are weak, i.e. the very dilute regime. Connected to this, one of the main parts of this Thesis deals with the realization of this phase diagram by using the Diffusion Monte Carlo methods developed for SOC potentials. In this way, Diffusion Monte Carlo is able to extend the phase diagram to a regime where inter-atomic correlations are not negligible. Results concerning this are presented in Chapter 3.

Beyond mean field calculations of several observables have also been performed for Raman SOC systems in all three phases. The excitation spectrum of the plane wave and single minimum phases [61], and that of the stripe phase [4], have already been computed following the Bogoliubov-de Gennes formalism. Also, the static structure factor and the superfluid fraction have been obtained [62, 63]. The Lee-Huang-Yang (LHY) energy, which yields the first order correction in terms of density and scattering length to the mean field energy, has been obtained in the plane wave and single minimum phases [3]. However, no LHY correction has been derived for a system in the stripe phase. We evaluate this term in Chapter 4. The motivation behind this comes from the role played by quantum fluctuations in an attractive Bose-Bose mixture without SOC that is unstable at the mean field level [35]. In this case, the physics of the system are greatly modified by quantum fluctuations, as the LHY correction is able to stabilize the system, which is shown to present a liquid-like behaviour. For a finite number of particles, the system admits droplet-like ground state solutions. We check whether the same effect is present on a system under Raman SOC in the stripe phase, and if a droplet-like solution with density modulations exists as the ground state. Such a state combines liquid behaviour, density modulations reminiscent of solids, and superfluidity, which is a novel combination of properties in the field of ultracold atoms. As previously mentioned, this scenario, where mean field physics are drastically modified by beyond mean field effects, is present in other systems like dipoles. Experimentally, it has been possible to observe how the beyond mean field stabilization mechanisms lead to the formation of droplets both for unstable Bose-Bose mixtures [37, 38] and dipoles [9, 10]. While all the experiments published up to date in the field of SOC systems involve repulsive interactions, and thus do not experience a collapse, current state of the art experiments, which feature attractive inter-spin interactions, are pursuing the observation of Raman SOC striped self-bound droplets.

1.1 Objectives and outline

The goal of this Thesis is to compute properties of the ground state of a quantum many-body system with Spin-Orbit Coupling interactions out of the ultra-dilute regime, with special focus on Raman SOC. In order to achieve this, we follow two approaches. On one hand, we develop and use two Diffusion Monte Carlo methods suitable to study systems featuring SOC. On the other hand, we follow the Bogoliubov formalism to perform calculations beyond the mean field level. The contents of this Thesis are structured as follows:

- In Chapter 2, we briefly review the one-body Raman SOC problem, as it is very illustrative to understand the many-body picture discussed in other Chapters. We also review the derivation of the mean field Gross Pitaevskii equation for SOC systems and the dressed spin picture for Raman SOC of Ref. [1].

- In Chapter 3, we introduce the Monte Carlo methods of interest. We review the basic Variational and Diffusion Monte Carlo formalisms, and present the derivation and implementation of the Diffusion Monte Carlo algorithms adapted for the study of SOC systems, including numerical tests for both methods. Finally, we present the phase diagram for a Raman SOC system in three dimensions. We extend the pre-existing mean field diagram [25] to a region of gas parameters outside the regime of validity of the mean field approach and evaluate the effect of quantum correlations. We also report physical quantities like the pair-distribution function, the static structure factor, and the one-body density matrix.

  The main results of this Chapter are featured in the following publications:
  - J. Sánchez-Baena, J. Boronat, and F. Mazzanti, Diffusion Monte Carlo methods for spin-orbit-coupled ultracold Bose gases, Phys. Rev. A **98**, 053632 (2018).
  - J. Sánchez-Baena, J. Boronat, and F. Mazzanti, Supersolid stripes enhanced by correlations in a Raman spin-orbit-coupled system, Phys. Rev. A **101**, 043602 (2020).

- In Chapter 4, we review the Bogoliubov formalism to perform beyond mean field calculations in the absence of SOC and present the detailed extension of the formalism for Raman SOC systems in the stripe, plane wave and single minimum phases. We derive, for the first time, the Lee-Huang-Yang energy correction for a Raman SOC in the stripe phase. We present and discuss the technical details involved in the calculation. As an application, we evaluate the role played by quantum fluctuations in a Raman SOC system in the stripe phase that is unstable at the mean field level due to the presence of attractive enough inter-spin interactions. We characterize the phase diagram of the system stabilized by quantum fluctuations and study the presence of supersolid striped droplets.

The main results of this Chapter are featured in the following publications:
- J. Sánchez-Baena, J. Boronat, and F. Mazzanti, Supersolid striped droplets in a Raman spin-orbit-coupled system, arXiv:2007.04196 (2020) (accepted in Physical Review A as of October of 2020).

- In Chapter 5, we shift the focus to Spin Orbital Angular Coupling (SOAC). We review the derivation of an effective one-dimensional Gross Pitaevskii equation, useful to perform calculations at the mean field level. We also perform Diffusion Monte Carlo calculations of the ground state energy of a many-body system under a SOAC interaction in order to compare to mean field results.

Chapter 2

The Raman SOC one-body problem and the Mean Field regime

2.1 Introduction

We review in this Chapter several topics that are of relevance in the context of this Thesis. Since the systems of interest involve Raman SOC (except in Chapter 5), it is convenient to briefly review the physics of the one-body problem of a particle under Raman SOC. This simple case already showcases properties that are very useful to understand the many-body picture, such as the double degeneration in momentum space of the energy dispersion, which is related to the appearance of the stripe phase in the many-body case. As stated in Chapter 1, the mean field description of ultracold atom systems is of great importance due to its ability to quantitatively and qualitatively describe the majority of state-of-the-art experiments in the field. Motivated by this, we review in this Chapter the derivation of the Gross-Pitaevskii equation for SOC Hamiltonians, since the GPE represents a theoretical tool used recurrently throughout this Thesis.

This Chapter is organized as follows: in Sec. 2.2, we review the one-body problem for a particle under Raman SOC. In Sec. 2.3, we present a derivation of the Gross-Pitaevskii equation for Hamiltonians including SOC interactions. Finally, in Sec. 2.4, we review the dressed spin picture for a Raman SOC system at the mean field level, since it is of importance when studying the excitations of a Raman SOC system.

2.2 The one-body Raman SOC problem

We present in this Section a brief review of the one-body problem for a single particle under Raman SOC. We do so in order to illustrate the fundamental physics of this interaction, since the majority of the results presented in this Thesis involve it. Furthermore, useful expressions employed in Chapter 4 are also derived. The Hamiltonian we solve is:

$$\hat{H} = \frac{\hat{P}^2}{2m} + \hat{W}^{\text{Raman}} \tag{2.1}$$

$$\hat{W}^{\text{Raman}} = \frac{\lambda\hbar}{m}\hat{P}^x\hat{\sigma}^z + \frac{\lambda^2\hbar^2}{2m} - \frac{\Omega}{2}\hat{\sigma}^x \tag{2.2}$$

Notice that $[\hat{H}, \hat{\vec{P}}] = 0$, which means that we can build a basis of eigenstates of $\hat{H}$ that are also eigenstates of the momentum operator. Thus, in momentum space, the eigenvalue problem can be written as:

$$\begin{pmatrix} \frac{p^2}{2m} + \frac{\lambda\hbar p_x}{m} + \frac{\lambda^2\hbar^2}{2m} & -\frac{\Omega}{2} \\ -\frac{\Omega}{2} & \frac{p^2}{2m} - \frac{\lambda\hbar p_x}{m} + \frac{\lambda^2\hbar^2}{2m} \end{pmatrix} \begin{pmatrix} \phi_+ \\ \phi_- \end{pmatrix} = E \begin{pmatrix} \phi_+ \\ \phi_- \end{pmatrix} \tag{2.3}$$

where the + and − subindexes indicate the spin component. The eigenvalues of the Hamiltonian can be computed by finding the zeros of the characteristic polynomial, i.e. by imposing the matrix in Eq. (2.3) to have a determinant equal to zero. This yields

$$\begin{aligned}
&\left(\frac{p^2}{2m} + \frac{\lambda\hbar p_x}{m} + \frac{\lambda^2\hbar^2}{2m} - E\right)\left(\frac{p^2}{2m} - \frac{\lambda\hbar p_x}{m} + \frac{\lambda^2\hbar^2}{2m} - E\right) - \left(\frac{\Omega}{2}\right)^2 = 0 \\
&\left(\frac{p^2}{2m} + \frac{\lambda^2\hbar^2}{2m} - E\right)^2 - \left(\frac{\lambda\hbar p_x}{m}\right)^2 = \left(\frac{\Omega}{2}\right)^2 \\
&\frac{p^2}{2m} + \frac{\lambda^2\hbar^2}{2m} - E = \pm\sqrt{\left(\frac{\lambda\hbar p_x}{m}\right)^2 + \left(\frac{\Omega}{2}\right)^2} \\
&E_{\mp}(\vec{p}) = \frac{p^2}{2m} + \frac{\lambda^2\hbar^2}{2m} \mp \sqrt{\left(\frac{\hbar\lambda p_x}{m}\right)^2 + \left(\frac{\Omega}{2}\right)^2} \qquad (2.4)
\end{aligned}$$

As we can see, the energy dispersion has two branches, the lower branch being E_-. The eigenvector of the lower branch is

$$\begin{aligned}
&\left(\frac{p^2}{2m} - \frac{\lambda\hbar p_x}{m} + \frac{\lambda^2\hbar^2}{2m} - E_-\right)\phi_- - \frac{\Omega}{2}\phi_+ = 0 \\
&\phi_+ = \phi_-\left(\frac{2}{\Omega}\left(\frac{p^2}{2m} - \frac{\lambda\hbar p_x}{m} + \frac{\lambda^2\hbar^2}{2m} - E_-\right)\right) \\
&\phi_+ = \phi_-\left(-\frac{2\lambda\hbar p_x}{\Omega m} + \frac{2}{\Omega}\sqrt{\left(\frac{\hbar\lambda p_x}{m}\right)^2 + \left(\frac{\Omega}{2}\right)^2}\right) \\
&\phi_+ = \phi_-\left(\frac{2\hbar\lambda p_x}{\Omega m}\left[-1 + \frac{p_x}{|p_x|}\sqrt{1 + \left(\frac{\Omega m}{2\hbar\lambda p_x}\right)^2}\right]\right) \qquad (2.5)
\end{aligned}$$

where ϕ_+ and ϕ_- indicate the components of the vector in Eq. (2.3). Analogously, the eigenvector of the higher branch is given by

$$\phi_+ = \phi_- \left(\frac{2\hbar\lambda p_x}{\Omega m} \left[-1 - \frac{p_x}{|p_x|} \sqrt{1 + \left(\frac{\Omega m}{2\hbar\lambda p_x} \right)^2} \right] \right) \tag{2.6}$$

Thus, in position space, the eigenfunctions associated to each branch are:

$$\psi_\mp(\vec{r}) = \exp\left(i\vec{k}\vec{r} \right) \left\{ \frac{2\hbar^2\lambda k_x}{\Omega m} \left[-1 \pm \frac{k_x}{|k_x|} \sqrt{1 + \left(\frac{\Omega m}{2\hbar^2\lambda k_x} \right)^2} \right] |{+1}\rangle + |{-1}\rangle \right\} \tag{2.7}$$

with $\vec{p} = \hbar\vec{k}$. The eigenfunctions of the Hamiltonian correspond to plane waves because the Hamiltonian commutes with the momentum operator. Therefore, it is possible to obtain an eigenbasis composed by eigenstates that have definite momentum. The ground state momentum can be obtained by minimizing the energy. It is given by:

$$k_{\perp,\text{g.s.}} = 0 \qquad\qquad k_{x,\text{g.s.},} = \begin{cases} 0 & \text{if } \left(\frac{\Omega m}{2\lambda^2\hbar^2} \right) > 1 \\ \pm\lambda\sqrt{1 - \left(\frac{\Omega m}{2\lambda^2\hbar^2} \right)^2} & \text{if } \left(\frac{\Omega m}{2\lambda^2\hbar^2} \right) < 1 \end{cases} \tag{2.8}$$

where $k_{\perp,\text{g.s.}} = \sqrt{k_{y,\text{g.s.}}^2 + k_{z,\text{g.s.}}^2}$. Notice that the ground state shows a single minimum for $\left(\frac{\Omega m}{2\lambda^2\hbar^2} \right) > 1$, whereas for $\left(\frac{\Omega m}{2\lambda^2\hbar^2} \right) < 1$ the ground state is degenerate in momentum space, with two states with opposite x-momentum component having the same energy. This degeneracy hints to the appearance of the stripe phase, which consists on a superposition of states with opposite momenta. Notice that the appearance of a double minima in the energy spectrum is the cause of a second order phase transition, where a spontaneous symmetry breaking process takes place. This is illustrated in Fig. 2.1, where we show the lower branch of the dispersion relation and the ground state values of the momentum for different values of Ω.

The ground state energy is given by:

$$E_{\text{g.s.}} = \begin{cases} \frac{\lambda^2\hbar^2}{2m} - \frac{\Omega}{2} & \text{if } \left(\frac{\Omega m}{2\lambda^2\hbar^2} \right) > 1 \\ -\frac{\Omega^2 m}{8\hbar^2\lambda^2} & \text{if } \left(\frac{\Omega m}{2\lambda^2\hbar^2} \right) < 1 \end{cases} \tag{2.9}$$

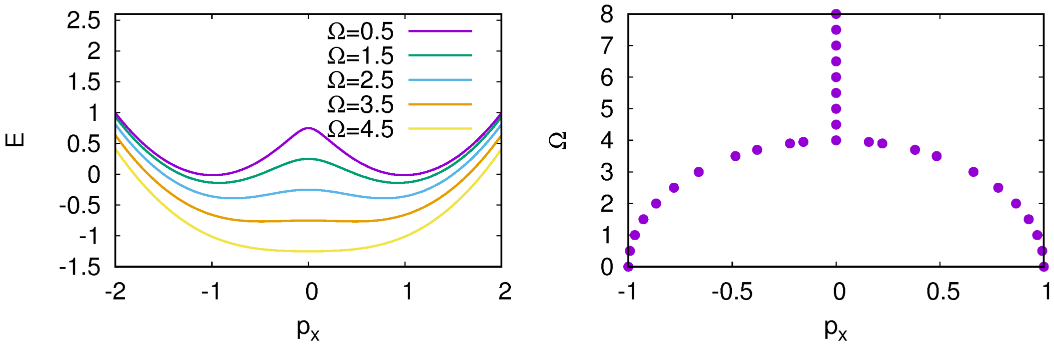

Fig. 2.1 Lowest energy branch for different values of the Raman coupling (left plot) and ground state momentum vs Raman coupling (right plot). All quantities are expressed in reduced units, with the characteristic length and energy scales given by $a_0 = \frac{1}{\lambda}$ and $\epsilon_0 = \frac{\hbar^2\lambda^2}{2m}$, respectively.

For $\frac{\Omega m}{2\lambda^2\hbar^2} < 1$, the ground state wave function can be written as:

$$\begin{aligned}\psi_-(\vec{r}) &= \exp(ik_x x)\left\{\left[-\frac{2\hbar^2\lambda k_x}{\Omega m} + \sqrt{1+\left(\frac{2\hbar^2\lambda k_x}{\Omega m}\right)^2}\right]|{+1}\rangle + |{-1}\rangle\right\} \\ &= \exp(ik_x x)\sqrt{1+\left(\frac{2\hbar^2\lambda k_x}{\Omega m}\right)^2}\left\{\left[-\frac{\frac{2\hbar^2\lambda k_x}{\Omega m}}{\sqrt{1+\left(\frac{2\hbar^2\lambda k_x}{\Omega m}\right)^2}} + 1\right]|{+1}\rangle + \frac{1}{\sqrt{1+\left(\frac{2\hbar^2\lambda k_x}{\Omega m}\right)^2}}|{-1}\rangle\right\}\end{aligned} \tag{2.10}$$

We define:

$$\sin\theta_k = \frac{\frac{2\hbar^2\lambda k_x}{\Omega m}}{\sqrt{1+\left(\frac{2\hbar^2\lambda k_x}{\Omega m}\right)^2}} \tag{2.11}$$

$$\cos\theta_k = \frac{1}{\sqrt{1+\left(\frac{2\hbar^2\lambda k_x}{\Omega m}\right)^2}} \tag{2.12}$$

such that:

$$\psi_-(\vec{r}) = \exp(ik_x x)\frac{1}{\cos\theta_k}\left\{\left[-\sin\theta_k + 1\right]|{+1}\rangle + \cos\theta_k\,|{-1}\rangle\right\} \tag{2.13}$$

Next, we normalize the wave function to get:

$$\begin{aligned}\psi_-(\vec{r}) &= \exp(ik_x x)\left\{\frac{1-\sin\theta_k}{\sqrt{2(1-\sin\theta_k)}}|{+1}\rangle + \frac{\cos\theta_k}{\sqrt{2(1-\sin\theta_k)}}|{-1}\rangle\right\}\ , \\ &= \exp(ik_x x)\left\{\sqrt{\frac{1-\sin\theta_k}{2}}|{+1}\rangle + \sqrt{\frac{1+\sin\theta_k}{2}}|{-1}\rangle\right\}\ ,\end{aligned} \tag{2.14}$$

and defining:

$$\sin\chi_k = \sqrt{\frac{1-\sin\theta_k}{2}} \tag{2.15}$$

$$\cos\chi_k = \sqrt{\frac{1+\sin\theta_k}{2}} \tag{2.16}$$

we can write:

$$\psi_-(\vec{r}) = \exp(ik_x x)\left\{\sin\chi_k\left|+1\right\rangle + \cos\chi_k\left|-1\right\rangle\right\} \tag{2.17}$$

Eqs. (2.11), (2.12), (2.15), (2.16), (2.17) are used in Chapter 4.

2.3 The Gross-Pitaevskii equation for a SOC Hamiltonian

We present here the derivation of the Gross-Pitaevskii equation (GPE) for Hamiltonians with SOC interactions. We derive the formalism for Raman SOC (see Eq. (2.2)), but an analogous procedure can be carried out for different SOC interactions, like Rashba or Weyl. In the mean field approximation, we write the many-body wave function of the system as:

$$\begin{aligned}\Psi(\vec{r}_1,\ ...,\vec{r}_N) &= \sum_{s_1,\ ...,s_N}\Psi(\vec{r}_1,s_1,\ ...,\vec{r}_N,s_N)\left|s_1,\ ...,s_N\right\rangle = \sum_{s_1,\ ...,s_N}\left(\prod_{i=1}^{N}\psi(\vec{r}_i,s_i)\left|s_i\right\rangle\right)\\ &= \prod_{i=1}^{N}\left(\psi_+(\vec{r}_i)\left|+1\right\rangle + \psi_-(\vec{r}_i)\left|-1\right\rangle\right)\end{aligned} \tag{2.18}$$

where $\vec{r}_i$ and $s_i = \pm 1$ are the position and spin coordinates of the i-th particle and $\psi_\pm(\vec{r}_i) = \psi(\vec{r}_i,\pm 1)$ are single-particle wave functions. This form for the wave function is a valid approximation of the exact many-body wave function as long as the system remains in the dilute regime. The wave function is normalized if:

$$\int d\vec{r}\left(\left|\psi_+(\vec{r})\right|^2 + \left|\psi_-(\vec{r})\right|^2\right) = 1\ . \tag{2.19}$$

The interactions between particles are modeled by a two-body contact potential, i.e.

$$\hat{V}_{ij} = \sum_{s_1,s_2}\frac{4\pi\hbar^2 a_{s_1,s_2}}{m}\delta(\vec{r}_i-\vec{r}_j)\left|s_1,s_2\right\rangle\left\langle s_1,s_2\right|\ , \tag{2.20}$$

with m the mass and a_{s_1,s_2} the spin-dependent scattering lengths, with $a_{+1,-1} = a_{-1,+1}$. Under these conditions, we can compute the energy of the system, which is given by:

$$
\begin{aligned}
E(\psi,\psi^\dagger) &= \frac{\langle\Psi|\,\hat{H}\,|\Psi\rangle}{\langle\Psi|\Psi\rangle} \\
&= N\int d\vec{r}\,\Big(\psi_+^*(\vec{r})\,\langle+1| + \psi_-^*(\vec{r})\,\langle-1|\Big)\left(-\frac{\hbar^2}{2m}\nabla^2\right)\big(\psi_+(\vec{r})\,|+1\rangle + \psi_-(\vec{r})\,|-1\rangle\big) \\
&+ N\int d\vec{r}\,\Big(\psi_+^*(\vec{r})\,\langle+1| + \psi_-^*(\vec{r})\,\langle-1|\Big)\left(-i\frac{\hbar^2\lambda}{m}\hat{\sigma_z}\frac{\partial}{\partial x}\right)\big(\psi_+(\vec{r})\,|+1\rangle + \psi_-(\vec{r})\,|-1\rangle\big) \\
&+ N\int d\vec{r}\,\Big(\psi_+^*(\vec{r})\,\langle+1| + \psi_-^*(\vec{r})\,\langle-1|\Big)\left(-\frac{\Omega}{2}\hat{\sigma_x} + \frac{\hbar^2\lambda^2}{2m}\right)\big(\psi_+(\vec{r})\,|+1\rangle + \psi_-(\vec{r})\,|-1\rangle\big) \\
&+ \frac{N(N-1)}{2}\int d\vec{r}_1 d\vec{r}_2\left[\prod_{i=1,2}\Big(\psi_+^*(\vec{r}_i)\,\langle+1| + \psi_-^*(\vec{r}_i)\,\langle-1|\Big)\right] \\
&\times\left(\sum_{s_1,s_2}\frac{4\pi\hbar^2 a_{s_1,s_2}}{m}\delta(\vec{r}_1-\vec{r}_2)\,|s_1,s_2\rangle\,\langle s_1,s_2|\right)\left[\prod_{i=1,2}\big(\psi_+(\vec{r}_i)\,|+1\rangle + \psi_-(\vec{r}_i)\,|-1\rangle\big)\right] \\
&= N\int d\vec{r}\left[-\frac{\hbar^2}{2m}\psi_+^*\nabla^2\psi_+ - \frac{\hbar^2}{2m}\psi_-^*\nabla^2\psi_- - i\frac{\hbar^2\lambda}{m}\psi_+^*\frac{\partial\psi_+}{\partial x}\right. \\
&+ i\frac{\hbar^2\lambda}{m}\psi_-^*\frac{\partial\psi_-}{\partial x} - \frac{\Omega}{2}\Big(\psi_-^*(\vec{r})\psi_+(\vec{r}) + \psi_+^*(\vec{r})\psi_-(\vec{r})\Big) \\
&\left.+ \frac{\hbar^2\lambda^2}{2m}\Big(\psi_+^*(\vec{r})\psi_+(\vec{r}) + \psi_-^*(\vec{r})\psi_-(\vec{r})\Big)\right] \\
&+ \frac{N(N-1)}{2}\int d\vec{r}\left[g_{+1,+1}|\psi_+(\vec{r})|^4 + g_{-1,-1}|\psi_-(\vec{r})|^4 + 2g_{+1,-1}|\psi_+(\vec{r})|^2|\psi_-(\vec{r})|^2\right] ,
\end{aligned}
\tag{2.21}
$$

with $g_{\pm1,\pm1} = \frac{4\pi\hbar^2}{m}a_{\pm1,\pm1}$ and $a_{\pm1,\pm1}$ the spin-dependent scattering lengths.

In order to obtain the GPE, we minimize the functional in Eq. (2.21) with the condition in Eq. (2.19). This is equivalent to minimizing the functional:

$$
F(\psi,\psi^\dagger) = E(\psi,\psi^\dagger) - \mu\left(\int d\vec{r}\,\Big(|\psi_+(\vec{r})|^2 + |\psi_-(\vec{r})|^2\Big) - 1\right) \tag{2.22}
$$

In order to do so, we evaluate $F(\psi_+^* + \delta\psi_+^*, \psi_-^* + \delta\psi_-^*, \psi_+, \psi_-)$, which results into:

$$
\begin{aligned}
F(\psi_+^* + \delta\psi_+^*, \psi_-^* + \delta\psi_-^*, \psi_+, \psi_-) &= \int d\vec{r}\epsilon(\psi,\psi^\dagger) + \int d\vec{r}\left(\frac{\delta\epsilon}{\delta\psi_+^*}\delta\psi_+^* + \frac{\delta\epsilon}{\delta\psi_-^*}\delta\psi_-^*\right) \\
&+ \mathcal{O}\Big((\delta\psi_+^*)^2, (\delta\psi_-^*)^2\Big)
\end{aligned}
\tag{2.23}
$$

with $\epsilon(\psi, \psi^\dagger)$ the energy density. Substituting, we find

$$\begin{aligned}
&F(\psi_+^* + \delta\psi_+^*, \psi_-^* + \delta\psi_-^*, \psi_+, \psi_-) = F(\psi_+^*, \psi_-^*, \psi_+, \psi_-) \\
&+ \int d\vec{r}\delta\psi_+^* \left[N\left(-\frac{\hbar^2}{2m}\nabla^2\psi_+ - i\frac{\hbar^2\lambda}{m}\frac{\partial\psi_+}{\partial x} - \frac{\Omega}{2}\psi_-(\vec{r}) + \frac{\hbar^2\lambda^2}{2m}\psi_+(\vec{r}) \right) \right. \\
&\left. + \frac{N(N-1)}{2}\left(2g_{+1,+1}|\psi_+(\vec{r})|^2\psi_+(\vec{r}) + 2g_{+1,-1}|\psi_-(\vec{r})|^2\psi_+(\vec{r}) \right) - \mu\psi_+(\vec{r}) \right] \\
&+ \int d\vec{r}\delta\psi_-^* \left[N\left(-\frac{\hbar^2}{2m}\nabla^2\psi_- + i\frac{\hbar^2\lambda}{m}\frac{\partial\psi_-}{\partial x} - \frac{\Omega}{2}\psi_+(\vec{r}) + \frac{\hbar^2\lambda^2}{2m}\psi_-(\vec{r}) \right) \right. \\
&\left. + \frac{N(N-1)}{2}\left(2g_{-1,-1}|\psi_-(\vec{r})|^2\psi_-(\vec{r}) + 2g_{+1,-1}|\psi_+(\vec{r})|^2\psi_-(\vec{r}) \right) - \mu\psi_-(\vec{r}) \right] . \qquad (2.24)
\end{aligned}$$

In order to minimize F $\forall$ $\delta\psi_+^*$, $\delta\psi_-^*$, we must set $\frac{\delta\epsilon}{\delta\psi_+^*} = 0$ and $\frac{\delta\epsilon}{\delta\psi_-^*} = 0$. Therefore:

$$\begin{aligned}
&-\frac{\hbar^2}{2m}\nabla^2\psi_+ - i\frac{\hbar^2\lambda}{m}\frac{\partial\psi_+}{\partial x} - \frac{\Omega}{2}\psi_-(\vec{r}) + \frac{\hbar^2\lambda^2}{2m}\psi_+(\vec{r}) \\
&+ N\left(g_{+1,+1}|\psi_+(\vec{r})|^2\psi_+(\vec{r}) + g_{+1,-1}|\psi_-(\vec{r})|^2\psi_+(\vec{r}) \right) = \mu\psi_+(\vec{r}) \qquad (2.25) \\
&-\frac{\hbar^2}{2m}\nabla^2\psi_- + i\frac{\hbar^2\lambda}{m}\frac{\partial\psi_-}{\partial x} - \frac{\Omega}{2}\psi_+(\vec{r}) + \frac{\hbar^2\lambda^2}{2m}\psi_-(\vec{r}) \\
&+ N\left(g_{-1,-1}|\psi_-(\vec{r})|^2\psi_-(\vec{r}) + g_{+1,-1}|\psi_+(\vec{r})|^2\psi_-(\vec{r}) \right) = \mu\psi_-(\vec{r}) \qquad (2.26)
\end{aligned}$$

where we have approximated $N-1 \simeq N$ in the thermodynamic limit. One can also compute $F(\psi_+^*, \psi_-^*, \psi_+ + \delta\psi_+, \psi_- + \delta\psi_-)$ and impose the terms proportional to $\delta\psi_+$, $\delta\psi_-$ to be zero, which yields an equivalent set of equations. By numerically solving Eqs. (2.25) and (2.26) one can obtain the condensate wave function of the system and, from it, any desired observable at the mean field level. The time-dependent version of the GPE can be obtained similarly following a variational approach: the minimization of the functional

$$F(\Psi^\dagger, \Psi) = \sum_{\vec{S},\vec{S}'} \int d\vec{R}d\vec{R}' \left[i\hbar\Psi^\dagger\frac{\partial\Psi}{\partial t}\delta(\vec{R}-\vec{R}')\delta(\vec{S}-\vec{S}') - \Psi^\dagger(\vec{R}',\vec{S}') \left\langle \vec{R}',\vec{S}' \right| \hat{H} \left| \vec{R},\vec{S} \right\rangle \Psi(\vec{R},\vec{S}) \right] \tag{2.27}$$

where $\hat{H}$ is the many-body Hamiltonian and $\Psi(\vec{R},\vec{S})$ the many-body wave function, with $\vec{R} = (\vec{r}_1, \ ..., \vec{r}_N)$, $\vec{S} = (s_1, \ ..., s_N)$. We define:

$$A = \int d\vec{r} \left(|\psi_+(\vec{r})|^2 + |\psi_-(\vec{r})|^2 \right) \ , \tag{2.28}$$

such that the functional in Eq. (2.27(can be rewritten as:

$$
\begin{aligned}
&F(\Psi^\dagger,\Psi) = A^{N-1}N\int \vec{dr}\; i\hbar\left(\psi_+^*\frac{\partial\psi_+}{\partial t}+\psi_-^*\frac{\partial\psi_-}{\partial t}\right)\\
&-NA^{N-1}\int \vec{dr}\left[-\frac{\hbar^2}{2m}\psi_+^*\nabla^2\psi_+ - \frac{\hbar^2}{2m}\psi_-^*\nabla^2\psi_- - i\frac{\hbar^2\lambda}{m}\psi_+^*\frac{\partial\psi_+}{\partial x}\right.\\
&+i\frac{\hbar^2\lambda}{m}\psi_-^*\frac{\partial\psi_-}{\partial x} - \frac{\Omega}{2}\Big(\psi_-^*(\vec{r})\psi_+(\vec{r})+\psi_+^*(\vec{r})\psi_-(\vec{r})\Big)\\
&\left.+\frac{\hbar^2\lambda^2}{2m}\Big(\psi_+^*(\vec{r})\psi_+(\vec{r})+\psi_-^*(\vec{r})\psi_-(\vec{r})\Big)\right]\\
&-\frac{N(N-1)}{2}A^{N-2}\int \vec{dr}\left[g_{+1,+1}|\psi_+(\vec{r})|^4+g_{-1,-1}|\psi_-(\vec{r})|^4+2g_{+1,-1}|\psi_+(\vec{r})|^2|\psi_-(\vec{r})|^2\right]\ .
\end{aligned}
\tag{2.29}
$$

Following the minimization procedure described above, we find:

$$
\begin{aligned}
&-\frac{\hbar^2}{2m}\nabla^2\psi_+ - i\frac{\hbar^2\lambda}{m}\frac{\partial\psi_+}{\partial x} - \frac{\Omega}{2}\psi_-(\vec{r}) + \frac{\hbar^2\lambda^2}{2m}\psi_+(\vec{r})\\
&+N\left(g_{+1,+1}\frac{|\psi_+(\vec{r})|^2}{A}\psi_+(\vec{r}) + g_{+1,-1}\frac{|\psi_-(\vec{r})|^2}{A}\psi_+(\vec{r})\right) = i\hbar\frac{\partial\psi_+}{\partial t}
\end{aligned}
\tag{2.30}
$$

$$
\begin{aligned}
&-\frac{\hbar^2}{2m}\nabla^2\psi_- + i\frac{\hbar^2\lambda}{m}\frac{\partial\psi_-}{\partial x} - \frac{\Omega}{2}\psi_+(\vec{r}) + \frac{\hbar^2\lambda^2}{2m}\psi_-(\vec{r})\\
&+N\left(g_{-1,-1}\frac{|\psi_-(\vec{r})|^2}{A}\psi_-(\vec{r}) + g_{+1,-1}\frac{|\psi_+(\vec{r})|^2}{A}\psi_-(\vec{r})\right) = i\hbar\frac{\partial\psi_-}{\partial t}\ ,
\end{aligned}
\tag{2.31}
$$

which corresponds to Eqs. (2.25) (2.26) replacing $\mu\psi_\pm(\vec{r})$ by $i\hbar\frac{\partial\psi_\pm}{\partial t}$ and setting the norm of the wave function to $A = 1$. In order to obtain the ground state of a system at the mean field level, one can solve these equations using imaginary time evolution setting $\tau = it/\hbar$. Starting from the initial wave function, imaginary time evolution leads to the mean field representation of the ground state of the system. For the particular case of an homogeneous system with Raman SOC, the mean field wave function only depends on x [25]. Therefore, in practice, the GPE to be solved is one-dimensional.

2.4 The dressed spin picture for a Raman SOC system at the mean field level

We now review the dressed spin picture introduced in Ref. [1], since it offers some useful physical insight on the existence of stripes in the mean field phase diagram of the Raman SOC system mentioned in Chapter 3. This picture is also relevant to understand the results presented in Chapter 4 regarding the excitation spectrum of the system.

The interaction part of the Hamiltonian for a system under Raman SOC with spin-dependent interactions at the mean field level can be written as:

$$\hat{H}_{\text{int.}} = \int d\vec{r} \frac{1}{2} \left[g_{+1,+1}\rho_{+1}^2 + g_{-1,-1}\rho_{+1}^2 + 2g_{+1,-1}\rho_{+1}\rho_{-1} \right] \tag{2.32}$$

where $\rho_{+1} = |\psi_{+1}|^2$, $\rho_{-1} = |\psi_{-1}|^2$. We define the dressed spin states as the spin components of the lowest energy eigenstates of the one-body problem in Sec. 2.2. These are:

$$\left|+1'\right\rangle = [\cos\chi_k \left|+1\right\rangle + \sin\chi_k \left|-1\right\rangle] \tag{2.33}$$

$$\left|-1'\right\rangle = [\sin\chi_k \left|+1\right\rangle + \cos\chi_k \left|-1\right\rangle] \tag{2.34}$$

with $k_0 = \lambda\sqrt{1 - \left(\frac{\Omega m}{2\lambda^2\hbar^2}\right)^2}$ the ground state momentum of the one-body system (see Sec. 2.2). In this Section, we want to rewrite the interaction of Eq. 2.32 in terms of the dressed spin states. We do so because the phases that arise in the mean field phase diagram of a Raman SOC system, which are the stripe, plane wave, and single minimum phases, are closely related to the dressed spin states [1, 25]. The mean field stripe phase wave function can be approximated by [25]:

$$\psi_{\text{stripe}}(\vec{r}) \simeq \exp(-ik_0x)\left|+1'\right\rangle + \exp(ik_0x)\left|-1'\right\rangle \tag{2.35}$$

whereas the mean field plane wave wave function can be approximated by:

$$\psi_{\text{pw}}(\vec{r}) \simeq \exp(-ik_0x)\left|+1'\right\rangle \tag{2.36}$$

or

$$\psi_{\text{pw}}(\vec{r}) \simeq \exp(ik_0x)\left|-1'\right\rangle \tag{2.37}$$

since both plane wave states yield the same energy. We have approximated the mean field momentum of each phase by the one-body ground state momentum. Therefore, the stripe phase corresponds to a miscible mixture of the $+1'$ and $-1'$ dressed spin states, whereas the plane wave phase corresponds to only one of them. Thus, the stripe-plane wave phase transition can be understood as a miscible-to-immiscible (or vice-versa) process between the dressed states [1]. By writing the interaction Hamiltonian in the dressed spin basis we can characterize the miscibility between these states.

Any wave function can be written as:

$$\begin{aligned}\psi(\vec{r}) &= \psi_{+1'}(\vec{r})\left|+1'\right\rangle + \psi_{-1'}(\vec{r})\left|-1'\right\rangle \\ &= \psi_{+1'}(\vec{r})\left[\cos\chi_k\left|+1\right\rangle + \sin\chi_k\left|-1\right\rangle\right] + \psi_{-1'}(\vec{r})\left[\sin\chi_k\left|+1\right\rangle + \cos\chi_k\left|-1\right\rangle\right]\ ,\end{aligned} \tag{2.38}$$

and thus, the two separate components of ψ can be written as:

$$\psi_{+1}(\vec{r}) = \cos\chi_k\psi_{+1'}(\vec{r}) + \sin\chi_k\psi_{-1'}(\vec{r}) \tag{2.39}$$

$$\psi_{-1}(\vec{r}) = \sin\chi_k\psi_{+1'}(\vec{r}) + \cos\chi_k\psi_{-1'}(\vec{r}) \tag{2.40}$$

Here we focus in the stripe phase wave function. In order to express the term in Eq. (2.32) in terms of the dressed state amplitudes, we transform the density terms.

$$\rho_{+1} = \cos^2\chi_k\rho_{+1'} + \sin^2\chi_k\rho_{-1'} + \sin\chi_k\cos\chi_k\left(\psi^*_{+1'}\psi_{-1'} + \psi^*_{-1'}\psi_{+1'}\right) \tag{2.41}$$

$$\rho_{-1} = \sin^2\chi_k\rho_{+1'} + \cos^2\chi_k\rho_{-1'} + \sin\chi_k\cos\chi_k\left(\psi^*_{+1'}\psi_{-1'} + \psi^*_{-1'}\psi_{+1'}\right) \tag{2.42}$$

$$\begin{aligned}\rho^2_{+1} = &\left(\cos^2\chi_k\rho_{+1'} + \sin^2\chi_k\rho_{-1'}\right)^2 + \sin^2\chi_k\cos^2\chi_k\left(\psi^*_{+1'}\psi_{-1'} + \psi^*_{-1'}\psi_{+1'}\right)^2 \\ &+ 2\left(\cos^2\chi_k\rho_{+1'} + \sin^2\chi_k\rho_{-1'}\right)\sin\chi_k\cos\chi_k\left(\psi^*_{+1'}\psi_{-1'} + \psi^*_{-1'}\psi_{+1'}\right)\end{aligned} \tag{2.43}$$

$$\begin{aligned}\rho^2_{-1} = &\left(\sin^2\chi_k\rho_{+1'} + \cos^2\chi_k\rho_{-1'}\right)^2 + \sin^2\chi_k\cos^2\chi_k\left(\psi^*_{+1'}\psi_{-1'} + \psi^*_{-1'}\psi_{+1'}\right)^2 \\ &+ 2\left(\sin^2\chi_k\rho_{+1'} + \cos^2\chi_k\rho_{-1'}\right)\sin\chi_k\cos\chi_k\left(\psi^*_{+1'}\psi_{-1'} + \psi^*_{-1'}\psi_{+1'}\right)\end{aligned} \tag{2.44}$$

$$\begin{aligned}\rho_{+1}\rho_{-1} = &\left(\cos^2\chi_k\rho_{+1'} + \sin^2\chi_k\rho_{-1'}\right)\left(\sin^2\chi_k\rho_{+1'} + \cos^2\chi_k\rho_{-1'}\right) \\ &+ \sin\chi_k\cos\chi_k\left(\psi^*_{+1'}\psi_{-1'} + \psi^*_{-1'}\psi_{+1'}\right)\left(\rho_{+1'} + \rho_{-1'}\right) \\ &+ \sin^2\chi_k\cos^2\chi_k\left(\psi^*_{+1'}\psi_{-1'} + \psi^*_{-1'}\psi_{+1'}\right)^2\end{aligned} \tag{2.45}$$

Notice that when substituting Eqs. (2.41)- (2.45) into Eq. (2.32) the terms proportional to $\psi^*_{+1'}\psi_{-1'}$ and $\psi^*_{-1'}\psi_{+1'}$ will vanish upon integration, since they are proportional to $\exp(2ik_0x)$ and $\exp(-2ik_0x)$. Therefore, performing the aforementioned substitution, Eq. (2.32) becomes:

$$\begin{aligned}\hat{H}_{\text{int.}} = &\int d\vec{r}\frac{1}{2}\left\{g_{+1,+1}\left[\cos^4\chi_k\rho^2_{+1'} + \sin^4\chi_k\rho^2_{-1'} + 4\sin^2\chi_k\cos^2\chi_k\rho_{+1'}\rho_{-1'}\right]\right. \\ &+g_{-1,-1}\left[\sin^4\chi_k\rho^2_{+1'} + \cos^4\chi_k\rho^2_{-1'} + 4\sin^2\chi_k\cos^2\chi_k\rho_{+1'}\rho_{-1'}\right] \\ &+2g_{+1,-1}\left[\sin^2\chi_k\cos^2\chi_k\left(\rho^2_{+1'} + \rho^2_{-1'}\right) + \rho_{+1'}\rho_{-1'}\left(\sin^4\chi_k + \cos^4\chi_k\right)\right. \\ &\left.\left.+2\sin^2\chi_k\cos^2\chi_k\rho_{+1'}\rho_{-1'}\right]\right\}\ .\end{aligned} \tag{2.46}$$

Expressing Eq. (2.46) in terms of powers of $\sin^2\chi_k$ only, we get:

$$\begin{aligned}\hat{H}_{\text{int.}} &= \int d\vec{r}\frac{1}{2}\Big\{g_{+1,+1}\Big[\rho^2_{+1'} - 2\sin^2\chi_k\rho^2_{+1'} + \sin^4\chi_k\rho^2_{+1'} \\ &+ \sin^4\chi_k\rho^2_{-1'} + 4\sin^2\chi_k\rho_{+1'}\rho_{-1'} - 4\sin^4\chi_k\rho_{+1'}\rho_{-1'}\Big] \\ &+ g_{-1,-1}\Big[\rho^2_{-1'} - 2\sin^2\chi_k\rho^2_{-1'} + \sin^4\chi_k\rho^2_{+1'} \\ &+ \sin^4\chi_k\rho^2_{-1'} + 4\sin^2\chi_k\rho_{+1'}\rho_{-1'} - 4\sin^4\chi_k\rho_{+1'}\rho_{-1'}\Big] \\ &+ 2g_{+1,-1}\left[\sin^2\chi_k\left(\rho^2_{+1'} + \rho^2_{-1'}\right) - \sin^4\chi_k\left(\rho^2_{+1'} + \rho^2_{-1'}\right) + \rho_{+1'}\rho_{-1'}\right]\Big\} \qquad (2.47) \\ &= \int d\vec{r}\frac{1}{2}\left[g_{+1',+1'}\rho^2_{+1'} + g_{-1',-1'}\rho^2_{+1'} + 2g_{+1',-1'}\rho_{+1'}\rho_{-1'}\right] \ . \qquad (2.48)\end{aligned}$$

The effective interactions in the dressed spin basis are:

$$g_{+1',+1'} = g_{+1,+1} + \sin^2\chi_k\left[2\left(g_{+1,-1} - g_{+1,+1}\right)\right] + \sin^4\chi_k\left[\left(g_{+1,+1} + g_{-1,-1} - 2g_{+1,-1}\right)\right] \qquad (2.49)$$

$$g_{-1',-1'} = g_{-1,-1} + \sin^2\chi_k\left[2\left(g_{+1,-1} - g_{-1,-1}\right)\right] + \sin^4\chi_k\left[\left(g_{+1,+1} + g_{-1,-1} - 2g_{+1,-1}\right)\right] \qquad (2.50)$$

$$g_{+1',-1'} = g_{+1,-1} + \sin^2\chi_k\left[2\left(g_{+1,+1} + g_{-1,-1}\right)\right] - \sin^4\chi_k\left[2\left(g_{+1,+1} + g_{-1,-1}\right)\right] \qquad (2.51)$$

Using Eqs. (2.15), (2.11), the term $\sin^2\chi_k$ can be expressed as:

$$\sin^2\chi_k = \frac{1}{2}\left[1 - \frac{\frac{2\hbar^2\lambda k_x}{\Omega m}}{\sqrt{1+\left(\frac{2\hbar^2\lambda k_x}{\Omega m}\right)^2}}\right] = \frac{1}{2}\left[1 - \frac{1}{\sqrt{1+\left(\frac{\Omega m}{2\hbar^2\lambda k_x}\right)^2}}\right] \ , \qquad (2.52)$$

while substituting k_x by the ground state momentum of the one-body system we obtain:

$$\sin^2\chi_k = \frac{1}{2}\left[1 - \sqrt{1 - \left(\frac{\Omega^2}{\left(4\epsilon_0\right)^2}\right)}\right] \qquad (2.53)$$

with $\epsilon_0 = \frac{\hbar^2\lambda^2}{2m}$. For $\frac{\Omega^2}{\left(4\epsilon_0\right)^2} \ll 1$, we can write:

$$\sin^2\chi_k \simeq \frac{1}{2}\left[1 - \left(1 - \frac{1}{2}\left(\frac{\Omega^2}{\left(4\epsilon_0\right)^2}\right)\right)\right] = \left(\frac{\Omega}{8\epsilon_0}\right)^2 \ , \qquad (2.54)$$

and thus, up to $\mathcal{O}\left(\left(\frac{\Omega}{8\epsilon_0}\right)^2\right)$, the effective interactions in the dressed spin basis are given by:

$$g_{+1',+1'} = g_{+1,+1} + \left(\frac{\Omega}{8\epsilon_0}\right)^2 \left[2\left(g_{+1,-1} - g_{+1,+1}\right)\right] \tag{2.55}$$

$$g_{-1',-1'} = g_{-1,-1} + \left(\frac{\Omega}{8\epsilon_0}\right)^2 \left[2\left(g_{+1,-1} - g_{-1,-1}\right)\right] \tag{2.56}$$

$$g_{+1',-1'} = g_{+1,-1} + \frac{1}{2}\left(\frac{\Omega}{8\epsilon_0}\right)^2 \left[4\left(g_{+1,+1} + g_{-1,-1}\right)\right] \tag{2.57}$$

For the experiment of Ref. [1], where ^{87}Rb atoms are employed, $g_{+1,+1} \simeq g_{-1,-1} \simeq g_{+1,-1}$, so that the relative difference $\Delta g = |g_{+1,+1} - g_{+1,-1}|/g_{+1,+1}$ is considered to be a small parameter. Under these conditions:

$$g_{+1',+1'} = g_{+1,+1} + \mathcal{O}\left(\Delta g\left(\frac{\Omega}{8\epsilon_0}\right)^2\right) \tag{2.58}$$

$$g_{-1',-1'} = g_{-1,-1} + \mathcal{O}\left(\Delta g\left(\frac{\Omega}{8\epsilon_0}\right)^2\right) \tag{2.59}$$

$$g_{+1',-1'} = g_{+1,-1} + 4g_{+1,+1}\left(\frac{\Omega}{8\epsilon_0}\right)^2 + \mathcal{O}\left(\Delta g\left(\frac{\Omega}{8\epsilon_0}\right)^2\right) \tag{2.60}$$

Eq. (2.60) recovers the effective dressed spin inter-species interaction given in Ref. [1]. Even though in ^{87}Rb experiments $g_{+1,-1} \simeq g_{+1,+1}$, a stripe ground state exists for the system because $g_{+1,-1} < g_{+1,+1}$ [1, 25]. As mentioned previously, the stripe state can be understood as a miscible mixture of the two dressed spin states. Since the effective inter-species interaction in the dressed spin basis depends on the Raman coupling, Ω, there is only a given range of Ω values where the dressed spins are miscible, and thus, where the stripe phase can exist as the ground state. In general, the spin components of a system that features spin-dependent interactions are miscible at the mean field level if [1]

$$a_{+1,-1} < \sqrt{a_{+1,+1}a_{-1,-1}} \tag{2.61}$$

Therefore, the dressed spin components are miscible if

$$g_{+1',-1'} < \sqrt{g_{+1',+1'}g_{-1',-1'}} = \sqrt{g_{+1,+1}g_{-1,-1}} \tag{2.62}$$

The limiting value of Ω regarding the miscibility of the system is:

$$\begin{aligned} g_{+1',-1'} &= g_{+1,-1} + 4g_{+1,+1}\left(\frac{\Omega}{8\epsilon_0}\right)^2 < \sqrt{g_{+1,+1}g_{-1,-1}} \\ \Omega &< \epsilon_0\sqrt{\frac{16\left(\sqrt{g_{+1,+1}g_{-1,-1}} - g_{+1,-1}\right)}{g_{+1,+1}}} \end{aligned} \tag{2.63}$$

This threshold value of Ω regarding the miscibility of the system is only valid for low enough values of $ng_{\pm1,\pm1}$, since in the expansion of the stripe wave function in terms of the dressed states (given in Eq. (2.35)) we neglect inter-atomic interactions.

Chapter 3

Quantum Monte Carlo methods for Spin-Orbit interactions

3.1 Introduction

Even though mean field theories represent a powerful tool when describing ultracold atom systems, they lack the ability to account for inter-atomic correlations at all orders. Therefore, when the *gas parameter* of a given system, defined as $x_g = na^3$, with n the density and a the scattering length, surpasses a given threshold, mean field theories start to fail qualitatively and quantitatively in the description of many-body systems. In this regime, other approaches to calculate observables must be followed. In particular, quantum Monte Carlo methods represent a reliable option in these cases. Unlike mean field theories, Monte Carlo methods are able to account for inter-atomic correlations at all orders, and can therefore provide an accurate description of a many-body system at larger gas parameters. However, the computational cost of these methods is much higher, and such cost is directly related to the number of particles of the system. Because of this, Monte Carlo methods are only able to simulate rather small systems compared to the typical experimental scales regarding the number of particles. Nevertheless, they still constitute one of the premier options for the description of correlated many-body systems. In this Chapter, we present two types of Diffusion Monte Carlo methods suitable for the study of SOC systems: the Discrete Spin T-moves DMC (DTDMC), which corresponds to an adaptation to discrete spins of the method presented in Ref. [19], and the Spin-Integrated DMC (SIDMC), which is a completely original method developed during this Thesis that bypasses the effective Hamiltonian definition of the DTDMC by propagating the spin integrated wave function of the system in imaginary time. We also review the basic Variational and Diffusion Monte Carlo algorithms suited to study systems without SOC. Finally, as an application of the derived DMC methods, we present the phase diagram of a Raman SOC system and its comparison with the mean field case, together with some observables of the system obtained at the Monte Carlo level.

This Chapter is organized as follows: in Sec. 3.2 we introduce the relevant SOC Hamiltonians for this Chapter, together with the reduced units of choice. In Sec. 3.3, we present the basics of the Variational Monte Carlo method and briefly discuss its implementation for SOC Hamiltonians. In Sec. 3.4, we introduce the standard Diffusion Monte Carlo method, suited for the study of many-body non-SOC systems. Finally, in Sec. 3.5, we present the derivation of both the DTDMC and the SIDMC, discuss their implementation, show the results for some test cases and present the results for the phase diagram of a Raman SOC system.

3.2 Spin-Orbit Coupled Hamiltonians

In this Chapter, we study ultracold gases of N bosons of mass m with pseudo-spin 1/2 under the effect of synthetic spin-orbit coupling. The generic form of the Hamiltonian is

$$\hat{H} = \sum_{k=1}^{N} \left[\frac{\hat{P}_k^2}{2m} + \hat{V}_k^{\text{1b}} + \hat{W}_k^{\text{SOC}} \right] + \hat{V}^{\text{2b}} \ , \tag{3.1}$$

with $\hat{V}_k^{\text{1b}}$ and $\hat{V}^{\text{2b}}$ momentum independent, local, one- and two-body interactions, respectively, while $\hat{V}^{\text{2b}}$ can depend on the spin configuration. In much the same way, $\hat{W}_k^{\text{SOC}}$ stands for a one-body, momentum- and spin-dependent potential. The ones considered in this Chapter are the Rashba, Weyl and Raman, given by

$$\hat{W}_k^{\text{Rs}} = \frac{\lambda_{\text{Rs}}\hbar}{2} \left[\hat{P}_k^y \hat{\sigma}_k^x - \hat{P}_k^x \hat{\sigma}_k^y \right] \tag{3.2}$$

$$\hat{W}_k^{\text{Rm}} = \frac{\lambda_{\text{Rm}}\hbar}{m} \hat{P}_k^x \hat{\sigma}_k^z + \frac{\lambda_{\text{Rm}}^2 \hbar^2}{2m} - \frac{\Omega}{2} \hat{\sigma}_k^x \tag{3.3}$$

$$\hat{W}_k^{\text{We}} = \frac{\lambda_{\text{We}}\hbar}{m} \left[\hat{P}_k^x \hat{\sigma}_k^x + \hat{P}_k^y \hat{\sigma}_k^y + \hat{P}_k^z \hat{\sigma}_k^z \right] + \frac{\lambda_{\text{We}}^2 \hbar^2}{2m} \ , \tag{3.4}$$

with $\hat{P}_k^\alpha$ the α-component of the momentum operator of particle k, $\hat{\sigma}_k^{x,y,z}$ the Pauli matrices associated to the k-th particle, Ω the Rabi frequency, and λ_α ($\alpha = \{$ Rs, We, Rm$\}$) the strength of the corresponding SOC interaction. The general form of the two-body potential is:

$$\hat{V}^{\text{2b}} = \sum_{k<l} \left[\sum_{s_k, s_l} V_{s_k,s_l}^{\text{2b}}(r_{kl}) |s_k, s_l\rangle\langle s_k, s_l| \right] \ , \tag{3.5}$$

where s_k, s_l assign values ± 1 to the z-component of the spin of particles k and l, while $V_{s_k,s_l}^{\text{2b}}(r_{kl})$ is a central, short-ranged potential that can be different for the different channels corresponding to s_k and s_l. For instance, in the numerical examples of Sec. 3.5.3 we use a soft-core spin-dependent potential for simplicity, defined by:

$$V_{s_k,s_l}(r) = V_0(s_k, s_l)\, \theta(R_0(s_k, s_l) - r)) \ . \tag{3.6}$$

If the two-body interaction is taken to be spin-independent, $V_0(s_k, s_l) = V_0$ and $R_0(s_k, s_l) = R_0$. In much the same way, the one-body potential used in some of the calculations of Sec. 3.5.3 is a harmonic trapping interaction

$$\hat{V}^{1\mathrm{b}} = \frac{1}{2} m\omega^2 (\hat{X}^2 + \hat{Y}^2 + \hat{Z}^2) \; . \tag{3.7}$$

3.2.1 Reduced units for the different kinds of SOC interactions

Due to the different spin dependence, we define different length and energy scales in each case. For the Rashba interaction, we use

$$a_{\mathrm{Rs}} = \frac{1}{\lambda_{\mathrm{Rs}} m} \;,\; e_{\mathrm{Rs}} = \frac{\hbar^2}{2ma_{\mathrm{Rs}}^2} = \frac{\hbar^2 \lambda_{\mathrm{Rs}}^2 m}{2} \;, \tag{3.8}$$

while for the Raman interaction, we employ

$$a_{\mathrm{Rm}} = \frac{\eta_{\mathrm{Rm}}}{\lambda_{\mathrm{Rm}}} \;,\; e_{\mathrm{Rm}} = \frac{\hbar^2}{2ma_{\mathrm{Rm}}^2} = \frac{\hbar^2 \lambda_{\mathrm{Rm}}^2}{2m\eta_{\mathrm{Rm}}^2} \;. \tag{3.9}$$

with η_{Rm} a dimensionless scaling factor that we vary depending on the density. This only modifies the length scale of choice for reduced units. Finally, for the Weyl Hamiltonian we use

$$a_{\mathrm{We}} = \frac{\eta_{\mathrm{We}}}{2\lambda_{\mathrm{We}}} \;,\; e_{\mathrm{We}} = \frac{\hbar^2}{2ma_{\mathrm{We}}^2} = \frac{2\hbar^2 \lambda_{\mathrm{We}}^2}{m\eta_{\mathrm{We}}^2} \;. \tag{3.10}$$

In terms of these, the interactions read

$$\hat{W}_k^{\mathrm{Rashba}} = \left[\hat{P}_k^y \hat{\sigma}_k^x - \hat{P}_k^x \hat{\sigma}_k^y\right] \tag{3.11}$$

$$\hat{W}_k^{\mathrm{Raman}} = 2\eta_{\mathrm{Rm}} \hat{P}_k^x \hat{\sigma}_k^z + \eta_{\mathrm{Rm}}^2 - \frac{\Omega}{2} \hat{\sigma}_k^x \tag{3.12}$$

$$\hat{W}_k^{\mathrm{Weyl}} = \eta_{\mathrm{We}} \left[\hat{P}_k^x \hat{\sigma}_k^x + \hat{P}_k^y \hat{\sigma}_k^y + \hat{P}_k^z \hat{\sigma}_k^z\right] + \frac{\eta_{\mathrm{We}}^2}{4} \tag{3.13}$$

where all quantities written in dimensionless form. The same applies to the soft-core potential and harmonic trap of Eqs. (3.6) and (3.7).

3.3 The Variational Monte Carlo method

We present in this Section a brief overview of the Variational Monte Carlo (VMC) method and address how to include Spin-Orbit interactions. The VMC method allows to estimate properties of an N-particle quantum system described by the many-body wave function $\psi_T(\vec{R})$. Typically, $\psi_T(\vec{R})$ is usually referred as the trial wave function, and is an approximation to the actual ground state wave function, $\psi_0(\vec{R})$. The estimators of the properties of the system can be written as

$$O = \frac{\langle\psi_T|\,\hat{O}\,|\psi_T\rangle}{\langle\psi_T|\psi_T\rangle} = \frac{\int d\vec{R}\left[\int d\vec{R}'\left\langle\vec{R}'\middle|\,\hat{O}\,\middle|\vec{R}\right\rangle\frac{\psi_T(\vec{R}')}{\psi_T(\vec{R})}\right]\left|\psi_T(\vec{R})\right|^2}{\langle\psi_T|\psi_T\rangle} = \frac{\int d\vec{R}\,O_L(\vec{R})\left|\psi_T(\vec{R})\right|^2}{\langle\psi_T|\psi_T\rangle} \tag{3.14}$$

where:

$$O_L(\vec{R}) = \int d\vec{R}'\left\langle\vec{R}'\middle|\,\hat{O}\,\middle|\vec{R}\right\rangle\frac{\psi_T(\vec{R}')}{\psi_T(\vec{R})} \tag{3.15}$$

If the $\hat{O}$ operator is local (i.e. $\left\langle\vec{R}'\middle|\,\hat{O}\,\middle|\vec{R}\right\rangle = O(\vec{R})\delta(\vec{R}'-\vec{R})$), this expression reduces to:

$$O_L(\vec{R}) = O(\vec{R}) \ . \tag{3.16}$$

Within the VMC framework, one first generates a set of coordinates $\vec{R}_i = (\vec{r}_{i,1} \ ... \ \vec{r}_{i,N})$ that statistically represent $\left|\psi_T(\vec{R})\right|^2$. This can be done by means of the Metropolis algorithm [64, 65]. From the Central Limit Theorem [64], we know that Eq. (3.14) can be evaluated by employing the unbiased estimator of the mean, i.e.

$$O = \frac{1}{N_w}\sum_{i=1}^{N_w} O_L(\vec{R}_i) \ , \tag{3.17}$$

where N_w is the number of sets of coordinates. This procedure is performed multiple times, referred as iterations, so that a set of estimations is obtained, i.e. $\{O_j\}$, where $j = 1, 2, ..., N_{\text{it}}$, with N_{it} the total number of iterations. The final result for the observable $\langle\hat{O}\rangle$ is given by the average over iterations, i.e.

$$\langle\hat{O}\rangle = \frac{1}{N_{\text{it}}}\sum_{i=1}^{N_{\text{it}}} O_j \tag{3.18}$$

The estimation of $\langle\hat{O}\rangle$ has a variance associated, which can be computed as:

$$\sigma_O^2 = \frac{1}{N_{\text{b}}-1}\sum_{j=1}^{N_{\text{b}}}\langle\hat{O}^2\rangle_j - \langle\hat{O}\rangle_j^2 \tag{3.19}$$

Here, $\langle\hat{O}^2\rangle_j$ and $\langle\hat{O}\rangle_j$ correspond to averages over a given number of iterations, conforming a block, while N_b denotes the number of blocks. This block averaging procedure is carried out in order to reduce correlations between samples, since the sampling from the Metropolis algorithm is correlated. In this way, Eq. (3.19) corresponds to the variance.

The trial wave function is usually written in terms of a set of variational parameters $\{\alpha\}$, so that $\psi_T(\vec{R}, \vec{\alpha})$, that are tuned so that the energy obtained with VMC is minimized. The best approximation to the unknown ground state wave function is then taken as $\psi_T(\vec{R}, \vec{\alpha}_{\text{min}})$, with $\vec{\alpha}_{\text{min}}$ the set of variational parameters that minimizes the energy. This variational estimation of the energy corresponds to an upper bound to the ground state energy. The optimized trial wave function can then be used as an input to the Diffusion Monte Carlo method described in the Sec. 3.4.

The implementation of SOC Hamiltonians requires spin sampling together with position sampling. Therefore, the set of coordinates obtained with the Metropolis algorithm now includes spins, i.e. $\vec{X}_i = (\vec{r}_{i,1}, s_{i,1} \ldots \vec{r}_{i,N}, s_{i,N})$. We denote by $\vec{S}$ a vector containing the spins of the N particles. Also, the wave function employed as a trial factor is generally complex. Given the Hamiltonian of Eq. (3.1), the energy is estimated as:

$$\begin{aligned} E = \frac{\langle\psi_T|\,\hat{H}\,|\psi_T\rangle}{\langle\psi_T|\psi_T\rangle} &= \frac{\sum_{\vec{S}}\int d\vec{R}'\left|\psi_T(\vec{R}',\vec{S}')\right|^2\left[\sum_{\vec{S}}\int d\vec{R}\left\langle\vec{R}',\vec{S}'\right|\hat{H}\left|\vec{R},\vec{S}\right\rangle\frac{\psi_T(\vec{R},\vec{S})}{\psi_T(\vec{R}',\vec{S}')}\right]}{\langle\psi_T|\psi_T\rangle} \\ &= \frac{\sum_{\vec{S}'}\int d\vec{R}'\; E_L(\vec{R}',\vec{S}')\left|\psi_T(\vec{R}',\vec{S}')\right|^2}{\langle\psi_T|\psi_T\rangle} \end{aligned} \tag{3.20}$$

Since the energy is a real quantity, one generally works with the real part of $E_L(\vec{R}, \vec{S})$, which is commonly referred as the local energy, since the imaginary part vanishes upon integration. Thus, with $\psi_T(\vec{R}, \vec{S}) = \rho_T(\vec{R}, \vec{S}) \exp\left(i\Phi_T(\vec{R}, \vec{S})\right)$, one computes $E_L(\vec{R}, \vec{S})$ as:

$$\begin{aligned} E_L(\vec{R},\vec{S}) = \sum_{k=1}^{N}\Bigg[&-\frac{\hbar^2}{2m}\frac{\nabla_k^2\rho_T(\vec{R},\vec{S})}{\rho_T(\vec{R},\vec{S})} + \left|\vec{\nabla}_k\Phi_T(\vec{R},\vec{S})\right|^2 + V_k^{1\text{b}}(\vec{r}_k) \\ &+\sum_{\vec{S}'}\int d\vec{R}'\left\langle\vec{R}',\vec{S}'\right|\hat{w}_{\text{Re},k}\left|\vec{R},\vec{S}\right\rangle\frac{\rho_T(\vec{R}',\vec{S}')}{\rho_T(\vec{R},\vec{S})}\Bigg] + V^{2\text{b}}(\vec{R},\vec{S})\ , \end{aligned} \tag{3.21}$$

where

$$\langle\vec{R}',\vec{S}'|\,\hat{w}_{\text{Re},k}\,|\vec{R},\vec{S}\rangle = \text{Re}\left\{\langle\vec{R}',\vec{S}'|\,\hat{W}_k^{\text{SOC}}\,|\vec{R},\vec{S}\rangle\,\frac{e^{i\Phi_T(\vec{R},\vec{S},\tau)}}{e^{i\Phi_T(\vec{R}',\vec{S}',\tau)}}\right\}\ . \tag{3.22}$$

For the SOC Hamiltonians of the previous Section, the integral appearing in Eq. (3.15), which arises from the non-local character of the SOC potential, can be computed analytically.

3.4 The standard Diffusion Monte Carlo method

We introduce in this Section the basics of the standard Diffusion Monte Carlo (DMC) method. This algorithm enables the computation of observables of the ground state of a quantum many-body system. The main principle behind the method is the propagation in imaginary time of a wave function. Given a quantum state $|\psi_0\rangle$ and an N-particle Hamiltonian $\hat{H}$, the application of the imaginary time evolution operator $\exp\left(-\tau\hat{H}\right)$ yields:

$$\begin{aligned}|\psi(\tau)\rangle &= \exp\left(-\hat{H}\tau\right)|\psi_0\rangle = \sum_{E,\alpha}\exp\left(-\hat{H}\tau\right)|\phi_{E,\alpha}\rangle\langle\phi_{E,\alpha}|\psi_0\rangle \\ &= \sum_{E,\alpha}\exp\left(-E\tau\right)|\phi_{E,\alpha}\rangle\langle\phi_{E,\alpha}|\psi_0\rangle \end{aligned} \tag{3.23}$$

with $\tau = it/\hbar$ the imaginary time and $|\phi_{E,\alpha}\rangle$ the eigenvectors of eigenvalue E and quantum number α of $\hat{H}$. By performing the limit $\tau \to \infty$ and normalizing the evolved state, we get:

$$\lim_{\tau\to\infty}\frac{|\psi(\tau)\rangle}{\sqrt{\langle\psi(\tau)|\psi(\tau)\rangle}} = \lim_{\tau\to\infty}\frac{\sum_{E,\alpha}\exp\left(-E\tau/\hbar\right)|\phi_{E,\alpha}\rangle\langle\phi_{E,\alpha}|\psi_0\rangle}{\sqrt{\langle\psi(\tau)|\psi(\tau)\rangle}} \propto |\phi_{E_0,\alpha}\rangle \tag{3.24}$$

where $\phi_{E_0,\alpha}$ is the ground state of the system. Therefore, as long as $\langle\phi_{E,\alpha}|\psi_0\rangle \neq 0$, imaginary time evolution leads to the ground state of $\hat{H}$. DMC implements the imaginary time evolution stochastically: first, the initial wave function is sampled by the use of the Metropolis algorithm [64, 65], typically in position space, which results into a set of N-particle coordinates, $\vec{R}_i = (\vec{r}_{i,1} \,...\, \vec{r}_{i,N})$. Each set of coordinates is commonly known as a *walker*, with i being the walker index. Then, a given set of transformations is applied to these points iteratively such that, after a sufficiently high number of iterations, the coordinates represent statistically the true ground state wave function of the system. We denote by $\Delta\tau$ the imaginary time-step. The evolved wave function can be written as

$$\psi(\vec{R}', \tau + \Delta\tau) = \int d\vec{R}\,\langle\vec{R}'|\exp\left[-\Delta\tau\hat{H}\right]|\vec{R}\rangle\,\psi(\vec{R},\tau)\ , \tag{3.25}$$

Given a set of walkers statistically representing $\psi(\vec{R},\tau)$, the transformations to be applied in order to get a representation of $\psi(\vec{R}', \tau+\Delta\tau)$ are obtained by interpreting $\langle\vec{R}'|\exp\left[-\Delta\tau\hat{H}\right]|\vec{R}\rangle$ as a probability distribution. Up to $\mathcal{O}(\Delta\tau)$, this matrix element is given by [64]:

$$\langle \vec{R}'|\exp\left[-\Delta\tau\hat{H}\right]|\vec{R}\rangle = \exp\left[-\frac{m}{2\hbar^2\Delta\tau}\left(\vec{R}'-\vec{R}\right)^2\right]\exp\left[\Delta\tau\left(-\frac{V(\vec{R}')+V(\vec{R})}{2}\right)\right] + \mathcal{O}\left(\Delta\tau^2\right) . \tag{3.26}$$

Here, $V(\vec{R})$ is a many-body interaction potential consisting on a sum of two-body interactions. The expansion of the propagator of Eq. (3.26) can be obtained as follows. First, the imaginary time evolution operator is spit as

$$\exp\left\{-\tau\hat{H}\right\} = \prod_{k=1}^{N_\tau}\exp\left\{-\Delta\tau\hat{H}\right\} + \mathcal{O}\left(\Delta\tau^2\right) \tag{3.27}$$

with $\tau = N_\tau\Delta\tau$. Next, we split the contributions from the kinetic and potential terms as

$$\exp\left\{-\tau\hat{H}\right\} = \prod_{k=1}^{N_\tau}\exp\left\{-\Delta\tau\hat{V}/2\right\}\exp\left\{-\Delta\tau\hat{T}\right\}\exp\left\{-\Delta\tau\hat{V}/2\right\} + \mathcal{O}\left(\Delta\tau^2\right) \tag{3.28}$$

where $\hat{T}$ is the kinetic energy operator and $\hat{V}$ is the potential. In the position representation,

$$\langle \vec{R}'|\exp\left[-\Delta\tau\hat{H}\right]|\vec{R}\rangle = \langle \vec{R}'|\exp\left[-\Delta\tau\hat{T}\right]|\vec{R}\rangle\exp\left[\Delta\tau\left(-\frac{V(\vec{R}')+V(\vec{R})}{2}\right)\right] + \mathcal{O}\left(\Delta\tau^2\right) . \tag{3.29}$$

It can be shown that [64]

$$\langle \vec{R}'|\exp\left[-\Delta\tau\hat{T}\right]|\vec{R}\rangle = \exp\left[-\frac{m}{2\hbar^2\Delta\tau}\left(\vec{R}'-\vec{R}\right)^2\right] . \tag{3.30}$$

In DMC, one evolves the product $\psi_T(\vec{R})\psi(\vec{R},\tau)$ in imaginary time, with $\psi_T(\vec{R})$ a trial wave function, instead of just $\psi(\vec{R},\tau)$. This is done in order to reduce the variance of the measured observables. The imaginary-time evolution equation thus becomes:

$$\psi_T(\vec{R}')\psi(\vec{R}',\tau+\Delta\tau) = \int d\vec{R}\frac{\psi_T(\vec{R}')}{\psi_T(\vec{R})}\langle \vec{R}'|\exp\left[-\Delta\tau\hat{H}\right]|\vec{R}\rangle\,\psi_T(\vec{R})\psi(\vec{R},\tau) , \tag{3.31}$$

It can be shown that the transformations to be applied to the set of walkers, obtained by interpreting the object $\frac{\psi_T(\vec{R}')}{\psi_T(\vec{R})}\langle \vec{R}'|\exp\left[-\Delta\tau\hat{H}\right]|\vec{R}\rangle$ as a probability distribution, consist of a Gauss-Drift-Branching (GDB) process [64]. The Gauss-Drift step performs a shift of the coordinates of the walker, $\vec{R}_i \to \vec{R}_i'$, given by the sum of two factors: a multidimensional Gaussian random variable drawn from the probability distribution:

$$P(\vec{\chi}) = \mathcal{N} \exp\left[-\frac{m\chi^2}{2\hbar^2\Delta\tau}\right] \tag{3.32}$$

with $\mathcal{N}$ the normalization factor, plus a factor determined by the trial wave function. The resulting shift in coordinates is given by:

$$\vec{R}' = \vec{R} + \frac{\hbar^2\Delta\tau}{m}\frac{\vec{\nabla}\psi_T}{\psi_T} + \vec{\chi} \tag{3.33}$$

Finally, the Branching step arises from the fact that the object $\frac{\psi_T(\vec{R}')}{\psi_T(\vec{R})}\langle\vec{R}'|\exp\left[-\Delta\tau\hat{H}\right]|\vec{R}\rangle$ can not be normalized. It consists on replicating and eliminating walkers, with their multiplicities given by [64]:

$$B = \text{Int.}\left\{\exp\left[\Delta\tau\left(E_s - \frac{E_L(\vec{R}') + E_L(\vec{R})}{2}\right)\right] + \xi\right\} \tag{3.34}$$

with ξ an instance of a uniformly distributed random variable between 0 and 1. Here, $E_L(\vec{R})$ is the local energy, defined as $E_L(\vec{R}) = \frac{\hat{H}\psi_T(\vec{R})}{\psi_T(\vec{R})}$. The quantity E_s is an energy shift that is constantly updated during imaginary time evolution with the estimated value of the energy. In this way, during the simulation, walkers with local energy lower than E_s produce higher branching factors, while those with local energy higher than E_s are more likely removed.

Observables within the DMC framework are then computed as:

$$O = \frac{\langle\psi_T|\hat{O}|\psi(\tau)\rangle}{\langle\psi_T|\psi(\tau)\rangle} = \frac{\int d\vec{R}\frac{\hat{O}\psi_T}{\psi_T}\psi_T(\vec{R})\psi(\vec{R},\tau)}{\langle\psi_T|\psi(\tau)\rangle} = \frac{\int d\vec{R}O_L(\vec{R})\psi_T(\vec{R})\psi(\vec{R},\tau)}{\langle\psi_T|\psi(\tau)\rangle} \tag{3.35}$$

and approximating the integral using the unbiased estimator of the mean, as in the previous Section. Since the walkers represent statistically $\langle\psi_T|\psi(\tau)\rangle$, the observable O can be estimated at a given iteration as:

$$O = \frac{1}{N_w}\sum_{i=1}^{N_w} O_L(\vec{R}_i) \tag{3.36}$$

with N_w the number of walkers. Notice that, since $\lim_{\tau\to\infty}\psi_T(\vec{R})\psi(\vec{R},\tau) = \psi_T(\vec{R})\psi_0(\vec{R})$, with $\psi_0(\vec{R})$ the ground state wave function of $\hat{H}$, the estimation of the energy (and any quantity commuting with $\hat{H}$) is exact, i.e.

$$E = \frac{\langle\psi_T|\hat{H}|\psi_0\rangle}{\langle\psi_T|\psi_0\rangle} = E_0 \tag{3.37}$$

with E_0 the ground state energy. The estimators obtained with DMC depend on the time step $\Delta\tau$. For the description presented in this work, this dependence is linear, so one should set several DMC runs for different values of the time step and perform a linear extrapolation to $\Delta\tau \to 0$. Another important remark is that the DMC estimates have statistical variance, i.e. even when the steady state has been reached, DMC estimations oscillate around the mean for different iterations. As in the previous Section, this variance can be estimated as:

$$\sigma_O^2 = \frac{1}{N_b - 1} \sum_{i=1}^{N_b} \langle \hat{O}^2 \rangle_i - \langle \hat{O} \rangle_i^2 \tag{3.38}$$

$$\langle \hat{O} \rangle_i = \frac{1}{N_b^{\text{it}} N_w} \sum_{i=1}^{N_b^{\text{it}}} \sum_{j=1}^{N_w} O_L(\vec{R}_j^{(i)}) \tag{3.39}$$

$$\langle \hat{O}^2 \rangle_i = \frac{1}{N_b^{\text{it}} N_w} \sum_{i=1}^{N_b^{\text{it}}} \sum_{j=1}^{N_w} O_L^2(\vec{R}_j^{(i)}) \ . \tag{3.40}$$

Here N_b denotes the number of blocks, N_b^{it} the number of iterations per block and $\vec{R}_j^{(i)}$ indicates the position coordinates of the j-th walker at the i-th iteration.

3.5 Diffusion Monte Carlo methods for Spin-Orbit interactions

As mentioned in Chapter 1, the standard Diffusion Monte Carlo method reviewed in Sec. 3.4 can not deal with SOC interactions. This is mainly due to the non-local character of SOC potentials, which feature linear momentum terms that are non-local in the position representation. This non-locality induces the emergence of new terms in the propagator that must be obtained and included in the imaginary time propagation process of the DMC algorithm. Another difficulty associated to the presence of SOC is the emergence of an imaginary part in the ground state wave function. Since DMC algorithms are unable to simultaneously propagate in imaginary time the modulus and the phase of a wave function, one must resort to the fixed phase approximation (FPA) [40]. Within this approach, the phase of the wave function is held constant, while the modulus is propagated in imaginary time. As a consequence, one can only obtain the best possible estimates of physical quantities according to a given phase constraint. We have developed two DMC methods able to deal with SOC terms in the Hamiltonian: the Discrete Spin T-moves DMC, an adaptation to discrete spins of the method developed in Ref. [19] and the Spin Integrated DMC. While the DTDMC approach resorts into the definition of an effective Hamiltonian to bypass a sign problem in the matrix elements of the propagator, the SIDMC method is able to avoid the definition of such effective Hamiltonian by propagating the spin-integrated wave function of the system. Avoiding the use of the effective Hamiltonian improves the quality of the estimates.

In this Section, we present the formalism of the two DMC methods able to sample SOC Hamiltonians previously mentioned: the SIDMC (see Sec. 3.5.1) and the DTDMC (see Sec. 3.5.2). We first derivate the propagator for Hamiltonians featuring SOC interactions and then proceed to discuss its numerical implementation.

3.5.1 The Spin-integrated DMC (SIDMC) method

In this Section, we derive the SIDMC method. As mentioned previously, the spin-integrated wave function of the system is propagated in imaginary time, as this avoids the need to define an effective Hamiltonian to bypass the sign problem of the propagator. As a consequence, the quality of the estimates is improved with respect to the DTDMC approach, although the SIDMC method needs the imposition of constraints on the two-body interaction and the trial wave function (both of which can not be spin-dependent). Within the SIDMC formalism, SOC terms are accounted by an extra branching process performed after a standard Gauss-Drift-Branching process. We show that the computation of this secondary branching factor is numerically efficient. In order to derive the SIDMC method, we start by deriving the propagator in the FPA, and writing the imaginary time evolution equation for the spin-integrated probability density. In the following, we assume that the two-body interaction is spin-independent. We also present a scheme of the SIDMC algorithm and address some relevant technical details.

3.5.1.1 Formalism

We first derive a suitable form of the propagator required to simulate spin-orbit problems, under the assumption that the two-body interaction $\hat{V}^{2\mathrm{b}}$ is spin-independent. The imaginary time evolution of state $|\Psi(\tau)\rangle$ is given by

$$|\Psi(\tau+\Delta\tau)\rangle = \exp\left[-\Delta\tau\hat{H}\right]|\Psi(\tau)\rangle \ . \tag{3.41}$$

Projecting on $\langle\vec{R}',\vec{S}'|$ and introducing an identity, Eq. (3.41) can be written as:

$$\psi(\vec{R}',\vec{S}',\tau+\Delta\tau) = \sum_{\vec{S}}\int d\vec{R}\,\langle\vec{R}',\vec{S}'|\exp\left[-\Delta\tau\hat{H}\right]|\vec{R},\vec{S}\rangle\,\psi(\vec{R},\vec{S},\tau)\ , \tag{3.42}$$

where $\vec{R}$ and $\vec{S}$ stand for the position and spin coordinates of the N particles, and $\psi(\vec{R},\vec{S},\tau) = \langle \vec{R},\vec{S}|\Psi(\tau)\rangle$. For the sake of clarity, we also define

$$\hat{H}_0 = \sum_{k=1}^{N} \left[\frac{P_k^2}{2m} + \hat{V}_k^{1\mathrm{b}} + \sum_{l<k}^{N} \hat{V}_{k,l}^{2\mathrm{b}} \right] \tag{3.43}$$

$$\hat{W} = \sum_{k=1}^{N} \hat{W}_k^{\mathrm{SOC}} \ . \tag{3.44}$$

where $\hat{V}_{k,l}^{2\mathrm{b}}$ is spin-independent. Up to $\mathcal{O}(\Delta\tau)$, Eq. (3.42) can be written as:

$$\begin{aligned}\psi(\vec{R}',\vec{S}',\tau+\Delta\tau) = \sum_{\vec{S}} \int d\vec{R} \int d\vec{R}'' \, \langle \vec{R}',\vec{S}'| \exp\left[-\Delta\tau \hat{W}\right] |\vec{R}'',\vec{S}\rangle \\ \times \, \langle \vec{R}''| \exp\left[-\Delta\tau \hat{H}_0\right] |\vec{R}\rangle \, \psi(\vec{R},\vec{S},\tau) + \mathcal{O}\Big(\Delta\tau^2\Big) \ ,\end{aligned} \tag{3.45}$$

where $\hat{H}_0$ stands for all terms of $\hat{H}$ in the propagator that are spin-independent.

In this way, the propagator reads:

$$G(\vec{R},\vec{S} \to \vec{R}',\vec{S}') = \int d\vec{R}'' \, \langle \vec{R}',\vec{S}'| \exp\left[-\Delta\tau \hat{W}\right] |\vec{R}'',\vec{S}\rangle \, \langle \vec{R}''| \exp\left[-\Delta\tau \hat{H}_0\right] |\vec{R}\rangle \ . \tag{3.46}$$

As mentioned previously, the ground state wave function of a SOC Hamiltonian is, in general, imaginary. Since DMC is unable to simultaneously propagate the modulus and the phase of the wave function, we resort to the fixed-phase approximation [19], [40] where all quantities involved are real.

Knowing the general expression of the propagator written above, we can deduce its equivalent form within the fixed-phase approximation. This can be done by comparing the imaginary-time Schrödinger equation for the wave function and for its modulus, which is the main quantity of interest in the FPA. For the full wave function, one has

$$\begin{aligned}-\frac{\partial \psi(\vec{R},\vec{S})}{\partial \tau} = \left[\sum_{k=1}^{N} \left(-\frac{\hbar^2}{2m} \nabla_k^2 + V_k^{1\mathrm{b}}(\vec{r}_k) + \sum_{l<k}^{N} \hat{V}_{k,l}^{2\mathrm{b}}(r_{kl}) \right) \right] \psi(\vec{R},\vec{S},\tau) \\ + \sum_{\vec{S}'} \int d\vec{R}' \, \langle \vec{R},\vec{S}| \, \hat{W} \, |\vec{R}',\vec{S}'\rangle \, \psi(\vec{R}',\vec{S}',\tau) \ ,\end{aligned} \tag{3.47}$$

while for the modulus $\rho(\vec{R},\vec{S})$ of $\psi(\vec{R},\vec{S})$ the equation reads

$$\begin{aligned}-\frac{\partial \rho(\vec{R},\vec{S})}{\partial \tau} = \left[\sum_{k=1}^{N} \left(-\frac{\hbar^2}{2m} \nabla_k^2 + \frac{\hbar^2}{2m} |\vec{\nabla}_k \Phi(\vec{R},\vec{S},\tau)|^2 + V_k^{1\mathrm{b}}(\vec{r}_k) + \sum_{l<k}^{N} \hat{V}_{k,l}^{2\mathrm{b}}(\vec{r}_k,\vec{r}_l) \right) \right] \rho(\vec{R},\vec{S},\tau) \\ + \sum_{\vec{S}'} \int d\vec{R}' \, \langle \vec{R},\vec{S}| \, \hat{w}_{\mathrm{Re}} \, |\vec{R}',\vec{S}'\rangle \, \rho(\vec{R}',\vec{S}',\tau) \ ,\end{aligned} \tag{3.48}$$

where

$$\psi(\vec{R},\vec{S},\tau) = \rho(\vec{R},\vec{S},\tau)\exp\left[i\Phi(\vec{R},\vec{S},\tau)\right] \tag{3.49}$$

and

$$\langle\vec{R},\vec{S}|\,\hat{w}_{\text{Re}}\,|\vec{R}',\vec{S}'\rangle = \text{Re}\left\{\langle\vec{R},\vec{S}|\,\hat{W}\,|\vec{R}',\vec{S}'\rangle\,\frac{e^{i\Phi(\vec{R}',\vec{S}',\tau)}}{e^{i\Phi(\vec{R},\vec{S},\tau)}}\right\} . \tag{3.50}$$

In the FPA, $\Phi(\vec{R},\vec{S},\tau)$ is kept constant and:

$$\hat{V}_{\Phi} = \sum_{k=1}^{N}|\nabla_k\Phi(\vec{R},\vec{S})|^2 \tag{3.51}$$

becomes a local interaction in positions and spins. Eqs. (3.47) and (3.48) have a similar structure, and thus comparing terms in each, we can get the FPA form of the propagator in Eq. (3.46):

$$\begin{aligned} G_{\text{FP}}(\vec{R},\vec{S}\to\vec{R}',\vec{S}') =&\ \langle\vec{R}',\vec{S}'|\exp\left[-\Delta\tau\hat{H}^{\text{FP}}\right]|\vec{R},\vec{S}\rangle \\ =&\int d\vec{R}''\,\langle\vec{R}',\vec{S}'|\exp\left[-\Delta\tau\left(\hat{w}_{\text{Re}}+\hat{V}_{\Phi}\right)\right]|\vec{R}'',\vec{S}\rangle \\ &\times\ \langle\vec{R}''|\exp\left[-\Delta\tau\hat{H}_0\right]|\vec{R}\rangle+\mathcal{O}\left(\Delta\tau^2\right) , \end{aligned} \tag{3.52}$$

with

$$\hat{H}^{\text{FP}} = \hat{H}_0+\hat{w}_{\text{Re}}+\hat{V}_{\Phi} \tag{3.53}$$

the fixed-phase Hamiltonian. In this approximation one has to impose a certain form for the phase. In this work, we model it as a sum of one-body terms

$$\Phi(\vec{R},\vec{S}) = \sum_{k=1}^{N}\phi_k(\vec{r}_k,s_k) . \tag{3.54}$$

Due to the form of the spin-orbit potential, we can evaluate the integral in Eq. (3.52). For the Raman SOC of Eq. (3.3), the matrix element of the spin-dependent part of the potential is

$$\begin{aligned} \langle\vec{R}',\vec{S}'\hat{w}_{\text{Re}}+\hat{V}_{\Phi}\,|\vec{R}'',\vec{S}\rangle = \sum_{k=1}^{N}\left[\prod_{l\neq k}^{N}\delta_{\vec{r}'_l,\vec{r}''_l}\delta_{s'_l,s_l}\right]&\left[\frac{\lambda\hbar}{m}\delta_{y'_k,y''_k}\delta_{z'_k,z''_k}\frac{d\delta_{x'_k,x''_k}}{dx'_k}\,\langle s'_k|\,\hat{\sigma}^z_k\,|s_k\rangle\sin(\Delta\phi_k)\right. \\ &+\frac{\lambda^2}{2m}\delta_{\vec{r}'_k,\vec{r}''_k}\delta_{s'_k,s_k}+|\vec{\nabla}_k\phi_k|^2\delta_{\vec{r}'_k,\vec{r}''_k}\delta_{s'_k,s_k} \\ &\left.-\frac{\Omega}{2}\,\langle s'_k|\,\hat{\sigma}^x_k\,|s_k\rangle\cos(\Delta\phi_k)\delta_{\vec{r}'_k,\vec{r}''_k}\right] , \end{aligned} \tag{3.55}$$

where

$$\Delta\phi_k = \phi_k(\vec{r}''_k,s_k)-\phi_k(\vec{r}'_k,s'_k) . \tag{3.56}$$

Since the spinless part of the propagator is given in Eq. (3.26), the integral in Eq. (3.52) yields

$$
\begin{aligned}
G_{\mathrm{FP}}(\vec{R},\vec{S}\to\vec{R}',\vec{S}') = {} & \langle\vec{R}'|\exp\left[-\Delta\tau\hat{H}_0\right]|\vec{R}\rangle \\
& \times\left\{\delta_{\vec{S}',\vec{S}}-\Delta\tau\sum_{k=1}^{N}\left[\prod_{l\neq k}^{N}\delta_{s'_l,s_l}\right]\left[\frac{\lambda\hbar}{m}\langle s'_k|\,\hat{\sigma}^z_k\,|s_k\rangle\cos(\Delta\phi_k)\right.\right. \\
& \times\frac{\partial\phi_k}{\partial x''_k}+\frac{\lambda^2}{2m}\delta_{s'_k,s_k}-\frac{\Omega}{2}\langle s'_k|\,\hat{\sigma}^x_k\,|s_k\rangle\cos(\Delta\phi_k) \\
& \left.\left.+\left|\vec{\nabla}_k\phi_k\right|^2\delta_{s'_k,s_k}\right]\Big|_{\vec{R}''=\vec{R}'}\right\}.
\end{aligned}
\tag{3.57}
$$

For the Rashba and Weyl SOC interactions, a similar procedure has to be carried out. However, one has to expand the element $\langle\vec{R}',\vec{S}'|\exp\left[-\Delta\tau\left(\hat{w}_{\mathrm{Re}}+\hat{V}_{\Phi}\right)\right]|\vec{R}'',\vec{S}\rangle$ in Eq. (3.52) up to order $\Delta\tau^2$. This is because the terms originated from the matrix element of $\hat{w}_{\mathrm{Re}}$ are proportional to $\xi_k = r'_k - r_k$, and thus, the elements arising from $\hat{w}^2_{\mathrm{Re}}$ generate contributions of order ξ_k^2 and $\xi_k\xi_l$. Since ξ_k represents the displacement of particle k due to the standard DMC Gauss-Drift-Branching (GDB) process, this quantity is of $\mathcal{O}\left(\sqrt{\Delta\tau}\right)$. However, in our simulations, we have not found a significant impact on the results when these terms are ignored.

Following with the derivation of the propagator in Eq. (3.57), we define a new operator $\hat{O}$ as

$$
\langle\vec{S}'|\,\hat{O}(\vec{R}')\,|\vec{S}\rangle = \frac{G_{\mathrm{FP}}(\vec{R},\vec{S}\to\vec{R}',\vec{S}')}{\langle\vec{R}'|\exp\left[-\Delta\tau\hat{H}_0\right]|\vec{R}\rangle}\,. \tag{3.58}
$$

such that, up to $\mathcal{O}(\Delta\tau)$, Eq. (3.57) can be rewritten as:

$$
\begin{aligned}
& G_{\mathrm{FP}}(\vec{R},\vec{S}\to\vec{R}',\vec{S}') \simeq \langle\vec{R}'|\exp\left[-\Delta\tau\hat{H}_0\right]|\vec{R}\rangle\prod_{k=1}^{N}\left\{\delta_{s'_k,s_k}-\Delta\tau\left[\frac{\lambda\hbar}{m}\langle s'_k|\,\hat{\sigma}^z_k\,|s_k\rangle\cos(\Delta\phi_k)\right.\right. \\
& \left.\left.\times\frac{\partial\phi_k}{\partial x''_k}+\frac{\lambda^2}{2m}\delta_{s'_k,s_k}-\frac{\Omega}{2}\langle s'_k|\,\hat{\sigma}^x_k\,|s_k\rangle\cos(\Delta\phi_k)+\left|\vec{\nabla}_k\phi_k\right|^2\delta_{s'_k,s_k}\right]\Big|_{\vec{r}''_k=\vec{r}'_k}\right\} \\
& = \langle\vec{R}'|\exp\left[-\Delta\tau\hat{H}_0\right]|\vec{R}\rangle\prod_{k=1}^{N}\langle s'_k|\,\hat{O}_k(\vec{r}'_k)\,|s_k\rangle
\end{aligned}
\tag{3.59}
$$

where we have used the approximation $(1-\Delta t\sum x_i)\approx\prod(1-\Delta t x_i)$ which is exact to order Δt. In this way, the matrix element of the new operator $\hat{O}$ becomes the product of matrix elements of single-particle operators $\hat{O}_k$, as shown in the expression above.

Note that, for the Rashba and Weyl SOC potentials, the matrix elements $\langle s'_k|\,\hat{O}_k\,|s_k\rangle$ depend both on $\vec{r}'_k$ and $\vec{r}_k$. For the sake of simplicity, in the following we omit the r_k and r'_k labels. The imaginary time evolution equation for the modulus of the wave function, within the FPA and to order Δt, is then given by

$$\rho(\vec{R}', \vec{S}', \tau+\Delta\tau) = \sum_{\vec{S}} \int d\vec{R} \left\{ \left(\prod_{k=1}^{N} \langle s'_k | \hat{O}_k | s_k \rangle \right) \langle \vec{R}' | \exp\left[-\Delta\tau \hat{H}_0 \right] | \vec{R} \rangle \, \rho(\vec{R}, \vec{S}, \tau) \right\} . \tag{3.60}$$

However, in DMC simulations the object that is being propagated is $f(\vec{R}, \vec{S}, \tau) = \rho(\vec{R}, \vec{S}, \tau)\rho_T(\vec{R}, \vec{S})$, with $\rho_T(\vec{R}, \vec{S})$ the modulus of a given importance sampling trial function. From Eq. (3.60) one readily sees that

$$f(\vec{R}', \vec{S}', \tau+\Delta\tau) = \sum_{\vec{S}} \int d\vec{R} \left\{ \prod_{k=1}^{N} \langle s'_k | \hat{O}_k | s_k \rangle \, \langle \vec{R}' | \exp\left[-\Delta\tau \hat{H}_0 \right] | \vec{R} \rangle \, \frac{\rho_T(\vec{R}', \vec{S}')}{\rho_T(\vec{R}, \vec{S})} f(\vec{R}, \vec{S}, \tau) \right\} \tag{3.61}$$

In order to use this expression in the actual simulations, we need the propagator to be positive-definite. However, due to the spin-orbit coupling, the matrix elements of the propagator do not fulfill this condition. Despite this, if we propagate the spin-integrated form of the modulus of the importance sampling function of Eq. (3.61), this problem is greatly reduced. Therefore, we propagate the quantity

$$F(\vec{R}, \tau) = \sum_{\vec{S}} f(\vec{R}, \vec{S}, \tau) . \tag{3.62}$$

In order to progress, we also impose the modulus of the trial wave function to be spin-independent i.e. $\rho_T(\vec{R}, \vec{S}) = \rho_T(\vec{R})$. After j time steps, one gets

$$\begin{aligned} F(\vec{R}^{(j)}, j\Delta\tau) = \sum_{\vec{S}^{(j)},\ldots,\vec{S}^{(0)}} \int d\vec{R}^{(j-1)} \cdots d\vec{R}^{(0)} & \left[\prod_{n=1}^{j} \left(\prod_{k=1}^{N} \langle s_k^{(n)} | \hat{O}_k | s_k^{(n-1)} \rangle \right) \right] \\ \times & \left[\prod_{n=1}^{j} \langle \vec{R}^{(n)} | \exp\left[-\Delta\tau \hat{H}_0 \right] | \vec{R}^{(n-1)} \rangle \, \frac{\rho_T(\vec{R}^{(n)})}{\rho_T(\vec{R}^{(n-1)})} F(\vec{R}^{(0)}, 0) \right] , \end{aligned} \tag{3.63}$$

where $\vec{R}^{(n)}$ stand for the position coordinates of the walker, and $s_k^{(n)}$ for the spin of particle k in that walker, both at iteration n. We can understand this expression in a simple way. The last piece correspond to a standard GDB DMC process [64] for the spinless part of the Hamiltonian. On the other hand, the first part, incorporating the spin-dependent terms, can be implemented through a secondary branching process. This one must fulfill that, after j iterations, the weight carried by a given walker should be

$$w(j) = \sum_{\vec{S}^{(j)},\ldots,\vec{S}^{(0)}} \prod_{n=1}^{j} \left(\prod_{k=1}^{N} \langle s_k^{(n)} | \hat{O}_k | s_k^{(n-1)} \rangle \right) , \tag{3.64}$$

corresponding to the first term in Eq. (3.63). This is fulfilled by performing the secondary branching at iteration j using the weight

$$B(j) = \frac{w(j)}{w(j-1)} \tag{3.65}$$

with the initial condition $w(0) = 1$. The weights $w(j)$ are easily computed and read

$$w(j) = \prod_{k=1}^{N} \left(c_k^+(j) + c_k^-(j) \right) = \prod_{k=1}^{N} w_k(j) \ , \tag{3.66}$$

in terms of the spin weight factors

$$\begin{aligned} \begin{pmatrix} c_k^+(j) \\ c_k^-(j) \end{pmatrix} &= \left[\prod_{n=1}^{j} \begin{pmatrix} \langle\uparrow| \hat{O}_k |\uparrow\rangle & \langle\uparrow| \hat{O}_k |\downarrow\rangle \\ \langle\downarrow| \hat{O}_k |\uparrow\rangle & \langle\downarrow| \hat{O}_k |\downarrow\rangle \end{pmatrix} \right] \begin{pmatrix} 1 \\ 1 \end{pmatrix} \\ &= \begin{pmatrix} \langle\uparrow| \hat{O}_k |\uparrow\rangle & \langle\uparrow| \hat{O}_k |\downarrow\rangle \\ \langle\downarrow| \hat{O}_k |\uparrow\rangle & \langle\downarrow| \hat{O}_k |\downarrow\rangle \end{pmatrix} \begin{pmatrix} c_k^+(j-1) \\ c_k^-(j-1) \end{pmatrix} \ , \end{aligned} \tag{3.67}$$

where $|\uparrow\rangle$ and $|\downarrow\rangle$ stand for $|s = 1\rangle$ and $|s = -1\rangle$, respectively. In this way, in the proposed method each walker carries the evolution of both c^+ and c^- for every particle, instead of explicit spin variables. Notice that these factors constitute the fundamental quantities that define the secondary branching of Eq. (3.65). In this way, these factors account for the change in norm of the propagator.

We turn to the estimation of the energy within the SIDMC formalism. The DMC energy estimator in the FPA at iteration j is given by:

$$E_{\mathrm{DMC}}(j) = \sum_{\vec{S},\vec{S}'} \int d\vec{R}^{(j)} d\vec{R}' \, \langle \vec{R}', \vec{S}' | \, \hat{H}^{\mathrm{FP}} \, | \vec{R}^{(j)}, \vec{S} \rangle \, \frac{\rho_T(\vec{R}')}{\rho_T(\vec{R}^{(j)})} f(\vec{R}^{(j)}, \vec{S}, j\Delta\tau) \ , \tag{3.68}$$

with $\hat{H}^{\mathrm{FP}}$ defined in Eq. (3.53). The local energy is

$$E_L = \sum_{\vec{S}'} \int d\vec{R}' \, \langle \vec{R}', \vec{S}' | \, \hat{H}^{\mathrm{FP}} \, | \vec{R}^{(j)}, \vec{S} \rangle \, \frac{\rho_T(\vec{R}')}{\rho_T(\vec{R}^{(j)})} \ , \tag{3.69}$$

which depends on both $\vec{R}^{(j)}$ and $\vec{S}$, so that $E_L = E_L(\vec{R}^{(j)}, \vec{S})$. We can split it in two parts

$$E_L(\vec{R}^{(j)}, \vec{S}) = E_{L,0}(\vec{R}^{(j)}) + E_{L,\mathrm{S}}(\vec{R}^{(j)}, \vec{S}) \ , \tag{3.70}$$

corresponding the the spin-independent and spin-dependent contributions, respectively. The spin-independent part can be expressed in the form

$$E_{L,0}(\vec{R}^{(j)}) = \int d\vec{R}' \, \langle \vec{R}' | \, \hat{H}_0 \, | \vec{R}^{(j)} \rangle \, \frac{\rho_T(\vec{R}')}{\rho_T(\vec{R}^{(j)})} \ , \tag{3.71}$$

while

$$\begin{aligned} E_{L,S} &= \sum_{\vec{S}'} \int d\vec{R}' \, \langle \vec{R}', \vec{S}' | \, \hat{w}_{\mathrm{Re}} + \hat{V}_{\Phi} \, | \vec{R}^{(j)}, \vec{S} \rangle \, \frac{\rho_T(\vec{R}')}{\rho_T(\vec{R}^{(j)})} \\ &= \sum_{l=1}^{N} \epsilon_{L,S,l}(\vec{R}^{(j)}, s_l) \ , \end{aligned} \tag{3.72}$$

with $\epsilon_{L,S,l}$ the one-body contribution to the spin-dependent local energy corresponding to particle l (recall that $\hat{w}_{\mathrm{Re}} + \hat{V}_{\Phi}$ is a one-body operator). With all these definitions, Eq. (3.68) becomes

$$E_{\mathrm{DMC}}(j) = E_{\mathrm{DMC,0}}(j) + E_{\mathrm{DMC,S}}(j) \ . \tag{3.73}$$

The term $E_{\mathrm{DMC,0}}(j)$ contains all the spin-independent contributions, and can be written as

$$\begin{aligned} E_{\mathrm{DMC,0}}(j) &= \int d\vec{R}^{(j)} \ E_{L,0}(\vec{R}^{(j)}) \sum_{\vec{S}} f(\vec{R}^{(j)}, \vec{S}, j\Delta\tau) \\ &= \int d\vec{R}^{(j)} \ E_{L,0}(\vec{R}^{(j)}) F(\vec{R}^{(j)}, j\Delta\tau) \end{aligned} \tag{3.74}$$

with $F(\vec{R}, \tau)$ defined in Eq. (3.62). This part of the energy is evaluated as usual in DMC, so that

$$E_{\mathrm{DMC,0}}(j) = \frac{1}{N_w} \sum_{i_w=1}^{N_w} E_{L,0}^{(i_w)}(\vec{R}^{(j)}) \ , \tag{3.75}$$

where N_w is the total number of walkers in the simulation, and i_w specifies the walker index. In much the same way

$$\begin{aligned} E_{\mathrm{DMC,S}}(j) &= \sum_{l=1}^{N} \sum_{s_l=\pm 1} \int d\vec{R}^{(j)} \epsilon_{L,\mathrm{S},l}(\vec{R}^{(j)}, s_l) \\ &\times \ \tilde{F}(\vec{R}^{(j)}, s_l, j\Delta\tau) \end{aligned} \tag{3.76}$$

with

$$\tilde{F}(\vec{R}^{(j)}, s_l, j\Delta\tau) = \sum_{\vec{S}_{N-l}} f(\vec{R}^{(j)}, \vec{S}, j\Delta\tau) \Big|_{s_k=\pm 1} \tag{3.77}$$

where $\sum_{\vec{S}_{N-1}}$ sums over all particles but the k-th one. Therefore, one has to be able to sample $\tilde{F}(\vec{R}^{(j)}, s_l, j\Delta\tau)$ in order to evaluate $E_{\mathrm{DMC,S}}(j)$. This can be done by estimating $E_{\mathrm{DMC,S}}(j)$ as

$$\begin{aligned}
E_{\mathrm{DMC,S}}(j) &= \frac{1}{N_w}\Bigg(\sum_{i_w=1}^{N_w}\sum_{l=1}^{N}\frac{c^{+}_{l,i_w}(j)}{c^{+}_{l,i_w}(j)+c^{-}_{l,i_w}(j)}\epsilon^{(i_w)}_{L,\mathrm{S},l}(\vec{R}^{(j)},+1) \\
&+ \frac{c^{-}_{l,i_w}(j)}{c^{+}_{l,i_w}(j)+c^{-}_{l,i_w}(j)}\epsilon^{(i_w)}_{L,\mathrm{S},l}(\vec{R}^{(j)},-1)\Bigg) \\
&= \frac{1}{N_w}\sum_{i_w=1}^{N_w}\varepsilon^{(i_w)}_{L,\mathrm{S}}(\vec{R}^{(j)}) \ , \qquad (3.78)
\end{aligned}$$

This expression ensures that each local energy contribution $\epsilon^{(i_w)}_{L,\mathrm{S},l}(\vec{R}^{(j)},\pm 1)$ is averaged with an effective weight given by

$$\eta^{\pm}_{l}(j) = \frac{c^{\pm}_{l}(j)}{c^{+}_{l}(j)+c^{-}_{l}(j)}w(j) \ , \qquad (3.79)$$

which is the weight associated to the sampling of $\tilde{F}(\vec{R}^{(j)}, s_l = \pm 1, j\Delta\tau)$.

3.5.1.2 The SIDMC algorithm

In this section, we present a scheme of the Spin-integrated DMC algorithm. In the SIDMC method, a walker is represented by the set of quantities

$$\vec{v} = \left(\vec{r}_1,\ldots,\vec{r}_N, c^{+}_1, c^{-}_1,\ldots,c^{+}_N, c^{-}_N\right) \ . \qquad (3.80)$$

Particle positions are initialized as usual in Monte Carlo simulations, while the spin weight factors $c^{\pm}_k$ must be initialized to one

$$c^{\pm}_k = 1 \ \forall \ k \ . \qquad (3.81)$$

The first step in each iteration of the algorithm is to perform a standard GDB process using the spinless part of the Hamiltonian $\hat{H}_0$ and $\rho_T(\vec{R})$. Next, one has to update the $c^{\pm}_k$ coefficients according to the expression

$$\begin{pmatrix} c^{+}_k(j+1) \\ c^{-}_k(j+1)\end{pmatrix} = \boldsymbol{O}^{(j+1)}_k \begin{pmatrix} c^{+}_k(j) \\ c^{-}_k(j)\end{pmatrix} \ , \qquad (3.82)$$

which yields the new coefficients at iteration $j+1$ from the previous ones at iteration j. In this expression, $\boldsymbol{O}_k$ is the 2×2 matrix of Eq. (3.67). Once with these coefficients, one can obtain $w(j+1)$ according to

$$w(j+1) = \left[\prod_{k=1}^{N}\left(c^{+}_k(j+1)+c^{-}_k(j+1)\right)\right] \ , \qquad (3.83)$$

and from here, the secondary branching factor,

$$B(j+1) = \frac{w(j+1)}{w(j)} \; . \tag{3.84}$$

This weight is different for each walker, so in fact $B = B_{i_w}$ with i_w the walker index. The branching process with total replication factor $B_{\text{tot}}(j+1) = B_{\text{spinless}}(j+1)B(j+1)$ is in this way split in two parts, which are performed one after the other, for convenience.

In practice, it may happen that, along the simulation, the absolute value of the $c_k^{\pm}(j)$ coefficients keeps increasing unboundedly. However, the ratio of w's in this equation is always finite. On the other hand, it is better to use a mixed-branching strategy when dealing with the $B(j+1)$ terms, where walkers acquire a weight that is being updated at each block of iterations. The accumulated weight $\mathcal{B}_{i_w}$ at the end of the block is equal to the product of the weights at each iteration, for each walker. Once the block is finished, these weights are used to replicate the list of walkers.

In DMC simulations, the weight of the walkers is divided by a constant (equal to $e^{E_T \Delta\tau}$ with E_T the threshold energy and $\Delta\tau$ the time step) when performing the replication process [64]. One has to perform an equivalent renormalization with the secondary branching, while in this case the normalization constant can be computed in two forms. One way is to take the average over the final number of walkers of the accumulated B of the previous block. Another way is to use the B coefficients of the current block, accumulated over the previous iterations and averaged over the number of walkers. The best strategy is determined by the SOC model at hand, with the first choice being more suitable for the Raman interaction, and the latter performing better with the Weyl and Rashba models.

The energy at iteration i inside a block is estimated as:

$$E^{(i)}_{DMC} = \frac{\sum_{i_w=1}^{N_w} E^{(i)}_{i_w} \mathcal{B}_{i_w}}{\sum_{i_w=1}^{N_w} \mathcal{B}_{i_w}} \tag{3.85}$$

$$E^{(i)}_{i_w} = E^{(i_w)}_{L,0}(\vec{R}^{(i)}_{i_w}) + \varepsilon^{(i_w)}_{L,\text{S}}(\vec{R}^{(i)}_{i_w}) \; . \tag{3.86}$$

with $E^{(i_w)}_{L,0}(\vec{R}^{(i)}_{i_w})$ and $\varepsilon^{(i_w)}_{L,\text{S}}(\vec{R}^{(i)}_{i_w})$ given by

$$E^{(i_w)}_{L,0}(\vec{R}^{(i)}_{i_w}) = \int d\vec{R}' \, \langle \vec{R}' | \, \hat{H}_0 \, |\vec{R}^{(i)}_{i_w}\rangle \, \frac{\rho_T(\vec{R}')}{\rho_T(\vec{R}^{(i)}_{i_w})} \; , \tag{3.87}$$

$$\varepsilon^{(i_w)}_{L,\text{S}}(\vec{R}^{(i)}_{i_w}) = \sum_{l=1}^{N} \frac{c^+_{l,i_w}(i)}{c^+_{l,i_w}(i) + c^-_{l,i_w}(i)} \epsilon^{(i_w)}_{L,\text{S},l}(\vec{R}^{(i)}_{i_w}, +1) + \frac{c^-_{l,i_w}(i)}{c^+_{l,i_w}(i) + c^-_{l,i_w}(i)} \epsilon^{(i_w)}_{L,\text{S},l}(\vec{R}^{(i)}_{i_w}, -1) \tag{3.88}$$

$$\epsilon^{(i_w)}_{\mathrm{L,S},l}(\vec{R}^{(i)}_{i_w}, s^{i}_{l,i_w}) = \sum_{\vec{S}'} \int d\vec{R}' \, \langle \vec{R}', \vec{S}' | \, \hat{w}_{\mathrm{Re},l} + \hat{V}_{\Phi,l} \, | \vec{R}^{(i)}_{i_w}, \vec{S}^{(i)}_{i_w} \rangle \, \frac{\rho_T(\vec{R}')}{\rho_T(\vec{R}^{(i)}_{i_w})} \tag{3.89}$$

Here $\hat{w}_{\mathrm{Re},l}$ and $\hat{V}_{\Phi,l}$ are the contributions from particle l to the potentials $\hat{w}_{\mathrm{Re}}$ and $\hat{V}_{\Phi}$, defined in Eqs. (3.50) and (3.51) respectively. In Eq. (3.85), the sums run over the complete set of N_w walkers, obtained after the standard GDB process associated to the spinless part of the Hamiltonian. In this way, the expression implicitly includes the weighting of the standard branching. Eq. (3.85) represents the generalization of Eqs. (3.75) and (3.78) for the mixed-branching case.

An important remark concerning the secondary branching is that $B(j+1)$ in Eq. (3.84) is not positive definite. However, the fraction of walkers which generate a change in sign is found to be tiny in actual simulations, and thus walkers that produce this effect can be safely discarded. To quantify that, we monitor the quantity

$$\chi = \frac{N_e}{\langle N_w \rangle N_b^{\mathrm{it}}} \ , \tag{3.90}$$

with N_e and N_b^{it} the number of eliminated walkers and the number of iterations per block, and $\langle N_w \rangle$ the average number of walkers of the block. Our numerical results show that χ depends slightly on the value of the parameters chosen for the simulation, but it is always of the order of 10^{-3} or smaller.

3.5.2 Discrete spin T-moves DMC (DTDMC)

In this section we adapt the continuous spin T-moves method of Ref. [19] to a system of discrete spins under the SOC interactions analyzed in this work. In this method, the spin and position dependent wave function is propagated in imaginary time, with the matrix elements of the propagator giving the probability amplitudes of the imaginary time transitions. Due to SOC propagators being non-local, and generally non-positive definite, the definition of an effective Hamiltonian is necessary within the DTDMC formalism, so that the propagator to be implemented has non-local, positive matrix elements that can be interpreted as probabilities. Analogously to the standard DMC and SIDMC cases, a trial wave function is introduced to reduce the variance of the estimates. In the following, we assume the two-body interaction is spin-dependent, with (possibly) different contributions in each channel. In this method the walkers carry explicit spin variables together with the particle positions.

3.5.2.1 Basics of the DTDMC method

We start by presenting the derivation of the DTDMC algorithm [19] adapted to the discrete spin case. We first split the propagator in Eq. (3.52), rearranging terms as follows

$$G_{\mathrm{FP}}(\vec{R},\vec{S}\to\vec{R}',\vec{S}') = \int d\vec{R}'' \langle\vec{R}',\vec{S}'|\exp\left[-\Delta\tau\hat{w}_{\mathrm{Re}}\right]|\vec{R}'',\vec{S}\rangle \times \langle\vec{R}'',\vec{S}|\exp\left[-\Delta\tau\hat{H}_1\right]|\vec{R},\vec{S}\rangle + \mathcal{O}\Big(\Delta\tau^2\Big) \,, \tag{3.91}$$

where

$$\hat{H}_1 = \sum_{k=1}^{N}\left[\frac{P_k^2}{2m} + \hat{V}_k^{1\mathrm{b}} + |\vec{\nabla}_k\Phi_T(\vec{R},\vec{S})|^2\right] + \hat{V}^{2\mathrm{b}} \,. \tag{3.92}$$

We can introduce the importance sampling function inside this expression and write

$$\frac{\rho_T(\vec{R}',\vec{S}')}{\rho_T(\vec{R},\vec{S})}G_{\mathrm{FP}}(\vec{R},\vec{S}\to\vec{R}',\vec{S}') = \int d\vec{R}''\frac{\rho_T(\vec{R}',\vec{S}')}{\rho_T(\vec{R}'',\vec{S})}\langle\vec{R}',\vec{S}'|\exp\left[\Delta\tau\hat{w}_{\mathrm{Re}}\right]|\vec{R}'',\vec{S}\rangle \times \frac{\rho_T(\vec{R}'',\vec{S})}{\rho_T(\vec{R},\vec{S})}\langle\vec{R}'',\vec{S}|\exp\left[\Delta\tau\hat{H}_1\right]|\vec{R},\vec{S}\rangle + \mathcal{O}\Big(\Delta\tau^2\Big) \tag{3.93}$$

To order $\mathcal{O}(\Delta\tau)$, the first term inside the integral becomes

$$\frac{\rho_T(\vec{R}',\vec{S}')}{\rho_T(\vec{R}'',\vec{S})}\langle\vec{R}',\vec{S}'|\exp\left[-\Delta\tau\hat{w}_{\mathrm{Re}}\right]|\vec{R}'',\vec{S}\rangle \simeq \delta(\vec{R}'-\vec{R}'')\delta(\vec{S}'-\vec{S}) - \Delta\tau\langle\vec{R}',\vec{S}'|\hat{w}_{\mathrm{Re}}|\vec{R}'',\vec{S}\rangle\frac{\rho_T(\vec{R}',\vec{S}')}{\rho_T(\vec{R}'',\vec{S})} \tag{3.94}$$

However, for any kind of spin-orbit coupling the matrix element $\langle\vec{R}',\vec{S}'|\hat{w}_{\mathrm{Re}}|\vec{R}'',\vec{S}\rangle$ is not always negative, and thus Eq. (3.94) can not be interpreted as a probability distribution. In order to bypass this limitation and in the spirit of Refs. [19, 44, 45], we define an effective Hamiltonian that replaces the original one, and that leads to a variational upper bound to the fixed phase energy of the original Hamiltonian. We thus write

$$\hat{H}_{\mathrm{eff}}^{\mathrm{FP}} = \hat{H}_1 + \hat{w}_{\mathrm{Re,A}}^{\mathrm{eff}} + \hat{w}_{\mathrm{Re,B}}^{\mathrm{eff}} \,, \tag{3.95}$$

where the sum $\hat{w}_{\mathrm{Re,A}}^{\mathrm{eff}} + \hat{w}_{\mathrm{Re,B}}^{\mathrm{eff}}$ is an approximation to the original $\hat{w}_{\mathrm{Re}}$ of Eq. (3.50). This approximation is built such that the local energy of $\hat{H}_{\mathrm{eff}}^{\mathrm{FP}}$ and $\hat{H}^{\mathrm{FP}}$ are equal when they act on the modulus of the trial wave function. The matrix elements of these terms are given by

$$\langle\vec{R},\vec{S}|\hat{w}_{\mathrm{Re,A}}^{\mathrm{eff}}|\vec{R},\vec{S}\rangle = 0 \tag{3.96}$$

$$\langle\vec{R}',\vec{S}'|\hat{w}_{\mathrm{Re,A}}^{\mathrm{eff}}|\vec{R},\vec{S}\rangle = \begin{cases}\langle\vec{R}',\vec{S}'|\hat{w}_{\mathrm{Re}}|\vec{R},\vec{S}\rangle & \text{if } T<0\\ 0 & \text{if } T>0\end{cases}$$

with the transition coefficients

$$T = \langle \vec{R}', \vec{S}'| \, \hat{w}_{\text{Re}} \, |\vec{R}, \vec{S}\rangle \, \frac{\rho_T(\vec{R}', \vec{S}')}{\rho_T(\vec{R}, \vec{S})} \ , \tag{3.97}$$

while

$$\begin{aligned} \langle \vec{R}, \vec{S}| \, \hat{w}^{\text{eff}}_{\text{Re,B}} \, |\vec{R}, \vec{S}\rangle &= \sum_{\vec{s}} \int d\vec{X} \, \langle \vec{R}, \vec{S}| \, \hat{w}_{\text{Re}} \, |\vec{X}, \vec{s}\rangle \, \frac{\rho_T(\vec{X}, \vec{s})}{\rho_T(\vec{R}, \vec{S})} \\ \langle \vec{R}', \vec{S}'| \, \hat{w}^{\text{eff}}_{\text{Re,B}} \, |\vec{R}, \vec{S}\rangle &= 0 \end{aligned} \tag{3.98}$$

where in the last expression, the summation and the integration are restricted to those values such that $T > 0$. Using these definitions we avoid non-local matrix elements in the propagator producing negative transition probabilities at $\mathcal{O}(\Delta\tau)$. Notice also that the effective Hamiltonian depends on the modulus of the trial wave function, which means that the energy obtained also depends on its choice. The fixed-phase propagator for the effective Hamiltonian, with importance sampling, is thus:

$$\begin{aligned} \frac{\rho_T(\vec{R}', \vec{S}')}{\rho_T(\vec{R}, \vec{S})} G^{\text{eff}}_{\text{FP}}(\vec{R}, \vec{S} \to \vec{R}', \vec{S}') &= \int d\vec{R}'' \frac{\rho_T(\vec{R}', \vec{S}')}{\rho_T(\vec{R}'', \vec{S})} \langle \vec{R}', \vec{S}'| \exp\Big[- \Delta\tau \hat{w}^{\text{eff}}_{\text{Re,A}} \Big] |\vec{R}'', \vec{S}\rangle \\ \times \frac{\rho_T(\vec{R}'', \vec{S})}{\rho_T(\vec{R}, \vec{S})} \langle \vec{R}'', \vec{S}| \exp\Big[- \Delta\tau (\hat{H}_1 + \hat{w}^{\text{eff}}_{\text{Re,B}}) \Big] |\vec{R}, \vec{S}\rangle &+ \mathcal{O}\Big(\Delta\tau^2\Big) \ . \end{aligned} \tag{3.99}$$

This propagator is positive-definite, and thus we can interpret it as a probability distribution and sample from it. This can be implemented performing initially a Gauss-Drift-Branching process of the $\exp\Big[-\Delta\tau(\hat{H}_1 + \hat{w}^{\text{eff}}_{\text{Re,B}})\Big]$ part, with a branching factor that, according to Ref. [44], reads

$$B(\vec{R}, \vec{R}'', \vec{S}) = \exp\left[-\frac{\Delta\tau}{2} \Big[E_L(\vec{R}, \vec{S}) + E_L(\vec{R}'', \vec{S}) \Big] \right] \ , \tag{3.100}$$

with

$$E_L(\vec{R}, \vec{S}) = \sum_{\vec{S}'} \int d\vec{R}' \, \langle \vec{R}', \vec{S}'| \, \hat{H}^{\text{FP}}_{\text{eff}} \, |\vec{R}, \vec{S}\rangle \, \frac{\rho_T(\vec{R}', \vec{S}')}{\rho_T(\vec{R}, \vec{S})} \ , \tag{3.101}$$

to obtain the displacement $\vec{R} \to \vec{R}''$. In a second step, one performs a transition to a new position and spin coordinates, $(\vec{R}'', \vec{S}) \to (\vec{R}', \vec{S}')$, given by the probability

$$p(\vec{R}'', \vec{S} \to \vec{R}'\vec{S}') = \frac{P(\vec{R}'', \vec{S} \to \vec{R}'\vec{S}')}{\sum_{\vec{S}'} \int d\vec{R}' P(\vec{R}'', \vec{S} \to \vec{R}'\vec{S}')} \ , \tag{3.102}$$

where

$$P(\vec{R}'', \vec{S} \to \vec{R}'\vec{S}') = \delta(\vec{R}' - \vec{R}'')\delta(\vec{S}' - \vec{S}) - \Delta\tau \langle \vec{R}', \vec{S}'| \, \hat{w}^{\text{eff}}_{\text{Re,A}} \, |\vec{R}'', \vec{S}\rangle \frac{\rho_T(\vec{R}', \vec{S}')}{\rho_T(\vec{R}'', \vec{S})} \, . \tag{3.103}$$

Despite the sum in Eq. (3.102) involves the 2^N spin configurations, which sounds prohibitive for large N, it must be kept in mind that only one-body operators are involved so that the expression is greatly simplified. The two-body spin-dependent interaction is treated like any other local operator in DMC, and its contribution to the local energy is

$$\begin{aligned} V_{\text{L,2b}}(\vec{R}, \vec{S}) &= \sum_{\vec{S}'} \int d\vec{R}' \langle \vec{R}', \vec{S}'| \, \hat{V}_{\text{2b}} \, |\vec{R}, \vec{S}\rangle \frac{\rho_T(\vec{R}', \vec{S}')}{\rho_T(\vec{R}, \vec{S})} \\ &= \sum_{k<l} V^{\text{2b}}_{s_k, s_l}(r_{kl}) \ , \end{aligned} \tag{3.104}$$

where use has been made of the fact that the operator is local, meaning that it is proportional to $\delta(\vec{S}' - \vec{S})\delta(\vec{R} - \vec{R}')$. The two-body, spin-dependent potential is defined in Eqs. (3.5) and (3.6).

Finally, in order to estimate the energy, one computes:

$$\begin{aligned} E &= \frac{\sum_{\vec{S}} \int d\vec{R} \left[\sum_{\vec{S}'} \int d\vec{R}' \frac{\rho_T(\vec{R}', \vec{S}') \left\langle \vec{R}', \vec{S}' \middle| \hat{H}^{\text{FP}}_{\text{eff}} \middle| \vec{R}, \vec{S} \right\rangle}{\rho_T(\vec{R}, \vec{S})} \right] \rho_T(\vec{R}, \vec{S}) \rho(\vec{R}, \vec{S})}{\sum_{\vec{S}} \int d\vec{R} \ \rho_T(\vec{R}, \vec{S}) \rho(\vec{R}, \vec{S})} \\ &= \frac{\sum_{\vec{S}} \int d\vec{R} \ E_L(\vec{R}, \vec{S}) \rho_T(\vec{R}, \vec{S}) \rho(\vec{R}, \vec{S})}{\sum_{\vec{S}} \int d\vec{R} \ \rho_T(\vec{R}, \vec{S}) \rho(\vec{R}, \vec{S})} \end{aligned} \tag{3.105}$$

using the unbiased estimator of the mean, analogously to the previous Section. It must be remarked that the additional integral involved in the computation of the local energy due to the non-local character of the SOC potential can be computed analytically. As mentioned previously, this quantity corresponds to an upper bound to the fixed phase energy [19]

3.5.2.2 Application to synthetic SOC in ultracold gases

In this section we show how to apply the previous method to the SOC interactions of interest in the field of ultracold gases. We focus on the Weyl SOC, since it features the most general type of non-locality: momentum terms, which are non-local in position space, coupled to non-local spin terms. Nevertheless, the procedure we detail is analogous for the Rashba and Raman potentials. We start evaluating the matrix elements of $\hat{w}_{\rm Re}$, which are given by

$$\begin{aligned}\langle \vec{R}', \vec{S}' | \, \hat{w}_{\rm Re} \, | \vec{R}, \vec{S} \rangle = \frac{\lambda\hbar}{m} \sum_{k=1}^{N} & \left[\prod_{l\neq k} \delta(\vec{r}_l' - \vec{r}_l)\delta(s_l' - s_l) \right] \\ \times & \Bigg[\delta(y_k' - y_k)\delta(z_k' - z_k)\frac{d}{dx_k'}\delta(x_k' - x_k) \\ \times & \ \langle s_k' | \, \hat{\sigma}_{x,k} \, | s_k \rangle \sin\Big[-\phi_k(x_k', y_k, z_k, s_k') + \phi_k(\vec{r}_k, s_k) \Big] \\ + & \, \delta(x_k' - x_k)\delta(z_k' - z_k)\frac{d}{dy_k'}\delta(y_k' - y_k) \\ \times & \ \langle s_k' | - i\hat{\sigma}_{y,k} \, | s_k \rangle \cos\Big[-\phi_k(x_k, y_k', z_k, s_k') + \phi_k(\vec{r}_k, s_k) \Big] \\ + & \, \delta(x_k' - x_k)\delta(y_k' - y_k)\frac{d}{dz_k'}\delta(z_k' - z_k) \\ \times & \ \langle s_k' | \, \hat{\sigma}_{z,k} \, | s_k \rangle \sin\Big[-\phi_k(x_k, y_k, z_k', s_k') + \phi_k(\vec{r}_k, s_k) \Big] \Bigg] \end{aligned} \tag{3.106}$$

with ϕ_k the single-particle phase of Eq. (3.54). In this expression we have omitted the last term of Eq. (3.4) as it is a constant contribution that represents a shift of the total energy only. In order to construct the effective Hamiltonian, we must evaluate the matrix elements of $\hat{w}_{\rm Re}$ to check their sign. However, given two set of coordinates $\vec{r}_k$, $\vec{r}_k'$, terms of the form $\frac{\rm d}{{\rm d}x_k'}\left(\delta(x_k' - x_k)\right)$ are in general difficult to handle. In order to preserve the upper bound property of the effective Hamiltonian, we adopt the crude prescription

$$\frac{\rm d}{{\rm d}\xi_k'}\Big(\delta(\xi_k' - \xi_k)\Big) \sim \frac{1}{2\epsilon}\Big[\delta(\xi_k' + \epsilon - \xi_k) - \delta(\xi_k' - \epsilon - \xi_k)\Big] \tag{3.107}$$

with ϵ a small parameter. To order ϵ, this is equivalent to replacing the momentum operator with

$$\hat{p} \sim \frac{\hbar}{2i\epsilon}\left[\exp\left(i\frac{\hat{p}}{\hbar}\epsilon\right) - \exp\left(-i\frac{\hat{p}}{\hbar}\epsilon\right)\right] \ . \tag{3.108}$$

Notice that, in this form, the resulting operator is still hermitian, and for $\epsilon \to 0$, the energy is preserved. With this substitution, $\hat{w}_{\rm Re}$ is replaced by a new operator $\hat{w}_{{\rm Re},\epsilon}$, whose matrix elements are the same as in Eq. (3.106) with the derivatives of the deltas replaced as in Eq. (3.107). We can then construct the potential $\hat{w}^{\rm eff}_{{\rm Re},\epsilon,{\rm A}}$ using Eqs. (3.96).

Notice that, by introducing the prescription in Eq. (3.107), the SOC part of the propagator is accurate up to order $\mathcal{O}\Big(\frac{N\Delta\tau}{2\epsilon}\Big)$. This implies that the value of ϵ must be chosen so that

$$\begin{aligned}
1 &\gg \left| \Delta\tau \sum_{\vec{S}'} \int d\vec{R}' \, \langle \vec{R}', \vec{S}' | \, \hat{w}^{\text{eff}}_{\text{Re},\epsilon,\text{A}} \, | \vec{R}'', \vec{S} \rangle \, \frac{\rho_T(\vec{R}', \vec{S}')}{\rho_T(\vec{R}'', \vec{S})} \right| \\
1 &\gg \left| \Delta\tau \sum_{\vec{S}'} \int d\vec{R}' \, \langle \vec{R}', \vec{S}' | \, \hat{w}^{\text{eff}}_{\text{Re},\epsilon,\text{B}} \, | \vec{R}'', \vec{S} \rangle \, \frac{\rho_T(\vec{R}', \vec{S}')}{\rho_T(\vec{R}'', \vec{S})} \right| \\
&= \left| \Delta\tau \, \langle \vec{R}'', \vec{S} | \, \hat{w}^{\text{eff}}_{\text{Re},\epsilon,\text{B}} \, | \vec{R}'', \vec{S} \rangle \right| \, ,
\end{aligned} \tag{3.109}$$

with

$$\begin{aligned}
&\langle \vec{R}, \vec{S} | \, \hat{w}^{\text{eff}}_{\text{Re},\epsilon,\text{B}} \, | \vec{R}, \vec{S} \rangle = \sum_{\vec{s}} \int d\vec{X} \, \langle \vec{R}, \vec{S} | \, \hat{w}_{\text{Re},\epsilon} \, | \vec{X}, \vec{s} \rangle \, \frac{\rho_T(\vec{X}, \vec{s})}{\rho_T(\vec{R}, \vec{S})} \\
&\langle \vec{R}', \vec{S}' | \, \hat{w}^{\text{eff}}_{\text{Re},\epsilon,\text{B}} \, | \vec{R}, \vec{S} \rangle = 0 \, ,
\end{aligned} \tag{3.110}$$

where, in the last expression, the summation and the integration are restricted to values satisfying the condition $T > 0$, given in Eq. (3.97). We have seen in actual simulations that these condition can be somewhat relaxed. In any case, the precise value of ϵ chosen for the simulations should not affect the energy contribution from the SOC part of the Hamiltonian, i.e.

$$\begin{aligned}
&\sum_{\vec{S}'} \int d\vec{R}' \, \langle \vec{R}', \vec{S}' | \, \hat{w}^{\text{eff}}_{\text{Re},\epsilon,\text{A}} + \hat{w}^{\text{eff}}_{\text{Re},\epsilon,\text{B}} \, | \vec{R}, \vec{S} \rangle \, \frac{\rho_T(\vec{R}', \vec{S}')}{\rho_T(\vec{R}, \vec{S})} \simeq \\
&\sum_{\vec{S}'} \int d\vec{R}' \, \langle \vec{R}', \vec{S}' | \, \hat{w}_{\text{Re}} \, | \vec{R}, \vec{S} \rangle \, \frac{\rho_T(\vec{R}', \vec{S}')}{\rho_T(\vec{R}, \vec{S})} \, .
\end{aligned} \tag{3.111}$$

3.5.2.3 The DTDMC algorithm

In this Section we present a scheme of the DTDMC algorithm to better understand how to implement it in practice. A walker at the j-th iteration is denoted as

$$\vec{v}(j) = \left(\vec{r}^{\,(j)}_1, s^{(j)}_1, \ldots, \vec{r}^{\,(j)}_N, s^{(j)}_N \right) \, , \tag{3.112}$$

with $s_k = \pm 1$ the z-component of the spin of particle k and subindexes and superindexes standing for particles and iterations, respectively. The initial values of the position and spin coordinates are generally obtained sampling the trial wave function using the Metropolis algorithm.

The first step to be implemented at each iteration is a Gauss-Drift-Branching process with the branching factor given in Eq. (3.100), which produces a spatial translation $\vec{R}^{(j)} \to \vec{R}^{(j)}_A$. After that, one has to sample the part of the propagator which depends on the effective potential $\hat{w}_{\text{Re},\epsilon,\text{A}}$. In this second step, a transition

$(\vec{R}_A^{(j)}, \vec{S}^{(j)}) \rightarrow (\vec{R}^{(j+1)}, \vec{S}^{(j+1)})$ is performed with probability given by

$$p(\vec{R},\vec{S} \rightarrow \vec{R}'\vec{S}') = \frac{P(\vec{R},\vec{S} \rightarrow \vec{R}'\vec{S}')}{\sum_{\vec{S}'} \int d\vec{R}' P(\vec{R},\vec{S} \rightarrow \vec{R}'\vec{S}')} \tag{3.113}$$

$$\begin{aligned} P(\vec{R},\vec{S} \rightarrow \vec{R}'\vec{S}') &= \delta(\vec{R}'-\vec{R})\delta(\vec{S}'-\vec{S}) \\ &- \Delta\tau \, \langle \vec{R}', \vec{S}' | \, \hat{w}^{\text{eff}}_{\text{Re},\epsilon,\text{A}} \, | \vec{R}, \vec{S} \rangle \, \frac{\rho_T(\vec{R}',\vec{S}')}{\rho_T(\vec{R},\vec{S})} \end{aligned} \tag{3.114}$$

where one can identify $\vec{R} = \vec{R}_A^{(j)}$, $\vec{S} = \vec{S}^{(j)}$, $\vec{R}' = \vec{R}^{(j+1)}$ and $\vec{S}' = \vec{S}^{(j+1)}$. As an example, we explicitly report how this evolution is carried out for the Weyl SOC case. The transition probability is:

$$\begin{aligned} &P(\vec{R},\vec{S} \rightarrow \vec{R}',\vec{S}') = \delta(\vec{R}'-\vec{R})\delta(\vec{S}'-\vec{S}) \\ &- \Delta\tau \left\{ \sum_{k=1}^{N} \left[\prod_{l \neq k} \delta(\vec{r}_l\,' - \vec{r}_l)\delta(s_l' - s_l) \right] \right. \\ &\times \frac{\lambda\hbar}{m} \left[\delta(y_k' - y_k)\delta(z_k' - z_k)\frac{1}{2\epsilon}\delta(x_k' + \epsilon - x_k) \right. \\ &\times \langle s_k' | \, \hat{\sigma}_{x,k} \, | s_k \rangle \sin\Big[-\phi_k(x_k', y_k, z_k, s_k') + \phi_k(\vec{r}_k, s_k) \Big] \\ &- \delta(x_k' - x_k)\delta(z_k' - z_k)\frac{1}{2\epsilon}\delta(y_k' - \epsilon - y_k) \\ &\times \langle s_k' | - i\hat{\sigma}_{y,k} \, | s_k \rangle \cos\Big[-\phi_k(x_k, y_k', z_k, s_k') + \phi_k(\vec{r}_k, s_k) \Big] \\ &+ \delta(x_k' - x_k)\delta(y_k' - y_k)\frac{1}{2\epsilon}\Big(\delta(z_k' + \epsilon - z_k) - \delta(z_k' - \epsilon - z_k) \Big) \\ &\left. \left. \times \langle s_k' | \, \hat{\sigma}_{z,k} \, | s_k \rangle \sin\Big[-\phi_k(x_k, y_k, z_k', s_k') + \phi_k(\vec{r}_k, s_k) \Big] \right] \right\} \\ &\times \frac{\rho_T(\vec{R}',\vec{S}')}{\rho_T(\vec{R},\vec{S})} \end{aligned} \tag{3.115}$$

Notice that the terms appearing in $P(\vec{R},\vec{S} \rightarrow \vec{R}',\vec{S}')$ are different for each walker and each iteration. In general, one has to keep here only those terms of Eq. (3.106) (after the substitution of Eqs. (3.107) and (3.108)) that are strictly negative. This total transition probability is the sum of different transition probabilities $P_{t,k}^{(m)}$, so it can be written as

$$\begin{aligned}
&P(\vec{R},\vec{S}\to\vec{R}',\vec{S}') = P^{(0)}_{t,k}(\vec{R},\vec{S}\to\vec{R}\vec{S})\delta(\vec{R}'-\vec{R})\delta(\vec{S}'-\vec{S})\\
&+\sum_{k=1}^{N}\left[\prod_{l\neq k}\delta(\vec{r}_l'-\vec{r}_l)\delta(s_l'-s_l)\right]\Big\{\delta(y_k'-y_k)\delta(z_k'-z_k)\\
&\times\delta(x_k'+\epsilon-x_k)P^{(1)}_{t,k}(x_k,s_k\to x_k-\epsilon,-s_k)\\
&+\delta(x_k'-x_k)\delta(z_k'-z_k)\delta(y_k'-\epsilon-y_k)P^{(2)}_{t,k}(y_k,s_k\to y_k+\epsilon,-s_k)\\
&+\delta(x_k'-x_k)\delta(y_k'-y_k)\Big(\delta(z_k'+\epsilon-z_k)P^{(3)}_{t,k}(z_k,s_k\to z_k-\epsilon,s_k)\\
&+\delta(z_k'-\epsilon-z_k)P^{(4)}_{t,k}(z_k,s_k\to z_k+\epsilon,s_k)\Big)\Big\}
\end{aligned} \tag{3.116}$$

The probabilities $P^{(m)}_{t,k}$ depend on the coordinates of all particles, but, for the sake of simplicity, we only explicit the dependence on the coordinates that change under each transition. Notice that in this example there are $4N+1$ possible transitions. We define the cumulative distribution vector as

$$v_c(i_c) = \frac{\sum_{i=1}^{i_c} v_2(i)}{\sum_{i=1}^{4N+1} v_2(i)}\ ,\ i_c = 1,...,4N+1 \qquad v_c(0)=0 \tag{3.117}$$

with

$$v_2 = (1, P^{(1)}_{t,1}, P^{(2)}_{t,1}, P^{(3)}_{t,1}, P^{(4)}_{t,1}, ..., P^{(1)}_{t,N}, P^{(2)}_{t,N}, P^{(3)}_{t,N}, P^{(4)}_{t,N})\ . \tag{3.118}$$

Notice that $v_c(i_c)\in(0,1]\ \forall\ i_c$. Sampling this discrete probability distribution function can be done following the standard procedure: we generate a random number $\xi\in[0,1]$ and select the component of $v_c(i_{\text{trans}})$ that verifies

$$\begin{aligned}
&v_c(i_{\text{trans}}-1)<\xi\\
&v_c(i_{\text{trans}})>\xi\ .
\end{aligned} \tag{3.119}$$

Finally, one performs the transition associated to the quantity $v_2(i_{\text{trans}}) = v_c(i_{\text{trans}}) - v_c(i_{\text{trans}}-1)$, i.e., if $v_2(i_{\text{trans}}) = P^{(2)}_{t,k}$, the spin of particle k flips and its coordinates are modified according to $x_k' = x_k$, $y_k' = y_k+\epsilon$, $z_k' = z_k$, while the rest of the system is left unchanged.

3.5.3 Numerical results

We report in this Section results for the energy of different systems with SOC using both the SIDMC and the DTDMC methods. In Sec. 3.5.3.1 we evaluate the energy of a few one-body and two-body problems, while in Sec. 3.5.3.2 we report results for the energy of some many-body systems, both in the mean field regime and out of it. As a sanity check for the two SOC DMC algorithms for SOC systems, we compare the DMC energies with those obtained from the imaginary-time evolution of the Schrödinger equation (one and two-body cases) and the Gross-Pitaevskii equation (many-body in the dilute regime). We also comment on the technical issues mentioned in Secs. 3.5.1.2 and 3.5.2.3, mainly the removal of walkers in SIDMC and the influence of the parameter ϵ in the DTDMC method, as well as the dependence of the energy estimation on the time step. In all cases, the parameters of the Hamiltonian and the trial wave function are reported in reduced units (see Sec. 3.2.1).

3.5.3.1 One and two-body problems

We first show DMC results for the energy corresponding to four different physical systems involving one- and two-body problems: a three-dimensional (3D) one-body system with Weyl SOC, a 3D one-body system with Raman SOC, and two interacting two-dimensional (2D) two-body systems with Rashba SOC, one containing spin-independent two-body interactions, and another with spin-dependent ones. All systems are harmonically confined. We summarize our results in Table 3.1, which includes the DMC energies obtained with both algorithms together with the imaginary time evolution (ITE) estimates, both for the fixed-phase Hamiltonian (Eq. (3.53)) and the fixed-phase, effective Hamiltonian of the DTDMC approach. All SIDMC energies are obtained by performing several simulations, changing the parameter $\Delta\tau$, and then extrapolating the energy to the limit $\Delta\tau \to 0$. This is necessary because the propagator employed in DMC calculations is not exact at all orders of $\Delta\tau$, but only up to $\mathcal{O}(\Delta\tau)$. As a consequence, there is a dependence of the estimates on the time step employed in the simulations. Therefore, to get rid of such dependence, an extrapolation to zero time step is performed. In the Weyl and Rashba cases with DTDMC, it is necessary to perform extrapolations not only in the time step but also in ϵ, since the propagator is only exact in the limit $\Delta\tau \to 0$, $\epsilon \to 0$. Thus, one must carry out several calculations changing $\Delta\tau$ and ϵ and then extrapolate to the limits $\Delta\tau \to 0$, $\epsilon \to 0$, and $\frac{\Delta\tau}{\epsilon} \to 0$. We discuss below how to perform the triple limit involving $\Delta\tau$, ϵ, and $\frac{\Delta\tau}{\epsilon}$. This setup is not necessary in the Raman calculations since the SOC part of the propagator scales as $\mathcal{O}(N\Delta\tau)$ if ϵ is sufficiently small. This is because Raman SOC couples momentum with an operator local in spin space, $\hat{\sigma}_z$, when expressing the Hamiltonian in the basis of eigenstates of $\hat{\sigma}_z$. On the other hand, Rashba and Weyl SOC include couplings involving $\hat{\sigma}_x$ and $\hat{\sigma}_y$ (in the case of Rashba SOC) and all $\hat{\sigma}_x$, $\hat{\sigma}_y$ and $\hat{\sigma}_z$ (in the case of Weyl SOC).

The trial wave function for each Hamiltonian is important because it fixes the phase and, in all cases, reduces the variance via importance sampling. For the Raman

SOC problem with DTDMC, the trial wave function that we have used is

$$\Psi_T(\vec{r},s) = \rho_T(\vec{r},s)\exp\left[i\phi_T(\vec{r},s)\right] \tag{3.120}$$

$$\rho_T(\vec{r},s=+1) = \Big[C_1^2\sin^2\mu + C_2^2\cos^2\mu + 2\sin\mu\cos\mu C_1C_2\cos(2kx)\Big]^{1/2}\exp\left[-\frac{\omega}{2}\left(x^2+y^2+z^2\right)\right] \tag{3.121}$$

$$\rho_T(\vec{r},s=-1) = \Big[C_2^2\sin^2\mu + C_1^2\cos^2\mu + 2\sin\mu\cos\mu C_1C_2\cos(2kx)\Big]^{1/2}\exp\left[-\frac{\omega}{2}\left(x^2+y^2+z^2\right)\right] \tag{3.122}$$

$$\phi_T(\vec{r},s=+1) = \operatorname{atan}\left[\frac{(C_1\sin\mu - C_2\cos\mu)\sin(kx)}{(C_1\sin\mu + C_2\cos\mu)\cos(kx)}\right] \tag{3.123}$$

$$\phi_T(\vec{r},s=-1) = \operatorname{atan}\left[\frac{(C_1\cos\mu - C_2\sin\mu)\sin(kx)}{(C_1\cos\mu + C_2\sin\mu)\cos(kx)}\right] \tag{3.124}$$

with $\mu = \frac{1}{2}\operatorname{acos}\left(\frac{k}{\eta_{\mathrm{Rm}}}\right)$, k the reduced momentum and ω the harmonic oscillator strength. In these expressions, $\{k, C_1, C_2\}$ are taken as variational parameters. The SOC term of the trial wave function has the same form as the one used in Ref. [25], which consists on a superposition of two plane waves of opposed momenta. This SOC term represents an excellent approximation to the mean field ground state of the system. A Gaussian factor is incorporated to account for the presence of an harmonic trap. Since the modulus of the trial wave function must be independent of the spin in the SIDMC method, we have used

$$\rho_T(\vec{r}) = \Big[C_1^2 + C_2^2 + 2B_cC_1C_2\cos(2kx)\Big]^{1/2}\exp\left[-\frac{\omega}{2}\left(x^2+y^2+z^2\right)\right] \tag{3.125}$$

with B_c another variational parameter.

Concerning the Weyl model, the adopted trial wave function for DTDMC is

$$\rho_T(\vec{r},s=+1) = \exp\left[-\frac{\omega}{2}\left(x^2+y^2+z^2\right)\right] \tag{3.126}$$

$$\rho_T(\vec{r},s=-1) = \frac{(1+\cos\theta_k)}{\sin\theta_k}\exp\left[-\frac{\omega}{2}\left(x^2+y^2+z^2\right)\right] \tag{3.127}$$

$$\phi_T(\vec{r},s=+1) = \vec{k}\vec{r} \tag{3.128}$$

$$\phi_T(\vec{r},s=-1) = \vec{k}\vec{r} + \pi + \phi_k \tag{3.129}$$

where θ_k and ϕ_k are the polar and azimuthal angles of the momentum vector $\vec{k}$, respectively. This corresponds to a product of the ground state of the one-body Weyl SOC Hamiltonian times the harmonic oscillator ground state wave function. The adopted modulus of the trial wave function for the SIDMC case is

$$\rho_T(\vec{r}) = \exp\left[-\frac{\omega}{2}\left(x^2+y^2+z^2\right)\right] \tag{3.130}$$

Finally, the trial wave function used in the DTDMC two-body Rashba simulations is

$$\Psi_T(\vec{R},\vec{S}) = \left[\prod_{j=1}^{2} \rho_{T,1\mathrm{b}}(\vec{r}_j, s_j)\right] \rho_{T,2\mathrm{b}}(\vec{r}_1,\vec{r}_2) \exp\left[i \sum_{j=1}^{2} \phi_T(\vec{r}_j, s_j)\right] \tag{3.131}$$

$$\rho_{T,1\mathrm{b}}(\vec{r}, s=+1) = \exp\left[-\frac{\omega}{2}\left(x^2+y^2\right)\right] \tag{3.132}$$

$$\rho_{T,1\mathrm{b}}(\vec{r}, s=-1) = \exp\left[-\frac{\omega}{2}\left(x^2+y^2\right)\right] \tag{3.133}$$

$$\phi_T(\vec{r}, s=+1) = \vec{k}\vec{r} - \phi_k - \frac{\pi}{2} \tag{3.134}$$

$$\phi_T(\vec{r}, s=-1) = \vec{k}\vec{r} \tag{3.135}$$

with ϕ_k the angle of the momentum vector in polar coordinates. Again, the one-body terms in the trial wave function correspond to a product of the ground state of the one-body Rashba SOC Hamiltonian times the harmonic oscillator ground state wave function. In this expression, $\rho_{T,2\mathrm{b}}(\vec{r}_1,\vec{r}_2)$ is the exact solution of the two-body problem at low momentum ($k_{2\mathrm{b}} \sim 10^{-2}$) (without SOC) corresponding to the soft-sphere potential of Eq. (3.6), with parameters

$$\overline{V}_0 = \frac{V_0(1,1)+V_0(1,-1)+V_0(-1,1)+V_0(-1,-1)}{4} \tag{3.136}$$

$$\overline{R}_0 = \frac{R_0(1,1)+R_0(1,-1)+R_0(-1,1)+R_0(-1,-1)}{4}\ . \tag{3.137}$$

This choice makes the two-body trial wave function spin-independent for simplicity. We use the same function for the SIDMC simulations.

In DTDMC simulations, the time step is $\Delta\tau \sim \mathcal{O}\left(10^{-3}\right)$, while it is $\Delta\tau \sim \mathcal{O}\left(10^{-2}\right)$ in the SIDMC ones. The average number of walkers is kept stable along the simulations, and it is fixed to a value between 2000 and 3000, depending on the case. The parameter ϵ of DTDMC is fixed to $\epsilon = 100\Delta\tau$ in the Raman calculation, and to $\epsilon = 200\Delta\tau$ in the Rashba and Weyl cases. In the Weyl SIDMC calculations, the secondary branching weights $w(j)$ are accumulated in blocks of $N_b^{\mathrm{it}} = 10$ iterations. The ratio of discarded walkers is found to be $\chi < 0.001$. In the Rashba cases, we have $N_b^{\mathrm{it}} = 50$ and $\chi < 0.002$. Finally, for the Raman problem we have $N_b^{\mathrm{it}} = 10$ and $\chi = 0$ (see Sec. 3.5.1.2).

The parameters used in the Raman simulations are $\eta_{\mathrm{Rm}} = 1$, $\omega = 0.4$, $\Omega = 0.5$, $k = 0.7$, $C_1 = 0.6$, $C_2 = 0.8$, and $B_c = 0.5$. For the Weyl simulations we considered $\eta_{\mathrm{We}} = 1$, $\omega = 0.4$, $k = 0.5$, $\theta_k = \frac{\pi}{4}$, and $\phi_k = 0.3$. Finally, the parameters for the two-body Rashba simulations in the two-body spin-independent case are $V_0 = 1.5$, $R_0 = 3.5$, $k = 0.5$, $\phi_k = 0.1$, and $\omega = 0.4$. The two-body spin-dependent Rashba case shares the same values, except for $V_0(+1,+1) = V_0(-1,-1) = 2.5$ and $V_0(+1,-1) = V_0(-1,+1) = 1.5$.

We show in Fig. 3.1 the energy as a function of the imaginary-time step for the two-body Rashba calculations. We can clearly see the linear dependence of the energy

	SIDMC	ITE FPA	DTDMC	DTDMC fixed ϵ	ITE FPA eff. H
Raman	1.368 ± 0.001	1.3667 ± 0.0005	1.368 ± 0.001		1.3679 ± 0.0005
Weyl	1.095 ± 0.002	1.0780 ± 0.0005	1.197 ± 0.002	1.190 ± 0.002	1.1887 ± 0.0005
Rashba 2-b NS	1.064 ± 0.002	1.058 ± 0.003	1.148 ± 0.003	1.132 ± 0.002	1.133 ± 0.003
Rashba 2-b S			1.279 ± 0.002	1.262 ± 0.002	1.258 ± 0.003

Table 3.1 Estimation of the energy (in reduced units, see Sec. 3.2.1) for the few-body systems described in Sec. 3.5.3.1. Results for the Raman and Weyl cases correspond to the total energy while results for the Rashba case correspond to the energy per particle. "2b-S" stands for spin-dependent two-body interaction while "2b-NS" stands for spin-independent two-body interaction.

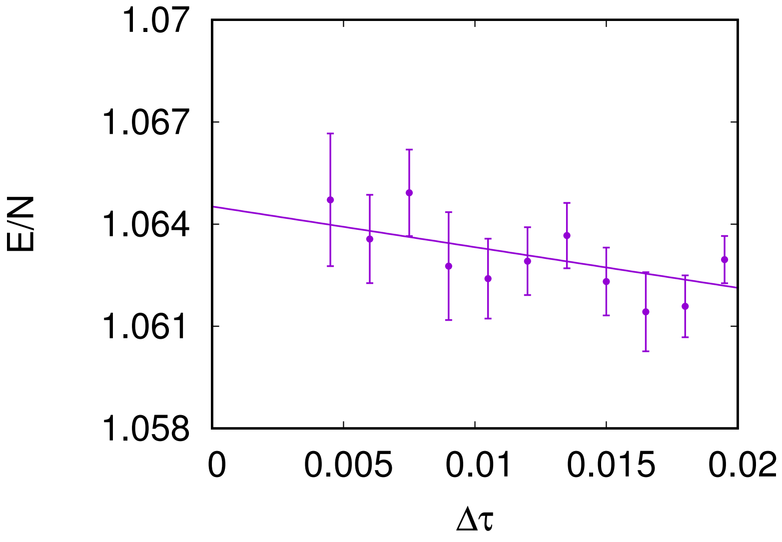

Fig. 3.1 Dependence of the DMC energy per particle on the imaginary-time step using the SIDMC method for a two-body system with Rashba SOC and harmonic confinement. The line corresponds to the linear extrapolation of the DMC energies. Quantities are dimensionless, with the energy and length scales defined in Eq. (3.8).

on the time step, as it corresponds to a linear approximation to the exact propagator. In the DTDMC method, and as stated previously, three limits have to be simultaneously satisfied in order to obtain the energy: $\Delta\tau \to 0$, $\epsilon \to 0$, and $\frac{\Delta\tau}{\epsilon} \to 0$. The extrapolation according to these limits can be performed in several ways. Here, we discuss two of them. Method 1 consists in performing N_{sets} sets of N_{sim} simulations setting $\Delta\tau \to 0$, $\epsilon \to 0$, with $\frac{\Delta\tau}{\epsilon} \ll 1$ fixed. After this, one ends up with N_{sets} estimations of the energy, each one associated to a given $\frac{\Delta\tau}{\epsilon}$ value. In general, if the value of $\frac{\Delta\tau}{\epsilon}$ is small enough, there is no need to perform an extrapolation $\frac{\Delta\tau}{\epsilon} \to 0$ and one can just retain the estimation associated to the lowest $\frac{\Delta\tau}{\epsilon}$ value. In Method 2 one also performs N_{sets} sets of N_{sim} simulations with $\Delta\tau \to 0$, $\frac{\Delta\tau}{\epsilon} \to 0$, and fixed ϵ. After this, one ends up with N_{sets} estimations of the energy, each one associated to a small but finite ϵ. Then, one extrapolates these results to $\epsilon \to 0$.

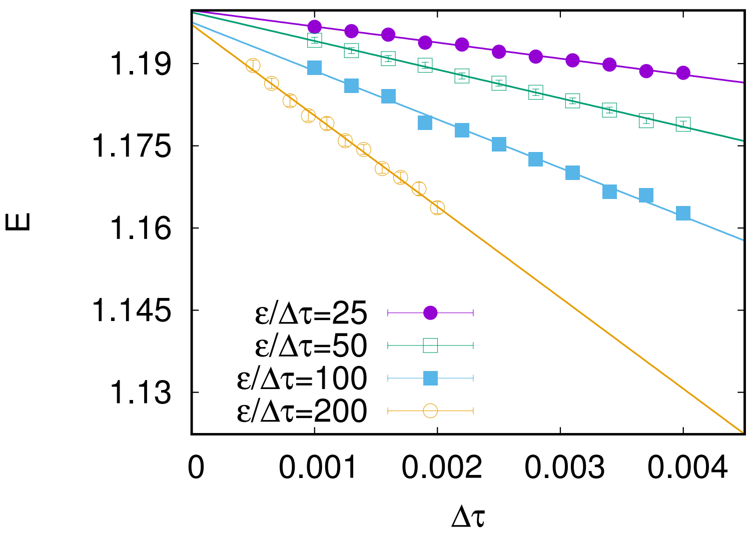

Fig. 3.2 Estimation of the DTDMC energy using Method 1 (see the main text) for a harmonically trapped one-body system with Weyl SOC. Also shown are the linear extrapolations of the DMC energies to $\Delta\tau \to 0$. Quantities are dimensionless, with the energy and length scales defined in Eq. (3.10).

In Figs. 3.2 and 3.3, we show the estimations obtained using Method 1 and Method 2, respectively, for the one-body system with Weyl SOC in a harmonic trap. As we can see, the dependence of the extrapolated energies on $\frac{\Delta\tau}{\epsilon}$ is much weaker than their dependence on ϵ. Therefore, Method 1 is preferred and is the one that we have used to provide the DTDMC energy. We can also see from the figures that the dependence of the energy with respect to $\Delta\tau$, when ϵ or $\frac{\Delta\tau}{\epsilon}$ are fixed, is linear in both cases. This is because the non-SOC terms of the propagator are exact up to $\mathcal{O}(\Delta\tau)$ while the SOC terms are exact up to $\mathcal{O}\left(\frac{\Delta\tau}{\epsilon}\right)$. For all the chosen values of ϵ, the conditions in Eq. (3.109) are satisfied, with the r.h.s being $\sim 10^{-2}$. Also, the condition in Eq. (3.111) is satisfied since the difference between the r.h.s. and the l.h.s. is at most a 3% of the SOC local energy contribution.

From Table 3.1, we can see that both DMC methods provide energies that agree with the result of the imaginary-time evolution within a 2% error. We can also see that SIDMC provides lower energies than DTDMC. This is due to the fixed-phase nature of the energies obtained with SIDMC, which does not require to use an effective Hamiltonian, as does DTDMC. We can see that this effect is enhanced in the harmonically trapped systems with Rashba and Weyl SOCs. For the cases with two-body spin-dependent interactions, only T-moves results are reported, since SIDMC can not deal with these potentials. It must be noticed that, while in the T-moves calculations one performs the triple extrapolation $\Delta\tau \to 0$, $\epsilon \to 0$, and $\frac{\Delta\tau}{\epsilon} \to 0$, calculations with ITE are performed at fixed ϵ ($\epsilon = 0.1$ and $\epsilon = 0.3$ in the Weyl and Rashba cases, respectively). This is due to the computational cost associated to

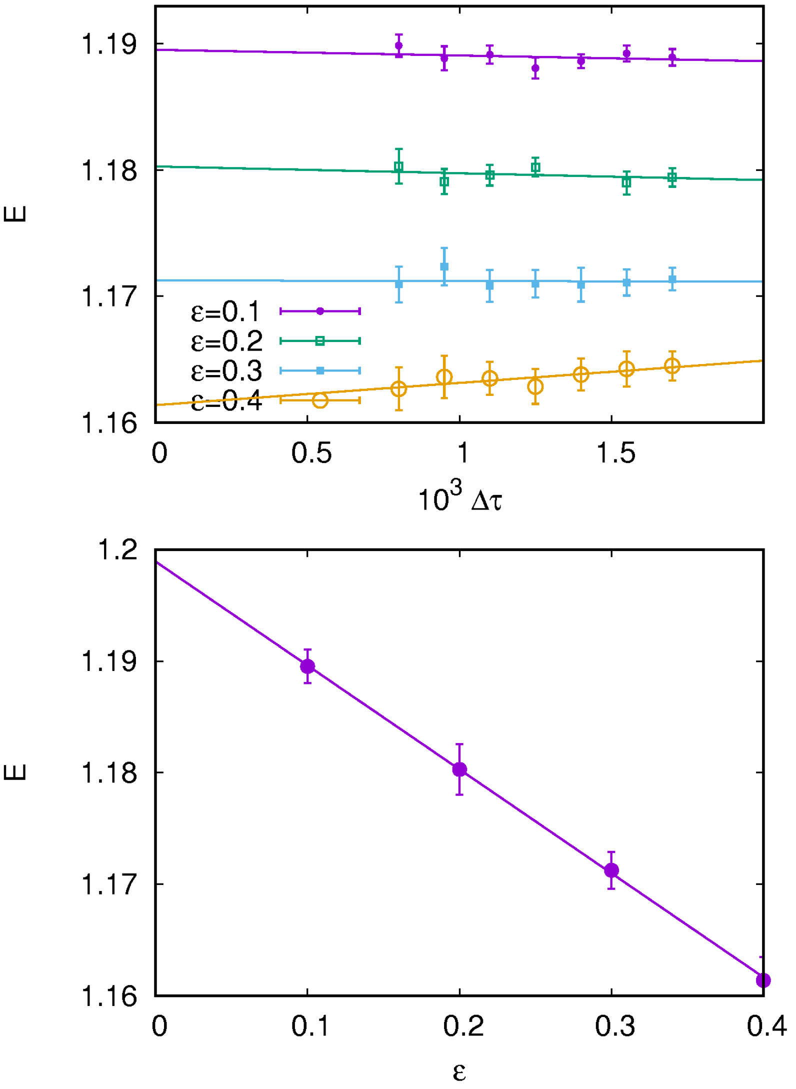

Fig. 3.3 Estimation of the DTDMC energy using Method 2 (see the main text) for a one-body system with Weyl SOC on a harmonic trap. The lines are used to extrapolate the DMC energies. The quantities shown are dimensionless.

decreasing ϵ when discretizing the Schrödinger equation in the position representation, since ϵ is taken as the point-to-point distance of the mesh. In order to check that both DTDMC and ITE give compatible estimates, we also provide in Table 3.1 DMC energies corresponding to fixed ϵ. This is not necessary in the Raman case since the Raman Hamiltonian is independent of ϵ if this parameter is sufficiently small, as mentioned previously. Notice also that the errors corresponding to the ITE results in the two-body 2D Rashba cases are larger than the ones in the 3D one-body Raman and Weyl cases. This is due to the higher number of dimensions that must be discretized in the latter case.

	SIDMC	GPE FPA	DTDMC	DTDMC fixed ϵ	GPE FPA eff. H
Rm. 2-b NS	-0.0496 ± 0.0002	-0.04964 ± 0.00005	-0.0496 ± 0.0004		-0.04962 ± 0.00005
Rm. 2-b S			0.00946 ± 0.00004		0.009370 ± 0.000005
Wy. 2-b NS	0.1125 ± 0.0003	0.11217 ± 0.00005	0.1444 ± 0.0002	0.1423 ± 0.0002	0.14239 ± 0.00005
Wy. 2-b NS 2			0.1122 ± 0.00015	0.1123 ± 0.00015	0.11225 ± 0.000005
Wy. 2-b S			0.0602 ± 0.0001	0.0602 ± 0.0001	0.06029 ± 0.00005

Table 3.2 Results of the energy per particle (in reduced units, see Sec. 3.2.1) for the many-body systems in the dilute regime, as described in Sec. 3.5.3.3. "2-b S" stands for spin-dependent two-body interaction while "2-b NS" stands for spin-independent two-body interaction, while "Rm." (Raman) and "Wy." (Weyl) indicate the type of SOC.

3.5.3.2 Many-body calculations

We now report the DMC energies corresponding to the many-body Raman and Weyl SOC Hamiltonians. We first focus on the dilute regime with a finite number of particles imposing periodic boundary conditions (PBC). We compare the DMC energy estimations with the energies obtained from the imaginary time propagation solution of the Gross-Pitaevskii equation (GPE), both for the fixed-phase Hamiltonian (Eq. (3.53)) and the fixed-phase, effective Hamiltonian of the DTDMC approach. In the case of the Rashba SOC, we do not know the scattering length of the complete interaction, and thus a direct comparison to the GPE results is not possible. Finally, we compare the energy estimations of both DMC methods out of the ultra dilute regime.

3.5.3.3 Dilute regime

Table 3.2 reports the DMC energy per particle, together with the corresponding Gross-Pitaevskii energy per particle, for four different physical systems: Raman and Weyl SOCs, both with spin-independent and spin-dependent two-body interactions. Moreover, we include the DTDMC energy per particle using two different trial wave functions in the two-body spin-independent Weyl case, in order to showcase the variational dependence of this method on the modulus of the trial wave function.

For the GPE calculations involving Raman and Weyl SOCs, we use the free-space scattering length, i.e., the scattering length obtained for the Hamiltonian removing the SOC terms [66].

In all cases, the trial wave function is of the form

$$\Psi_T(\vec{R},\vec{S}) = \left[\prod_{j=1}^{N} \rho_{T,1\mathrm{b}}(\vec{r}_j, s_j)\right] \left[\prod_{\substack{i,j=1 \\ i<j}}^{N} \bar{\rho}_{T,2\mathrm{b}}(\vec{r}_i,\vec{r}_j)\right] \exp\left[i\sum_{j=1}^{N}\phi_T(\vec{r}_j, s_j)\right] , \qquad (3.138)$$

with

$$\overline{\rho}_{T,2\mathrm{b}}(r_{ij}) = \begin{cases} \frac{\rho_{T,2\mathrm{b}}(r_{ij})+\rho_{T,2\mathrm{b}}(L-r_{ij})}{2\rho_{T,2\mathrm{b}}(L/2)} & \text{if } r_{ij} < L/2 \\ 1 & \text{if } r_{ij} > L/2 \end{cases} \tag{3.139}$$

and $r_{ij} = |\vec{r}_j - \vec{r}_j|$. The function $\rho_{T,2\mathrm{b}}(r_{ij})$ is the modulus of a spin-independent two-body trial wave function analogous to the one presented in Sec. 3.5.3.1 (here $k_{2\mathrm{b}} \sim 10^{-6}$). The modulus of the one-body terms for the DTDMC "Raman 2-b NS" and "Raman 2-b S" cases of Table 3.2 are given in Eqs. (3.121) and (3.122). For the SIDMC "Raman 2-b NS" case we use the expression in Eq. (3.125). Both DTDMC and SIDMC "Weyl 2-b NS" cases are done with the terms in Eq. (3.130), while in the DTDMC "Weyl 2-b NS 2" and "Weyl 2-b S" cases we use the one-body forms of Eqs. (3.126) and (3.127). In all cases no harmonic trap has been used, therefore we drop the harmonic oscillator ground state wave function from all the aforementioned expressions (as an example, the "Weyl 2-b NS" cases are performed setting $\rho_T(\vec{r}) = 1$). The trial phases for each case are analogous to the ones in Eqs. (3.123), (3.124), (3.128), and (3.129).

The average number of walkers is set to $N_w = 1,000$, and the time step is $\Delta\tau \sim \mathcal{O}\left(10^{-3}\right)$. The parameter ϵ in the DTDMC is fixed to $\epsilon = 100\Delta\tau$. All the values of ϵ employed in order to perform the extrapolations previously discussed satisfy the condition of Eq. (3.111), with a discrepancy between the r.h.s. and the l.h.s. of at most $\sim 1\%$. Also, the r.h.s of both expressions in Eq. (3.109) equals 0.08 at most, which implies that the maximum error in the approximation to the propagator is $e_{\max} \sim e^{0.08} - (1 + 0.08) \simeq 0.0033$. In the Weyl SIDMC calculations, the length of a simulation block is set to $N_b^{\mathrm{it}} = 10$. The ratio of discarded walkers is found to be $\chi < 0.0002$. For the Raman SIDMC calculations, we set $N_b^{\mathrm{it}} = 10$ and find $\chi = 0$ (see Sec. 3.5.1.2).

The Raman simulations are carried out with $N = 40$ particles, $\eta_{\mathrm{Rm}} = 0.4$, $L_x = L_y = L_z = 16.899$ (box length) and $k = k_x = \frac{2\pi}{L_x}$. In the two-body spin-independent case we have $V_0 = 75$, $R_0 = 0.25$, $\Omega = 0.4$, $C_1 = 0$, $C_2 = 1$ and $B_c = 0.5$, while in the two-body spin-dependent case we have $V_0(+1,+1) = V_0(-1,-1) = 75$, $V_0(+1,-1) = V_0(-1,+1) = 50$, $R_0 = 0.25$, $\Omega = 0.1$, $C_1 = 0.6$, $C_2 = 0.8$. The gas parameter for these systems is $na^3 \simeq 10^{-6}$. Here, n is the density and a corresponds to the scattering length of the interaction in the spin-independent cases, and the maximum scattering length in the spin-dependent ones.

In the Weyl simulations, and for the two-body spin-independent case, we use $N = 45$ particles, $\eta_{\mathrm{We}} = 0.25$, $L_x = L_y = L_z = 20$, $\vec{k} = (k_x, 0, k_z)$ with $k_i = \frac{2\pi}{L_i}$, $V_0 = 75$, $R_0 = 0.3$, with a gas parameter of $na^3 = 1.7 \times 10^{-5}$. In the two-body spin-dependent case we use $N = 35$, $\eta_{\mathrm{We}} = 0.25$, $L_x = L_y = L_z = 18$, $k = k_x = \frac{2\pi}{L_x}$,

	SIDMC	DTDMC
Raman PBC 2-b no spin	3.673 ± 0.002	3.681 ± 0.002
Raman PBC 2-b spin trial 1		5.356 ± 0.003
Raman PBC 2-b spin trial 2		5.358 ± 0.002
Weyl PBC 2-b no spin	3.773 ± 0.003	3.798 ± 0.003
Weyl PBC 2-b no spin trial 2		4.050 ± 0.005
Weyl PBC 2-b spin		5.633 ± 0.005
Weyl HO 2-b no spin	2.236 ± 0.001	2.302 ± 0.002

Table 3.3 Energies per particle (in reduced units, see Sec. 3.2.1) for the many-body systems out of the dilute regime, as described in Sec. 3.5.3.4.

$V_0(+1,+1) = V_0(-1,-1) = 75$, $V_0(+1,-1) = V_0(-1,+1) = 50$, $R_0 = 0.3$, with a gas parameter of $na^3 \sim 10^{-5}$.

We can see from Table 3.2 that the DMC energies agree with the GPE calculations up to a $\sim 1\%$. As in the previous Section, only DTDMC results are reported for the spin-dependent two-body cases, since the SIDMC method can not handle two-body spin-dependent interactions. We can also see from the two-body spin-independent cases that DTDMC is able to recover almost completely the fixed-phase energy, although we know it always provides an upper bound. On the other hand, SIDMC recovers the complete fixed-phase energy. The DTDMC Weyl two-body spin-independent calculations illustrate the variational property with respect to the modulus of the trial wave function of this method. Notice that two different modulus ("Weyl 2-b NS" and "Weyl 2-b NS 2" cases) provide two different energy estimations.

3.5.3.4 Beyond the dilute regime

In this Section we compare the performance of the two DMC algorithms discussed when applied to several homogeneous many-body systems beyond the dilute regime. We analyze a few systems under Raman and Weyl SOC interactions using periodic boundary conditions and a two-body spin-independent interaction. We show again an example of the variation of the DTDMC energy when the modulus of the trial wave function is changed. We also provide DTDMC energy estimations of systems under Raman and Weyl SOCs with a spin-dependent two-body interaction. Finally, we compare both DMC estimations in a many-body harmonically confined system with Weyl SOC. Results are presented in Table 3.3.

The general form of the trial wave function is given in Eq. (3.138). The DTDMC calculations corresponding to the cases "Raman PBC 2-b no spin", "Raman PBC 2-b spin trial 1" and "Raman PBC 2-b spin trial 2" have been evaluated using the one-body terms of Eqs. (3.121) and (3.122), while for the SIDMC "Raman PBC 2-b no spin" calculation, Eq. (3.125) has been employed. For DTDMC corresponding to the cases "Weyl PBC 2-b no spin", "Weyl PBC 2-b spin" and "Weyl HO 2-b no spin" use has been made of the expressions in Eqs. (3.126) and (3.127). Finally, for the DTDMC "Weyl PBC 2-b no spin trial 2" case, we use

$$\rho_T(\vec{r}, s = +1) = \gamma \tag{3.140}$$

$$\rho_T(\vec{r}, s = -1) = \sqrt{1-\gamma^2}\frac{(1+\cos\theta_k)}{\sin\theta_k} \tag{3.141}$$

$$\gamma = 0.6 \tag{3.142}$$

This form is used to illustrate the variational property of the T-moves method with respect to the modulus of the trial wave function. The SIDMC "Weyl PBC 2-b no spin" and "Weyl HO 2-b no spin" calculations use the expressions in Eq. (3.130). As in the previous Section, the harmonic oscillator wave function is dropped from the aforementioned equations when PBC are considered. Again, the trial phases for each case are given in Eqs. (3.123), (3.124), (3.128), and (3.129).

In the two-body spin-independent calculations, the two-body trial terms in all PBC cases are the same as in Sec. 3.5.3.3. Concerning the two-body spin-dependent calculations, we report the energy in the Weyl case using a spin-independent two-body correlation factor analogous to the one in Sec. 3.5.3.3. In the Raman case, though, we compare the energy estimated using a spin-independent two-body factor with the estimation from a spin-dependent one, again with the same form as in Sec. 3.5.3.3. Finally, in the "Weyl HO 2-body no spin" case we set $\overline{\rho}_{T,2\mathrm{b}}(r_{ij}) = \rho_{T,2\mathrm{b}}(r_{ij})$ in Eq. (3.139) because we do not impose PBC.

The average number of walkers is set to $N_w = 1000$, the time step $\Delta\tau \in (10^{-4}, 10^{-3})$, and the DTDMC ϵ parameter is fixed such that $\frac{\epsilon}{\Delta\tau} \in (100, 400)$ for Weyl SOC . All the used values of ϵ satisfy the condition in Eq. (3.111), with a discrepancy between the r.h.s. and the l.h.s. of at most 3%. Also, the r.h.s of both expressions in Eq. (3.109) equals 0.3 at most, which implies that the maximum error in the approximation to the propagator is $e_{\max} \sim e^{0.3} - (1 + 0.3) \simeq 0.05$. The length of a simulation block in the Weyl PBC SIDMC calculations is set to $N_b^{\mathrm{it}} = 10$. The ratio of discarded walkers is found to be $\chi < 0.006$. The harmonically trapped Weyl simulations share the same parameters except for the ratio χ, which turns out to be $\chi < 0.001$. For the Raman calculations one has $N_b^{\mathrm{it}} = 10$ and finds $\chi = 0$ (see Sec. 3.5.1.2).

In the Raman case we use $N = 50$ particles, $\eta_{\mathrm{Rm}} = 1.5$, $\Omega = 0.4$, $L_x = L_y = L_z = 4.5$, $V_0 = 1$, $R_0 = 1.5$, $k = \frac{2\pi}{L_x}$, and $C_1 = 0.6$, $C_2 = 0.8$. In the SIDMC simulations we also have $B_c = 0.5$. The two-body spin-dependent case shares the same parameters with $V_0(+1, +1) = V_0(-1, -1) = 2$, $V_0(+1, -1) = V_0(-1, +1) = 1$. The gas parameter for the up-down channels is $na^3_{+1,-1} \sim 10^{-2}$ while for the up-up and down-down channels we set $na^3_{+1,+1} \sim 0.1$. In the PBC two-body spin-independent Weyl case we simulate $N = 25$ particles with $\eta_{\mathrm{We}} = 3.590$, $L_x = L_y = L_z = 3.5$, $V_0 = 1$, $R_0 = 1.5$, and

$\vec{k} = (k_x, 0, 0)$ $k_x = \frac{2\pi}{L_x}$, $V_0(+1,+1) = V_0(-1,-1) = 2$, $V_0(+1,-1) = V_0(-1,+1) = 1$, with $R_0 = 1.5$. The gas parameter for each channel is of the same order of magnitude that the one in the Raman case. Finally, in the harmonically trapped Weyl simulations we use $N = 30$ particles, $\eta_{\text{We}} = 1$, $\omega = 0.4$, $V_0 = 1$, $R_0 = 1.5$, $k = 0.5$, $\theta_k = 1.31$, and $\phi_k = 0.3$.

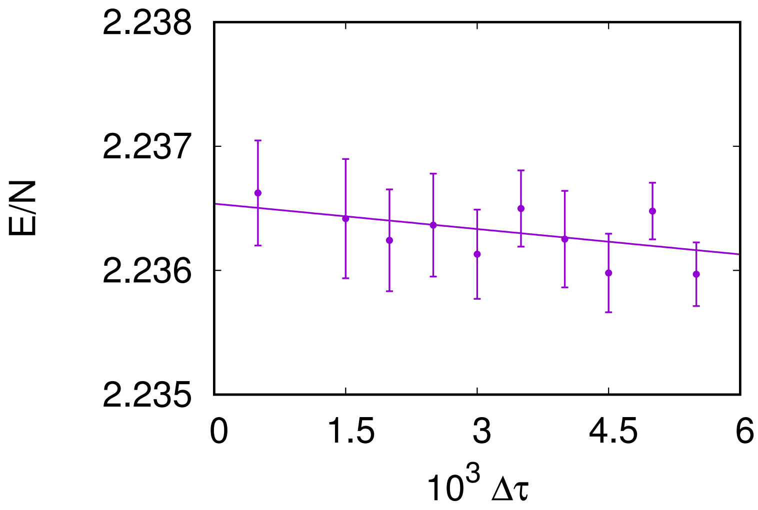

Fig. 3.4 Dependence of the DMC energy per particle on the imaginary time-step for SIDMC for a many-body system with Weyl SOC and a harmonic trap. The line corresponds to the linear extrapolation of the DMC energies. The shown quantities are dimensionless.

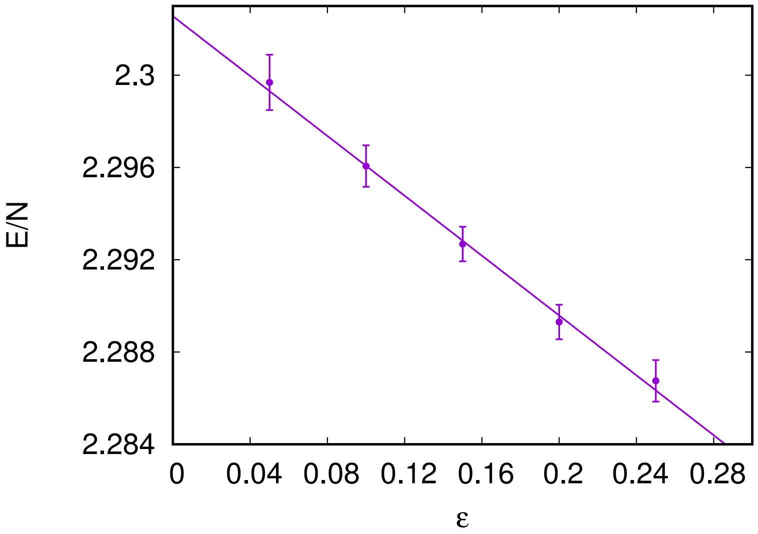

Fig. 3.5 Estimation of the DTDMC energy per particle using Method 2 (see Sec. 3.5.3.1) for a many-body system with Weyl SOC and a harmonic trap. The line corresponds to the linear extrapolation of the DMC energies. All quantities are dimensionless.

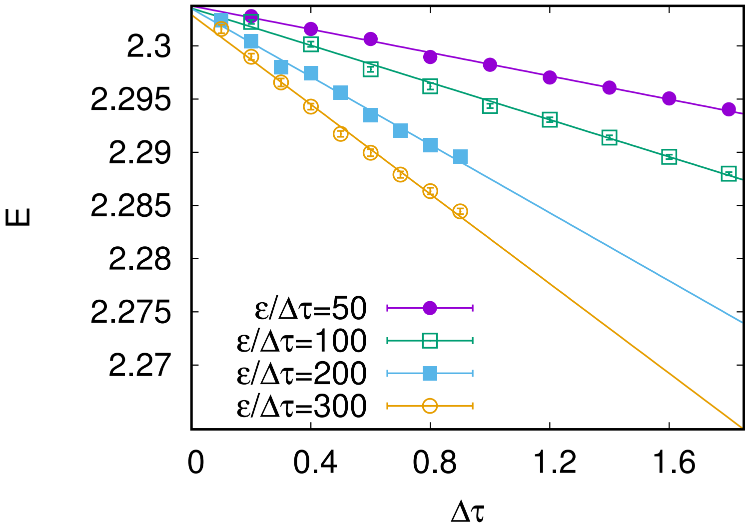

Fig. 3.6 Estimation of the DTDMC energy per particle using Method 1 (see Sec. 3.5.3.1) for a many-body system with Weyl SOC and a harmonic trap. The lines correspond to the linear extrapolation of the DMC energies. The shown quantities are dimensionless.

In Fig. 3.4, we show the energy dependence on the imaginary time-step corresponding to the SIDMC simulations of trapped Weyl gases. We see from the Figure the linear dependence of the energy with respect to $\Delta\tau$. In Figs. 3.6 and 3.5, we show DTDMC results for the two methods mentioned in Sec. 3.5.3.1 to estimate the triple limit $\Delta\tau \to 0$, $\epsilon \to 0$, and $\frac{\Delta\tau}{\epsilon} \to 0$. The observed behavior is consistent with the previous results obtained in the one-body case.

In Table 3.3, we report the DMC energies per particle for the analyzed cases. From these results, we can see that DTDMC is able to almost exactly recover the fixed-phase energy of the bulk gases. In the trapped Weyl gas, the difference with respect to the fixed-phase energy obtained with SIDMC is larger. We can also see how the improvement of the modulus of the trial wave function in the two-body spin-independent PBC Weyl simulation produces better energies as a consequence of the variational nature of the DTDMC method. Finally, our results show that using a spin-dependent two-body trial correlation factor does not lead to any significant improvement in the two-body spin-dependent PBC Raman cases performed.

3.6 The Phase Diagram of a Raman Spin-Orbit Coupled system

As mentioned in Chapter 1, the phase diagram of an interacting system of atoms under Raman SOC has been reported previously [25, 60]. However, the diagram is obtained within the mean field regime, valid only for very low gas parameter values $\lesssim 10^{-4}$. In order to extend these results to a more strongly interacting regime, and to deal with the non-local character of the SOC interaction, we use the DTDMC method introduced previously to study the system from a microscopic point of view.

We study a three-dimensional system of N bosons of mass m under periodic boundary conditions described by the Hamiltonian in Eq. (3.1), with $\hat{W}_k^{\mathrm{SOC}} = \hat{W}_k^{\mathrm{Rm}}$ (see Eq. (3.3)) and $V^{\mathrm{2b}}_{s_i,s_j}$ (see Eq. (3.5)) a short-range, two-body, spin-dependent interaction. We use two model interactions: a soft-sphere (SS) potential of strength $V_0(s_i, s_j)$ and range $R_0(s_i, s_j)$, and a Lennard-Jones (LJ) force $V^{\mathrm{2b}}_{s_i,s_j}(r_{ij}) = \left(\frac{\sigma_{12}(s_i,s_j)}{r_{ij}}\right)^{12} - \left(\frac{\sigma_6(s_i,s_j)}{r_{ij}}\right)^{6}$. Here, r_{ij} is the distance between the i-th and j-th particles and $s_i, s_j = \pm 1$ are their spins. The trial wave function used for importance sampling in the DTDMC method, that also fixes the phase, is chosen as a product of one-body and two-body (Jastrow) terms. It is given by Eqs. (3.121) (3.122) (3.123) /3.124) with $C_1 = C_2 = 1/\sqrt{2}$ and $k \in [0, k_0]$ optimized variationally, although the harmonic confinement is dropped since we are studying an homogeneous system. This corresponds to the expression reported in Ref. [25], with the sign of the spin-down component changed due to the different sign of the Ω term in the Hamiltonian, and the up and down components exchanged due to the different sign of the $\hat{P}^x \hat{\sigma}^z$ term. The Jastrow factor depends on the interaction $\hat{V}_{ij}$. For the SS potentials, we adopt the zero-energy solution of the averaged interaction along the different spin channels (see Eqs. (3.136), (3.137)). This prescription provides a lower variational energy than a spin-dependent two-body Jastrow factor in the case considered in this work. In the case of the LJ interaction, we use a McMillan factor of the form $f(r) = e^{-(b/r)^5}$. The constant b is fixed so that the highest order divergence of the LJ potential is suppressed at the two-body level (cusp condition). Thus, we set to zero the highest order divergence arising in the expression:

$$-\frac{\hbar^2}{m}\nabla^2 f(r) + \left[\left(\frac{\sigma_{12}(s_i, s_j)}{r_{ij}}\right)^{12} - \left(\frac{\sigma_6(s_i, s_j)}{r_{ij}}\right)^{6}\right] f(r) = 0 \tag{3.143}$$

which is of $\mathcal{O}\Big(1/r^{12}\Big)$. Assuming σ_{12} is spin-independent, this is achieved by setting:

$$b = \left(\sigma_{12}^{12}\frac{m}{25\hbar^2}\right)^{1/10} . \tag{3.144}$$

As it is common in systems with periodic boundary conditions, the two-body Jastrow factor is set to a constant for inter-particle distances greater than $L/2$ (as shown in Sec. 3.5.3). However, in this case we employ a different prescription for the trial factor with respect to the previous Section. The Jastrow factor $f_{\rm 2b}(r_{ij})$ employed is:

$$f_{\rm 2b}(r_{ij}) = \begin{cases} \rho_{\rm 2b,T}(r_{ij}) / \left(C_A \exp\left(-\frac{C_B}{(L/2)^2} - \frac{C_B}{(L/2)^2} \right) \right) & r_{ij} < R^* \\ C_A \exp\left(-\frac{C_B}{r^2} - \frac{C_B}{(L-r)^2} \right) / \left(C_A \exp\left(-\frac{C_B}{(L/2)^2} - \frac{C_B}{(L/2)^2} \right) \right) & R^* < r < L/2 \\ 1 & r_{ij} > L/2 \end{cases} \tag{3.145}$$

with:

$$C_A = \rho_{\rm 2b,T}(R^*) \exp\left(\frac{C_B}{(R^*)^2} + \frac{C_B}{(L-(R^*)^2)} \right) \tag{3.146}$$

$$C_B = \frac{1}{\rho_{\rm 2b,T}(R^*)} \left. \frac{{\rm d}\rho_{\rm 2b,T}}{{\rm d}r_{ij}} \right|_{R^*} \frac{1}{2\left(\frac{1}{(R^*)^3} - \frac{1}{(L-R^*)^3} \right)} \tag{3.147}$$

Here $\rho_{\rm 2b,T}(r_{ij})$ is the two-body factor described previously, which depends on the interaction potential, and R^* is a matching point. This Jastrow factor corresponds to the matching of $\rho_{\rm 2b,T}(r_{ij})$ to a phonon-like wave function, $C_A \exp\left(-\frac{C_B}{r^2} - \frac{C_B}{(L-r)^2} \right)$. Eqs. (3.146) and (3.147) are obtained by imposing continuity and differentiability in the matching point. We have not seen a strong variational influence of the parameter R^*, which is set to $R^* = 0.22L$. No significant changes are seen when setting $R^* = 0.4L$ in the tested cases. The number of walkers in the DMC simulations is set to $N_w = 1000$ while the time-step range is chosen in the range $\Delta\tau \in [7 \times 10^{-4}, 5.6 \times 10^{-3}]$.

The choice of the parameters of the two-body interaction $\hat{V}_{ij}$ determines the different channel scattering lengths $a_{s,s'}$, as according to Ref. [66] the inclusion or not of the SOC term does not appreciably change them. The values used in this Section fulfill the condition $a_{+1,+1} = a_{-1,-1} > a_{+1,-1} = a_{-1,+1}$, as in the experiments of Ref. [2]. Finally, we express all quantities in dimensionless form, with the characteristic energy and length scales given in Sec. 3.2.1 with $\eta_{\rm Rm.} = 1$.

In order to characterize the phase diagram of the model, we use the standard gas parameter na^3, with $a = a_{+1,+1}$ the scattering length of the interaction in the $(+1,+1)$ channel. It should be noted that, for this system, na^3 is not a scaling parameter. However, we use it to characterize the combined effect of the density and the interaction. We have checked, though, that for very low values of na^3 one recovers the mean field results, while for larger values, the DTDMC simulations reveal that the extension of the stripe phase domain is increased with respect to the mean field prediction. This may be a relevant issue for experiments willing to detect and/or characterize the stripe phase. In order to illustrate that, we set the density to $n = 3.7 \times 10^{-3}$, with the number of particles $N \in [50, 120]$ and the size of the simulation box changing as a function of the momentum of the trial wave function. We tune the spin-dependent scattering lengths such that $na^3 \in (10^{-4}, 10^{-1})$ by changing the two-body potential parameters. In this sense, increasing the gas parameter is equivalent to increasing the range and strength of the interactions, which enhances the effect of correlations in the medium. We set the interaction contrast $\gamma = (a - a_{+1,-1})/(a + a_{+1,-1})$ to $\gamma = 0.4$, since non-zero values of this quantity are necessary for the existence of a stripe ground state [25]. This contrast is employed for the elaboration of the phase diagram, and the computation of the pair correlation functions and the one-body density matrix. However, the quantitative characterization of the superfluidity in the stripe phase and the computation of the static structure factor is performed with the contrast used in Ref. [2], $\gamma = 0.904$. It must be remarked that the quantity γ is a tunable property in the experimental setup of Ref. [2].

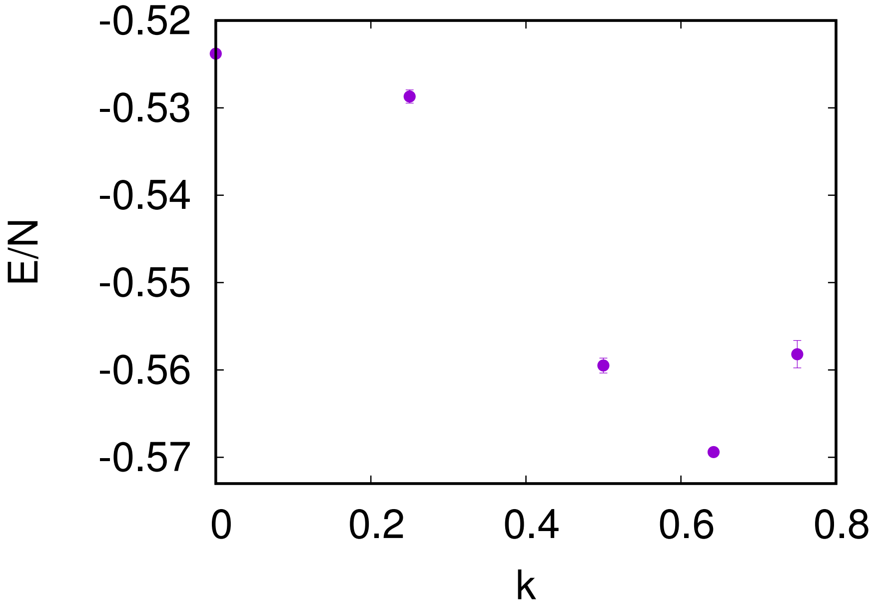

Fig. 3.7 Variational energy per particle of the system under Raman SOC in the stripe phase for $\Omega = 3.1$, $na^3 = 10^{-3}$ as a function of the variational momentum k. All quantities are reported in reduced units.

In order to illustrate the Variational Monte Carlo method introduced in Sec. 3.3, we present in Fig. 3.7 the variational energy of the system in the stripe phase with a SS interaction for $\Omega = 3.1$, $na^3 = 10^{-3}$, $V_0 = 4$, $R_0(+1,+1) = R_0(-1,-1) = 1.315$, $R_0(+1,-1) = R_0(-1,+1) = 0.871$, as a function of the variational momentum k. The value of k employed in the trial wave function for the DMC simulations in this case is the one corresponding to the energy minimum, $k = 0.64$, which is the optimal value of the momentum in the dilute regime [25].

The DTDMC phase diagram of the SOC system is reported in Fig. 3.8 for fixed density and varying scattering length. The upper and middle plots correspond to the DTDMC results for the SS and LJ interactions, respectively, while the lower plot

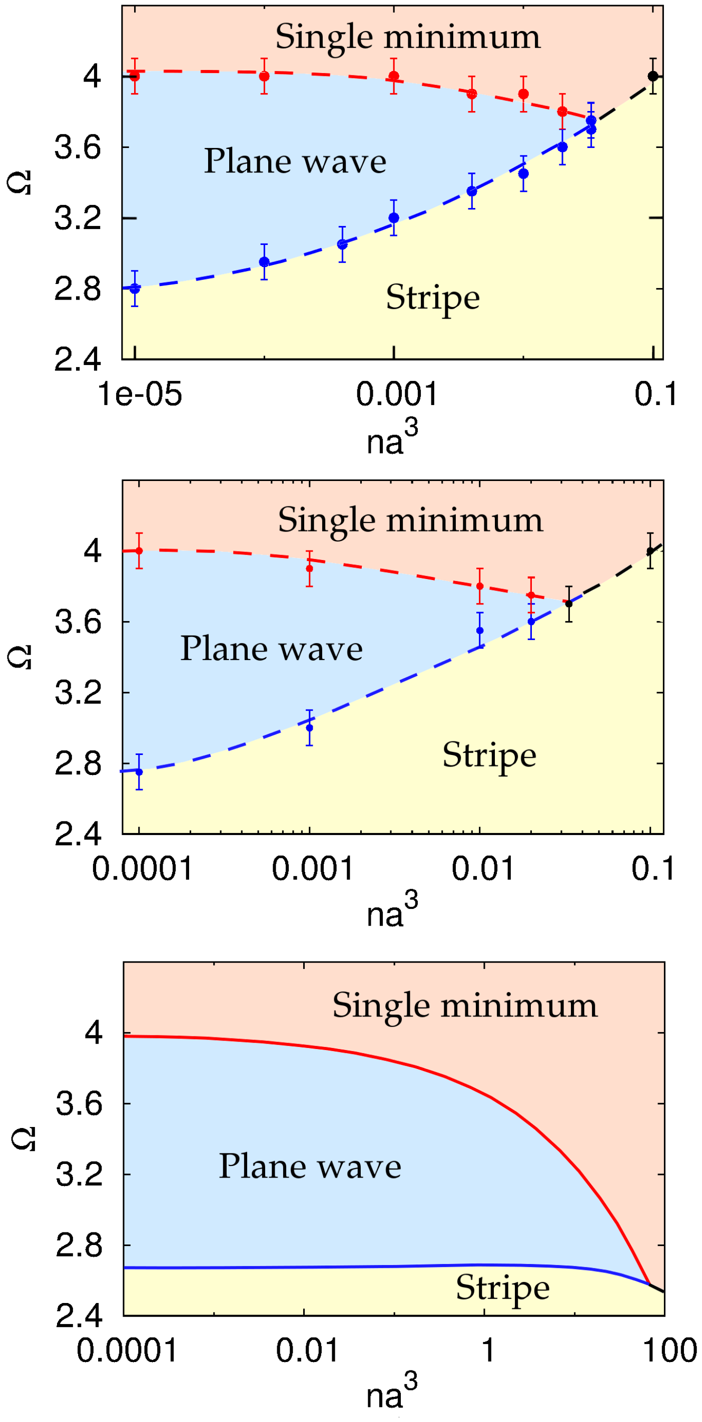

Fig. 3.8 DTDMC Phase diagram of the many-body system with Raman Spin Orbit Coupling. The upper plot corresponds to the DTDMC diagram using the SS potential, while the middle one corresponds to the LJ potential. Dashed lines are a guide to the eye. In the lower plot, we report the mean field phase diagram.

shows the mean field phase diagram. The points indicate the computed transition lines between the different phases. Errorbars in the DTDMC results account for

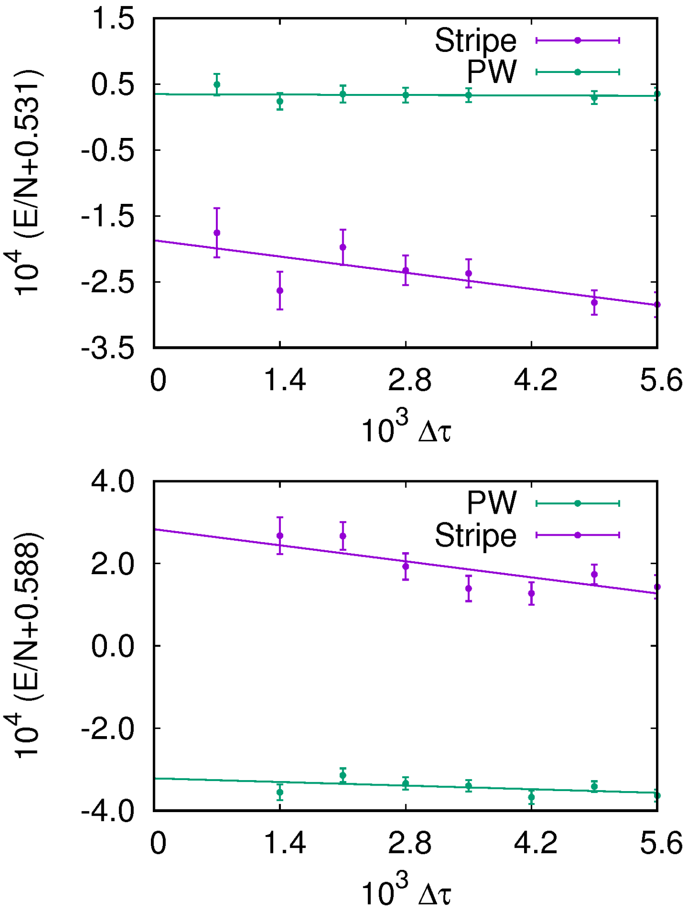

Fig. 3.9 Rescaled DMC energies per particle as a function of the imaginary time step for $na^3 = 10^{-4}$, $\Omega = 2.9$ (top) and $\Omega = 3.1$ (bottom), for the SS interaction. All quantities are reported in reduced units.

the statistical variance of the energy estimations. In order to provide an illustrative example of phase characterization, we show in Fig. 3.9 the DMC energies as a function of the imaginary time step for the stripe and plane wave phases, for $na^3 = 10^{-4}$ with $\Omega = 2.9$ and $\Omega = 3.1$, for the SS interaction. We see that at $\Omega = 2.9$ the stripe phase provides a statistically significant lower energy than the plane wave phase, while at $\Omega = 3.1$ the opposite happens. We have omitted the single minimum energy since it lays above both of them.

Looking at the DTDMC phase diagrams it can be seen that, as the two-body scattering length increases, the value of the reduced Raman coupling at which the plane wave-stripe phase transition takes place, also increases. Remarkably, this effect is absent at the mean field level, and is also robust with respect to the interaction employed. Based on this, we conclude that the enhancement of the stripe phase in the DTDMC phase diagrams is produced by the increase of inter-atomic correlations. This enhancement takes place because the DTDMC correction to the mean field energy of the stripe ($\Delta E_{\mathrm{DMC,S}}$) and plane wave ($\Delta E_{\mathrm{DMC,PW}}$) phases and the energy difference between these phases at the mean field level (ΔE_{MF}) fulfill $\left|\frac{\Delta E_{\mathrm{DMC,S}}}{\Delta E_{\mathrm{MF}}}\right| \simeq \left|\frac{\Delta E_{\mathrm{DMC,PW}}}{\Delta E_{\mathrm{MF}}}\right| \simeq 1$ over a wide region of the phase diagram. Not only do the DTDMC phase boundaries depart from the mean field prediction as the gas parameter increases, but also the energies of each phase do. To show this, we present in Table 3.4 the DMC energies per particle of the stripe wave function for both the SS and LJ interactions, together with the mean field energy. We report the same for the plane wave wave function in Table 3.5. We remark that the $\{\Omega, na^3\}$ points where the energy is reported do not necessarily correspond to points in the diagram where a given phase dominates. As the gas parameter increases, we can see how the DTDMC energy departs from the mean field result, and also how the energy obtained when employing different interactions depart from each other.

The stripe phase is favored over the plane wave phase in the DTDMC diagram because of the different polarization between phases: while the stripe phase is always unpolarized, the plane wave phase has non-zero polarization. Since the potentials employed in this work are less repulsive in the $(+1, -1)$ and $(-1, +1)$ channels in accordance to the experiment of Ref. [2], the beyond mean field corrections favor an unpolarized state over a polarized one. In this sense, the DTDMC corrections drastically determine the transition line. In order to showcase the different polarizations of each phase, we show in Fig. 3.10 the average of the z-component of the spin for these two phases as a function of the imaginary time step, with $na^3 = 10^{-4}$, $\Omega = 2.9$ for the stripe phase and $\Omega = 3.1$ for the plane wave phase.

In contrast to the case discussed above, the single minimum region of the diagram is only slightly changed by DTDMC with respect to the mean field prediction. This is because the energy gap in mean field between this phase and the stripe and plane wave phases is larger in absolute value than the DTDMC corrections over the majority of the phase diagram.

In mean field, the stripe-plane wave and the stripe-single minimum transitions are of first order, while the plane wave-single minimum transition is of second order according to Refs. [25, 60]. This is directly reflected in the value of the momentum that minimizes the energy in each phase at the mean field level: while there is a

na^3	Ω	DMC SS	DMC LJ	MF
10^{-3}	3.1	-0.5721 ± 0.0001	-0.5711 ± 0.0002	-0.5723
10^{-2}	3.4	-0.6485 ± 0.0005	-0.6508 ± 0.0005	-0.6590
2×10^{-2}	3.6	-0.7037 ± 0.0004	-0.7160 ± 0.0007	-0.7276
3.33×10^{-2}	3.6	-0.6720 ± 0.0003	-0.6964 ± 0.0005	-0.7124

Table 3.4 Results for the energy per particle estimation (in reduced units) for the stripe trial wave function for several points of the $\{\Omega, na^3\}$ diagram. "DMC SS" indicates the DMC energies per particle with a SS two-body interaction, "DMC LJ" indicates the same for the LJ potential and "MF" indicates the mean field energies per particle.

na^3	Ω	DMC SS	DMC LJ	MF
10^{-3}	3.1	-0.5717 ± 0.0001	-0.5715 ± 0.0002	-0.5754
10^{-2}	3.4	-0.6466 ± 0.0002	-0.6437 ± 0.0003	-0.6706
2×10^{-2}	3.6	-0.7037 ± 0.0002	-0.7177 ± 0.0005	-0.7468
3.33×10^{-2}	3.6	-0.6683 ± 0.0001	-0.6951 ± 0.0005	-0.7352

Table 3.5 Same quantities as in Table 3.4 for the plane wave trial wave function.

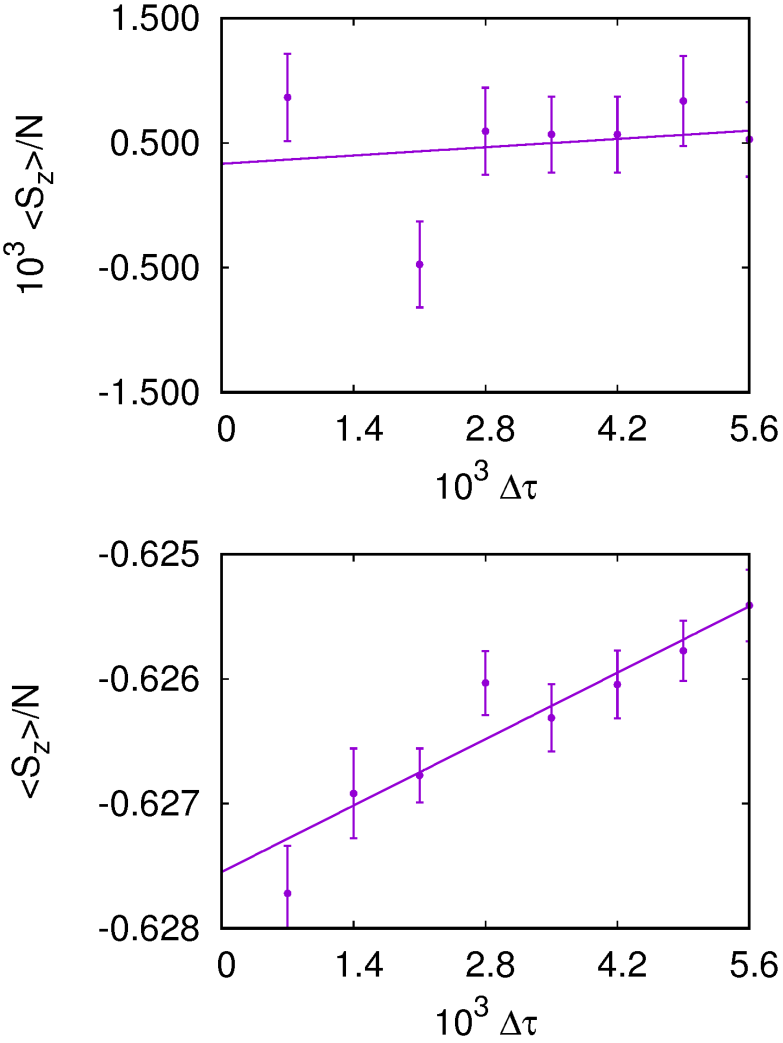

Fig. 3.10 DMC average of the z-component of the spin per particle as a function of the imaginary time step for $na^3 = 10^{-4}$, $\Omega = 2.9$ (stripe phase, top) and $\Omega = 3.1$ (plane wave phase, bottom), for the SS interaction. Notice that the values displayed for the stripe phase have largely been rescaled.

discontinuity in this parameter between the stripe and the other two phases at the transition, the optimal momentum changes continuously from the plane wave to the single minimum phase [25, 60]. We believe that the inclusion of correlations in the DTDMC calculation does not change the nature of any of these phase transitions.

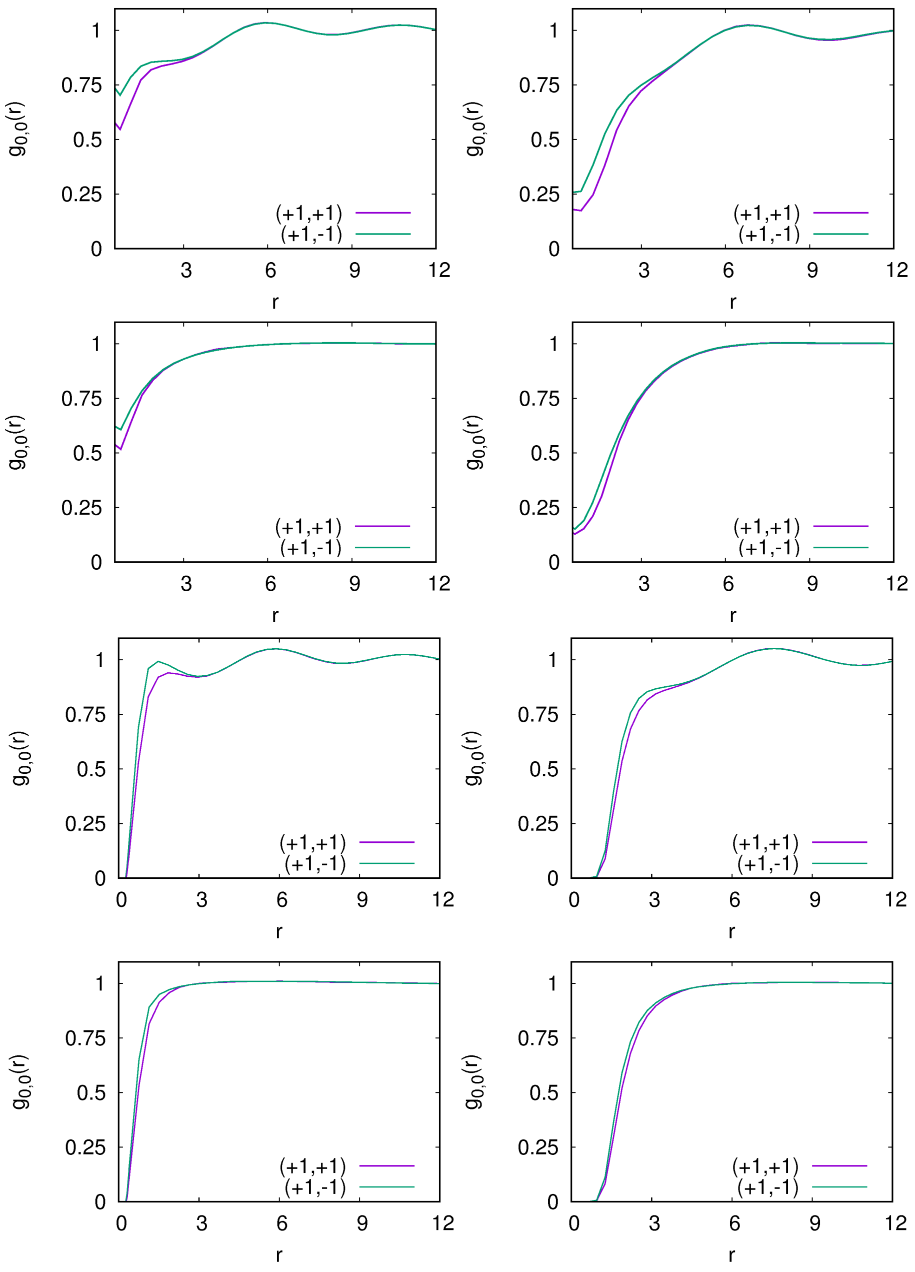

Fig. 3.11 Isotropic contribution to the pair distribution function for the $(+1,+1)$ and $(+1,-1)$ channels of the SS interaction (four top plots) and the LJ interaction (bottom plots). For each interaction, the two upper plots correspond to the stripe phase, while the bottom ones correspond to the plane wave phase. Left and right plots correspond to $na^3 = 10^{-3}$ and $na^3 = 10^{-2}$, respectively.

The presence of inter-atomic correlations can be seen in the pair distribution function, $g(\vec{r}_i - \vec{r}_j)$, which yields the probability of finding two particles with a relative position vector $\vec{r}_i - \vec{r}_j$. For an isotropic system, $g(\vec{r})$ depends on $|\vec{r}|$, while for a non-isotropic system, as it is the case of the stripe phase, an expansion in partial waves of the form $g(\vec{r}_i - \vec{r}_j) = \sum_{l,m} g_{l,m}(r_{ij}) Y_l^m(\theta, \phi)$ yields non-zero contributions for

$l > 0$. Notice that, in this expression, θ is the angle formed by $\vec{r}$ and the x-axis, while the stripes are formed along planes perpendicular to that direction. The short range behaviour of the pair distribution function depends on the specific model potential employed, and is also sensitive to the gas parameter of the system. In order to illustrate this, we report in Fig. 3.11 the isotropic mode ($l = 0$) for the plane wave and stripe phases, for both the SS and LJ interactions, and for two different values of the gas parameter $na^3 = (10^{-2}, 10^{-3})$. In the figures, $g_{0,0}(r)$ is normalized such that $\lim_{r\to\infty} g_{0,0}(r) = 1$ for all spin channels. As can be seen from the Figure, an increase of the gas parameter leads to lower values of $g_{0,0}(r)$ at short distances for both phases and model potentials, which is the result of the stronger repulsion induced by the interaction. The Figure also shows that the pair distribution function of the LJ interaction approaches zero at short inter-particle distances, while this is not the case for the SS interaction. This is a consequence of the infinite repulsion of the LJ potential as $r \to 0$. Remarkably, $g_{0,0}(r)$ is sensitive to the different spatial symmetries present between the plane wave and stripe phases, since small oscillations can be seen in the stripe case. These oscillations are induced by the periodic density modulations of the stripes. As mentioned, the two phases are clearly distinguished when looking at the leading correction to the isotropic mode, which is reported in Fig. 3.12, for $\Omega = 3.1$, $na^3 = 10^{-3}$. Only the $(+1, +1)$ component is reported since results for the other two-body channels are similar. The Figure depicts the $l = 2, m = 0$ modes for the SS interaction. It should be pointed out that, for the specific type of interactions used in this work, only the $m = 0$ contributions survive. As one can see, $g_{2,0}(r_{ij})$ is zero in the plane wave phase, while it yields a non-vanishing contribution in the stripe phase. This reflects the different spatial symmetries associated to each phase [25]. This quantity also vanishes for the single minimum phase. Very similar results hold for the LJ interaction.

Since in the stripe phase the x-axis is transverse to the stripe planes, the static structure factor along the x-direction, $S(k_x)$, develops a peak at a momentum proportional to the inverse of the characteristic distance separating the stripes, a feature also present at the Bogoliubov level [4]. We show in the upper panel of Fig. 3.13 the static structure factor $S(\vec{k})$ for conditions similar to the experiment of Ref. [2] ($\gamma = 0.904$, $\Omega = 0.3131$ and $na^3 = 5 \times 10^{-5}$). The lower panel shows the same quantities for $\Omega = 2.8$, where the stripe modulation is much more apparent due to the higher value of Ω compared to E_0. In accordance to that experiment, where reduced Raman coupling values lay in the interval $\Omega_{\text{exp}} \in [0,\ 0.4]$, we recover the stripe phase as the lowest energy state. The periodicity of the stripes has been quantitatively characterized before both in the mean field regime [25, 4] and in experiments [2]. The static structure factor does not show any peak in the plane wave and single minimum phases, a consequence of the lack of density modulations in these phases [25].

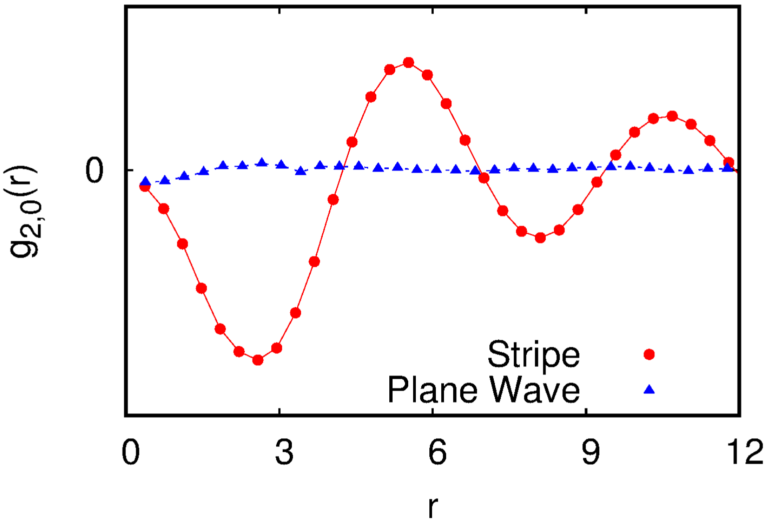

Fig. 3.12 Leading correction to the isotropic contribution of the pair distribution function in the $(+1, +1)$ channel, corresponding to $l = 2, m = 0$, for the SS interaction.

Next, we characterize the superfluidity of the system in the stripe phase, where other systems have shown a non-trivial dependence along different directions [47]. In order to recreate the conditions of contrast and diluteness of Ref. [2], we set $\gamma = 0.904$ and use gas parameters spanning the range $na^3 \in [5\times10^{-5},\ 2\times10^{-4}]$. We measure the superfluid density using the zero-temperature limit of the winding number estimator [67], which is extracted from the mean squared displacement of the center of mass of the particles during imaginary time evolution. The superfluid fraction along a given direction u is computed as [47]

$$\frac{\rho_s^u}{\rho} = \lim_{\tau\to\infty} \frac{N}{2\tau}\langle |u_{\text{c.m.}}(\tau) - u_{\text{c.m.}}(0)|^2\rangle \tag{3.148}$$

with $u_{\text{c.m.}} = \sum_{k=1}^{N} \frac{u_i}{N}$, $u = x,\ y,\ z$. The superfluid fraction is normalized such that it yields unity if a system is fully superfluid along a given direction. We show in Fig. 3.14 results for the superfluid fraction ρ_s^x in the stripe phase along the x direction as a function of Ω, and for three different values of the gas parameter, $na^3 = 5\times10^{-5}, 1\times10^{-4}$, and 2×10^{-4}. The reported values are close to those present in Ref. [49], obtained at the mean field level using the twisted phase method. We see from the plot that the main parameter governing changes in ρ_s^x is Ω, while little dependence on the specific value of the gas parameter is found. As Ω increases, the system becomes less superfluid in the x direction. This is a direct consequence of the fact that the amplitude of the density modulation increases with Ω, as already seen in mean field theory. For large values of Ω, exchanges of particles between different stripe planes are less favored, and thus localization along the x axis is enhanced. In the

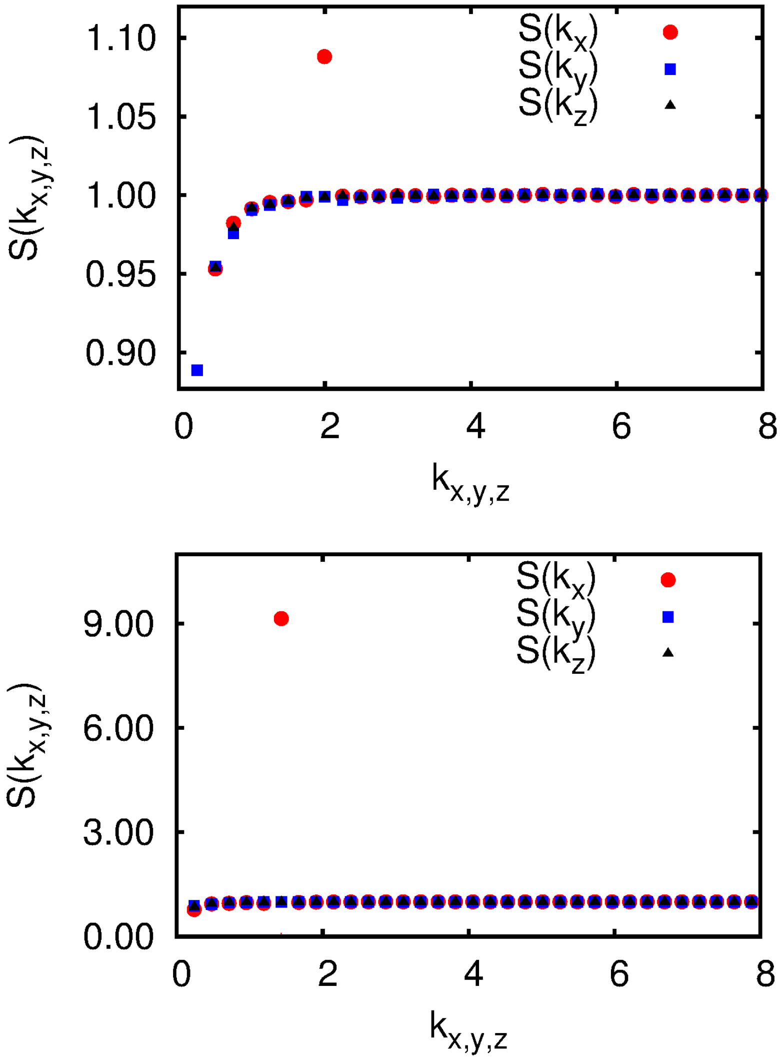

Fig. 3.13 Static structure factors for the SS interaction, for two different points with $na^3 = 5 \times 10^{-5}$ and $\gamma = 0.904$, both corresponding to the stripe phase. The upper and lower panels correspond to $\Omega = 0.3131$ and $\Omega = 2.8$, respectively.

other two directions, parallel to the stripe planes, the system remains fully superfluid ($\rho_s^y = \rho_s^z = 1$). Notice also that, for the values of Ω employed in the experiment of Ref. [2], the superfluid fraction ρ_s^x equals one. This, together with the periodic density modulations in the static structure factor reported in Fig. 3.13, yields a quantitative indication of simultaneous spatial periodicity and superfluidity in the system.

The superfluid fraction for the plane wave and single minimum phases has been obtained at the mean field level using the phase twist method [49] and in the Bogoliubov model through the evaluation of the transverse current operator [68]. In this case, the superfluidity along y and z equals unity, while ρ_x^s shows a dependence on the Raman coupling. We recover these results with DTDMC for the gas parameters mentioned previously by using the expression for the normal density of Ref. [68], replacing the

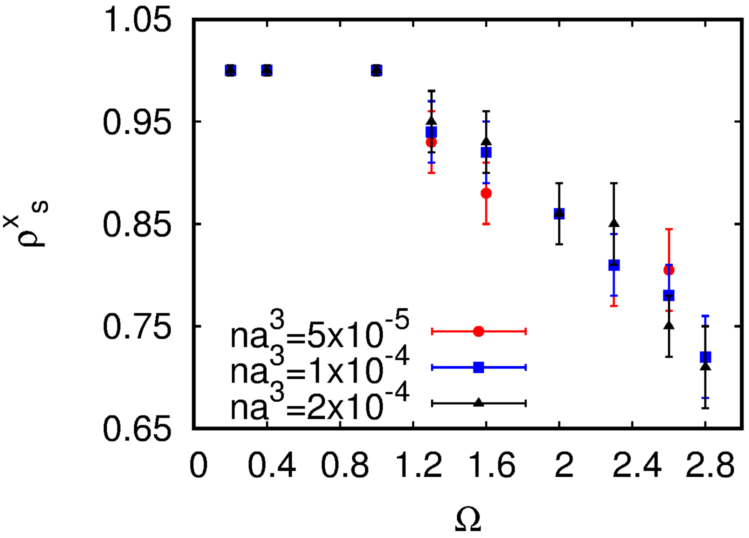

Fig. 3.14 Superfluid fraction along the direction transverse to the stripe planes, as a function of the reduced Raman coupling, for $na^3 = 5 \times 10^{-5}$ and $\gamma = 0.904$.

mean field value of $\langle \hat{\sigma}_x \rangle$ with the value obtained with DTDMC. For the plane wave phase, this corresponds to:

$$\frac{\rho_s^x}{\rho} = 1 - \frac{\Omega}{(2 - 2G_2)(2 - 2G_2 k_1)} \langle \hat{\sigma}_x \rangle \tag{3.149}$$

$$k_1 = \sqrt{1 - \frac{\Omega^2}{4(2 - 2G_2)^2}} \tag{3.150}$$

while for the single minimum phase, we have:

$$\frac{\rho_s^x}{\rho} = 1 - \frac{4}{\Omega - 4G_2} \langle \hat{\sigma}_x \rangle \tag{3.151}$$

where $G_2 = 8\pi n(a_{+1,+1} - a_{+1,-1})/4$ and all quantities are expressed in reduced units. The difference in sign of the terms proportional to $\langle \hat{\sigma}_x \rangle$ with respect to the expressions reported in Ref. [68] account for the different sign of the term proportional to Ω in Eq. (3.3).

Finally, we report the one-body density matrix of the system, $\rho(\vec{r}_i - \vec{r}_i')$, defined as:

$$\rho(\vec{r} - \vec{r}') = \frac{\sum_{\vec{S}} \int d\vec{R}_{N-1} \; \Psi^*(\vec{r}, \vec{R}_{N-1}, \vec{S}) \Psi(\vec{r}', \vec{R}_{N-1}, \vec{S})}{\langle \Psi | \Psi \rangle} \; . \tag{3.152}$$

Here, $\vec{R}_{N-1}$ stands for the position vector of an $N-1$ particle system. As other quantities, this function presents in general both radial and angular dependences, although for isotropic systems the latter is missing. However, the condensate fraction of the system is obtained from the long distance value of the s-wave component of

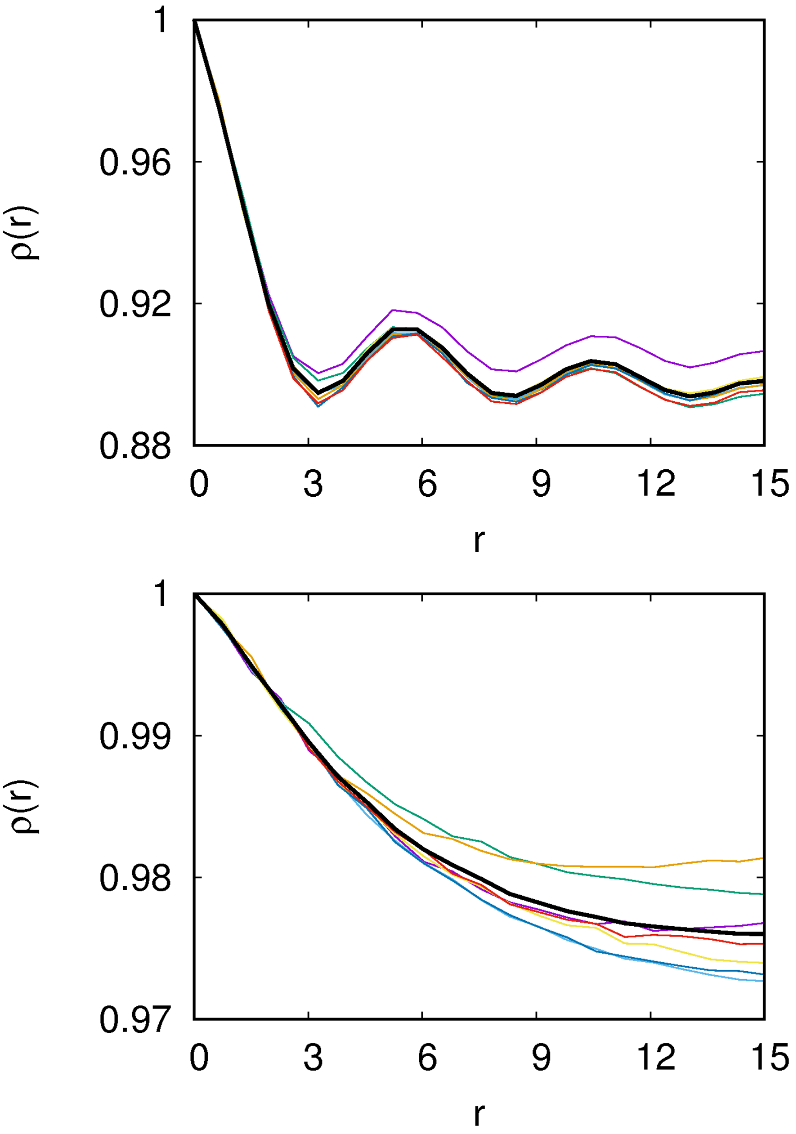

Fig. 3.15 Several realizations of the one-body density matrix and its average (wider line) for the stripe (upper plot, $\Omega = 3.1$, $na^3 = 10^{-3}$) and plane wave (lower plot, $\Omega = 3.3$, $na^3 = 10^{-3}$) phases. γ is set to $\gamma = 0.4$.

$\rho(\vec{r} - \vec{r}')$ [47]. Thus, we show in Fig. 3.16 the isotropic contribution to the one-body density matrix for the plane wave and stripe trial wave functions. Results for the single minimum are not reported as they are qualitatively equivalent to those of the plane wave phase. For the stripe case these are calculated at $\{\Omega, na^3\}$ equal to $\{2.4,\ 10^{-4}\}$ and $\{3.1,\ 10^{-3}\}$, while for the plane wave case these are computed at $\{\Omega, na^3\} = \{3.1,\ 10^{-4}\}$ and $\{3.3,\ 10^{-3}\ \}$. In all cases, the two-body interaction is of SS type. In order to obtain the data shown in Fig. 3.16 we have averaged the s-wave component of $\rho(\vec{r})$ obtained from seven realizations of the simulation. We show in Fig. 3.15 some of these realization and its average for both the stripe and plane wave cases at $\{\Omega = 3.1,\ na^3 = 10^{-3}\}$ and $\{\Omega = 3.3,\ na^3 = 10^{-3}\}$ respectively. In order to obtain a condensate fraction for the stripe phase, we take the value of the one-body density matrix at the highest possible $|\vec{r}|$ and incorporate an errorbar which accounts for the small oscillations. Looking at Fig. 3.16 we can see that the stripe phase has always a lower condensate fraction than the plane wave phase. We can also see how the condensate fraction on both phases decreases as the gas parameter increases, which is already expected. Finally, notice how $\rho(r)$ shows marked oscillations in the stripe phase. This is caused by the periodicity of the stripes.

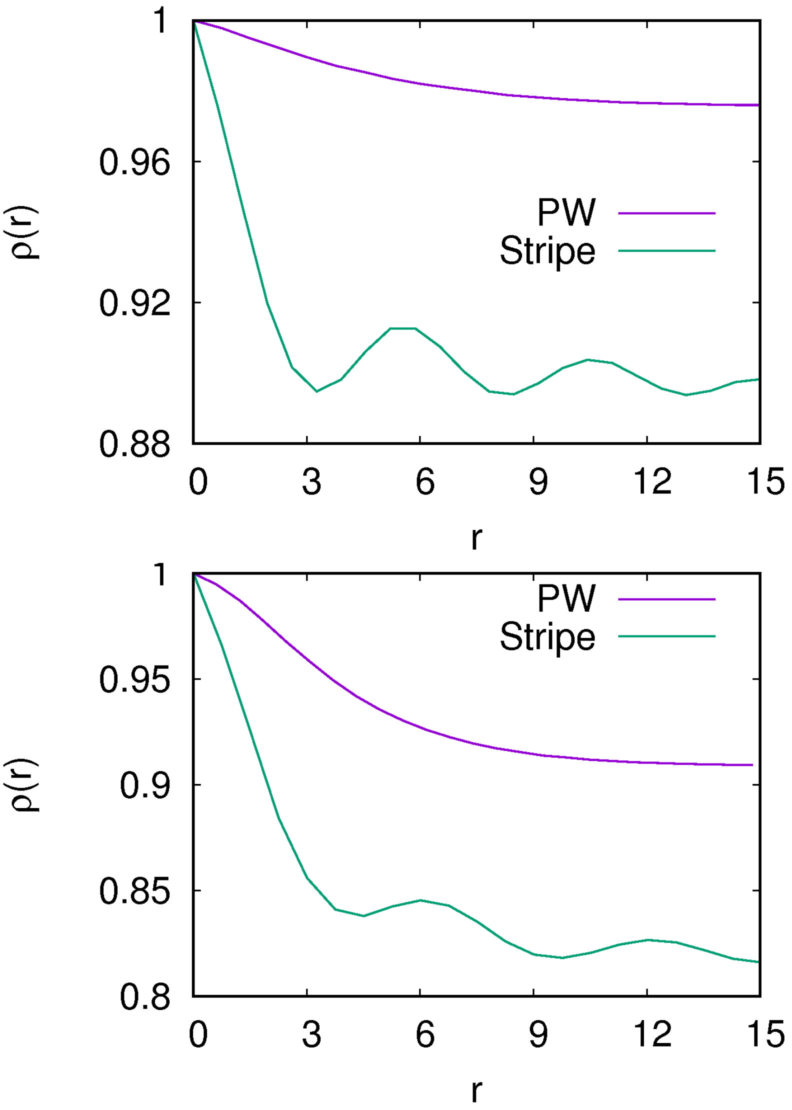

Fig. 3.16 One-body density matrix for the stripe and plane wave phases. The upper plot corresponds to $\Omega = 3.3$ and $na^3 = 10^{-3}$, while the lower plot corresponds to $\Omega = 3.5$ and $na^3 = 10^{-2}$. $\gamma = 0.4$ in both cases.

Chapter 4

Beyond Mean Field Effects in Raman Spin-Orbit Coupled Systems

4.1 Introduction

As stated in Chapter 1, despite the large number of experiments accurately described by mean field theories, these approaches have some limitations. On one hand, they are unable to account for inter-atomic correlations for large enough gas parameters. On the other hand, one can find some examples of systems for which the mean field approximation predicts a collapse while experiments do not show so. This is the case for dipolar systems in three dimensions [9, 10] and ultra-dilute unstable Bose-Bose mixtures [35, 37, 36]. In this context, it is necessary to account for correlations at a higher order in order to provide a quantitatively accurate description of the many-body system. The first correction to the mean field prediction can be obtained by following Beyond Mean Field prescriptions. In this context, a system is modeled as a mostly populated BEC with a small fraction of particles excited out of the condensate due to the effect of interactions. These approaches can not account for inter-atomic correlations at the same level as Monte Carlo methods, but have the advantage of being generally of much lower computational cost, and the ability to simulate arbitrarily large systems. On top of this, the only parameter to be considered from interactions is the scattering length, which means that the results obtained from Beyond Mean Field calculations are independent of the details of the potential, so they are universal. While for non-SOC systems, Beyond Mean Field methods are strictly less accurate than Monte Carlo methods, in the case of SOC systems they are complementary. While, as previously mentioned, Monte Carlo methods account for inter-atomic correlations exactly, they resort to the fixed phase approximation, whereas this is not the case with Beyond Mean Field techniques. We present in this Chapter a review of the theoretical framework needed to include beyond mean field terms in Raman Spin-Orbit

Coupling systems. We discuss two approaches: a matrix variation [3] of the standard Bogoliubov formalism. [69] (see Sec. 4.2), and the Bogoliubov-de Gennes method [70] (see Sec. 4.3). We first recover the known results for a non-SOC system and then extend both formalisms to the Raman SOC case, for all the stripe, plane wave and single minimum phases. We obtain, for the first time, the Lee-Huang-Yang (LHY) correction for the stripe phase of a Raman SOC system. Afterwards, we present an application of this calculation: we study how the beyond mean field energy correction stabilizes a Raman SOC system in the stripe phase that is unstable at the mean field level (see Sec. 4.4). The mean field instability in this system is induced by an attractive inter-spin interaction. We characterize the phases that emerge in the system stabilized by the beyond mean field effects, also known as quantum fluctuations: the gas and the liquid phases. We also show that the stabilized system admits droplet-like solutions that feature a striped density pattern, which we call supersolid striped droplets.

Through all this Chapter, the SOC Hamiltonian is defined as:

$$\hat{H}_{\mathrm{SOC}} = \sum_{k=1}^{N} \left[\frac{\hat{P}_k^2}{2M} + \hat{W}_k^{\mathrm{SOC}} \right] + \sum_{\substack{k,j=1 \\ k<j}}^{N} \hat{V}_{k,j}^{\mathrm{2b}} \ , \tag{4.1}$$

with N the number of particles enclosed in a volume V. Through this Section, we use M to denote the mass instead of m, since the letter m is employed as a summation index in several expressions. The potentials are given by:

$$\hat{W}_k^{\mathrm{SOC}} = \frac{\lambda\hbar}{M}\hat{P}_k^x\hat{\sigma}_k^z + \frac{\lambda^2\hbar^2}{2M} - \frac{\Omega}{2}\hat{\sigma}_k^x \tag{4.2}$$

$$V_{k,j}^{\mathrm{2b}}\left(\vec{r}_k,\vec{r}_j,s_k,s_j\right) = \frac{4\pi\hbar^2 a_{s_k,s_j}}{M}\delta\left(\vec{r}_k-\vec{r}_j\right) \ , \tag{4.3}$$

with a_{s_k,s_j} the spin-dependent scattering length, which fulfills $a_{+1,-1} = a_{-1,+1}$. We set $a_{+1,+1} = a_{-1,-1}$. We define the parameter $\gamma = (a_{+1,+1} - a_{+1,-1})/(a_{+1,+1} + a_{+1,-1})$, which accounts for the contrast of the two-body spin-dependent interaction. All results are reported in reduced units. We chose the length and energy scales to be:

$$a_0 = \frac{1}{\lambda} \ , \ \epsilon_0 = \frac{\hbar^2}{2Ma_0^2} = \frac{\hbar^2\lambda^2}{2M} \ . \tag{4.4}$$

which correspond to the length and energy scales chosen in Chapter 3 with $\eta_{\mathrm{Rm.}} = 1$. The non-SOC Hamiltonian reads:

$$\hat{H}_{\text{no-SOC}} = \sum_{k=1}^{N} \frac{\hat{P}_k^2}{2M} + \sum_{\substack{k,j=1 \\ k<j}}^{N} \frac{4\pi\hbar^2 a}{M}\delta\left(\vec{r}_k-\vec{r}_j\right) \ . \tag{4.5}$$

In second quantization, any Hamiltonian $\hat{H}$ composed by the sum of one-body terms $\hat{H}_0$ and a local two-body interaction $\hat{V}$ can be written as [69]:

$$\hat{H} = \int d\vec{r}_1 d\vec{r}_2 \hat{\Psi}^\dagger\left(\vec{r}_1\right) \langle \vec{r}_1 | \, \hat{H}_0 \, | \vec{r}_2 \rangle \, \hat{\Psi}\left(\vec{r}_2\right) + \frac{1}{2} \int d\vec{r}_1 d\vec{r}_2 \hat{\Psi}^\dagger\left(\vec{r}_1\right) \hat{\Psi}^\dagger\left(\vec{r}_2\right) V\left(\vec{r}_1, \vec{r}_2\right) \hat{\Psi}\left(\vec{r}_1\right) \hat{\Psi}\left(\vec{r}_2\right) \ , \tag{4.6}$$

where $\hat{\Psi}\left(\vec{r}\right)$ stands for to the field operator.

4.2 Matrix formulation of the standard Bogoliubov formalism

4.2.1 Non-SOC case

The first steps to follow within this approach are analogous to the ones in Ref. [69]. We expand the field operator in eigenstates of the momentum operator:

$$\hat{\Psi}\left(\vec{r}\right) = \sum_{\vec{k}} \frac{1}{\sqrt{V}} e^{i\vec{k}\vec{r}} \hat{a}_{\vec{k}} \tag{4.7}$$

with $\hat{a}_{\vec{k}}$ the annihilation operator of momentum $\vec{k}$. We assume that the state of our system lies close to the mean field regime, i.e. the number of particles occupying the zero momentum state is orders of magnitude larger than the population of the $\vec{k} \neq 0$ states. We denote by N_0 the population of the condensate (zero momentum state in this case). This assumption allows us to treat the creation and annihilation operators of the zero-momentum state as complex numbers, i.e., $\hat{a}_0 \sim \hat{a}_0^\dagger \sim \sqrt{N_0}$ Expanding the Hamiltonian of the system in terms of the creation and annihilation operators yields [69]:

$$\hat{H} = \sum_{\vec{k} \neq 0} \frac{\hbar^2 k^2}{2M} \hat{a}_{\vec{k}}^\dagger \hat{a}_{\vec{k}} + \frac{2\pi\hbar^2 a}{MV} \sum_{\vec{q}_1, \vec{q}_2, \vec{k}} \hat{a}_{\vec{q}_1 - \vec{k}}^\dagger \hat{a}_{\vec{q}_2 + \vec{k}}^\dagger \hat{a}_{\vec{q}_1} \hat{a}_{\vec{q}_2} \tag{4.8}$$

where the momentum indexes of the two-body potential reflect the momentum conservation on a collision of particles, a consequence of the dependence of the two-body interaction on the relative distance between particles only. We now expand this expression in powers of $N_0^{1/2}$ and keep only the main contributions of the two-body interaction up to $\mathcal{O}(N_0)$, which results into:

$$\hat{H} = \sum_{\vec{k} \neq 0} \frac{\hbar^2 k^2}{2M} \hat{a}_{\vec{k}}^\dagger \hat{a}_{\vec{k}} + \frac{2\pi\hbar^2 a}{MV} \left[N_0^2 + 4N_0 \sum_{\vec{k} \neq 0} \hat{a}_{\vec{k}}^\dagger \hat{a}_{\vec{k}} + N_0 \sum_{\vec{k} \neq 0} \left(\hat{a}_{\vec{k}} \hat{a}_{-\vec{k}} + \hat{a}_{\vec{k}}^\dagger \hat{a}_{-\vec{k}}^\dagger \right) \right] \tag{4.9}$$

At the mean field level, we retain only the largest power in N_0 and consider that only the zero-momentum state is occupied, i.e. $N = N_0$, which yields the known result:

$$E_{\mathrm{MF}} = \frac{2\pi\hbar^2 a N^2}{MV} \tag{4.10}$$

In order to incorporate beyond mean field corrections, we must first discuss the conservation of the number of particles. Because of the dropped contributions to the two-body part of the exact Hamiltonian, the approximated Hamiltonian no longer commutes with the total number operator [71] $\hat{N} = \sum_{\vec{k}} \hat{a}^\dagger_{\vec{k}} \hat{a}_{\vec{k}} = N_0 + \delta\hat{N}$. In order to solve this issue, we work in the grand-canonical ensemble. By doing so, we recover the eigenvalues and eigenstates of Ref. [69]. The grand-canonical Hamiltonian, $\hat{K} = \hat{H} - \mu\hat{N}$ reads, up to $\mathcal{O}(N_0)$

$$\hat{K} = \sum_{\vec{k}\neq 0} \frac{\hbar^2 k^2}{2M} \hat{a}^\dagger_{\vec{k}} \hat{a}_{\vec{k}} + \frac{2\pi\hbar^2 a}{MV} \left[N_0^2 + 4N_0 \sum_{\vec{k}\neq 0} \hat{a}^\dagger_{\vec{k}} \hat{a}_{\vec{k}} + N_0 \sum_{\vec{k}\neq 0} \left(\hat{a}_{\vec{k}} \hat{a}_{-\vec{k}} + \hat{a}^\dagger_{\vec{k}} \hat{a}^\dagger_{-\vec{k}} \right) \right] - \mu N_0 - \mu \sum_{\vec{k}\neq 0} \hat{a}^\dagger_{\vec{k}} \hat{a}_{\vec{k}} \tag{4.11}$$

with μ the chemical potential and $\hat{N} = \sum_{\vec{k}} \hat{a}^\dagger_{\vec{k}} \hat{a}_{\vec{k}} = N_0 + \sum_{\vec{k}\neq 0} \hat{a}^\dagger_{\vec{k}} \hat{a}_{\vec{k}}$. The chemical potential is obtained as the eigenvalue of the time-independent Gross-Pitaevskii equation (tiGPE). For an homogeneous gas, the solution of the tiGPE is a constant wave function with eigenvalue

$$\mu = \frac{4\pi\hbar^2 a N_0}{MV} \ , \tag{4.12}$$

so upon substitution in the previous equation, the grand-canonical Hamiltonian becomes:

$$\hat{K} = \sum_{\vec{k}\neq 0} \frac{\hbar^2 k^2}{2M} \hat{a}^\dagger_{\vec{k}} \hat{a}_{\vec{k}} + \frac{2\pi\hbar^2 a}{MV} \left[2N_0 \sum_{\vec{k}\neq 0} \hat{a}^\dagger_{\vec{k}} \hat{a}_{\vec{k}} + N_0 \sum_{\vec{k}\neq 0} \left(\hat{a}_{\vec{k}} \hat{a}_{-\vec{k}} + \hat{a}^\dagger_{\vec{k}} \hat{a}^\dagger_{-\vec{k}} \right) \right] + \frac{2\pi\hbar^2 a N_0^2}{MV} - \mu N_0 \tag{4.13}$$

We can rewrite the sum over momenta as a sum running over $k_x > 0$ only, so that the grand-canonical Hamiltonian reads

$$\begin{aligned} \hat{K} = \sum_{k_x>0} \left(\frac{\hbar^2 k^2}{2M} + \frac{4\pi\hbar^2 a N_0}{MV} \right) \left(\hat{a}^\dagger_{\vec{k}} \hat{a}_{\vec{k}} + \hat{a}^\dagger_{-\vec{k}} \hat{a}_{-\vec{k}} \right) + \frac{4\pi\hbar^2 a N_0}{MV} \sum_{k_x>0} \left(\hat{a}_{\vec{k}} \hat{a}_{-\vec{k}} + \hat{a}^\dagger_{\vec{k}} \hat{a}^\dagger_{-\vec{k}} \right) \\ + \frac{2\pi\hbar^2 a N_0^2}{MV} - \mu N_0 \end{aligned} \tag{4.14}$$

We now proceed to diagonalize $\hat{K}$. We do so following the approach of Ref. [3]. We define:

$$\hat{\psi}_{\vec{k}} = \begin{pmatrix} \hat{a}_{\vec{k}} \\ \hat{a}^{\dagger}_{-\vec{k}} \end{pmatrix} \qquad \hat{\psi}^{\dagger}_{\vec{k}} = \begin{pmatrix} \hat{a}^{\dagger}_{\vec{k}} & \hat{a}_{-\vec{k}} \end{pmatrix} \tag{4.15}$$

and use them to write $\hat{K}$ in matrix form as:

$$\begin{aligned} \hat{K} &= \frac{2\pi\hbar^2 a N_0^2}{MV} - \mu N_0 + \sum_{k_x>0} \left[\hat{\psi}^{\dagger}_{\vec{k}} \begin{pmatrix} \frac{\hbar^2k^2}{2M} + \frac{4\pi\hbar^2 aN_0}{MV} & \frac{4\pi\hbar^2 aN_0}{MV} \\ \frac{4\pi\hbar^2 aN_0}{MV} & \frac{\hbar^2k^2}{2M} + \frac{4\pi\hbar^2 aN_0}{MV} \end{pmatrix} \hat{\psi}_{\vec{k}} - \frac{\hbar^2k^2}{2M} - \frac{4\pi\hbar^2 aN_0}{MV} \right] \\ &= \frac{2\pi\hbar^2 a N_0^2}{MV} - \mu N_0 + \sum_{k_x>0} \left[\hat{\psi}^{\dagger}_{\vec{k}} K_{\vec{k}} \hat{\psi}_{\vec{k}} - \frac{\hbar^2k^2}{2M} - \frac{4\pi\hbar^2 aN_0}{MV} \right] \end{aligned} \tag{4.16}$$

where we have used the commutation relation for boson operators, $[\hat{a}_{\vec{k}}\hat{a}^{\dagger}_{\vec{k}'}] = \delta_{\vec{k},\vec{k}'}$, to write

$$\sum_{k_x>0} \left(\frac{\hbar^2k^2}{2M} + \frac{4\pi\hbar^2 aN_0}{MV} \right) \hat{a}^{\dagger}_{-\vec{k}}\hat{a}_{-\vec{k}} = \sum_{k_x>0} \left(\frac{\hbar^2k^2}{2M} + \frac{4\pi\hbar^2 aN_0}{MV} \right) \hat{a}_{-\vec{k}}\hat{a}^{\dagger}_{-\vec{k}} - \frac{\hbar^2k^2}{2M} - \frac{4\pi\hbar^2 aN_0}{MV} \tag{4.17}$$

and we have defined

$$K_{\vec{k}} = \begin{pmatrix} \frac{\hbar^2k^2}{2M} + \frac{4\pi\hbar^2 aN_0}{MV} & \frac{4\pi\hbar^2 aN_0}{MV} \\ \frac{4\pi\hbar^2 aN_0}{MV} & \frac{\hbar^2k^2}{2M} + \frac{4\pi\hbar^2 aN_0}{MV} \end{pmatrix} \tag{4.18}$$

We want to diagonalize each one of the matrices $K_{\vec{k}}$, i.e. we want to find a vector of operators

$$\hat{\phi}_{\vec{k}} = \begin{pmatrix} \hat{b}_{\vec{k}} \\ \hat{b}^{\dagger}_{-\vec{k}} \end{pmatrix} \tag{4.19}$$

such that each matrix $K_{\vec{k}}$ can be written in diagonal form. This is equivalent to performing a Bogoliubov transformation. These vectors are related to the vectors $\hat{\psi}_{\vec{k}}$ defined in Eq. (4.15) by the transfer matrix $M_{\vec{k}}$, i.e.

$$\hat{\psi}_{\vec{k}} = M_{\vec{k}} \hat{\phi}_{\vec{k}} \ . \tag{4.20}$$

In this way, we can write

$$\begin{aligned}\hat{\psi}^{\dagger}_{\vec{k}}K_{\vec{k}}\hat{\psi}_{\vec{k}} - \frac{\hbar^2k^2}{2M} - \frac{4\pi\hbar^2aN_0}{MV} &= \hat{\phi}^{\dagger}_{\vec{k}}M^{\dagger}_{\vec{k}}K_{\vec{k}}M_{\vec{k}}\hat{\phi}_{\vec{k}} - \frac{\hbar^2k^2}{2M} - \frac{4\pi\hbar^2aN_0}{MV} \\ &= \hat{\phi}^{\dagger}_{\vec{k}}K_{d,\vec{k}}\hat{\phi}_{\vec{k}} - \frac{\hbar^2k^2}{2M} - \frac{4\pi\hbar^2aN_0}{MV} - E(-\vec{k}) + E(-\vec{k}) \\ &= E(-\vec{k})\hat{b}^{\dagger}_{-\vec{k}}\hat{b}_{-\vec{k}} + E(\vec{k})\hat{b}^{\dagger}_{\vec{k}}\hat{b}_{\vec{k}} - \frac{\hbar^2k^2}{2M} - \frac{4\pi\hbar^2aN_0}{MV} + E(-\vec{k}) \ ,\end{aligned} \tag{4.21}$$

with

$$K_{d,\vec{k}} = \begin{pmatrix} E(\vec{k}) & 0 \\ 0 & E(-\vec{k}) \end{pmatrix} = M^{\dagger}_{\vec{k}}K_{\vec{k}}M_{\vec{k}} \tag{4.22}$$

Here, $E(\vec{k})$ are the excitation spectrum energies. The commutation relation of the $\hat{a}_{\vec{k}}$, $\hat{a}^{\dagger}_{\vec{k}}$ operators can be written in matrix form as:

$$\hat{\psi}_{\vec{k}}\hat{\psi}^{\dagger}_{\vec{k}} - \left[\left(\hat{\psi}^{\dagger}_{\vec{k}}\right)^{\tau}\hat{\psi}^{\tau}_{\vec{k}}\right]^{\tau} = \tilde{I} = \begin{pmatrix} 1 & 0 \\ 0 & -1 \end{pmatrix} , \tag{4.23}$$

where τ indicates the transpose operation. It can be checked that:

$$\begin{aligned}\hat{\psi}_{\vec{k}}\hat{\psi}^{\dagger}_{\vec{k}} &= \begin{pmatrix} \hat{a}_{\vec{k}}\hat{a}^{\dagger}_{\vec{k}} & \hat{a}_{\vec{k}}\hat{a}_{-\vec{k}} \\ \hat{a}^{\dagger}_{-\vec{k}}\hat{a}^{\dagger}_{\vec{k}} & \hat{a}^{\dagger}_{-\vec{k}}\hat{a}_{-\vec{k}} \end{pmatrix} \\ \left[\left(\hat{\psi}^{\dagger}_{\vec{k}}\right)^{\tau}\hat{\psi}^{\tau}_{\vec{k}}\right]^{\tau} &= \begin{pmatrix} \hat{a}^{\dagger}_{\vec{k}}\hat{a}_{\vec{k}} & \hat{a}_{\vec{k}}\hat{a}_{-\vec{k}} \\ \hat{a}^{\dagger}_{-\vec{k}}\hat{a}^{\dagger}_{\vec{k}} & \hat{a}_{-\vec{k}}\hat{a}^{\dagger}_{-\vec{k}} \end{pmatrix}\end{aligned} \tag{4.24}$$

We want the $\hat{b}_{\vec{k}}$, $\hat{b}^{\dagger}_{\vec{k}}$ operators to be associated to the creation and annihilation of bosonic quasi-particles. Therefore, we impose

$$\begin{aligned}\hat{\phi}_{\vec{k}}\hat{\phi}^{\dagger}_{\vec{k}} - \left[\left(\hat{\phi}^{\dagger}_{\vec{k}}\right)^{\tau}\hat{\phi}^{\tau}_{\vec{k}}\right]^{\tau} &= \tilde{I} \\ \overline{M}_{\vec{k}}\hat{\psi}_{\vec{k}}\hat{\psi}^{\dagger}_{\vec{k}}\overline{M}^{\dagger}_{\vec{k}} - \left[\left(\overline{M}^{\dagger}_{\vec{k}}\right)^{\tau}\left(\hat{\psi}^{\dagger}_{\vec{k}}\right)^{\tau}\hat{\psi}^{\tau}_{\vec{k}}\overline{M}^{\tau}_{\vec{k}}\right]^{\tau} &= \tilde{I} \ ,\end{aligned} \tag{4.25}$$

where we have defined $\overline{M}_{\vec{k}} = M^{-1}_{\vec{k}}$. We now multiply both sides of Eq. (4.25) by $M_{\vec{k}}$ on the left and $M^{\dagger}_{\vec{k}}$ on the right, which results into

$$\hat{\psi}_{\vec{k}}\hat{\psi}^{\dagger}_{\vec{k}} - \left[\left(\hat{\psi}^{\dagger}_{\vec{k}}\right)^{\tau}\hat{\psi}^{\tau}_{\vec{k}}\right]^{\tau} = M_{\vec{k}}\tilde{I}M^{\dagger}_{\vec{k}} \ , \tag{4.26}$$

and thus, the matrix $M_{\vec{k}}$ must fulfill the condition

$$M_{\vec{k}}\tilde{I}M_{\vec{k}}^{\dagger} = \tilde{I} \ , \tag{4.27}$$

We can get an additional property of the $M_{\vec{k}}$ matrices from Eq. (4.27). If we multiply both sides of the Equation by $M_{\vec{k}}^{\dagger}\tilde{I}$ in the left and $\tilde{I}M_{\vec{k}}$ in the right we get

$$M_{\vec{k}}^{\dagger}\tilde{I}M_{\vec{k}}\tilde{I}M_{\vec{k}}^{\dagger}\tilde{I}M_{\vec{k}} = M_{\vec{k}}^{\dagger}\tilde{I}\tilde{I}\tilde{I}M_{\vec{k}} = M_{\vec{k}}^{\dagger}\tilde{I}M_{\vec{k}} \ . \tag{4.28}$$

By defining $A = M_{\vec{k}}^{\dagger}\tilde{I}M_{\vec{k}}$ we can write:

$$A\tilde{I}A = A \ , \tag{4.29}$$

Assuming that A^{-1} exists, we can write this expression in the form

$$\tilde{I}A = I \ , \tag{4.30}$$

which implies $A = \tilde{I}$. Therefore, $M_{\vec{k}}$ fulfills the relation

$$M_{\vec{k}}^{\dagger}\tilde{I}M_{\vec{k}} = \tilde{I} \tag{4.31}$$

This expression is useful when deriving the Bogoliubov amplitudes. Multiplying both sides of Eq. (4.22) by $M_{\vec{k}}\tilde{I}$ and using Eq. (4.27) we get:

$$M_{\vec{k}}\tilde{I}K_{d,\vec{k}} = \tilde{I}K_{\vec{k}}M_{\vec{k}} \ . \tag{4.32}$$

From Eq. (4.32) we can see that the columns of the matrix $M_{\vec{k}}$ correspond to the eigenvectors of $K_{\vec{k}}^{\text{eff}} = \tilde{I}K_{\vec{k}}$, while the eigenvalues are $E(\vec{k})$ and $-E(-\vec{k})$. We can compute the excitation spectrum and the Bogoliubov amplitudes following this prescription. The matrix to be diagonalized is:

$$K_{\vec{k}}^{\text{eff}} = \begin{pmatrix} \frac{\hbar^2 k^2}{2M} + \frac{4\pi\hbar^2 a N_0}{MV} & \frac{4\pi\hbar^2 a N_0}{MV} \\ -\frac{4\pi\hbar^2 a N_0}{MV} & -\frac{\hbar^2 k^2}{2M} - \frac{4\pi\hbar^2 a N_0}{MV} \end{pmatrix} \tag{4.33}$$

The eigenvalues $\epsilon_{\vec{k}}$ of $K_{\vec{k}}^{\text{eff}}$ are given by

$$\epsilon_{\vec{k}}^{\pm} = \pm\sqrt{\left(\frac{\hbar^2 k^2}{2M}\right)^2 + 2\left(\frac{\hbar^2 k^2}{2M}\right)\frac{4\pi\hbar^2 a N_0}{MV}} = \pm E(\pm\vec{k}) \ , \tag{4.34}$$

while its eigenvectors are given by

$$v^+ = \begin{pmatrix} 1 \\ -\xi_{\vec{k}} \end{pmatrix} \quad v^- = \begin{pmatrix} -\xi_{\vec{k}} \\ 1 \end{pmatrix} \quad \xi_{\vec{k}} = \frac{MV}{4\pi\hbar^2 aN_0}\left(\frac{\hbar^2 k^2}{2M} + \frac{4\pi\hbar^2 aN_0}{MV} - E(\vec{k})\right) , \tag{4.35}$$

The normalization of the eigenvectors is obtained from Eq. (4.31), i.e.

$$\begin{aligned} (v_1^+)^2 - (v_2^+)^2 &= 1 \\ (v_1^-)^2 - (v_2^-)^2 &= -1 \end{aligned} \tag{4.36}$$

Thus, the normalized eigenvectors are:

$$v^+ = \begin{pmatrix} \frac{1}{\sqrt{1-\xi_{\vec{k}}^2}} \\ -\frac{\xi_{\vec{k}}}{\sqrt{1-\xi_{\vec{k}}^2}} \end{pmatrix} \qquad v^- = \begin{pmatrix} -\frac{\xi_{\vec{k}}}{\sqrt{1-\xi_{\vec{k}}^2}} \\ \frac{1}{\sqrt{1-\xi_{\vec{k}}^2}} \end{pmatrix} \tag{4.37}$$

with the matrix $M_{\vec{k}}$ given by

$$M_{\vec{k}} = \begin{pmatrix} \frac{1}{\sqrt{1-\xi_{\vec{k}}^2}} & -\frac{\xi_{\vec{k}}}{\sqrt{1-\xi_{\vec{k}}^2}} \\ -\frac{\xi_{\vec{k}}}{\sqrt{1-\xi_{\vec{k}}^2}} & \frac{1}{\sqrt{1-\xi_{\vec{k}}^2}} \end{pmatrix} \tag{4.38}$$

In this way, we recover the eigenvalues and the Bogoliubov amplitudes of Ref. [69]. The lowest eigenvalue of the operator $\hat{K}$ corresponds to $\vec{k} = 0$ and can be inferred from Eqs. (4.16) and (4.21). It is given by:

$$K_0 = \frac{2\pi\hbar^2 aN_0^2}{MV} - \mu N_0 + \sum_{k_x>0}\left(-\frac{\hbar^2 k^2}{2M} - \frac{4\pi\hbar^2 aN_0}{MV} + E(-\vec{k})\right) , \tag{4.39}$$

Transforming the sum into an integral, we obtain

$$\begin{aligned} K_0 &= \frac{2\pi\hbar^2 aN_0^2}{MV} - \mu N_0 + \int_{k_x>0} d\vec{k}\frac{V}{(2\pi)^3}\left(-\frac{\hbar^2 k^2}{2M} - \frac{4\pi\hbar^2 aN_0}{MV} + E(-\vec{k})\right) \\ &= \frac{2\pi\hbar^2 aN_0^2}{MV} - \mu N_0 + \frac{V}{(2\pi)^2}\int_0^\infty dk k^2\left(-\frac{\hbar^2 k^2}{2M} - \frac{4\pi\hbar^2 aN_0}{MV} + E(-\vec{k})\right) \quad . \end{aligned} \tag{4.40}$$

The integral in Eq. (4.40) is divergent. This can be seen by computing the $k \to \infty$ limit of the integrand, which yields

$$
\begin{aligned}
&\lim_{k\to\infty} k^2\left(-\frac{\hbar^2k^2}{2M}-\frac{4\pi\hbar^2aN_0}{MV}+E(-\vec{k})\right)\\
&=\lim_{k\to\infty} k^2\left(-\frac{\hbar^2k^2}{2M}-\frac{4\pi\hbar^2aN_0}{MV}+\left(\frac{\hbar^2k^2}{2M}\right)\sqrt{1+2\left(\frac{4\pi\hbar^2aN_0}{MV}\right)\left(\frac{2M}{\hbar^2k^2}\right)}\right)\\
&=\lim_{k\to\infty} k^2\left(-\frac{\hbar^2k^2}{2M}-\frac{4\pi\hbar^2aN_0}{MV}+\left(\frac{\hbar^2k^2}{2M}\right)\left(1+\left(\frac{4\pi\hbar^2aN_0}{MV}\right)\left(\frac{2M}{\hbar^2k^2}\right)-\frac{1}{2}\left(\frac{4\pi\hbar^2aN_0}{MV}\right)^2\left(\frac{2M}{\hbar^2k^2}\right)^2\right)\right)\\
&=-\left(\frac{4\pi\hbar^2aN_0}{MV}\right)^2\left(\frac{M}{\hbar^2}\right)
\end{aligned}
\tag{4.41}
$$

i.e. the integrand tends to a constant. In order to regularize the integral, we apply Dimensional Regularization [72, 73]. We start by rewriting K_0 as:

$$
\begin{aligned}
K_0=\frac{2\pi\hbar^2aN_0^2}{MV}-\mu N_0+\frac{V}{(2\pi)^2}\int_0^\infty dk k^2\left(-\frac{\hbar^2k^2}{2M}-\frac{4\pi\hbar^2aN_0}{MV}+E(-\vec{k})\right.\\
\left.+\left(\frac{4\pi\hbar^2aN_0}{MV}\right)^2\left(\frac{M}{\hbar^2(k^2+c^2)}\right)\right)-\frac{1}{2}\frac{V}{(2\pi)^3}\int d\vec{k}\left(\frac{4\pi\hbar^2aN_0}{MV}\right)^2\left(\frac{M}{\hbar^2(k^2+c^2)}\right)\ .
\end{aligned}
\tag{4.42}
$$

where we have just added and subtracted to Eq. (4.40) the quantity $\int_{k_x>0} d\vec{k}\left(\frac{4\pi\hbar^2aN_0}{MV}\right)^2\left(\frac{M}{\hbar^2(k^2++c^2)}\right)$, with c a real parameter, and have also used that

$$
\int_{k_x>0} d\vec{k}\left(\frac{4\pi\hbar^2aN_0}{MV}\right)^2\left(\frac{M}{\hbar^2(k^2+c^2)}\right)=\frac{1}{2}\int d\vec{k}\left(\frac{4\pi\hbar^2aN_0}{MV}\right)^2\left(\frac{M}{\hbar^2(k^2+c^2)}\right)\ .
\tag{4.43}
$$

Now, the first integral of Eq. (4.42) is convergent for all values of c, while the second can be regularized via Dimensional Regularization.

In Dimensional Regularization, one first generalizes the integral to be regularized by turning the dimensionality of the space into a continuous variable. Afterwards, one computes it in the domain of the dimensionality where it converges. Finally, one performs the analytical continuation of the converged result, which can be shown to be unique [73] and provides the numerical value of the regularized integral at the dimensionality of interest, in our case $d = 3$. Let us illustrate this process. We want to regularize the second integral in Eq. (4.42),

$$I = \frac{1}{2}\frac{V}{(2\pi)^3}\int d\vec{k}\left(\frac{4\pi\hbar^2 aN_0}{MV}\right)^2\left(\frac{M}{\hbar^2(k^2+c^2)}\right) = \frac{V}{(2\pi)^3}\left(\frac{4\pi\hbar^2 aN_0}{MV}\right)^2\frac{M}{\hbar^2}\frac{4\pi}{2}\int_0^\infty dk\frac{k^2}{k^2+c^2}\ . \tag{4.44}$$

We now assume that the dimensionality of the space, d, is a continuous parameter. The generalized integral then becomes

$$I_d = \frac{V}{(2\pi)^3}\left(\frac{4\pi\hbar^2 aN_0}{MV}\right)^2\frac{M}{\hbar^2}\frac{S_d}{2}\int_0^\infty dk\frac{k^{d-1}}{k^2+c^2} = C_d\int_0^\infty dk\frac{k^{d-1}}{k^2+c^2} = C_d\tilde{I}_d\ . \tag{4.45}$$

with S_d the integral of the solid angle in d dimensions. Notice that I_d converges for $d \in [1,2]$. We can rewrite $\tilde{I}_d$ using the relation:

$$a^{-z} = \frac{1}{\Gamma(z)}\int_0^\infty dt\ t^{z-1}\exp(-at) \tag{4.46}$$

with $\Gamma(z)$ the Euler-Gamma function. This results into:

$$\begin{aligned}\tilde{I}_d &= \int_0^\infty dk\int_0^\infty dt\ k^{d-1}\exp\left(-t\left(k^2+c^2\right)\right)\\ &= \int_0^\infty dt\ \exp\left(-tc^2\right)\int_0^\infty dk\ k^{d-1}\exp\left(-tk^2\right)\ .\end{aligned} \tag{4.47}$$

We now perform the change of variables, $y = k^2$, to find

$$\begin{aligned}\tilde{I}_d &= \int_0^\infty dt\ \exp\left(-tc^2\right)\int_0^\infty dy\frac{1}{2\sqrt{y}}y^{(d-1)/2}\exp\left(-ty\right)\\ &= \frac{1}{2}\int_0^\infty dt\ \exp\left(-tc^2\right)\int_0^\infty dy\ y^{d/2-1}\exp\left(-ty\right)\\ &= \frac{1}{2}\Gamma\left(\frac{d}{2}\right)\int_0^\infty dt\ \exp\left(-tc^2\right)t^{-d/2}\\ &= \frac{c^{d-2}}{2}\Gamma\left(\frac{d}{2}\right)\Gamma\left(1-\frac{d}{2}\right)\ ,\ .\end{aligned} \tag{4.48}$$

We can now perform the analytical continuation of $\tilde{I}$ by using the well-known analytical continuation of the Gamma function, which extends $\Gamma(z)$ to $z < 0$. Notice that Eq. (4.48) involves positive arguments of the Gamma function for $d \in (1,2)$, the convergence interval of the unregularized integral. One can now obtain the regularized integral I by substituting $\tilde{I}_d$ in Eq. (4.44) and particularizing the result to $d = 3$.

$$I = \frac{V}{(2\pi)^2}\left(\frac{4\pi\hbar^2 aN_0}{MV}\right)^2\frac{M}{\hbar^2}\frac{c}{2}\Gamma\left(\frac{3}{2}\right)\Gamma\left(-\frac{1}{2}\right) \tag{4.49}$$

Substituting in Eq. (4.42) we write K_0 as

$$K_0 = \frac{2\pi\hbar^2 aN_0^2}{MV} - \mu N_0 + \frac{V}{(2\pi)^2}\int_0^\infty dkk^2 \left(-\frac{\hbar^2k^2}{2M} - \frac{4\pi\hbar^2 aN_0}{MV} + E(-\vec{k}) + \left(\frac{4\pi\hbar^2 aN_0}{MV}\right)^2 \left(\frac{M}{\hbar^2(k^2+c^2)}\right)\right) - \frac{V}{(2\pi)^2}\left(\frac{4\pi\hbar^2 aN_0}{MV}\right)^2 \frac{M}{\hbar^2}\frac{c}{2}\Gamma\left(\frac{3}{2}\right)\Gamma\left(-\frac{1}{2}\right) . \tag{4.50}$$

It must be remarked that the above result is independent of the chosen value of c. In particular, it can be shown in the framework of Dimensional Regularization, that for $c = 0$ one has [72]:

$$I = 0 \tag{4.51}$$

$$K_0 = \frac{2\pi\hbar^2 aN_0^2}{MV} - \mu N_0 + \frac{V}{(2\pi)^2}\int_0^\infty dkk^2 \left(-\frac{\hbar^2k^2}{2M} - \frac{4\pi\hbar^2 aN_0}{MV} + E(-\vec{k}) + \left(\frac{4\pi\hbar^2 aN_0}{MV}\right)^2 \left(\frac{M}{\hbar^2(k^2)}\right)\right) , \tag{4.52}$$

and the integration yields [69]

$$K_0 = \frac{2\pi\hbar^2 aN_0^2}{MV}\left(1 + \frac{128}{15\sqrt{\pi}}\sqrt{\frac{N_0}{V}a^3}\right) - \mu N_0 \tag{4.53}$$

However, this is the lowest eigenvalue of the grand-canonical Hamiltonian. In order to obtain the ground state energy of the system, we must obtain the lowest eigenvalue of the Hamiltonian.

$$\begin{aligned}
E_{\text{g.s.}} &= \frac{2\pi\hbar^2 aN_0^2}{MV}\left(1 + \frac{128}{15\sqrt{\pi}}\sqrt{\frac{N_0}{V}a^3}\right) - \mu N_0 + \mu N \\
&= \frac{2\pi\hbar^2 a(N_0 + \delta N -)^2}{MV}\left(1 + \frac{128}{15\sqrt{\pi}}\sqrt{\frac{N_0 + \delta N - \delta N}{V}a^3}\right) + \mu\delta N \\
&= \frac{2\pi\hbar^2 a(N - \delta N)^2}{MV}\left(1 + \frac{128}{15\sqrt{\pi}}\sqrt{\frac{N - \delta N}{V}a^3}\right) + \mu\delta N \\
&= \frac{2\pi\hbar^2 aN^2}{MV}\left(1 + \frac{128}{15\sqrt{\pi}}\sqrt{\frac{N - \delta N}{V}a^3}\right) - 2\delta N\frac{2\pi\hbar^2 a}{MV}\left(1 + \frac{128}{15\sqrt{\pi}}\sqrt{\frac{N - \delta N}{V}a^3}\right) + \mu\delta N
\end{aligned}$$

where $N = N_0 + \delta N$, with N the total number of particles in the system and δN the fraction of particles outside of the condensate. Using Eq. (4.12) and the fact that

$\mu\delta N = \delta N\frac{4\pi\hbar^2 aN}{MV} + \mathcal{O}\Big(\delta N^2\Big)$, we get

$$\frac{E_{\text{g.s.}}}{N} = \frac{2\pi\hbar^2 aN}{MV}\left(1+\frac{128}{15\sqrt{\pi}}\sqrt{\frac{N-\delta N}{V}a^3}\right) - 2\frac{\delta N}{N}\frac{2\pi\hbar^2 a}{MV}\left(\frac{128}{15\sqrt{\pi}}\sqrt{\frac{N-\delta N}{V}a^3}\right) . \tag{4.54}$$

By computing the condensate fraction, it can be shown that:

$$\frac{128}{15\sqrt{\pi}}\sqrt{\frac{N}{V}a^3} \sim \mathcal{O}\left(\frac{\delta N}{N}\right) \tag{4.55}$$

Therefore, one can write:

$$\frac{E_{\text{g.s.}}}{N} = \frac{2\pi\hbar^2 an}{M}\left(1+\frac{128}{15\sqrt{\pi}}\sqrt{na^3}\right) + \mathcal{O}\left(\left(\frac{\delta N}{N}\right)^2\right) . \tag{4.56}$$

where $n = N/V$ is the density. In this way, we have recovered the well-known Lee-Huang-Yang correction to the mean field energy.

4.2.2 Raman SOC case: Plane Wave and Single Minimum phases

We now present the application of the formalism introduced in the previous Section to a system under Raman SOC in the plane wave and single minimum phases [3], focusing on the computation of the excitation spectrum and the LHY energy correction to the mean field prediction. We start by expanding the field operator in terms of linear combinations of eigenstates of the one-body Hamiltonian

$$\hat{H}_{\text{SOC,1b}} = \frac{\hat{P}^2}{2M} + \frac{\lambda\hbar}{M}\hat{P}^x\hat{\sigma}^z + \frac{\lambda^2\hbar^2}{2M} - \frac{\Omega}{2}\hat{\sigma}_x \tag{4.57}$$

Therefore, we write the field operator as

$$\hat{\Psi}\left(\vec{r}\right) = \sum_{\vec{k},d}\frac{1}{\sqrt{V}}\exp\left(i\vec{k}\vec{r}\right)\hat{a}_{\vec{k},d}\left|d(\vec{k})\right\rangle \tag{4.58}$$

where $\vec{k}$ denotes the momentum and $d = \pm 1$ denotes the branch index, since the excitation spectrum of the system has two distinct branches due to the spin degrees of freedom. Furthermore (see Chapter 2):

$$\left|d=+1(\vec{k})\right\rangle = \sin\theta\left|\tilde{\uparrow}\right\rangle_{\vec{k}} + \cos\theta\left|\tilde{\downarrow}\right\rangle_{\vec{k}} \tag{4.59}$$

$$\left|d=-1(\vec{k})\right\rangle = -\cos\theta\left|\tilde{\uparrow}\right\rangle_{\vec{k}} + \sin\theta\left|\tilde{\downarrow}\right\rangle_{\vec{k}} \tag{4.60}$$

$$\left|\tilde{\uparrow}\right\rangle_{\vec{k}} = \sin\chi_k\left|+1\right\rangle + \cos\chi_k\left|-1\right\rangle \tag{4.61}$$

$$\left|\tilde{\downarrow}\right\rangle_{\vec{k}} = -\cos\chi_k\left|+1\right\rangle + \sin\chi_k\left|-1\right\rangle \tag{4.62}$$

$$\sin\chi_k = \sqrt{\frac{1-\sin\theta_k}{2}} \tag{4.63}$$

$$\cos\chi_k = \sqrt{\frac{1+\sin\theta_k}{2}} \tag{4.64}$$

$$\sin\theta_k = \frac{(2\hbar^2\lambda k_x)/(\Omega M)}{\sqrt{1+\left((2\hbar^2\lambda k_x)/(\Omega M)\right)^2}} \tag{4.65}$$

Here, $\exp\left(i\vec{k}\vec{r}\right)\left|\tilde{\uparrow}\right\rangle_{\vec{k}}$ and $\exp\left(i\vec{k}\vec{r}\right)\left|\tilde{\downarrow}\right\rangle_{\vec{k}}$ are the eigenstates of the one-body Hamiltonian of Eq. (4.57), obtained in Chapter 2. Therefore, the states $\exp\left(i\vec{k}\vec{r}\right)\left|d=\pm1(\vec{k})\right\rangle$ that appear in Eq. (4.58) correspond to linear combinations of these eigenstates. The states $|\pm1\rangle$ appearing in Eqs. (4.61) and (4.62) are the eigenstates of the $\hat{\sigma}_z$ operator. We assume that the condensation state is $\exp\left(i\vec{k}_0\vec{r}\right)\left|d=-1(\vec{k}_0)\right\rangle$. The values for θ and $\vec{k}_0$ (the ground state momentum) will be obtained by diagonalizing the Hamiltonian in second quantization up to $\mathcal{O}\left(N_0^{3/2}/V\right)$ and minimizing its lowest eigenvalue. This procedure leads to the same condensate wave function as that of Ref. [25]. We can express the states $|d=\pm1\rangle_{\vec{k}}$ in terms of $|\pm1\rangle$ as:

$$\left|d=+1(\vec{k})\right\rangle = -\cos\alpha_k\left|+1\right\rangle + \sin\alpha_k\left|-1\right\rangle \tag{4.66}$$

$$\left|d=-1(\vec{k})\right\rangle = -\sin\alpha_k\left|+1\right\rangle - \cos\alpha_k\left|-1\right\rangle \tag{4.67}$$

with $\alpha_k = \theta + \chi_k$. We now write the Hamiltonian of the system in second quantization, starting with the one-body terms. These are given by:

$$\begin{aligned}\int d\vec{r}_1 d\vec{r}_2 \hat{\Psi}^\dagger(\vec{r}_1)\left\langle\vec{r}_1\right|\hat{H}_0\left|\vec{r}_2\right\rangle\hat{\Psi}(\vec{r}_2) &= \int d\vec{r}_1 d\vec{r}_2 \sum_{\vec{k},\vec{k}',d,d'} \hat{a}^\dagger_{\vec{k},d}\hat{a}_{\vec{k}',d'} e^{-i\vec{k}\vec{r}_1}\left\langle d(\vec{k})\right|\left\langle\vec{r}_1\right|\hat{H}_0\left|\vec{r}_2\right\rangle\left|d'(\vec{k}')\right\rangle e^{i\vec{k}'\vec{r}_2} \\ &= \sum_{\vec{k},d,d'} \hat{a}^\dagger_{\vec{k},d'}\hat{a}_{\vec{k},d} E_{1\mathrm{b}}(\vec{k},d,d')\end{aligned} \tag{4.68}$$

where:

$$E_{1\mathrm{b}}(\vec{k},+1,+1)=\sin^2\theta\ E_{1\mathrm{b}}(\vec{k},\tilde{\uparrow})+\cos^2\theta\ E_{1\mathrm{b}}(\vec{k},\tilde{\downarrow}) \tag{4.69}$$

$$E_{1\mathrm{b}}(\vec{k},-1,-1)=\cos^2\theta\ E_{1\mathrm{b}}(\vec{k},\tilde{\uparrow})+\sin^2\theta\ E_{1\mathrm{b}}(\vec{k},\tilde{\downarrow}) \tag{4.70}$$

$$E_{1\mathrm{b}}(\vec{k},+1,-1)=E_{1\mathrm{b}}(\vec{k},-1,+1)=\sin\theta\cos\theta(-E_{1\mathrm{b}}(\vec{k},\tilde{\uparrow})+E_{1\mathrm{b}}(\vec{k},\tilde{\downarrow}))\ , \tag{4.71}$$

where we have used the fact that the states $e^{i\vec{k}\vec{r}}\left|\tilde{\updownarrow}\right\rangle_{\vec{k}}$ are eigenstates of $\hat{H}_0$ corresponding to an energy $E_{1\mathrm{b}}(\vec{k},\tilde{\updownarrow})$ and that they are orthogonal to each other (see Chapter 2). The two-body terms are given by:

$$\begin{aligned}&\frac{1}{2}\int d\vec{r}_1 d\vec{r}_2 \hat{\Psi}^\dagger(\vec{r}_1)\,\hat{\Psi}^\dagger(\vec{r}_2)\,V(\vec{r}_1,\vec{r}_2)\,\hat{\Psi}(\vec{r}_1)\,\hat{\Psi}(\vec{r}_2)=\\&\frac{2\pi\hbar^2}{MV}\sum_{\substack{\vec{q}_1,\vec{q}_2,\vec{k}\\ d_1,d_2\\ d_1',d_2'}}\left[\sum_{s_A,s_B} a_{s_A,s_B}\,\langle d_1'(\vec{q}_1-\vec{k})|s_A\rangle\,\langle d_2'(\vec{q}_1+\vec{k})|s_B\rangle\,\langle s_A|d_1(\vec{q}_1)\rangle\,\langle s_B|d_2(\vec{q}_2)\rangle\right]\\&\times\hat{a}^\dagger_{d_1',\vec{q}_1-\vec{k}}\hat{a}^\dagger_{d_2',\vec{q}_2+\vec{k}}\hat{a}_{d_1,\vec{q}_1}\hat{a}_{d_2,\vec{q}_2}\end{aligned} \tag{4.72}$$

where $|s_{A,B}=\pm1\rangle$ are the eigenstates of the $\hat{\sigma}_z$ operator. We have followed the same steps as in [69] to express the two-body interaction in terms of the creation and annihilation operators. Assuming that the condensation state is macroscopically occupied, we can write $\hat{a}_{-1,\vec{k}_0}\sim\sqrt{N_0}$. We now retain the two-body contributions up to $\mathcal{O}\Big(N_0\sqrt{N_0}/V\Big)$:

$$\begin{aligned}&\frac{1}{2}\int d\vec{r}_1 d\vec{r}_2 \hat{\Psi}^\dagger(\vec{r}_1)\,\hat{\Psi}^\dagger(\vec{r}_2)\,V(\vec{r}_1,\vec{r}_2)\,\hat{\Psi}(\vec{r}_1)\,\hat{\Psi}(\vec{r}_2)\simeq\\&N_0^2\frac{2\pi\hbar^2}{MV}\sum_{s_A,s_B}a_{s_A,s_B}\left|\Big\langle -1(\vec{k}_0)\Big|s_A\Big\rangle\right|^2\left|\Big\langle s_B\Big|-1(\vec{k}_0)\Big\rangle\right|^2\\&+N_0\sqrt{N_0}\frac{4\pi\hbar^2}{MV}\sum_{s_A,s_B}a_{s_A,s_B}\left|\Big\langle -1(\vec{k}_0)\Big|s_A\Big\rangle\right|^2\Big\langle -1(\vec{k}_0)\Big|s_B\Big\rangle\Big\langle s_B\Big|+1(\vec{k}_0)\Big\rangle\Big(\hat{a}_{+1,\vec{k}_0}+\hat{a}^\dagger_{+1,\vec{k}_0}\Big)\end{aligned} \tag{4.73}$$

where we have used that the products $\Big\langle d(\vec{k})\Big|s\Big\rangle$ are real. Therefore, the Hamiltonian up to $\mathcal{O}\Big(N_0\sqrt{N_0}/V\Big)$ is given by

$$\begin{aligned}\hat{H}\simeq\ &E_{1\mathrm{b}}(\vec{k}_0,-1,-1)N_0+N_0^2\frac{2\pi\hbar^2}{MV}\sum_{s_A,s_B}a_{s_A,s_B}\left|\Big\langle -1(\vec{k}_0)\Big|s_A\Big\rangle\right|^2\left|\Big\langle s_B\Big|-1(\vec{k}_0)\Big\rangle\right|^2\\&+N_0\sqrt{N_0}\left[E_{1\mathrm{b}}(\vec{k},+1,-1)+\frac{4\pi\hbar^2}{MV}\sum_{s_A,s_B}a_{s_A,s_B}\left|\Big\langle -1(\vec{k}_0)\Big|s_A\Big\rangle\right|^2\Big\langle -1(\vec{k}_0)\Big|s_B\Big\rangle\Big\langle s_B\Big|+1(\vec{k}_0)\Big\rangle\right]\\&\times\Big(\hat{a}_{+1,\vec{k}_0}+\hat{a}^\dagger_{+1,\vec{k}_0}\Big)\end{aligned} \tag{4.74}$$

We now find the value of the condensation momentum $\vec{k}_0$ and the superposition angle θ by imposing:

$$E_{1\mathrm{b}}(\vec{k},+1,-1)+\frac{4\pi\hbar^2}{MV}\sum_{s_A,s_B}a_{s_A,s_B}\left|\left\langle -1(\vec{k}_0)\middle|s_A\right\rangle\right|^2\left\langle -1(\vec{k}_0)\middle|s_B\right\rangle\left\langle s_B\middle|+1(\vec{k}_0)\right\rangle=0 \tag{4.75}$$

i.e. by making the non-diagonal contributions to the Hamiltonian vanish. In this way, we are diagonalizing the Hamiltonian. This gives a set of $\{\vec{k}_0,\ \theta\}$ values. We then minimize:

$$E_{MF}=E_{1\mathrm{b}}(\vec{k}_0,-1,-1)N_0+N_0^2\frac{2\pi\hbar^2}{MV}\sum_{s_A,s_B}a_{s_A,s_B}\left|\left\langle -1(\vec{k}_0)\middle|s_A\right\rangle\right|^2\left|\left\langle s_B\middle|-1(\vec{k}_0)\right\rangle\right|^2 \tag{4.76}$$

i.e. the mean field energy, with respect to $\vec{k}_0$ and θ, and set the final values for these parameters as the ones that minimize E_{MF}. This process can be carried out numerically. As mentioned previously, this approach yields the same condensation state and mean field energy as the ones provided by the ansatz used in Ref. [25].

Once the mean field ground state is obtained, we can go further by retaining higher order terms of the two-body part of the Hamiltonian. As in the previous Section, we must work with the grand-canonical Hamiltonian due to its non-commutativity with the number operator when these terms are retained. The chemical potential of the condensate state corresponds to the eigenvalue of the Gross-Pitaevskii equation, which is given by:

$$\mu=E_{1\mathrm{b}}(\vec{k}_0,-1,-1)+\frac{4\pi\hbar^2N_0}{MV}\sum_{s_A,s_B}a_{s_A,s_B}\left|\left\langle -1(\vec{k}_0)\middle|s_A\right\rangle\right|^2\left|\left\langle s_B\middle|-1(\vec{k}_0)\right\rangle\right|^2 \tag{4.77}$$

Up to $\mathcal{O}\left(\frac{N_0}{V}\right)$, $\hat{K}=\hat{H}-\mu\hat{N}$ can be written as:

$$\begin{aligned}\hat{K}\simeq{}&E_{1\mathrm{b}}(\vec{k}_0,-1,-1)N_0+N_0^2\frac{2\pi\hbar^2}{MV}\sum_{s_A,s_B}a_{s_A,s_B}\left|\left\langle -1(\vec{k}_0)\middle|s_A\right\rangle\right|^2\left|\left\langle s_B\middle|-1(\vec{k}_0)\right\rangle\right|^2-\mu N_0\\&+\sum_{\substack{\vec{k}\neq\vec{k}_0\\d,d'}}\left(E_{1\mathrm{b}}(\vec{k},d,d')-E_{1\mathrm{b}}(\vec{k}_0,-1,-1)\right)\hat{a}^\dagger_{\vec{k},d'}\hat{a}_{\vec{k},d}\\&+\frac{2\pi\hbar^2N_0}{MV}\sum_{\substack{\vec{k}\neq0\\d_1',d_2'}}\left[\sum_{s_A,s_B}a_{s_A,s_B}\left\langle d_1'(\vec{k}_0-\vec{k})\middle|s_A\right\rangle\left\langle d_2'(\vec{k}_0+\vec{k})\middle|s_B\right\rangle\left\langle s_A\middle|-1(\vec{k}_0)\right\rangle\left\langle s_B\middle|-1(\vec{k}_0)\right\rangle\right]\\&\times\hat{a}^\dagger_{d_1',\vec{k}_0-\vec{k}}\hat{a}^\dagger_{d_2',\vec{k}_0+\vec{k}}\end{aligned}$$

$$
\begin{aligned}
&+ \frac{4\pi\hbar^2 N_0}{MV} \sum_{\substack{\vec{q}_1 \neq \vec{k}_0 \\ d_1, d_1'}} \left[\sum_{s_A, s_B} a_{s_A, s_B} \left\langle d_1'(\vec{q}_1) \middle| s_A \right\rangle \left\langle -1(\vec{k}_0) \middle| s_B \right\rangle \langle s_A | d_1(\vec{q}_1) \rangle \left\langle s_B \middle| -1(\vec{k}_0) \right\rangle \right] \\
&\times \hat{a}^\dagger_{d_1', \vec{q}_1} \hat{a}_{d_1, \vec{q}_1} \\
&+ \frac{4\pi\hbar^2 N_0}{MV} \sum_{\substack{\vec{k} \neq 0 \\ d_1, d_2'}} \left[\sum_{s_A, s_B} a_{s_A, s_B} \left\langle -1(\vec{k}_0) \middle| s_A \right\rangle \left\langle d_2'(\vec{k}_0 + \vec{k}) \middle| s_B \right\rangle \left\langle s_A \middle| d_1(\vec{k}_0 + \vec{k}) \right\rangle \left\langle s_B \middle| -1(\vec{k}_0) \right\rangle \right] \\
&\times \hat{a}^\dagger_{d_2', \vec{k}_0 + \vec{k}} \hat{a}_{d_1, \vec{k}_0 + \vec{k}} \\
&+ \frac{2\pi\hbar^2 N_0}{MV} \sum_{\substack{\vec{k} \neq 0 \\ d_1, d_2}} \left[\sum_{s_A, s_B} a_{s_A, s_B} \left\langle -1(\vec{k}_0) \middle| s_A \right\rangle \left\langle -1(\vec{k}_0) \middle| s_B \right\rangle \left\langle s_A \middle| d_1(\vec{k}_0 + \vec{k}) \right\rangle \left\langle s_B \middle| d_2(\vec{k}_0 - \vec{k}) \right\rangle \right] \\
&\times \hat{a}_{d_1, \vec{k}_0 + \vec{k}} \hat{a}_{d_2, \vec{k}_0 - \vec{k}} \\
&- \frac{4\pi\hbar^2 N_0}{MV} \sum_{\substack{\vec{k} \neq \vec{k}_0 \\ d, d'}} \left[\sum_{s_A, s_B} a_{s_A, s_B} \left| \left\langle -1(\vec{k}_0) \middle| s_A \right\rangle \right|^2 \left| \left\langle s_B \middle| -1(\vec{k}_0) \right\rangle \right|^2 \right] \hat{a}^\dagger_{\vec{k}, d'} \hat{a}_{\vec{k}, d} \, , \qquad (4.78)
\end{aligned}
$$

where we have neglected the terms involving the operators $\hat{a}_{\vec{k}_0, +1}$, $\hat{a}^\dagger_{\vec{k}_0, +1}$. This is equivalent to not computing the value of the excitation spectrum of the system at a single point in momentum space. Therefore, this approximation has no effect in the quantities we report later in this Section. It is convenient to rewrite the grand-canonical Hamiltonian as [3]:

$$
\begin{aligned}
\hat{K} \simeq\ & E_{1\text{b}}(\vec{k}_0, -1, -1) N_0 + N_0^2 \frac{2\pi\hbar^2}{MV} \sum_{s_A, s_B} a_{s_A, s_B} \left| \left\langle -1(\vec{k}_0) \middle| s_A \right\rangle \right|^2 \left| \left\langle s_B \middle| -1(\vec{k}_0) \right\rangle \right|^2 - \mu N_0 \\
&+ \sum_{\substack{k_x > 0 \\ d, d'}} \left[\left(E_{1\text{b}}(\vec{k}_0 + \vec{k}, d, d') - E_{1\text{b}}(\vec{k}_0, -1, -1) \right) \hat{a}^\dagger_{\vec{k}_0 + \vec{k}, d'} \hat{a}_{\vec{k}_0 + \vec{k}, d} \right. \\
&\left. + \left(E_{1\text{b}}(\vec{k}_0 - \vec{k}, d, d') - E_{1\text{b}}(\vec{k}_0, -1, -1) \right) \hat{a}^\dagger_{\vec{k}_0 - \vec{k}, d'} \hat{a}_{\vec{k}_0 - \vec{k}, d} \right] \\
&+ \frac{2\pi\hbar^2 N_0}{MV} \sum_{\substack{k_x > 0 \\ d_1', d_2'}} \left\{ \left[\sum_{s_A, s_B} a_{s_A, s_B} \left\langle d_1'(\vec{k}_0 - \vec{k}) \middle| s_A \right\rangle \left\langle d_2'(\vec{k}_0 + \vec{k}) \middle| s_B \right\rangle \left\langle s_A \middle| -1(\vec{k}_0) \right\rangle \left\langle s_B \middle| -1(\vec{k}_0) \right\rangle \right] \right. \\
&\times \hat{a}^\dagger_{d_1', \vec{k}_0 - \vec{k}} \hat{a}^\dagger_{d_2', \vec{k}_0 + \vec{k}} + \left[\sum_{s_A, s_B} a_{s_A, s_B} \left\langle d_1'(\vec{k}_0 + \vec{k}) \middle| s_A \right\rangle \left\langle d_2'(\vec{k}_0 - \vec{k}) \middle| s_B \right\rangle \left\langle s_A \middle| -1(\vec{k}_0) \right\rangle \left\langle s_B \middle| -1(\vec{k}_0) \right\rangle \right] \\
&\left. \times \hat{a}^\dagger_{d_1', \vec{k}_0 + \vec{k}} \hat{a}^\dagger_{d_2', \vec{k}_0 - \vec{k}} \right\}
\end{aligned}
$$

$$
\begin{aligned}
&+\frac{4\pi\hbar^2 N_0}{MV}\sum_{\substack{k_x>0\\ d_1,d_1'}}\Bigg\{\Bigg[\sum_{s_A,s_B} a_{s_A,s_B}\left\langle d_1'(\vec{k}_0+\vec{k})\middle|s_A\right\rangle\left\langle -1(\vec{k}_0)\middle|s_B\right\rangle\left\langle s_A\middle|d_1(\vec{k}_0+\vec{k})\right\rangle\left\langle s_B\middle|-1(\vec{k}_0)\right\rangle\Bigg]\\
&\times\hat{a}^\dagger_{d_1',\vec{k}_0+\vec{k}}\hat{a}_{d_1,\vec{k}_0+\vec{k}}+\Bigg[\sum_{s_A,s_B} a_{s_A,s_B}\left\langle d_1'(\vec{k}_0-\vec{k})\middle|s_A\right\rangle\left\langle -1(\vec{k}_0)\middle|s_B\right\rangle\left\langle s_A\middle|d_1(\vec{k}_0-\vec{k})\right\rangle\left\langle s_B\middle|-1(\vec{k}_0)\right\rangle\Bigg]\\
&\times\hat{a}^\dagger_{d_1',\vec{k}_0-\vec{k}}\hat{a}_{d_1,\vec{k}_0-\vec{k}}\Bigg\}\\
&+\frac{4\pi\hbar^2 N_0}{MV}\sum_{\substack{k_x>0\\ d_1,d_2'}}\Bigg\{\Bigg[\sum_{s_A,s_B} a_{s_A,s_B}\left\langle -1(\vec{k}_0)\middle|s_A\right\rangle\left\langle d_2'(\vec{k}_0+\vec{k})\middle|s_B\right\rangle\left\langle s_A\middle|d_1(\vec{k}_0+\vec{k})\right\rangle\left\langle s_B\middle|-1(\vec{k}_0)\right\rangle\Bigg]\\
&\times\hat{a}^\dagger_{d_2',\vec{k}_0+\vec{k}}\hat{a}_{d_1,\vec{k}_0+\vec{k}}+\Bigg[\sum_{s_A,s_B} a_{s_A,s_B}\left\langle -1(\vec{k}_0)\middle|s_A\right\rangle\left\langle d_2'(\vec{k}_0-\vec{k})\middle|s_B\right\rangle\left\langle s_A\middle|d_1(\vec{k}_0-\vec{k})\right\rangle\left\langle s_B\middle|-1(\vec{k}_0)\right\rangle\Bigg]\\
&\times\hat{a}^\dagger_{d_2',\vec{k}_0-\vec{k}}\hat{a}_{d_1,\vec{k}_0-\vec{k}}\Bigg\}\\
&+\frac{2\pi\hbar^2 N_0}{MV}\sum_{\substack{k_x>0\\ d_1,d_2}}\Bigg\{\Bigg[\sum_{s_A,s_B} a_{s_A,s_B}\left\langle -1(\vec{k}_0)\middle|s_A\right\rangle\left\langle -1(\vec{k}_0)\middle|s_B\right\rangle\left\langle s_A\middle|d_1(\vec{k}_0+\vec{k})\right\rangle\left\langle s_B\middle|d_2(\vec{k}_0-\vec{k})\right\rangle\Bigg]\\
&\times\hat{a}_{d_1,\vec{k}_0+\vec{k}}\hat{a}_{d_2,\vec{k}_0-\vec{k}}+\Bigg[\sum_{s_A,s_B} a_{s_A,s_B}\left\langle -1(\vec{k}_0)\middle|s_A\right\rangle\left\langle -1(\vec{k}_0)\middle|s_B\right\rangle\left\langle s_A\middle|d_1(\vec{k}_0-\vec{k})\right\rangle\left\langle s_B\middle|d_2(\vec{k}_0+\vec{k})\right\rangle\Bigg]\\
&\times\hat{a}_{d_1,\vec{k}_0-\vec{k}}\hat{a}_{d_2,\vec{k}_0+\vec{k}}\Bigg\}\\
&-\frac{4\pi\hbar^2 N_0}{MV}\sum_{\substack{k_x>0\\ d,d'}}\Bigg[\sum_{s_A,s_B} a_{s_A,s_B}\left|\left\langle -1(\vec{k}_0)\middle|s_A\right\rangle\right|^2\left|\left\langle s_B\middle|-1(\vec{k}_0)\right\rangle\right|^2\Bigg]\left(\hat{a}^\dagger_{\vec{k}_0+\vec{k},d'}\hat{a}_{\vec{k}_0+\vec{k},d}+\hat{a}^\dagger_{\vec{k}_0-\vec{k},d'}\hat{a}_{\vec{k}_0-\vec{k},d}\right)
\end{aligned}
\tag{4.79}
$$

Analogously to the previous Section, we introduce the vectors:

$$
\hat{\psi}_{\vec{k}}=\begin{pmatrix}\hat{a}_{\vec{k}_0+\vec{k},-1}\\ \hat{a}_{\vec{k}_0+\vec{k},+1}\\ \hat{a}^\dagger_{\vec{k}_0-\vec{k},-1}\\ \hat{a}^\dagger_{\vec{k}_0-\vec{k},+1}\end{pmatrix}\qquad \hat{\psi}^\dagger_{\vec{k}}=\left(\hat{a}^\dagger_{\vec{k}_0+\vec{k},-1}\hat{a}^\dagger_{\vec{k}_0+\vec{k},+1}\hat{a}_{\vec{k}_0-\vec{k},-1}\hat{a}_{\vec{k}_0-\vec{k},+1}\right)\tag{4.80}
$$

$$
\hat{\phi}_{\vec{k}}=\begin{pmatrix}\hat{b}_{\vec{k}_0+\vec{k},-1}\\ \hat{b}_{\vec{k}_0+\vec{k},+1}\\ \hat{b}^\dagger_{\vec{k}_0-\vec{k},-1}\\ \hat{b}^\dagger_{\vec{k}_0-\vec{k},+1}\end{pmatrix}\qquad \hat{\phi}^\dagger_{\vec{k}}=\left(\hat{b}^\dagger_{\vec{k}_0+\vec{k},-1}\hat{b}^\dagger_{\vec{k}_0+\vec{k},+1}\hat{b}_{\vec{k}_0-\vec{k},-1}\hat{b}_{\vec{k}_0-\vec{k},+1}\right)\tag{4.81}
$$

In terms of these vectors, $\hat{K}$ can be written as:

$$\begin{aligned}\hat{K} \simeq{}& E_{1\mathrm{b}}(\vec{k}_0,-1,-1)N_0 + N_0^2\frac{2\pi\hbar^2}{MV}\sum_{s_A,s_B} a_{s_A,s_B}\left|\left\langle -1(\vec{k}_0)\middle|s_A\right\rangle\right|^2\left|\left\langle s_B\middle|-1(\vec{k}_0)\right\rangle\right|^2 - \mu N_0\\ &+ \sum_{k_x>0}\left[\hat{\psi}^\dagger_{\vec{k}}K_{\vec{k}}\hat{\psi}_{\vec{k}} - K_{\vec{k}}(3,3) - K_{\vec{k}}(4,4)\right]\end{aligned} \tag{4.82}$$

where $K_{\vec{k}}(i,j)$ indicates the element in the i-th row and the j-th column of the matrix $K_{\vec{k}}$. Its elements are given by:

$$\begin{aligned}K_{\vec{k}}(1,1) ={}& E_{1\mathrm{b}}(\vec{k}_0+\vec{k},-1,-1) - E_{1\mathrm{b}}(\vec{k}_0,-1,-1)\\ &+ \frac{4\pi\hbar^2 N_0}{MV}\left[\sum_{s_A,s_B} a_{s_A,s_B}\left\langle -1(\vec{k}_0+\vec{k})\middle|s_A\right\rangle\left\langle -1(\vec{k}_0)\middle|s_B\right\rangle\left\langle s_A\middle|-1(\vec{k}_0+\vec{k})\right\rangle\left\langle s_B\middle|-1(\vec{k}_0)\right\rangle\right]\\ &+ \frac{4\pi\hbar^2 N_0}{MV}\left[\sum_{s_A,s_B} a_{s_A,s_B}\left\langle -1(\vec{k}_0)\middle|s_A\right\rangle\left\langle -1(\vec{k}_0+\vec{k})\middle|s_B\right\rangle\left\langle s_A\middle|-1(\vec{k}_0+\vec{k})\right\rangle\left\langle s_B\middle|-1(\vec{k}_0)\right\rangle\right]\\ &- \frac{4\pi\hbar^2 N_0}{MV}\left[\sum_{s_A,s_B} a_{s_A,s_B}\left|\left\langle -1(\vec{k}_0)\middle|s_A\right\rangle\right|^2\left|\left\langle s_B\middle|-1(\vec{k}_0)\right\rangle\right|^2\right]\end{aligned} \tag{4.83}$$

$$\begin{aligned}K_{\vec{k}}(1,2) ={}& E_{1\mathrm{b}}(\vec{k}_0+\vec{k},+1,-1)\\ &+ \frac{4\pi\hbar^2 N_0}{MV}\left[\sum_{s_A,s_B} a_{s_A,s_B}\left\langle -1(\vec{k}_0+\vec{k})\middle|s_A\right\rangle\left\langle -1(\vec{k}_0)\middle|s_B\right\rangle\left\langle s_A\middle|+1(\vec{k}_0+\vec{k})\right\rangle\left\langle s_B\middle|-1(\vec{k}_0)\right\rangle\right]\\ &+ \frac{4\pi\hbar^2 N_0}{MV}\left[\sum_{s_A,s_B} a_{s_A,s_B}\left\langle -1(\vec{k}_0)\middle|s_A\right\rangle\left\langle -1(\vec{k}_0+\vec{k})\middle|s_B\right\rangle\left\langle s_A\middle|+1(\vec{k}_0+\vec{k})\right\rangle\left\langle s_B\middle|-1(\vec{k}_0)\right\rangle\right]\end{aligned} \tag{4.84}$$

$$K_{\vec{k}}(1,3) = \frac{4\pi\hbar^2 N_0}{MV}\left[\sum_{s_A,s_B} a_{s_A,s_B}\left\langle -1(\vec{k}_0-\vec{k})\middle|s_A\right\rangle\left\langle -1(\vec{k}_0+\vec{k})\middle|s_B\right\rangle\left\langle s_A\middle|-1(\vec{k}_0)\right\rangle\left\langle s_B\middle|-1(\vec{k}_0)\right\rangle\right] \tag{4.85}$$

$$K_{\vec{k}}(1,4) = \frac{4\pi\hbar^2 N_0}{MV}\left[\sum_{s_A,s_B} a_{s_A,s_B}\left\langle -1(\vec{k}_0+\vec{k})\middle|s_A\right\rangle\left\langle +1(\vec{k}_0-\vec{k})\middle|s_B\right\rangle\left\langle s_A\middle|-1(\vec{k}_0)\right\rangle\left\langle s_B\middle|-1(\vec{k}_0)\right\rangle\right] \tag{4.86}$$

$$\begin{aligned}
K_{\vec{k}}(2,2) &= E_{1\mathrm{b}}(\vec{k}_0+\vec{k},+1,+1) - E_{1\mathrm{b}}(\vec{k}_0,-1,-1) \\
&+ \frac{4\pi\hbar^2 N_0}{MV}\left[\sum_{s_A,s_B} a_{s_A,s_B}\left\langle +1(\vec{k}_0+\vec{k})\middle|s_A\right\rangle\left\langle -1(\vec{k}_0)\middle|s_B\right\rangle\left\langle s_A\middle|+1(\vec{k}_0+\vec{k})\right\rangle\left\langle s_B\middle|-1(\vec{k}_0)\right\rangle\right] \\
&+ \frac{4\pi\hbar^2 N_0}{MV}\left[\sum_{s_A,s_B} a_{s_A,s_B}\left\langle -1(\vec{k}_0)\middle|s_A\right\rangle\left\langle +1(\vec{k}_0+\vec{k})\middle|s_B\right\rangle\left\langle s_A\middle|+1(\vec{k}_0+\vec{k})\right\rangle\left\langle s_B\middle|-1(\vec{k}_0)\right\rangle\right] \\
&- \frac{4\pi\hbar^2 N_0}{MV}\left[\sum_{s_A,s_B} a_{s_A,s_B}\left|\left\langle -1(\vec{k}_0)\middle|s_A\right\rangle\right|^2\left|\left\langle s_B\middle|-1(\vec{k}_0)\right\rangle\right|^2\right]
\end{aligned}\tag{4.87}$$

$$K_{\vec{k}}(2,3) = \frac{4\pi\hbar^2 N_0}{MV}\left[\sum_{s_A,s_B} a_{s_A,s_B}\left\langle +1(\vec{k}_0+\vec{k})\middle|s_A\right\rangle\left\langle -1(\vec{k}_0-\vec{k})\middle|s_B\right\rangle\left\langle s_A\middle|-1(\vec{k}_0)\right\rangle\left\langle s_B\middle|-1(\vec{k}_0)\right\rangle\right]\tag{4.88}$$

$$K_{\vec{k}}(2,4) = \frac{4\pi\hbar^2 N_0}{MV}\left[\sum_{s_A,s_B} a_{s_A,s_B}\left\langle +1(\vec{k}_0-\vec{k})\middle|s_A\right\rangle\left\langle +1(\vec{k}_0+\vec{k})\middle|s_B\right\rangle\left\langle s_A\middle|-1(\vec{k}_0)\right\rangle\left\langle s_B\middle|-1(\vec{k}_0)\right\rangle\right]\tag{4.89}$$

$$\begin{aligned}
K_{\vec{k}}(3,3) &= E_{1\mathrm{b}}(\vec{k}_0-\vec{k},-1,-1) - E_{1\mathrm{b}}(\vec{k}_0,-1,-1) \\
&+ \frac{4\pi\hbar^2 N_0}{MV}\left[\sum_{s_A,s_B} a_{s_A,s_B}\left\langle -1(\vec{k}_0-\vec{k})\middle|s_A\right\rangle\left\langle -1(\vec{k}_0)\middle|s_B\right\rangle\left\langle s_A\middle|-1(\vec{k}_0-\vec{k})\right\rangle\left\langle s_B\middle|-1(\vec{k}_0)\right\rangle\right] \\
&+ \frac{4\pi\hbar^2 N_0}{MV}\left[\sum_{s_A,s_B} a_{s_A,s_B}\left\langle -1(\vec{k}_0)\middle|s_A\right\rangle\left\langle -1(\vec{k}_0-\vec{k})\middle|s_B\right\rangle\left\langle s_A\middle|-1(\vec{k}_0-\vec{k})\right\rangle\left\langle s_B\middle|-1(\vec{k}_0)\right\rangle\right] \\
&- \frac{4\pi\hbar^2 N_0}{MV}\left[\sum_{s_A,s_B} a_{s_A,s_B}\left|\left\langle -1(\vec{k}_0)\middle|s_A\right\rangle\right|^2\left|\left\langle s_B\middle|-1(\vec{k}_0)\right\rangle\right|^2\right]
\end{aligned}\tag{4.90}$$

$$\begin{aligned}
K_{\vec{k}}(3,4) &= E_{1\mathrm{b}}(\vec{k}_0-\vec{k},+1,-1) \\
&+ \frac{4\pi\hbar^2 N_0}{MV}\left[\sum_{s_A,s_B} a_{s_A,s_B}\left\langle -1(\vec{k}_0-\vec{k})\middle|s_A\right\rangle\left\langle -1(\vec{k}_0)\middle|s_B\right\rangle\left\langle s_A\middle|+1(\vec{k}_0-\vec{k})\right\rangle\left\langle s_B\middle|-1(\vec{k}_0)\right\rangle\right] \\
&+ \frac{4\pi\hbar^2 N_0}{MV}\left[\sum_{s_A,s_B} a_{s_A,s_B}\left\langle -1(\vec{k}_0)\middle|s_A\right\rangle\left\langle -1(\vec{k}_0-\vec{k})\middle|s_B\right\rangle\left\langle s_A\middle|+1(\vec{k}_0-\vec{k})\right\rangle\left\langle s_B\middle|-1(\vec{k}_0)\right\rangle\right]
\end{aligned}\tag{4.91}$$

$$\begin{aligned}
K_{\vec{k}}(4,4) &= E_{1\mathrm{b}}(\vec{k}_0-\vec{k},+1,+1) - E_{1\mathrm{b}}(\vec{k}_0,-1,-1) \\
&+ \frac{4\pi\hbar^2 N_0}{MV}\left[\sum_{s_A,s_B} a_{s_A,s_B}\left\langle +1(\vec{k}_0-\vec{k})\middle|s_A\right\rangle\left\langle -1(\vec{k}_0)\middle|s_B\right\rangle\left\langle s_A\middle|+1(\vec{k}_0-\vec{k})\right\rangle\left\langle s_B\middle|-1(\vec{k}_0)\right\rangle\right] \\
&+ \frac{4\pi\hbar^2 N_0}{MV}\left[\sum_{s_A,s_B} a_{s_A,s_B}\left\langle -1(\vec{k}_0)\middle|s_A\right\rangle\left\langle +1(\vec{k}_0-\vec{k})\middle|s_B\right\rangle\left\langle s_A\middle|+1(\vec{k}_0-\vec{k})\right\rangle\left\langle s_B\middle|-1(\vec{k}_0)\right\rangle\right] \\
&- \frac{4\pi\hbar^2 N_0}{MV}\left[\sum_{s_A,s_B} a_{s_A,s_B}\left|\left\langle -1(\vec{k}_0)\middle|s_A\right\rangle\right|^2\left|\left\langle s_B\middle|-1(\vec{k}_0)\right\rangle\right|^2\right]
\end{aligned}\tag{4.92}$$

Since $K_{\vec{k}}$ is an hermitian matrix (due to the hermiticity of the grand-canonical Hamiltonian), the rest of the elements can be obtained using that $K_{\vec{k}}(j,i) = K_{\vec{k}}(i,j)$. We have omitted the complex conjugate because all the terms in Eqs. (4.83)- (4.92), which denote the components of the $K_{\vec{k}}$ matrix, are real. We can now apply the prescription introduced in the previous Section: by diagonalizing $K^{\text{eff}}_{\vec{k}} = \tilde{I} K_{\vec{k}}$ with:

$$\tilde{I} = \begin{pmatrix} 1 & 0 & 0 & 0 \\ 0 & 1 & 0 & 0 \\ 0 & 0 & -1 & 0 \\ 0 & 0 & 0 & -1 \end{pmatrix} , \tag{4.93}$$

we can compute the matrix of Bogoliubov amplitudes, $M_{\vec{k}}$, which fulfills Eqs. (4.20), (4.31), and the excitation spectrum. The four eigenvalues obtained at each momentum when diagonalizing $K^{\text{eff}}_{\vec{k}}$ are $E(\vec{k}_0 + \vec{k}, -1)$, $E(\vec{k}_0 + \vec{k}, +1)$, -$E(\vec{k}_0 - \vec{k}, -1)$ and -$E(\vec{k}_0 - \vec{k}, +1)$ respectively. As a benchmark, we show in Fig. 4.1, the excitation spectrum for the plane wave and the single minimum phases in the same conditions of Ref. [3], and as can be seen from the Figure, we recover their results. Remarkably, the excitation spectrum shows a roton in the plane wave phase, which is absent in the single minimum phase. The roton present in the plane wave spectrum is reminiscent of the double well structure of the energy dispersion in the one-body problem (see Chapter 2).

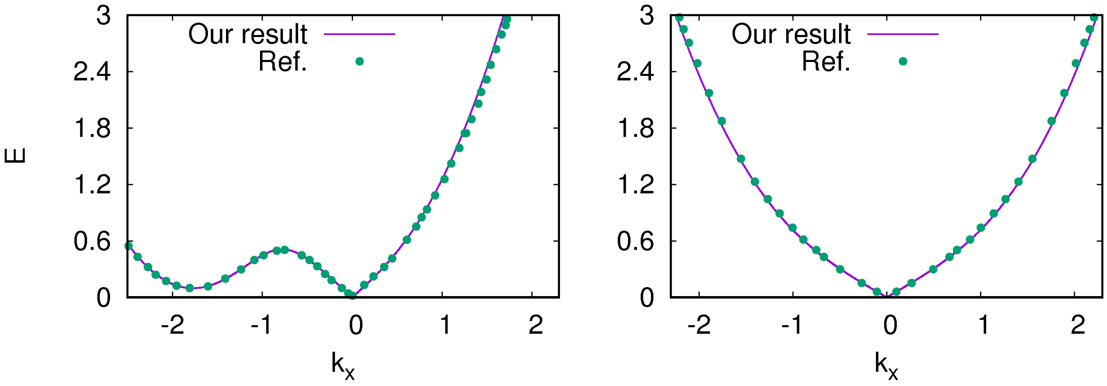

Fig. 4.1 Lowest branch of the excitation spectrum for the plane wave ($\Omega = 2$) and the single minimum ($\Omega = 6$) phases, for $a = a_{+1,+1} = a_{+1,-1} = a_{-1,+1} = a_{-1,-1}$ and $gn/\left(\frac{\hbar^2\lambda^2}{2M}\right) = 0.5$ with $g = \frac{4\pi\hbar^2 a}{M}$, as in Ref. [3]. The lines correspond to our results while points correspond to the results of Ref. [3]. All quantities are expressed in reduced units. The horizontal axis is shifted by $k_{0,x}$, with $k_{0,x}$ the ground state momentum.

Analogously to the previous Section, the lowest eigenvalue of the operator $\hat{K}$ is given by:

$$\begin{aligned} K_0 = E_{1\mathrm{b}}(\vec{k}_0, -1, -1)N_0 + N_0^2 \frac{2\pi\hbar^2}{MV} \sum_{s_A, s_B} a_{s_A, s_B} \left| \left\langle -1(\vec{k}_0) \middle| s_A \right\rangle \right|^2 \left| \left\langle s_B \middle| -1(\vec{k}_0) \right\rangle \right|^2 - \mu N_0 \\ + \frac{V}{(2\pi)^2} \int_0^\infty dk k^2 \left(-K_{\vec{k}}(3,3) - K_{\vec{k}}(4,4) + E(\vec{k}_0 - \vec{k}, -1) + E(\vec{k}_0 - \vec{k}, +1) \right) . \end{aligned} \tag{4.94}$$

It can be seen numerically that the above integral has the same divergent behaviour as in the non-SOC case (the integrand tends to a constant as k goes to infinity). Therefore, the divergence can be eliminated by adding and subtracting a function of the type $f_{\mathrm{reg}}(k) = \eta/(k^2)$ and applying Dimensional Regularization to the integral of this function. It can be checked that the coefficient η that cures the divergence is given by:

$$\eta = \left(\frac{4\pi\hbar^2 N_0}{MV} \right)^2 \sum_{s_A, s_B} a_{s_A, s_B}^2 \left| \left\langle -1(\vec{k}_0) \middle| s_A \right\rangle \right|^2 \left| \left\langle s_B \middle| -1(\vec{k}_0) \right\rangle \right|^2 \left(\frac{M}{\hbar^2} \right) \tag{4.95}$$

Therefore, after regularizing K_0 analogously to what was done in the previous Section, we obtain:

$$\begin{aligned} K_0 = E_{1\mathrm{b}}(\vec{k}_0, -1, -1)N_0 + N_0^2 \frac{2\pi\hbar^2}{MV} \sum_{s_A, s_B} a_{s_A, s_B} \left| \left\langle -1(\vec{k}_0) \middle| s_A \right\rangle \right|^2 \left| \left\langle s_B \middle| -1(\vec{k}_0) \right\rangle \right|^2 - \mu N_0 \\ + \frac{V}{(2\pi)^2} \int_0^\infty dk k^2 \Big(-K_{\vec{k}}(3,3) - K_{\vec{k}}(4,4) + E(\vec{k}_0 - \vec{k}, -1) + E(\vec{k}_0 - \vec{k}, +1) \\ + \left(\frac{4\pi\hbar^2 N_0}{MV} \right)^2 \sum_{s_A, s_B} a_{s_A, s_B}^2 \left| \left\langle -1(\vec{k}_0) \middle| s_A \right\rangle \right|^2 \left| \left\langle s_B \middle| -1(\vec{k}_0) \right\rangle \right|^2 \left(\frac{M}{\hbar^2 (k^2)} \right) \Big) . \end{aligned} \tag{4.96}$$

We can express the integral as:

$$\begin{aligned} \frac{V}{(2\pi)^2} \int_0^\infty dk k^2 \Big(-K_{\vec{k}}(3,3) - K_{\vec{k}}(4,4) + E(\vec{k}_0 - \vec{k}, -1) + E(\vec{k}_0 - \vec{k}, +1) \\ + \left(\frac{4\pi\hbar^2 N_0}{MV} \right)^2 \sum_{s_A, s_B} a_{s_A, s_B}^2 \left| \left\langle -1(\vec{k}_0) \middle| s_A \right\rangle \right|^2 \left| \left\langle s_B \middle| -1(\vec{k}_0) \right\rangle \right|^2 \left(\frac{M}{\hbar^2 (k^2)} \right) \Big) \\ = \Gamma_{\mathrm{LHY}}(N_0) \frac{2\pi\hbar^2 N_0^2}{MV} \sum_{s_A, s_B} a_{s_A, s_B} \left| \left\langle -1(\vec{k}_0) \middle| s_A \right\rangle \right|^2 \left| \left\langle s_B \middle| -1(\vec{k}_0) \right\rangle \right|^2 \end{aligned} \tag{4.97}$$

where we have defined $\Gamma_{\mathrm{LHY}}(N_0)$, which corresponds to the ratio between the integral and the mean field interaction energy. In this way, K_0 can be written as:

$$K_0 = E_{1\mathrm{b}}(\vec{k}_0, -1, -1)N_0 + \frac{2\pi\hbar^2 N_0^2}{MV} \sum_{s_A, s_B} a_{s_A, s_B} \left|\left\langle -1(\vec{k}_0)\middle| s_A \right\rangle\right|^2 \left|\left\langle s_B \middle| -1(\vec{k}_0)\right\rangle\right|^2 (1 + \Gamma_{\mathrm{LHY}}(N_0)) - \mu N_0 \ . \tag{4.98}$$

We now compute the ground state energy as we did in the previous Section. We use that $\Gamma_{\mathrm{LHY}}(N_0) = \Gamma_{\mathrm{LHY}}(N) + \mathcal{O}\left(\delta N^2\right)$, since the ratio between the LHY correction and the interaction mean field energy, Γ_{LHY}, is of $\mathcal{O}(\delta N)$. We reach

$$\begin{aligned} E_0 = K_0 + \mu N = E_{1\mathrm{b}}(\vec{k}_0, -1, -1)N \\ + \frac{2\pi\hbar^2 N^2}{MV} \sum_{s_A, s_B} a_{s_A, s_B} \left|\left\langle -1(\vec{k}_0)\middle| s_A \right\rangle\right|^2 \left|\left\langle s_B \middle| -1(\vec{k}_0)\right\rangle\right|^2 (1 + \Gamma_{\mathrm{LHY}}(N)) \end{aligned} \tag{4.99}$$

We report in Fig. 4.2 results for Γ_{LHY} in the same conditions as in Ref. [3] as a test to our calculations. As we can see from the Figure, we recover the results from Ref. [3]. Remarkably, Γ_{LHY} decreases with respect to Ω in the plane wave phase ($\Omega < 4$), while this trend is reversed in the single minimum phase ($\Omega > 4$).

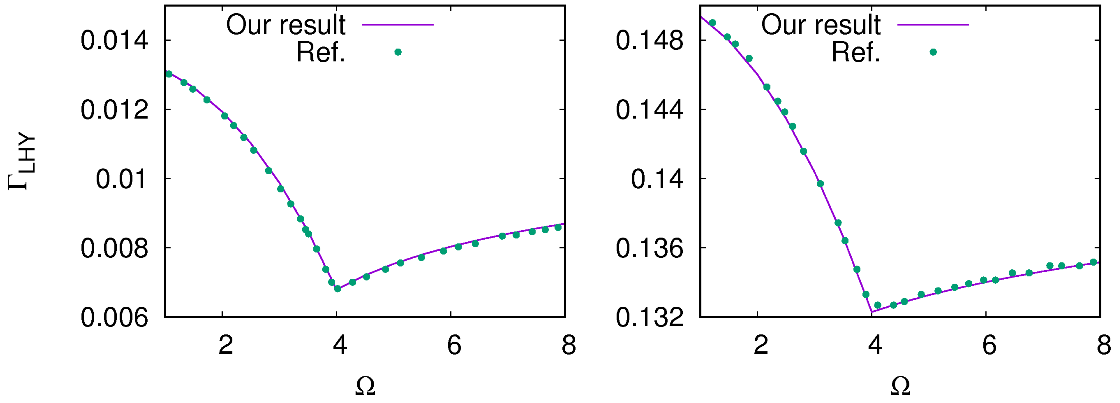

Fig. 4.2 Results for Γ_{LHY} for different values of Ω, for $a = a_{+1,+1} = a_{+1,-1} = a_{-1,+1} = a_{-1,-1}$ and $n/\lambda^3 = 1$ as in Ref. [3]. The left and right panels correspond to $na^3 = 8 \times 10^{-6}$ and $na^3 = 1 \times 10^{-3}$, respectively. The lines show our results while points denote the results of Ref. [3]. All quantities are expressed in reduced units.

4.3 The Bogoliubov-de Gennes formalism

We present in this Section an alternative formalism to the one previously discussed in order to compute beyond mean field properties. This formalism is more convenient to perform calculations for a Raman SOC system in the stripe phase. As in the previous Section, we first solve the non-SOC case and discuss the Raman SOC case afterwards. We focus on the computation of the excitation spectrum and the LHY energy correction, although we also report the static structure factor for the Raman stripe phase.

4.3.1 Non-SOC case

The Heisenberg equation of motion for the field operator corresponding to a system under two-body contact interactions characterized by a scattering length a is given by [74]:

$$i\hbar\frac{\mathrm{d}\hat{\Psi}(t)}{\mathrm{d}t} = \hat{H}_0\hat{\Psi} + \frac{4\pi\hbar^2 a}{M}\hat{\Psi}^\dagger\hat{\Psi}\hat{\Psi} \ , \tag{4.100}$$

while the time-dependent field operator reads [70]:

$$\hat{\Psi}(t) = e^{-i\mu t/\hbar}\left(\hat{\psi}_0 + \delta\hat{\Psi}(t)\right) \tag{4.101}$$

with $\hat{\psi}_0$ the condensate state and μ the chemical potential. As it can be seen, we are separating the condensate contribution, denoted by $\hat{\psi}_0$, from the rest, denoted by $\delta\hat{\Psi}(t)$, which is often referred as the quantum fluctuations part. We assume that the majority of the particles of the system lay in the condensate. We substitute Eq. (4.101) into Eq. (4.100), we obtain

$$\begin{aligned}\mu\psi_0(\vec{r}) + i\hbar\frac{\mathrm{d}\delta\hat{\Psi}}{\mathrm{d}t} &= \hat{H}_0\psi_0(\vec{r}) + \frac{4\pi\hbar^2 a}{M}|\psi_0(\vec{r})|^2\psi_0(\vec{r}) \\ &+ \hat{H}_0\delta\hat{\Psi}(t) + \frac{8\pi\hbar^2 a}{M}|\psi_0(\vec{r})|^2\delta\hat{\Psi}(t) + \frac{4\pi\hbar^2 a}{M}|\psi_0(\vec{r})|^2\delta\hat{\Psi}^\dagger(t) - \mu\delta\hat{\Psi}(t) = 0\end{aligned} \tag{4.102}$$

This equation is fulfilled if

$$\mu\psi_0(\vec{r}) = \hat{H}_0\psi_0(\vec{r}) + \frac{4\pi\hbar^2 a}{M}|\psi_0(\vec{r})|^2\psi_0(\vec{r}) \tag{4.103}$$

$$i\hbar\frac{\mathrm{d}\delta\hat{\Psi}}{\mathrm{d}t} = \hat{H}_0\delta\hat{\Psi}(t) + \frac{8\pi\hbar^2 a}{M}|\psi_0(\vec{r})|^2\delta\hat{\Psi}(t) + \frac{4\pi\hbar^2 a}{M}|\psi_0(\vec{r})|^2\delta\hat{\Psi}^\dagger(t) - \mu\delta\hat{\Psi}(t) \tag{4.104}$$

Notice that Eq. (4.103) corresponds to the time-independent Gross-Pitaevskii equation for the condensate state, while Eq. (4.104) governs the dynamics of the quantum fluctuations. Analogously to Sec. 4.2, we use a basis of momentum states to expand the field operator. Assuming that particles condensate at $\vec{k} = 0$, we can write

$$\hat{\psi}_0 = \frac{1}{\sqrt{V}}\hat{a}_0 \sim \sqrt{N_0/V} \ , \tag{4.105}$$

with N_0 the number of particles in the condensate. In much the same way, we write $\delta\hat{\Psi}(t)$ as:

$$
\begin{aligned}
\delta\hat{\Psi}(t) &= \sum_{\vec{k}\neq 0}\frac{1}{\sqrt{V}}e^{i\vec{k}\vec{r}}\hat{a}_{\vec{k}}(t) = \sum_{\vec{k}\neq 0}\frac{1}{\sqrt{V}}e^{i\vec{k}\vec{r}}\left(u(\vec{k})\hat{b}_{\vec{k}}(t) + v^*(-\vec{k})\hat{b}^\dagger_{-\vec{k}}(t)\right)\\
&= \frac{1}{\sqrt{V}}\sum_{\vec{k}\neq 0}\left(u(\vec{k},\vec{r})\hat{b}_{\vec{k}}(t) + v^*(-\vec{k},\vec{r})\hat{b}^\dagger_{-\vec{k}}(t)\right)\ . \qquad (4.106)
\end{aligned}
$$

where

$$
\begin{aligned}
u(\vec{k},\vec{r}) &= e^{i\vec{k}\vec{r}}u(\vec{k}) \qquad (4.107)\\
v^*(-\vec{k},\vec{r}) &= e^{i\vec{k}\vec{r}}v^*(-\vec{k})\ . \qquad (4.108)
\end{aligned}
$$

With a suitable election, the chosen dependence on the $\hat{b}_{\vec{k}}(t)$, $\hat{b}^\dagger_{-\vec{k}}(t)$ decouples Eq. (4.104), as can be checked by plugging Eq. (4.106) into Eq. (4.104).

$$
\begin{aligned}
&\sum_{\vec{k}\neq 0} i\hbar u(\vec{k},\vec{r})\frac{\mathrm{d}\hat{b}_{\vec{k}}(t)}{\mathrm{d}t} + i\hbar v^*(-\vec{k},\vec{r})\frac{\mathrm{d}\hat{b}^\dagger_{-\vec{k}}(t)}{\mathrm{d}t} = \sum_{\vec{k}\neq 0}\left(\hat{H}_0 + \frac{8\pi\hbar^2 aN_0}{MV} - \mu\right)u(\vec{k},\vec{r})\hat{b}_{\vec{k}}(t)\\
&+\left(\hat{H}_0 + \frac{8\pi\hbar^2 aN_0}{MV} - \mu\right)v^*(-\vec{k},\vec{r})\hat{b}^\dagger_{-\vec{k}}(t) + \frac{4\pi\hbar^2 aN_0}{MV}u^*(\vec{k},\vec{r})\hat{b}^\dagger_{\vec{k}}(t)\\
&+\frac{4\pi\hbar^2 aN_0}{MV}v(-\vec{k},\vec{r})\hat{b}_{-\vec{k}}(t)\ . \qquad (4.109)
\end{aligned}
$$

The above Equation is fulfilled if we impose for each $\hat{b}_{\vec{k}}$, $\hat{b}^\dagger_{-\vec{k}}$ that:

$$
i\hbar u(\vec{k},\vec{r})\frac{\mathrm{d}\hat{b}_{\vec{k}}(t)}{\mathrm{d}t} = \left(\hat{H}_0 + \frac{8\pi\hbar^2 aN_0}{MV} - \mu\right)u(\vec{k},\vec{r})\hat{b}_{\vec{k}}(t) + \frac{4\pi\hbar^2 aN_0}{MV}v(\vec{k},\vec{r})\hat{b}_{\vec{k}}(t) \qquad (4.110)
$$

$$
i\hbar v^*(-\vec{k},\vec{r})\frac{\mathrm{d}\hat{b}^\dagger_{-\vec{k}}(t)}{\mathrm{d}t} = \left(\hat{H}_0 + \frac{8\pi\hbar^2 aN_0}{MV} - \mu\right)v^*(-\vec{k},\vec{r})\hat{b}^\dagger_{-\vec{k}}(t) + \frac{4\pi\hbar^2 aN_0}{MV}u^*(-\vec{k},\vec{r})\hat{b}^\dagger_{-\vec{k}}(t) \qquad (4.111)
$$

Changing $-\vec{k}\to\vec{k}$ in Eq. 4.111, we obtain a system of two equations, for $\hat{b}_{\vec{k}}$ and $\hat{b}^\dagger_{\vec{k}}$, with two unknowns, $u(\vec{k},\vec{r})$ and $v(\vec{k},\vec{r})$, i.e

$$
i\hbar u(\vec{k},\vec{r})\frac{\mathrm{d}\hat{b}_{\vec{k}}(t)}{\mathrm{d}t} = \left(\hat{H}_0 + \frac{8\pi\hbar^2 aN_0}{MV} - \mu\right)u(\vec{k},\vec{r})\hat{b}_{\vec{k}}(t) + \frac{4\pi\hbar^2 aN_0}{MV}v(\vec{k},\vec{r})\hat{b}_{\vec{k}}(t) \qquad (4.112)
$$

$$
i\hbar v^*(\vec{k},\vec{r})\frac{\mathrm{d}\hat{b}^\dagger_{\vec{k}}(t)}{\mathrm{d}t} = \left(\hat{H}_0 + \frac{8\pi\hbar^2 aN_0}{MV} - \mu\right)v^*(\vec{k},\vec{r})\hat{b}^\dagger_{\vec{k}}(t) + \frac{4\pi\hbar^2 aN_0}{MV}u^*(\vec{k},\vec{r})\hat{b}^\dagger_{\vec{k}}(t) \qquad (4.113)
$$

Since Eqs. (4.112) and (4.113) are differential equations with constant coefficients with respect to t, the system admits a solution for $\hat{b}_{\vec{k}}(t)$ of the form:

$$\hat{b}_{\vec{k}}(t) = \exp\left(-itE(\vec{k})/\hbar\right)\hat{b}_{\vec{k}} \qquad \hat{b}^{\dagger}_{\vec{k}}(t) = \exp\left(itE(\vec{k})/\hbar\right)\hat{b}^{\dagger}_{\vec{k}} \tag{4.114}$$

The coefficients in the exponent of the imaginary exponentials are the excitation energies, since the operators $\hat{b}_{\vec{k}}$, $\hat{b}^{\dagger}_{\vec{k}}$ diagonalize the beyond mean field Hamiltonian. Substituting Eqs. (4.114) into Eqs. (4.111) we obtain:

$$E(\vec{k})u(\vec{k},\vec{r}) = \left(\hat{H}_0 + \frac{8\pi\hbar^2 aN_0}{MV} - \mu\right)u(\vec{k},\vec{r}) + \frac{4\pi\hbar^2 aN_0}{MV}v(\vec{k},\vec{r}) \tag{4.115}$$

$$-E(\vec{k})v^*(\vec{k},\vec{r}) = \left(\hat{H}_0 + \frac{8\pi\hbar^2 aN_0}{MV} - \mu\right)v^*(\vec{k},\vec{r}) + \frac{4\pi\hbar^2 aN_0}{MV}u^*(\vec{k},\vec{r}) \tag{4.116}$$

Using Eqs. (4.107) and (4.108), the system can be written in matrix form. Also, we use that $|\psi_0(\vec{r})|^2 = N_0$ and Eq. (4.12) to get:

$$\begin{pmatrix} \frac{\hbar^2k^2}{2M} + \frac{4\pi\hbar^2 aN_0}{MV} & \frac{4\pi\hbar^2 aN_0}{MV} \\ -\frac{4\pi\hbar^2 aN_0}{MV} & -\frac{\hbar^2k^2}{2M} - \frac{4\pi\hbar^2 aN_0}{MV} \end{pmatrix}\begin{pmatrix} u(\vec{k}) \\ v(\vec{k}) \end{pmatrix} = E(\vec{k})\begin{pmatrix} u(\vec{k}) \\ v(\vec{k}) \end{pmatrix} \tag{4.117}$$

Similarly, the equations for $\hat{b}_{-\vec{k}}$, $\hat{b}^{\dagger}_{-\vec{k}}$, which are obtained by applying a change $\vec{k} \to -\vec{k}$ to Eqs. (4.112) and (4.113), yield

$$\begin{pmatrix} \frac{\hbar^2k^2}{2M} + \frac{4\pi\hbar^2 aN_0}{MV} & \frac{4\pi\hbar^2 aN_0}{MV} \\ -\frac{4\pi\hbar^2 aN_0}{MV} & -\frac{\hbar^2k^2}{2M} - \frac{4\pi\hbar^2 aN_0}{MV} \end{pmatrix}\begin{pmatrix} v(-\vec{k}) \\ u(-\vec{k}) \end{pmatrix} = -E(-\vec{k})\begin{pmatrix} v(-\vec{k}) \\ u(-\vec{k}) \end{pmatrix} \tag{4.118}$$

Notice that the matrix in Eqs. (4.117) (4.118) is the same as the one in Eq. (4.33), obtained through the previous approach. Therefore, by diagonalizing Eqs. (4.117) (4.118) one can obtain the excitation spectrum and the Bogoliubov amplitudes. These fulfill the normalization condition of Eq. (4.31), i.e.

$$u^2(\vec{k}) - v^2(\vec{k}) = 1 \tag{4.119}$$

$$v^2(-\vec{k}) - u^2(-\vec{k}) = -1 \tag{4.120}$$

We now compute the Lee-Huang-Yang correction. Since the Bogoliubov Hamiltonian does not commute with $\hat{N}$, as stated in the previous Section, one must work in the grand-canonical ensemble. In the following, we refer to the ground state of the Bogoliubov Hamiltonian as $|0_b\rangle$. We can write:

$$\begin{aligned} E_{\text{g.s.}} &= K_{\text{g.s.}} + \mu N = \langle 0_b|\,\hat{H} - \mu\hat{N}\,|0_b\rangle\,(N_0) + \mu N \\ &= K_{\text{M.F.}}(N_0) + K_{\text{LHY}}(N_0) + \mu N \end{aligned} \tag{4.121}$$

where we have split the ground state of the grand-canonical Hamiltonian into a mean field contribution and a Lee-Huang-Yang term. Using Eq. (4.10) for the mean field energy and Eq. (4.12) for the chemical potential, we can write $K_{\text{M.F.}}(N_0) + \mu N$ as:

$$K_{\text{M.F.}}(N_0) + \mu N = \frac{2\pi\hbar^2 a N_0^2}{MV} - \frac{4\pi\hbar^2 a N_0^2}{MV} + \frac{4\pi\hbar^2 a N_0 N}{MV} \tag{4.122}$$

We decompose the total number of particles, N, as $N = N_0 + \delta N$, with δN the depletion of the condensate. Therefore:

$$\begin{aligned} K_{\text{M.F.}}(N_0) + \mu N &= \frac{2\pi\hbar^2 a N_0^2}{MV} - \frac{4\pi\hbar^2 a N_0^2}{MV} + \frac{4\pi\hbar^2 a N_0 N}{MV} \\ &= \frac{4\pi\hbar^2 a N^2}{MV} + \mathcal{O}\Big(\delta N^2\Big) \\ &= E_{\text{M.F.}}(N) + \mathcal{O}\Big(\delta N^2\Big) \ , \end{aligned} \tag{4.123}$$

so that

$$\begin{aligned} E_{\text{g.s.}} &= E_{\text{M.F.}}(N) + K_{\text{LHY}}(N_0) + \mathcal{O}\Big(\delta N^2\Big) \\ &= E_{\text{M.F.}}(N) + K_{\text{LHY}}(N) + \mathcal{O}\Big(\delta N^2\Big) \end{aligned} \tag{4.124}$$

which implies that $E_{\text{LHY}}(N) = K_{\text{LHY}}(N)$. We proceed to compute $K_{\text{LHY}}(N)$. In order to do so, we write the Hamiltonian in terms of the field operator and decompose it using Eq. (4.101), which leads to

$$\begin{aligned} K_{\text{LHY}}(N) &= \langle 0_b| \hat{H} - \mu\hat{N} |0_b\rangle (N) - K_{\text{M.F.}}(N) \\ &= \langle 0_b| \int d\vec{r}_1 d\vec{r}_2 \delta\hat{\Psi}^\dagger(\vec{r}_1) \Big(\langle \vec{r}_1| \hat{H}_0 |\vec{r}_2\rangle - \mu\delta\left(\vec{r}_2 - \vec{r}_1\right)\Big) \delta\hat{\Psi}(\vec{r}_2) |0_b\rangle \\ &+ \frac{2\pi\hbar^2 a}{M} \langle 0_b| \int d\vec{r} \psi_0^*(\vec{r})\psi_0^*(\vec{r})\delta\hat{\Psi}(\vec{r})\delta\hat{\Psi}(\vec{r}) |0_b\rangle \\ &+ \frac{8\pi\hbar^2 a}{M} \langle 0_b| \int d\vec{r} \psi_0^*(\vec{r})\delta\hat{\Psi}^\dagger(\vec{r})\psi_0(\vec{r})\delta\hat{\Psi}(\vec{r}) |0_b\rangle \\ &+ \frac{2\pi\hbar^2 a}{M} \langle 0_b| \int d\vec{r} \delta\hat{\Psi}^\dagger(\vec{r})\delta\hat{\Psi}^\dagger(\vec{r})\psi_0(\vec{r})\psi_0(\vec{r}) |0_b\rangle \end{aligned} \tag{4.125}$$

where $|0_b\rangle$ is the beyond mean field ground state. At this point we have already retained all the terms containing an even number of $\delta\hat{\Psi}(\vec{r})$, $\delta\hat{\Psi}^\dagger(\vec{r})$ operators, since only terms proportional to $\hat{b}_{\vec{k}}\hat{b}^\dagger_{\vec{k}}$ survive, as all $\hat{b}_{\vec{k}}$ operators with $\vec{k} \neq 0$ annihilate the beyond mean field ground state. One should now decompose the quantum fluctuations operator according to Eq. (4.106) and perform the sum in momentum space. After applying the regularization scheme presented in the previous Section, this calculation is the same as the one performed in Ref. [69], which yields the Lee-Huang-Yang energy correction previously obtained.

4.3.2 Raman SOC case: Plane Wave and Single Minimum phases

We now apply the Bogoliubov-de Gennes formalism to a Raman SOC system in the plane wave and single minimum phases in order to obtain the LHY energy correction and the excitation spectrum. The Heisenberg equation of motion for the field operator of a system governed by the Hamiltonian of Eq. (4.1) is given by [61]:

$$i\hbar\frac{\mathrm{d}\hat{\Psi}(t)}{\mathrm{d}t}=\hat{H}_0\hat{\Psi}+\left[\frac{2G_1}{n}\hat{\Psi}^\dagger\hat{\Psi}+\frac{2G_2}{n}\left(\hat{\Psi}^\dagger\hat{\sigma}_z\hat{\Psi}\right)\hat{\sigma}_z\right]\hat{\Psi}\ . \tag{4.126}$$

where

$$G_1=\frac{n\left(g_{+1,+1}+g_{+1,-1}\right)}{4} \tag{4.127}$$

$$G_2=\frac{n\left(g_{+1,+1}-g_{+1,-1}\right)}{4}\ . \tag{4.128}$$

Again, we write the time-dependent field operator as:

$$\hat{\Psi}(t)=e^{-i\mu t/\hbar}\left(\hat{\psi}_0+\delta\hat{\Psi}(t)\right) \tag{4.129}$$

where, analogously to what has been done in Sec. 4.2.2:

$$\hat{\psi}_0=\frac{1}{\sqrt{V}}e^{i\vec{k}_0\vec{r}}\hat{a}_{\vec{k}_0,-1}\left|d=-1\right\rangle_{\vec{k}_0}\sim\sqrt{\frac{N_0}{V}}e^{i\vec{k}_0\vec{r}}\left|d=-1\right\rangle_{\vec{k}_0}=e^{i\vec{k}_0\vec{r}}\vec{\phi}_0 \tag{4.130}$$

$$\delta\hat{\Psi}\left(\vec{r},t\right)=\sum_{\vec{k}\neq k_0,d}\frac{1}{\sqrt{V}}u^d_{\vec{k}}(\vec{r})\hat{a}_{\vec{k},d}(t)\left|d\right\rangle_{\vec{k}}+\frac{1}{\sqrt{V}}u^{+1}_{\vec{k}_0}(\vec{r})\hat{a}_{\vec{k}_0,+1}(t)\left|+1\right\rangle_{\vec{k}_0} \tag{4.131}$$

with $\left|d=-1\right\rangle_{\vec{k}_0}$ for the condensate state and $\left|d\right\rangle_{\vec{k}}$ given by a linear combination of the eigenstates of momentum $\vec{k}$ of the Hamiltonian in Eq. (4.57) (see Sec. 4.2.2). As we did in Sec. 4.2.2, we have neglected, for simplicity, the terms proportional to the operators $\hat{a}_{\vec{k}_0,+1}$, $\hat{a}^\dagger_{\vec{k}_0,+1}$ in the expansion of $\delta\hat{\Psi}\left(\vec{r},t\right)$, since this is equivalent to not computing the value of the excitation spectrum of the system at a single point in momentum space. Thus, we write:

$$\delta\hat{\Psi}\left(\vec{r},t\right)=\sum_{\vec{k}\neq k_0,d}\frac{1}{\sqrt{V}}u^d_{\vec{k}}(\vec{r})\hat{a}_{\vec{k},d}(t)\left|d\right\rangle_{\vec{k}}\ . \tag{4.132}$$

Substituting Eq. (4.129) into 4.126) we obtain, to first order in $\delta\hat{\Psi}$:

$$\mu\psi_0=\hat{H}_0\psi_0+\left[\frac{2G_1}{n}|\psi_0|^2+\frac{2G_2}{n}\left(\psi_0^*\hat{\sigma}_z\psi_0\right)\hat{\sigma}_z\right]\psi_0\ . \tag{4.133}$$

$$\begin{aligned}\mu\delta\hat{\Psi} + i\hbar\frac{\mathrm{d}\delta\hat{\Psi}}{\mathrm{d}t} &= \hat{H}_0\delta\hat{\Psi} + \frac{2G_1}{n}\left[|\psi_0|^2\delta\hat{\Psi} + \psi_0^*\delta\hat{\Psi}\psi_0 + \delta\hat{\Psi}^\dagger\psi_0\psi_0\right] \\ &+ \frac{2G_2}{n}\left[\psi_0^*\hat{\sigma}_z\psi_0\hat{\sigma}_z\delta\hat{\Psi} + \psi_0^*\hat{\sigma}_z\delta\hat{\Psi}\hat{\sigma}_z\psi_0 + \delta\hat{\Psi}^\dagger\hat{\sigma}_z\psi_0\hat{\sigma}_z\psi_0\right] \qquad (4.134)\end{aligned}$$

We now expand the quantum fluctuations contribution to the field operator as [3, 70]:

$$\begin{aligned}\delta\hat{\Psi}\left(\vec{r},t\right) &= \sum_{k_x>0,d}\frac{1}{\sqrt{V}}e^{i(\vec{k}_0+\vec{k})\vec{r}}\hat{a}_{\vec{k_0}+\vec{k},d}(t)\left|d\right\rangle_{\vec{k_0}+\vec{k}} + \frac{1}{\sqrt{V}}e^{i(\vec{k}_0-\vec{k})\vec{r}}\hat{a}_{\vec{k_0}-\vec{k},d}(t)\left|d\right\rangle_{\vec{k_0}-\vec{k}} \\ &= \frac{1}{\sqrt{V}}\sum_{k_x>0,d}\vec{f}_{\vec{k_0}+\vec{k},d}(\vec{k},\vec{r})\hat{b}_{\vec{k_0}+\vec{k},d}(t) + \vec{f}^*_{\vec{k_0}-\vec{k},d}(\vec{k},\vec{r})\hat{b}^\dagger_{\vec{k_0}-\vec{k},d}(t) \\ &+ \vec{g}_{\vec{k_0}-\vec{k},d}(\vec{k},\vec{r})\hat{b}_{\vec{k_0}-\vec{k},d}(t) + \vec{g}^*_{\vec{k_0}+\vec{k},d}(\vec{k},\vec{r})\hat{b}^\dagger_{\vec{k_0}+\vec{k},d}(t) \qquad (4.135)\end{aligned}$$

where $\vec{f}_{\vec{k_0}+\vec{k},d}(\vec{k},\vec{r})$, $\vec{f}^*_{\vec{k_0}-\vec{k},d}(\vec{k},\vec{r})$, $\vec{g}_{\vec{k_0}-\vec{k},d}(\vec{k},\vec{r})$ and $\vec{g}^*_{\vec{k_0}+\vec{k},d}(\vec{k},\vec{r})$ are two-component spinors that can be written as

$$\vec{f}_{\vec{k_0}+\vec{k},d}(\vec{k},\vec{r}) = e^{i(\vec{k}_0+\vec{k})\vec{r}}\vec{f}_{\vec{k_0}+\vec{k},d} \qquad (4.136)$$

$$\vec{f}^*_{\vec{k_0}-\vec{k},d}(\vec{k},\vec{r}) = e^{i(\vec{k}_0+\vec{k})\vec{r}}\vec{f}^*_{\vec{k_0}-\vec{k},d} \qquad (4.137)$$

$$\vec{g}_{\vec{k_0}-\vec{k},d}(\vec{k},\vec{r}) = e^{i(\vec{k}_0-\vec{k})\vec{r}}\vec{g}_{\vec{k_0}-\vec{k},d} \qquad (4.138)$$

$$\vec{g}^*_{\vec{k_0}+\vec{k},d}(\vec{k},\vec{r}) = e^{i(\vec{k}_0-\vec{k})\vec{r}}\vec{g}^*_{\vec{k_0}+\vec{k},d}\,. \qquad (4.139)$$

Since the only time-dependent terms in Eq. (4.134) are the $\hat{b}_{\vec{k},d}(t)$ operators, contained inside $\delta\hat{\Psi}$, their time-dependent part is given by:

$$\hat{b}_{\vec{k_0}+\vec{k},d}(t) = e^{-iE_{\vec{k_0}+\vec{k},d}t/\hbar}\hat{b}_{\vec{k_0}+\vec{k},d} \qquad (4.140)$$

$$\hat{b}_{\vec{k_0}-\vec{k},d}(t) = e^{-iE_{\vec{k_0}-\vec{k},d}t/\hbar}\hat{b}_{\vec{k_0}-\vec{k},d} \qquad (4.141)$$

$$\hat{b}^\dagger_{\vec{k_0}+\vec{k},d}(t) = e^{iE_{\vec{k_0}+\vec{k},d}t/\hbar}\hat{b}^\dagger_{\vec{k_0}+\vec{k},d} \qquad (4.142)$$

$$\hat{b}^\dagger_{\vec{k_0}-\vec{k},d}(t) = e^{iE_{\vec{k_0}-\vec{k},d}t/\hbar}\hat{b}^\dagger_{\vec{k_0}-\vec{k},d} \qquad (4.143)$$

We now insert Eq. (4.135) into Eq. (4.134) obtain:

$$\begin{aligned}(\mu + E_{\vec{k_0}+\vec{k},d})\vec{f}_{\vec{k_0}+\vec{k},d} &= \hat{H}_0(\vec{k_0}+\vec{k})\vec{f}_{\vec{k_0}+\vec{k},d} + \frac{2G_1}{n}\left[\left|\vec{\phi}_0\right|^2\vec{f}_{\vec{k_0}+\vec{k},d}\right. \\ &\left. +\vec{\phi}_0^\dagger\vec{f}_{\vec{k_0}+\vec{k},d}\vec{\phi}_0 + \vec{g}^\tau_{\vec{k_0}+\vec{k},d}\vec{\phi}_0\vec{\phi}_0\right] \\ &+ \frac{2G_2}{n}\left[\vec{\phi}_0^\dagger\hat{\sigma}_z\vec{\phi}_0\hat{\sigma}_z\vec{f}_{\vec{k_0}+\vec{k},d} + \vec{\phi}_0^\dagger\hat{\sigma}_z\vec{f}_{\vec{k_0}+\vec{k},d}\hat{\sigma}_z\vec{\phi}_0\right. \\ &\left. +\vec{g}^\tau_{\vec{k_0}+\vec{k},d}\hat{\sigma}_z\vec{\phi}_0\hat{\sigma}_z\vec{\phi}_0\right] \qquad (4.144)\end{aligned}$$

$$\begin{aligned}(\mu - E_{\vec{k_0}+\vec{k},d})\vec{g}^{*}_{\vec{k_0}+\vec{k},d} &= \hat{H}_0(\vec{k_0}-\vec{k})\vec{g}^{*}_{\vec{k_0}+\vec{k},d} + \frac{2G_1}{n}\left[\left|\vec{\phi}_0\right|^2 \vec{g}^{*}_{\vec{k_0}+\vec{k},d}\right. \\ &\left. +\vec{\phi}_0^{\dagger}\vec{g}^{*}_{\vec{k_0}+\vec{k},d}\vec{\phi}_0 + \vec{f}^{\dagger}_{\vec{k_0}+\vec{k},d}\vec{\phi}_0\vec{\phi}_0\right] \\ &+ \frac{2G_2}{n}\left[\vec{\phi}_0^{\dagger}\hat{\sigma}_z\vec{\phi}_0\hat{\sigma}_z\vec{g}^{*}_{\vec{k_0}+\vec{k},d} + \vec{\phi}_0^{\dagger}\hat{\sigma}_z\vec{g}^{*}_{\vec{k_0}+\vec{k},d}\hat{\sigma}_z\vec{\phi}_0\right. \\ &\left. +\vec{f}^{\dagger}_{\vec{k_0}+\vec{k},d}\hat{\sigma}_z\vec{\phi}_0\hat{\sigma}_z\vec{\phi}_0\right]\end{aligned} \tag{4.145}$$

$$\begin{aligned}(\mu - E_{\vec{k_0}-\vec{k},d})\vec{f}^{*}_{\vec{k_0}-\vec{k},d} &= \hat{H}_0(\vec{k_0}+\vec{k})\vec{f}^{*}_{\vec{k_0}-\vec{k},d} + \frac{2G_1}{n}\left[\left|\vec{\phi}_0\right|^2 \vec{f}^{*}_{\vec{k_0}-\vec{k},d}\right. \\ &\left. +\vec{\phi}_0^{\dagger}\vec{f}^{*}_{\vec{k_0}-\vec{k},d}\vec{\phi}_0 + \vec{g}^{\dagger}_{\vec{k_0}-\vec{k},d}\vec{\phi}_0\vec{\phi}_0\right] \\ &+ \frac{2G_2}{n}\left[\vec{\phi}_0^{\dagger}\hat{\sigma}_z\vec{\phi}_0\hat{\sigma}_z\vec{f}^{*}_{\vec{k_0}-\vec{k},d} + \vec{\phi}_0^{\dagger}\hat{\sigma}_z\vec{f}^{*}_{\vec{k_0}-\vec{k},d}\hat{\sigma}_z\vec{\phi}_0\right. \\ &\left. +\vec{g}^{\dagger}_{\vec{k_0}-\vec{k},d}\hat{\sigma}_z\vec{\phi}_0\hat{\sigma}_z\vec{\phi}_0\right]\end{aligned} \tag{4.146}$$

$$\begin{aligned}(\mu + E_{\vec{k_0}-\vec{k},d})\vec{g}_{\vec{k_0}-\vec{k},d} &= \hat{H}_0(\vec{k_0}-\vec{k})\vec{g}_{\vec{k_0}-\vec{k},d} + \frac{2G_1}{n}\left[\left|\vec{\phi}_0\right|^2 \vec{g}_{\vec{k_0}-\vec{k},d}\right. \\ &\left. +\vec{\phi}_0^{\dagger}\vec{g}_{\vec{k_0}-\vec{k},d}\vec{\phi}_0 + \vec{f}^{\tau}_{\vec{k_0}-\vec{k},d}\vec{\phi}_0\vec{\phi}_0\right] \\ &+ \frac{2G_2}{n}\left[\vec{\phi}_0^{\dagger}\hat{\sigma}_z\vec{\phi}_0\hat{\sigma}_z\vec{g}_{\vec{k_0}-\vec{k},d} + \vec{\phi}_0^{\dagger}\hat{\sigma}_z\vec{g}_{\vec{k_0}-\vec{k},d}\hat{\sigma}_z\vec{\phi}_0\right. \\ &\left. +\vec{f}^{\tau}_{\vec{k_0}-\vec{k},d}\hat{\sigma}_z\vec{\phi}_0\hat{\sigma}_z\vec{\phi}_0\right]\end{aligned} \tag{4.147}$$

where $\hat{H}_0(\vec{k})$ corresponds to the Hamiltonian of Eq. (4.57) evaluated at momentum $\vec{k}$ (since $[\hat{H}_0\ ,\ \hat{\vec{p}}] = 0$), which is a two-by-two matrix. By using the relations $(\vec{x}^{\tau}\vec{v})\vec{w} = (\vec{w}\vec{v}^{\tau})\vec{x}$ and $(\vec{v}^{\tau}\vec{x})\vec{w} = (\vec{w}\vec{v}^{\tau})\vec{x}$, with $\vec{x}, \vec{v}, \vec{w}$ vectors, Eqs. (4.144) and (4.145) can be written as an eigenvalue problem of the form:

$$A(\vec{k})\begin{pmatrix}\vec{f}_{\vec{k_0}+\vec{k},d}\\ \vec{g}_{\vec{k_0}+\vec{k},d}\end{pmatrix} = E_{\vec{k_0}+\vec{k},d}\begin{pmatrix}\vec{f}_{\vec{k_0}+\vec{k},d}\\ \vec{g}_{\vec{k_0}+\vec{k},d}\end{pmatrix}\ , \tag{4.148}$$

while the corresponding system for Eqs. (4.146) and (4.147) is:

$$A(\vec{k})\begin{pmatrix}\vec{f}_{\vec{k_0}-\vec{k},d}\\ \vec{g}_{\vec{k_0}-\vec{k},d}\end{pmatrix} = -E_{\vec{k_0}-\vec{k},d}\begin{pmatrix}\vec{f}_{\vec{k_0}-\vec{k},d}\\ \vec{g}_{\vec{k_0}-\vec{k},d}\end{pmatrix}\ . \tag{4.149}$$

$A(k)$ is a 4×4 matrix that can be written as

$$A(k) = \begin{pmatrix}A(1,1) & A(1,2)\\ A(2,1) & A(2,2)\end{pmatrix} \tag{4.150}$$

with the 2×2 submatrices $A(i,j)$ given by

$$
\begin{aligned}
A(k)(1,1) &= \hat{H}_0(\vec{k}_0 + \vec{k}) + \frac{2G_1}{n}\left(\left|\vec{\phi}_0\right| + \vec{\phi}_0\vec{\phi}_0^{\dagger}\right) \\
&+ \frac{2G_2}{n}\left(\vec{\phi}_0^{\dagger}\hat{\sigma}_z\vec{\phi}_0\hat{\sigma}_z + \hat{\sigma}_z\vec{\phi}_0\vec{\phi}_0^{\dagger}\hat{\sigma}_z\right) - \mu \qquad (4.151) \\
A(k)(1,2) &= \frac{2G_1}{n}\vec{\phi}_0\vec{\phi}_0^{\tau} + \frac{2G_2}{n}\hat{\sigma}_z\vec{\phi}_0\vec{\phi}_0^{\tau}\hat{\sigma}_z \\
A(k)(2,1) &= -\frac{2G_1}{n}\vec{\phi}_0\vec{\phi}_0^{\tau} - \frac{2G_2}{n}\hat{\sigma}_z\vec{\phi}_0\vec{\phi}_0^{\tau}\hat{\sigma}_z \qquad (4.152) \\
A(k)(2,2) &= -\hat{H}_0(\vec{k}_0 - \vec{k}) - \frac{2G_1}{n}\left(\left|\vec{\phi}_0\right| + \vec{\phi}_0\vec{\phi}_0^{\dagger}\right) \\
&- \frac{2G_2}{n}\left(\vec{\phi}_0^{\dagger}\hat{\sigma}_z\vec{\phi}_0\hat{\sigma}_z + \hat{\sigma}_z\vec{\phi}_0\vec{\phi}_0^{\dagger}\hat{\sigma}_z\right) + \mu \qquad (4.153)
\end{aligned}
$$

Since both $A(k)$ and the excitation spectrum $E_{\vec{k}_0 \pm \vec{k},d}$ are real for all values of the momentum, we can assume the terms $\vec{f}_{\vec{k}_0 \pm \vec{k},d}$, $\vec{g}_{\vec{k}_0 \pm \vec{k},d}$ are also real. Notice that both eigenvalue problems are equivalent. This means that by diagonalizing

$$A(k)\vec{v} = E\vec{v} \qquad (4.154)$$

we obtain four eigenvalues, i.e. $E_{\vec{k}_0+\vec{k},-1}$, $E_{\vec{k}_0+\vec{k},+1}$, $-E_{\vec{k}_0-\vec{k},-1}$ and $-E_{\vec{k}_0-\vec{k},+1}$, corresponding to the two bands of the excitation spectrum. The eigenvalues $E_{\vec{k}_0+\vec{k},-1}$ and $E_{\vec{k}_0+\vec{k},+1}$ yield the two branches of the spectrum for $\vec{k}_0 + \vec{k}$ while $E_{\vec{k}_0-\vec{k},-1}$ and $E_{\vec{k}_0-\vec{k},+1}$ provide the excitation bands for $\vec{k}_0 - \vec{k}$. We also obtain four eigenvectors, i.e.

$$
\begin{aligned}
\vec{v}_{-1}(\vec{k}_0 + \vec{k}) &= \begin{pmatrix} \vec{f}_{\vec{k}_0+\vec{k},-1} \\ \vec{g}_{\vec{k}_0+\vec{k},-1} \end{pmatrix} \qquad & \vec{v}_{+1}(\vec{k}_0 + \vec{k}) &= \begin{pmatrix} \vec{f}_{\vec{k}_0+\vec{k},+1} \\ \vec{g}_{\vec{k}_0+\vec{k},+1} \end{pmatrix} \\
\vec{v}_{-1}(\vec{k}_0 - \vec{k}) &= \begin{pmatrix} \vec{f}_{\vec{k}_0-\vec{k},-1} \\ \vec{g}_{\vec{k}_0-\vec{k},-1} \end{pmatrix} \qquad & \vec{v}_{+1}(\vec{k}_0 - \vec{k}) &= \begin{pmatrix} \vec{f}_{\vec{k}_0-\vec{k},+1} \\ \vec{g}_{\vec{k}_0-\vec{k},+1} \end{pmatrix} \qquad (4.155)
\end{aligned}
$$

One can check that writing the system in the spin basis $\{|d=-1\rangle_{\vec{k}}, |d=+1\rangle_{\vec{k}}\}$ introduced in Sec. 4.2.2, the matrix $A(\vec{k})$ becomes the matrix $K^{\text{eff.}}_{\vec{k}} = \tilde{I}K_{\vec{k}}$ obtained in Sec. 4.2.2, with the matrix elements of $K_{\vec{k}}$ given in Eqs. (4.83)- (4.92) and $\tilde{I}$ given in Eq. (4.93). We must discuss now the normalization condition of these eigenvectors. In the spin basis $\{|d=-1\rangle_{\vec{k}}, |d=+1\rangle_{\vec{k}}\}$ the matrix of eigenvectors $M_{\vec{k}}$ satisfies the condition (see Secs. 4.2.1, 4.2.2):

$$M^{\dagger}_{\vec{k}}\tilde{I}M_{\vec{k}} = \tilde{I} \qquad (4.156)$$

where:

$$M_{\vec{k}} = \begin{pmatrix} \vec{f}_{\vec{k}_0+\vec{k},d=-1} & \vec{f}_{\vec{k}_0+\vec{k},d=+1} & \vec{f}_{\vec{k}_0-\vec{k},d=-1} & \vec{f}_{\vec{k}_0-\vec{k},d=+1} \\ \vec{g}_{\vec{k}_0+\vec{k},d=-1} & \vec{g}_{\vec{k}_0+\vec{k},d=+1} & \vec{g}_{\vec{k}_0-\vec{k},d=-1} & \vec{g}_{\vec{k}_0-\vec{k},d=+1} \end{pmatrix} \tag{4.157}$$

However, for practical reasons it is convenient to choose the eigenbasis of $\hat{\sigma_z}$ when diagonalizing Eq. (4.154). We denote the matrix of eigenvectors in this basis by $M^z_{\vec{k}}$, which becomes

$$M^z_{\vec{k}} = \begin{pmatrix} -\cos\alpha_{k_0+k} & -\sin\alpha_{k_0+k} & 0 & 0 \\ \sin\alpha_{k_0+k} & -\cos\alpha_{k_0+k} & 0 & 0 \\ 0 & 0 & -\cos\alpha_{k_0-k} & -\sin\alpha_{k_0-k} \\ 0 & 0 & \sin\alpha_{k_0-k} & -\cos\alpha_{k_0-k} \end{pmatrix} M_{\vec{k}} = U_{\vec{k}} M_{\vec{k}} \ , \tag{4.158}$$

where the subindexes k and k_0 of the angles refer only to the x component of the momentum and we have defined the matrix $U_{\vec{k}}$. The angles α_k are introduced in Eqs. (4.66) and (4.67). Notice that the matrix $U_{\vec{k}}$ is unitary. We can write

$$M^\dagger_{\vec{k}} \tilde{I} M_{\vec{k}} = (U^\dagger_{\vec{k}} M^z_{\vec{k}})^\dagger \tilde{I} U^\dagger_{\vec{k}} M^z_{\vec{k}} = M^{z,\dagger}_{\vec{k}} U_{\vec{k}} \tilde{I} U^\dagger_{\vec{k}} M^z_{\vec{k}} \ . \tag{4.159}$$

Using the expression for $\tilde{I}$ (given in Eq. 4.93), one has

$$M^{z,\dagger}_{\vec{k}} U_{\vec{k}} \tilde{I} U^\dagger_{\vec{k}} M_{\vec{k}} = M^{z,\dagger}_{\vec{k}} \tilde{I} M^z_{\vec{k}} \tag{4.160}$$

which implies

$$M^{z,\dagger}_{\vec{k}} \tilde{I} M^z_{\vec{k}} = \tilde{I} \tag{4.161}$$

i.e. the normalization condition remains unchanged.

We proceed now to compute the beyond mean field energy of the system. Following the prescription of Sec. 4.3.1, we write:

$$E_{\text{g.s.}} = E_{\text{M.F.}}(N) + K_{\text{LHY}}(N_0) + \mathcal{O}\Big(\delta N^2\Big) \tag{4.162}$$

$$K_{\text{LHY}}(N_0) = \langle 0_b | \hat{H} - \mu\hat{N} | 0_b \rangle (N_0) - K_{\text{M.F.}}(N_0) \tag{4.163}$$

$$K_{\text{M.F.}}(N_0) = E_{\text{M.F.}}(N_0) - \mu N_0 \tag{4.164}$$

with $E_{\text{M.F.}}$ given in Eq. (4.76) and μ given in Eq. (4.77). We need to compute $K_{\text{LHY}}(N_0)$. As in the previous Section, we write the Hamiltonian of the system in terms of the field operator and decompose it as a mean field contribution plus the quantum fluctuations correction.

$$\begin{aligned}
K_{\mathrm{LHY}}(N_0) &= \langle 0_b| \hat{H} - \mu\hat{N} |0_b\rangle (N_0) - K_{\mathrm{M.F.}}(N_0) \\
&= \langle 0_b| \int d\vec{r}_1 d\vec{r}_2 \hat{\Psi}^\dagger(\vec{r}_1) \Big(\langle\vec{r}_1| \hat{H}_0 |\vec{r}_2\rangle - \mu\delta\left(\vec{r}_2 - \vec{r}_1\right) \Big) \hat{\Psi}(\vec{r}_2) |0_b\rangle \\
&+ \frac{1}{2} \langle 0_b| \int d\vec{r}_1 d\vec{r}_2 \hat{\Psi}^\dagger(\vec{r}_1)\hat{\Psi}^\dagger(\vec{r}_2) V(\vec{r}_1,\vec{r}_2) \hat{\Psi}(\vec{r}_1)\hat{\Psi}(\vec{r}_2) |0_b\rangle - K_{\mathrm{M.F.}}(N_0) \\
&= \langle 0_b| \int d\vec{r}_1 d\vec{r}_2 \hat{\psi}_0^\dagger(\vec{r}_1) \Big(\langle\vec{r}_1| \hat{H}_0 |\vec{r}_2\rangle - \mu\delta\left(\vec{r}_2 - \vec{r}_1\right) \Big) \hat{\psi}_0(\vec{r}_2) |0_b\rangle \\
&+ \langle 0_b| \int d\vec{r}_1 d\vec{r}_2 \delta\hat{\Psi}^\dagger(\vec{r}_1) \Big(\langle\vec{r}_1| \hat{H}_0 |\vec{r}_2\rangle - \mu\delta\left(\vec{r}_2 - \vec{r}_1\right) \Big) \delta\hat{\Psi}(\vec{r}_2) |0_b\rangle \\
&+ \frac{1}{2} \langle 0_b| \int d\vec{r}_1 d\vec{r}_2 \hat{\psi}_0^\dagger(\vec{r}_1)\hat{\psi}_0^\dagger(\vec{r}_2) V(\vec{r}_1,\vec{r}_2) \hat{\psi}_0(\vec{r}_1)\hat{\psi}_0(\vec{r}_2) |0_b\rangle \\
&+ \langle 0_b| \int d\vec{r}_1 d\vec{r}_2 \hat{\psi}_0^\dagger(\vec{r}_1)\hat{\psi}_0^\dagger(\vec{r}_2) V(\vec{r}_1,\vec{r}_2) \delta\hat{\Psi}(\vec{r}_1)\delta\hat{\Psi}(\vec{r}_2) |0_b\rangle \\
&+ \langle 0_b| \int d\vec{r}_1 d\vec{r}_2 \hat{\psi}_0^\dagger(\vec{r}_1)\delta\hat{\Psi}^\dagger(\vec{r}_2) V(\vec{r}_1,\vec{r}_2) \hat{\psi}_0(\vec{r}_1)\delta\hat{\Psi}(\vec{r}_2) |0_b\rangle \\
&+ \langle 0_b| \int d\vec{r}_1 d\vec{r}_2 \delta\hat{\Psi}^\dagger(\vec{r}_1)\hat{\psi}_0^\dagger(\vec{r}_2) V(\vec{r}_1,\vec{r}_2) \hat{\psi}_0(\vec{r}_1)\delta\hat{\Psi}(\vec{r}_2) |0_b\rangle - K_{\mathrm{M.F.}}(N_0) \ ,
\end{aligned} \tag{4.165}$$

where we have kept only the terms containing an even number of $\delta\hat{\Psi}$ operators, since terms with an odd number vanish (analogously to the calculation in Sec. 4.3.1). Again, $|0_b\rangle$ corresponds to the beyond mean field ground state. We have also used the fact that:

$$\begin{aligned}
&\langle 0_b| \int d\vec{r}_1 d\vec{r}_2 \hat{\psi}_0^\dagger(\vec{r}_1)\hat{\psi}_0^\dagger(\vec{r}_2) V(\vec{r}_1,\vec{r}_2) \delta\hat{\Psi}(\vec{r}_1)\delta\hat{\Psi}(\vec{r}_2) |0_b\rangle \\
&= \langle 0_b| \int d\vec{r}_1 d\vec{r}_2 \delta\hat{\Psi}^\dagger(\vec{r}_1)\delta\hat{\Psi}^\dagger(\vec{r}_2) V(\vec{r}_1,\vec{r}_2) \delta\hat{\psi}_0(\vec{r}_1)\hat{\psi}_0(\vec{r}_2) |0_b\rangle
\end{aligned} \tag{4.166}$$

$$\begin{aligned}
&\langle 0_b| \int d\vec{r}_1 d\vec{r}_2 \hat{\psi}_0^\dagger(\vec{r}_1)\delta\hat{\Psi}^\dagger(\vec{r}_2) V(\vec{r}_1,\vec{r}_2) \hat{\psi}_0(\vec{r}_1)\delta\hat{\Psi}(\vec{r}_2) |0_b\rangle \\
&= \langle 0_b| \int d\vec{r}_1 d\vec{r}_2 \delta\hat{\Psi}^\dagger(\vec{r}_1)\hat{\psi}_0^\dagger(\vec{r}_2) V(\vec{r}_1,\vec{r}_2) \delta\hat{\Psi}(\vec{r}_1)\hat{\psi}_0(\vec{r}_2) |0_b\rangle
\end{aligned} \tag{4.167}$$

$$\begin{aligned}
&\langle 0_b| \int d\vec{r}_1 d\vec{r}_2 \delta\hat{\Psi}^\dagger(\vec{r}_1)\hat{\psi}_0^\dagger(\vec{r}_2) V(\vec{r}_1,\vec{r}_2) \hat{\psi}_0(\vec{r}_1)\delta\hat{\Psi}(\vec{r}_2) |0_b\rangle \\
&= \langle 0_b| \int d\vec{r}_1 d\vec{r}_2 \hat{\psi}_0^\dagger(\vec{r}_1)\delta\hat{\Psi}^\dagger(\vec{r}_2) V(\vec{r}_1,\vec{r}_2) \delta\hat{\Psi}(\vec{r}_1)\hat{\psi}_0(\vec{r}_2) |0_b\rangle
\end{aligned} \tag{4.168}$$

Now, since

$$\begin{aligned}
K_{\mathrm{M.F.}}(N_0) &= \langle 0_b| \int d\vec{r}_1 d\vec{r}_2 \hat{\psi}_0^\dagger(\vec{r}_1) \Big(\langle\vec{r}_1| \hat{H}_0 |\vec{r}_2\rangle - \mu\delta\left(\vec{r}_2 - \vec{r}_1\right) \Big) \hat{\psi}_0(\vec{r}_2) |0_b\rangle \\
&+ \frac{1}{2} \langle 0_b| \int d\vec{r}_1 d\vec{r}_2 \hat{\psi}_0^\dagger(\vec{r}_1)\hat{\psi}_0^\dagger(\vec{r}_2) V(\vec{r}_1,\vec{r}_2) \hat{\psi}_0(\vec{r}_1)\hat{\psi}_0(\vec{r}_2) |0_b\rangle \ ,
\end{aligned} \tag{4.169}$$

we can write

$$\begin{aligned}
K_{\mathrm{LHY}}(N_0) &= \langle 0_b| \int d\vec{r}_1 d\vec{r}_2 \delta\hat{\Psi}^\dagger(\vec{r}_1) \Big(\langle \vec{r}_1 | \hat{H}_0 | \vec{r}_2 \rangle - \mu\delta\left(\vec{r}_2 - \vec{r}_1\right) \Big) \delta\hat{\Psi}(\vec{r}_2) |0_b\rangle \\
&+ \langle 0_b| \int d\vec{r}_1 d\vec{r}_2 \hat{\psi}_0^\dagger(\vec{r}_1) \hat{\psi}_0^\dagger(\vec{r}_2) V(\vec{r}_1, \vec{r}_2) \delta\hat{\Psi}(\vec{r}_1) \delta\hat{\Psi}(\vec{r}_2) |0_b\rangle \\
&+ \langle 0_b| \int d\vec{r}_1 d\vec{r}_2 \hat{\psi}_0^\dagger(\vec{r}_1) \delta\hat{\Psi}^\dagger(\vec{r}_2) V(\vec{r}_1, \vec{r}_2) \hat{\psi}_0(\vec{r}_1) \delta\hat{\Psi}(\vec{r}_2) |0_b\rangle \\
&+ \langle 0_b| \int d\vec{r}_1 d\vec{r}_2 \delta\hat{\Psi}^\dagger(\vec{r}_1) \hat{\psi}_0^\dagger(\vec{r}_2) V(\vec{r}_1, \vec{r}_2) \hat{\psi}_0(\vec{r}_1) \delta\hat{\Psi}(\vec{r}_2) |0_b\rangle \\
&= K_{\mathrm{LHY},0} + K_{\mathrm{LHY},1} + K_{\mathrm{LHY},2} + K_{\mathrm{LHY},3} \ . \qquad (4.170)
\end{aligned}$$

We now compute each one of these terms:

$$\begin{aligned}
K_{\mathrm{LHY},0} &= \langle 0_b| \int d\vec{r}_1 d\vec{r}_2 \delta\hat{\Psi}^\dagger(\vec{r}_1) \Big(\langle \vec{r}_1 | \hat{H}_0 | \vec{r}_2 \rangle - \mu\delta\left(\vec{r}_2 - \vec{r}_1\right) \Big) \delta\hat{\Psi}(\vec{r}_2) |0_b\rangle \\
&= \frac{1}{V} \langle 0_b| \int d\vec{r}_1 d\vec{r}_2 \Bigg\{ \sum_{k_x>0,d} f_{\vec{k}_0+\vec{k},d} e^{i(\vec{k}_0+\vec{k})\vec{r}_1} \hat{b}_{\vec{k}_0+\vec{k},d} + f^*_{\vec{k}_0-\vec{k},d} e^{i(\vec{k}_0+\vec{k})\vec{r}_1} \hat{b}^\dagger_{\vec{k}_0-\vec{k},d} \\
&+ \vec{g}_{\vec{k}_0-\vec{k},d} e^{i(\vec{k}_0-\vec{k})\vec{r}_1} \hat{b}_{\vec{k}_0-\vec{k},d} + \vec{g}^*_{\vec{k}_0+\vec{k},d} e^{i(\vec{k}_0-\vec{k})\vec{r}_1} \hat{b}^\dagger_{\vec{k}_0+\vec{k},d} \Bigg\}^\dagger \Big(\langle \vec{r}_1 | \hat{H}_0 | \vec{r}_2 \rangle - \mu\delta\left(\vec{r}_2 - \vec{r}_1\right) \Big) \\
&\times \Bigg\{ \sum_{k_x>0,d} f_{\vec{k}_0+\vec{k},d} e^{i(\vec{k}_0+\vec{k})\vec{r}_2} \hat{b}_{\vec{k}_0+\vec{k},d} + f^*_{\vec{k}_0-\vec{k},d} e^{i(\vec{k}_0+\vec{k})\vec{r}_2} \hat{b}^\dagger_{\vec{k}_0-\vec{k},d} \\
&+ \vec{g}_{\vec{k}_0-\vec{k},d} e^{i(\vec{k}_0-\vec{k})\vec{r}_2} \hat{b}_{\vec{k}_0-\vec{k},d} + \vec{g}^*_{\vec{k}_0+\vec{k},d} e^{i(\vec{k}_0-\vec{k})\vec{r}_2} \hat{b}^\dagger_{\vec{k}_0+\vec{k},d} \Bigg\} |0_b\rangle \\
&= \sum_{k_x>0,d,s_1,s_2} \Big\{ f_{\vec{k}_0-\vec{k},d,s_1} f^*_{\vec{k}_0-\vec{k},d,s_2} \Big[H_0(\vec{k}_0+\vec{k}, s_1, s_2) - \delta_{s_1,s_2}\mu \Big] \\
&+ g_{\vec{k}_0+\vec{k},d,s_1} g^*_{\vec{k}_0+\vec{k},d,s_2} \Big[H_0(\vec{k}_0-\vec{k}, s_1, s_2) - \delta_{s_1,s_2}\mu \Big] \Big\} \\
&= \sum_{d,s_1,s_2} \frac{V}{(2\pi)^3} \int_{k_x>0} d\vec{k} \Big\{ f_{\vec{k}_0-\vec{k},d,s_1} f^*_{\vec{k}_0-\vec{k},d,s_2} \Big[H_0(\vec{k}_0+\vec{k}, s_1, s_2) - \delta_{s_1,s_2}\mu \Big] \\
&+ g_{\vec{k}_0+\vec{k},d,s_1} g^*_{\vec{k}_0+\vec{k},d,s_2} \Big[H_0(\vec{k}_0-\vec{k}, s_1, s_2) - \delta_{s_1,s_2}\mu \Big] \Big\} \qquad (4.171)
\end{aligned}$$

where $H_0(\vec{k}, s_1, s_2)$ stands for $\langle s_1| H_0(\vec{k}) |s_2\rangle$, i.e. the matrix element of the one-body Hamiltonian in the momentum and spin-z representation. The other contributions yield:

$$\begin{aligned}
K_{\mathrm{LHY},1} &= \langle 0_b| \int d\vec{r}_1 d\vec{r}_2 \hat{\psi}_0^\dagger(\vec{r}_1) \hat{\psi}_0^\dagger(\vec{r}_2) V(\vec{r}_1, \vec{r}_2) \delta\hat{\Psi}(\vec{r}_1) \delta\hat{\Psi}(\vec{r}_2) |0_b\rangle \\
&= \frac{4\pi\hbar^2}{M} \langle 0_b| \int d\vec{r} \hat{\psi}_0^\dagger(\vec{r}) \hat{\psi}_0^\dagger(\vec{r}) \left[\sum_{s_1,s_2} a_{s_1,s_2} |s_1, s_2\rangle \langle s_1, s_2| \right] \delta\hat{\Psi}(\vec{r}) \delta\hat{\Psi}(\vec{r}) |0_b\rangle
\end{aligned}$$

$$
\begin{aligned}
&= \frac{4\pi\hbar^2}{M} \sum_{k_x>0,d,s_1,s_2} \Big[\phi^*_{0,s_1}\phi^*_{0,s_2} a_{s_1,s_2} f_{\vec{k_0}+\vec{k},d,s_1} g^*_{\vec{k_0}+\vec{k},d,s_2} \\
&+\phi^*_{0,s_1}\phi^*_{0,s_2} a_{s_1,s_2} g_{\vec{k_0}-\vec{k},d,s_1} f^*_{\vec{k_0}-\vec{k},d,s_2}\Big] \\
&= \frac{4\pi\hbar^2 V}{M(2\pi)^3} \sum_{d,s_1,s_2} \int_{k_x>0} d\vec{k} \Big[\phi^*_{0,s_1}\phi^*_{0,s_2} a_{s_1,s_2} f_{\vec{k_0}+\vec{k},d,s_1} g^*_{\vec{k_0}+\vec{k},d,s_2} \\
&+\phi^*_{0,s_1}\phi^*_{0,s_2} a_{s_1,s_2} g_{\vec{k_0}-\vec{k},d,s_1} f^*_{\vec{k_0}-\vec{k},d,s_2}\Big] \qquad (4.172)
\end{aligned}
$$

$$
\begin{aligned}
K_{\text{LHY},2} &= \frac{4\pi\hbar^2 V}{M(2\pi)^3} \sum_{d,s_1,s_2} \int_{k_x>0} d\vec{k} \Big[\phi^*_{0,s_1} f_{\vec{k_0}-\vec{k},d,s_2} a_{s_1,s_2} f^*_{\vec{k_0}-\vec{k},d,s_2} \phi_{0,s_1} \\
&+\phi^*_{0,s_1} g_{\vec{k_0}+\vec{k},d,s_2} a_{s_1,s_2} g^*_{\vec{k_0}+\vec{k},d,s_2} \phi_{0,s_1}\Big] \qquad (4.173)
\end{aligned}
$$

$$
\begin{aligned}
K_{\text{LHY},3} &= \frac{4\pi\hbar^2 V}{M(2\pi)^3} \sum_{d,s_1,s_2} \int_{k_x>0} d\vec{k} \Big[\phi^*_{0,s_1} f_{\vec{k_0}-\vec{k},d,s_2} a_{s_1,s_2} \phi_{0,s_2} f^*_{\vec{k_0}-\vec{k},d,s_1} \\
&+\phi^*_{0,s_1} g_{\vec{k_0}+\vec{k},d,s_2} a_{s_1,s_2} g^*_{\vec{k_0}+\vec{k},d,s_1} \phi_{0,s_2}\Big] \ . \qquad (4.174)
\end{aligned}
$$

In this way, collecting all these results we see that, for a system of N particles, the beyond mean field ground state energy is given by:

$$
\begin{aligned}
E_{\text{g.s.}} = E_{\text{M.F.}}(N) &+ \frac{V}{(2\pi)^3} \sum_{d,s_1,s_2} \int_{k_x>0} d\vec{k} \Bigg\{ \Big[f_{\vec{k_0}-\vec{k},d,s_1} f^*_{\vec{k_0}-\vec{k},d,s_1} \Big[H_0(\vec{k_0}+\vec{k}, s_1, s_2) - \delta_{s_1,s_2}\mu\Big] \\
&+ g_{\vec{k_0}+\vec{k},d,s_2} g^*_{\vec{k_0}+\vec{k},d,s_2} \Big[H_0(\vec{k_0}-\vec{k}, s_1, s_2) - \delta_{s_1,s_2}\mu\Big]\Big] \\
&+ \frac{4\pi\hbar^2 n}{M} \Big[\chi^*_{0,s_1}\chi^*_{0,s_2} a_{s_1,s_2} f_{\vec{k_0}+\vec{k},d,s_1} g^*_{\vec{k_0}+\vec{k},d,s_2} + \chi^*_{0,s_1}\chi^*_{0,s_2} a_{s_1,s_2} g_{\vec{k_0}-\vec{k},d,s_1} f^*_{\vec{k_0}-\vec{k},d,s_2}\Big] \\
&+ \frac{4\pi\hbar^2 n}{M} \Big[\chi^*_{0,s_1} f_{\vec{k_0}-\vec{k},d,s_2} a_{s_1,s_2} f^*_{\vec{k_0}-\vec{k},d,s_1} \chi_{0,s_2} + \chi^*_{0,s_1} g_{\vec{k_0}+\vec{k},d,s_2} a_{s_1,s_2} g^*_{\vec{k_0}+\vec{k},d,s_1} \chi_{0,s_2}\Big] \\
&+ \frac{4\pi\hbar^2 n}{M} \Big[\chi^*_{0,s_1} f_{\vec{k_0}-\vec{k},d,s_2} a_{s_1,s_2} f^*_{\vec{k_0}-\vec{k},d,s_2} \chi_{0,s_1} + \chi^*_{0,s_1} g_{\vec{k_0}+\vec{k},d,s_2} a_{s_1,s_2} g^*_{\vec{k_0}+\vec{k},d,s_2} \chi_{0,s_1}\Big]\Bigg\}
\end{aligned}
$$

(4.175)

with $n = N/V$ and $\vec{\phi}_0 = \sqrt{N/V}\vec{\chi}_0$.

Apart from the correction to the ground state energy, we can also compute other physical quantities like the static structure factor $S(\vec{k})$, the spin static structure factor $S_\sigma(\vec{k})$, and the condensate fraction $f_c = \delta N/N$. We proceed to compute these observables, although we focus on the k_x dependence of $S(\vec{k})$ and $S_\sigma(\vec{k})$, since the influence of SOC is mainly captured in the x-axis due to the contribution of Raman SOC proportional the x component of the momentum (see Eq. 4.57). The static structure factor is given by [4]:

$$
\begin{aligned}
S(q_x) &= \frac{1}{N} \langle 0_b | \left(\sum_{n=1}^{N} e^{iq_x x_n} \right) \left(\sum_{n=1}^{N} e^{-iq_x x_n} \right) | 0_b \rangle = \sum_{l,\vec{k}} \left| \frac{1}{\sqrt{N}} \langle 0_b | \left(\sum_{n=1}^{N} e^{iq_x x_n} \right) | l \rangle_{\vec{k}} \right|^2 \\
&= \sum_{l,\vec{k}} \left| s_{l,\vec{k}}(q_x) \right|^2
\end{aligned}
\tag{4.176}
$$

where we have introduced the identity $\hat{I} = \sum_{l,\vec{k}} |l\rangle_{\vec{k}} \langle l|_{\vec{k}}$ with $|l\rangle_{\vec{k}}$ the eigenstates associated to the creation operators $\hat{b}^{\dagger}_{\vec{k},l}$. The elements $s_{l,\vec{k}}(q_x)$ can be written in terms of the field operator as:

$$
\begin{aligned}
s_{l,\vec{k}}(q_x) &= \frac{1}{\sqrt{N}} \langle 0_b | \int d\vec{r} \hat{\Psi}^{\dagger}(\vec{r}) e^{iq_x x} \hat{\Psi}(\vec{r}) | l \rangle_{\vec{k}} \\
&= \frac{1}{\sqrt{N}} \langle 0_b | \int d\vec{r} \hat{\psi}_0^{\dagger}(\vec{r}) e^{iq_x x} \hat{\psi}_0(\vec{r}) | l \rangle_{\vec{k}} + \frac{1}{\sqrt{N}} \langle 0_b | \int d\vec{r} \delta\hat{\Psi}^{\dagger}(\vec{r}) e^{iq_x x} \hat{\psi}_0(\vec{r}) | l \rangle_{\vec{k}} \\
&+ \frac{1}{\sqrt{N}} \langle 0_b | \int d\vec{r} \hat{\psi}_0^{\dagger}(\vec{r}) e^{iq_x x} \delta\hat{\Psi}(\vec{r}) | l \rangle_{\vec{k}} + \frac{1}{\sqrt{N}} \langle 0_b | \int d\vec{r} \delta\hat{\Psi}^{\dagger}(\vec{r}) e^{iq_x x} \delta\hat{\Psi}(\vec{r}) | l \rangle_{\vec{k}}
\end{aligned}
\tag{4.177}
$$

The element $s_{l=0,\vec{k}=\vec{k}_0}(q_x)$, which corresponds to the lowest energy state, characterized by the quantum numbers $l = 0$ (lowest branch) and $\vec{k} = \vec{k}_0$ (condensate momentum), is proportional to $\delta[q_x]$, with $\delta[x]$ the Kronecker delta function. We focus on the terms which yield a non-trivial dependence on q_x of the static structure factor, which are:

$$
\begin{aligned}
s_{l,\vec{k}}(q_x)\Big|_{l\neq 0,\vec{k}\neq\vec{k}_0} &= \frac{1}{\sqrt{N}} \langle 0_b | \int d\vec{r} \delta\hat{\Psi}^{\dagger}(\vec{r}) e^{iq_x x} \hat{\psi}_0(\vec{r}) | l \rangle_{\vec{k}} + \frac{1}{\sqrt{N}} \langle 0_b | \int d\vec{r} \hat{\psi}_0^{\dagger}(\vec{r}) e^{iq_x x} \delta\hat{\Psi}(\vec{r}) | l \rangle_{\vec{k}} \\
&= s_{l,\vec{k},1}(q_x) + s_{l,\vec{k},2}(q_x)
\end{aligned}
\tag{4.178}
$$

We now evaluate each of these contribution separately. By setting $\vec{k} = \vec{k}_0 + \vec{k}'$, $k'_x > 0$:

$$
\begin{aligned}
s^{(+)}_{l,\vec{k},1}(q_x) &= \frac{1}{\sqrt{N}} \langle 0_b | \int d\vec{r} \delta\hat{\Psi}^{\dagger}(\vec{r}) e^{iq_x x} \hat{\psi}_0(\vec{r}) \hat{b}^{\dagger}_{\vec{k}_0+\vec{k}',l} | 0 \rangle_b = \frac{1}{V} \int d\vec{r} \vec{g}^{\tau}_{\vec{k}_0+\vec{k}',l} e^{i(-\vec{k}_0+\vec{k}')\vec{r}} e^{iq_x x} \vec{\chi}_0 e^{i\vec{k}_0\vec{r}} \\
&= \vec{g}^{\tau}_{\vec{k}_0+\vec{k}',l} \vec{\chi}_0 \delta[\vec{k}' + q_x]
\end{aligned}
\tag{4.179}
$$

while with $\vec{k} = \vec{k}_0 - \vec{k}'$, $k'_x > 0$ we obtain:

$$
\begin{aligned}
s^{(-)}_{l,\vec{k},1}(q_x) &= \frac{1}{\sqrt{N}} \langle 0_b | \int d\vec{r} \delta\hat{\Psi}^{\dagger}(\vec{r}) e^{iq_x x} \hat{\psi}_0(\vec{r}) \hat{b}^{\dagger}_{\vec{k}_0-\vec{k}',l} | 0 \rangle_b = \frac{1}{V} \int d\vec{r} \vec{f}^{\tau}_{\vec{k}_0-\vec{k}',l} e^{-i(\vec{k}_0+\vec{k}')\vec{r}} e^{iq_x x} \vec{\chi}_0 e^{i\vec{k}_0\vec{r}} \\
&= \vec{f}^{\tau}_{\vec{k}_0-\vec{k}',l} \vec{\chi}_0 \delta[\vec{k}' - q_x] \ .
\end{aligned}
\tag{4.180}
$$

Therefore:

$$
s^{(-)}_{l,\vec{k},1}(q_x) = \vec{g}^{\tau}_{\vec{k}_0+\vec{k}',l} \vec{\chi}_0 \delta[\vec{k}' + q_x] + \vec{f}^{\tau}_{\vec{k}_0-\vec{k}',l} \vec{\chi}_0 \delta[\vec{k}' - q_x] \ , \tag{4.181}
$$

and similarly:

$$s^{(+)}_{l,\vec{k},2}(q_x) = \vec{\chi}_0^{\tau} \vec{f}_{\vec{k}_0+\vec{k}',l} \delta[\vec{k}' + q_x] \tag{4.182}$$

$$s^{(-)}_{l,\vec{k},2}(q_x) = \vec{\chi}_0^{\tau} \vec{g}_{\vec{k}_0-\vec{k}',l} \delta[\vec{k}' - q_x] \ . \tag{4.183}$$

Collecting these results, we arrive at

$$S(q_x) = \sum_{l,k'_x>0} \left| \left(\vec{g}^{\tau}_{\vec{k}_0+\vec{k}',l} \vec{\chi}_0 + \vec{\chi}_0^{\tau} \vec{f}_{\vec{k}_0+\vec{k}',l} \right) \delta[\vec{k}' + q_x] \right|^2 + \left| \left(\vec{f}^{\tau}_{\vec{k}_0-\vec{k}',l} \vec{\chi}_0 + \vec{\chi}_0^{\tau} \vec{g}_{\vec{k}_0-\vec{k}',l} \right) \delta[\vec{k}' - q_x] \right|^2 . \tag{4.184}$$

Analogously, we can obtain the spin static structure factor $S_\sigma(\vec{k})$, defined as [4]:

$$S_\sigma(q_x) = \frac{1}{N} \langle 0_b | \left(\sum_{n=1}^{N} \hat{\sigma}_{z,n} e^{i q_x x_n} \right) \left(\sum_{n=1}^{N} \hat{\sigma}_{z,n} e^{-i q_x x_n} \right) | 0_b \rangle = \sum_{l,\vec{k}} \left| \frac{1}{\sqrt{N}} \langle 0_b | \left(\sum_{n=1}^{N} \hat{\sigma}_{z,n} e^{i q_x x_n} \right) | l \rangle_{\vec{k}} \right|^2 \tag{4.185}$$

which, in our case, reads

$$S_\sigma(q_x) = \sum_{l,k'_x>0} \left| \left(\vec{g}^{\tau}_{\vec{k}_0+\vec{k}',l} \hat{\sigma}_z \vec{\chi}_0 + \vec{\chi}_0^{\tau} \hat{\sigma}_z \vec{f}_{\vec{k}_0+\vec{k}',l} \right) \delta[\vec{k}' + q_x] \right| + \left| \left(\vec{f}^{\tau}_{\vec{k}_0-\vec{k}',l} \hat{\sigma}_z \vec{\chi}_0 + \vec{\chi}_0^{\tau} \hat{\sigma}_z \vec{g}_{\vec{k}_0-\vec{k}',l} \right) \delta[\vec{k}' - q_x] \right|^2 \tag{4.186}$$

Finally, we compute the condensate fraction of the system, which is defined as:

$$f_c = \frac{\langle 0_b | \delta N | 0_b \rangle}{N} = \frac{1}{N} \sum_{\vec{k} \neq 0, d} \langle 0_b | \hat{a}^{\dagger}_{\vec{k}_0+\vec{k},d} \hat{a}_{\vec{k}_0+\vec{k},d} | 0_b \rangle \tag{4.187}$$

The condensate fraction corresponds to the fraction of the particles that lay outside of the condensate state. It can be rewritten as

$$f_c = \frac{\delta N}{N} = \frac{1}{N} \sum_{k_x>0, d} \langle 0_b | \hat{a}^{\dagger}_{\vec{k}_0+\vec{k},d} \hat{a}_{\vec{k}_0+\vec{k},d} + \hat{a}^{\dagger}_{\vec{k}_0-\vec{k},d} \hat{a}_{\vec{k}_0-\vec{k},d} | 0_b \rangle \ , \tag{4.188}$$

and in terms of the vectors of Eq. (4.80), we can express it as:

$$f_c = \frac{1}{N} \sum_{k_x>0} \left(\langle 0_b | \hat{\psi}^{\dagger}_{\vec{k}} \hat{\psi}_{\vec{k}} - \sum_{d} 1 | 0_b \rangle \right) = \frac{1}{N} \sum_{k_x>0} \left(\langle 0_b | \hat{\phi}^{\dagger}_{\vec{k}} M^{\dagger}_{\vec{k}} M_{\vec{k}} \hat{\phi}_{\vec{k}} - \sum_{d} 1 | 0_b \rangle \right) \tag{4.189}$$

where we have used the commutation relation $[\hat{a}_{\vec{k}}, \hat{a}^{\dagger}_{\vec{k}'}] = \delta_{\vec{k},\vec{k}'}$ for the elements $\hat{a}^{\dagger}_{\vec{k}_0-\vec{k},d} \hat{a}_{\vec{k}_0-\vec{k},d}$, which explains the appearance of the contribution $\sum_d 1$. Using Eq. (4.158), this becomes

$$\begin{aligned} f_c &= \frac{1}{N}\sum_{k_x>0}\left(\langle 0_b|\,\hat{\phi}^{\dagger}_{\vec{k}}M^{z,\dagger}_{\vec{k}}M^{z}_{\vec{k}}\hat{\phi}_{\vec{k}} - \sum_{d} 1\,|0_b\rangle\right) \\ &= \frac{1}{N}\sum_{k_x>0}\left((M^{z,\dagger}_{\vec{k}}M^{z}_{\vec{k}})(3,3) + (M^{z,\dagger}_{\vec{k}}M^{z}_{\vec{k}})(4,4) - 2\right) \\ &= \frac{1}{(2\pi)^3 n}\int_{k_x>0} d\vec{k}\left((M^{z,\dagger}_{\vec{k}}M^{z}_{\vec{k}})(3,3) + (M^{z,\dagger}_{\vec{k}}M^{z}_{\vec{k}})(4,4) - 2\right) \end{aligned} \tag{4.190}$$

which is an expression that can be used to compute the condensate fraction once the matrix of eigenvectors $M^{z}_{\vec{k}}$ has been computed. It can be shown that the condensate fraction can be written as

$$f_c = \frac{1}{N}\langle 0_b|\int d\vec{r}_1 \delta\hat{\Psi}^{\dagger}(\vec{r}_1)\delta\hat{\Psi}(\vec{r}_1)\,|0_b\rangle \tag{4.191}$$

We employ this expression in Sec. 4.3.3.

4.3.3 Raman SOC case: Stripe phase

We proceed now to compute, for the stripe phase of a Raman SOC system, the beyond mean field corrections of the physical quantities previously introduced, following the Bogoliubov-de Gennes formalism. In this phase, the mean field wave function consists on a superposition of plane waves of opposite momenta [25, 70], which gives rise to a periodic density modulation. The first step is to obtain this wave function. More specifically, this implies obtaining the amplitudes multiplying each plane wave component. We write the wave function in the form [4, 70]:

$$\hat{\psi}_0(\vec{r}) = \sqrt{\frac{N_0}{V}}\sum_{n\in\mathbb{Z}} \vec{\psi}_{0,n} e^{ik_0x + 2ink_0x} \tag{4.192}$$

with $\vec{\psi}_{0,n}$ real spinors and k_0 the ground state momentum. As we can see from Eq. (4.192), this function features a superposition of plane waves of momenta $k_0 + 2nk_0$, $n \in \mathbb{Z}$. We can obtain the values of $\vec{\psi}_{0,n}$ and k_0 by minimizing the mean field energy per particle of the system in terms of these parameters. When the minimization is applied, the modulus of the wave function in Eq. (4.192) shows periodic density modulations, commonly known as *stripes*, unlike the plane wave and single minimum phases. Because of this modulations, the continuous translational symmetry of the wave function is broken. As a result of the periodicity, the excitation spectrum of the system features an infinite number of energy bands which are periodic in momentum space, where Brillouin Zones can be identified. Each Brillouin Zone spans the range $k_0 \in [nk_0,\ (n+2)k_0]$.

In order to carry out the aforementioned minimization procedure, we must obtain the mean field energy per particle, which is given by:

$$E_{\mathrm{M.F.}}/N_0 = \frac{1}{N_0}\int d\vec{r}\left(\hat{\psi}_0^\dagger \hat{H}_0 \hat{\psi}_0 + \frac{G_1}{n}\left|\hat{\psi}_0\right|^4 + \frac{G_2}{n}\left(\hat{\psi}_0^\dagger \hat{\sigma}_z \hat{\psi}_0\right)^2\right) \tag{4.193}$$

where, being ψ_0 the component of the condensate which is macroscopically occupied, it fulfills:

$$\langle \psi_0 | \psi_0 \rangle = N_0 = N_0 \sum_{n\in\mathbb{Z}} \vec{\psi}^\dagger_{0,n} \vec{\psi}_{0,n} \ . \tag{4.194}$$

Let us express $E_{\mathrm{M.F.}}/N_0$ in terms of the momentum amplitudes of $\psi_0(\vec{r})$.

$$\begin{aligned}
E_{\mathrm{M.F.}}/N_0 = \frac{1}{\sum_{v\in\mathbb{Z}} \vec{\psi}^\dagger_{0,v}\vec{\psi}_{0,v}} \Bigg[\sum_{v\in\mathbb{Z}} \Bigg(& \frac{\hbar^2 k_0^2 (2n+1)^2}{2M}\left(\left|\psi^{+1}_{0,v}\right|^2 + \left|\psi^{-1}_{0,v}\right|^2\right) \\
& + \frac{\hbar^2 \lambda k_0 (2n+1)}{M}\left(\left|\psi^{+1}_{0,v}\right|^2 - \left|\psi^{-1}_{0,v}\right|^2\right) + \frac{\hbar^2\lambda^2}{2M}\left(\left|\psi^{+1}_{0,v}\right|^2 + \left|\psi^{-1}_{0,v}\right|^2\right) - \Omega \psi^{+1}_{0,v}\psi^{-1}_{0,v}\Bigg) \\
& + \frac{G_1 N_0}{nV} \sum_{v,w,l,q\in n\in\mathbb{Z}} \left(\psi^{+1}_{0,w}\psi^{+1}_{0,v} + \psi^{-1}_{0,w}\psi^{-1}_{0,v}\right)\left(\psi^{+1}_{0,l}\psi^{+1}_{0,q} + \psi^{-1}_{0,l}\psi^{-1}_{0,q}\right)\delta[v-w+l-q] \\
& + \frac{G_2 N_0}{nV} \sum_{v,w,l,q\in n\in\mathbb{Z}} \left(\psi^{+1}_{0,w}\psi^{+1}_{0,v} - \psi^{-1}_{0,w}\psi^{-1}_{0,v}\right)\left(\psi^{+1}_{0,l}\psi^{+1}_{0,q} - \psi^{-1}_{0,l}\psi^{-1}_{0,q}\right)\delta[v-w+l-q] \Bigg] \ ,
\end{aligned} \tag{4.195}$$

where the spinors have been written in the eigenbasis of $\hat{\sigma}_z$. Notice that, given a term of the sum featuring indexes $j = v_0$,w_0,l_0,$q_0 > 0$; making the transformation $j \to (-j-1)$, $\psi^{+1}_{0,j} \to \psi^{-1}_{0,-j-1}$, $\psi^{-1}_{0,j} \to \psi^{+1}_{0,-j-1}$ leaves the term invariant. This is because $\hat{H}$ is also invariant under the transformation $\vec{k} \to -\vec{k}$, $\hat{\sigma_z} \to -\hat{\sigma_z}$ (see Eqs. (4.126) and (4.57)), thus the components of the wave function of opposite momentum have their spins flipped. We minimize the mean field energy per particle numerically, using the Simulated Annealing algorithm [75]. We denote by $N_c - 1$ the maximum value of the amplitude indexes to be retained in the minimization procedure, such that the condensate wave function reads

$$\psi_0(\vec{r}) = \sqrt{\frac{N_0}{V}} \sum_{n=-N_c}^{N_c-1} \vec{\psi}_{0,n} e^{ik_0x + 2ink_0x} \ . \tag{4.196}$$

Once we have the optimal amplitudes $\vec{\psi}_{0,n}$, we proceed to obtain the excitation spectrum and the Lee-Huang-Yang correction to the mean field energy. As in Sec. 4.3.2, we start from the Heisenberg equation of motion for the field operator, i.e.

$$i\hbar \frac{\mathrm{d}\hat{\Psi}(t)}{\mathrm{d}t} = \hat{H}_0 \hat{\Psi} + \left[\frac{2G_1}{n}\hat{\Psi}^\dagger\hat{\Psi} + \frac{2G_2}{n}\left(\hat{\Psi}^\dagger \hat{\sigma}_z \hat{\Psi}\right)\hat{\sigma}_z\right]\hat{\Psi} \ . \tag{4.197}$$

As we did in Sec. 4.3.2, we write the time-dependent field operator as

$$\hat{\Psi}(t) = e^{-i\mu t/\hbar}\left(\hat{\psi}_0 + \delta\hat{\Psi}(t)\right) . \tag{4.198}$$

Now, analogously to what was done in Sec. 4.3.2, one has

$$\hat{\psi}_0 = \frac{1}{\sqrt{V}}\sum_{n\in\mathbb{Z}} \vec{\psi}_{0,n} e^{ik_0x+2ink_0x}\hat{a}_{\vec{k}_0,l=0} \sim \sqrt{\frac{N_0}{V}}\sum_{n\in\mathbb{Z}} \vec{\psi}_{0,n} e^{ik_0x+2ink_0x} \tag{4.199}$$

$$\begin{aligned}\delta\hat{\Psi}\left(\vec{r},t\right) = \sum_{\substack{k_x>0,\vec{k}\in\mathrm{BZ}\\ l}} & \vec{f}_{\vec{k}_0+\vec{k},l}(\vec{k},\vec{r})\hat{b}_{\vec{k}_0+\vec{k},l}(t) + \vec{f}^{*}_{\vec{k}_0-\vec{k},l}(\vec{k},\vec{r})\hat{b}^{\dagger}_{\vec{k}_0-\vec{k},l}(t) \\ & + \vec{g}_{\vec{k}_0-\vec{k},l}(\vec{k},\vec{r})\hat{b}_{\vec{k}_0-\vec{k},l}(t) + \vec{g}^{*}_{\vec{k}_0+\vec{k},l}(\vec{k},\vec{r})\hat{b}^{\dagger}_{\vec{k}_0+\vec{k},l}(t)\end{aligned} \tag{4.200}$$

Here l is the band index, which replaces the index d of Sec. 4.3.2, which only took values $d = \pm 1$ because there are only two bands in the plane-wave and single minimum phases. Besides, $\vec{k}$ is restricted to the first Brillouin Zone of the system ($0 < k_x < 2k_0$) [70]. In the case of the stripe phase, l takes infinite values due to the periodicity of the system. Analogously to Sec. 4.3.2, we set the spatial dependence of the f and g functions to:

$$\vec{f}_{\vec{k}_0+\vec{k},l}(\vec{k},\vec{r}) = \frac{1}{\sqrt{V}}e^{i(\vec{k}_0+\vec{k})\vec{r}}\sum_{n\in\mathbb{Z}}\vec{f}_{\vec{k}_0+\vec{k},l,n}e^{2ink_0x} \tag{4.201}$$

$$\vec{f}^{*}_{\vec{k}_0-\vec{k},l}(\vec{k},\vec{r}) = \frac{1}{\sqrt{V}}e^{i(\vec{k}_0+\vec{k})\vec{r}}\sum_{n\in\mathbb{Z}}\vec{f}^{*}_{\vec{k}_0-\vec{k},l,n}e^{2ink_0x} \tag{4.202}$$

$$\vec{g}_{\vec{k}_0-\vec{k},l}(\vec{k},\vec{r}) = \frac{1}{\sqrt{V}}e^{i(\vec{k}_0-\vec{k})\vec{r}}\sum_{n\in\mathbb{Z}}\vec{g}_{\vec{k}_0-\vec{k},l,n}e^{2ink_0x} \tag{4.203}$$

$$\vec{g}^{*}_{\vec{k}_0+\vec{k},l}(\vec{k},\vec{r}) = \frac{1}{\sqrt{V}}e^{i(\vec{k}_0-\vec{k})\vec{r}}\sum_{n\in\mathbb{Z}}\vec{g}^{*}_{\vec{k}_0+\vec{k},l,n}e^{2ink_0x} \tag{4.204}$$

with $\vec{k}_0 = k_0\hat{u}_x$ and $\hat{u}_x$ the unitary vector along the x-axis. In these expressions we have expanded the f and g functions in Bloch waves due to the periodicity of the system. The position dependence of these functions matches the one from Ref. [70]. Also, analogously to Sec. 4.3.2, we set the time dependence of the $\hat{b}$ operators to:

$$\hat{b}_{\vec{k}_0+\vec{k},l}(t) = e^{-iE_{\vec{k}_0+\vec{k},l}t/\hbar}\hat{b}_{\vec{k}_0+\vec{k},l} \tag{4.205}$$

$$\hat{b}_{\vec{k}_0-\vec{k},l}(t) = e^{-iE_{\vec{k}_0-\vec{k},l}t/\hbar}\hat{b}_{\vec{k}_0-\vec{k},l} \tag{4.206}$$

$$\hat{b}^{\dagger}_{\vec{k}_0+\vec{k},l}(t) = e^{iE_{\vec{k}_0+\vec{k},l}t/\hbar}\hat{b}^{\dagger}_{\vec{k}_0+\vec{k},l} \tag{4.207}$$

$$\hat{b}^{\dagger}_{\vec{k}_0-\vec{k},l}(t) = e^{iE_{\vec{k}_0-\vec{k},l}t/\hbar}\hat{b}^{\dagger}_{\vec{k}_0-\vec{k},l} \tag{4.208}$$

The equation for $\delta\hat{\Psi}$ is given by (see Eq. (4.134))

$$\begin{aligned}\mu\delta\hat{\Psi}+i\hbar\frac{\mathrm{d}\delta\hat{\Psi}}{\mathrm{d}t}&=\hat{H}_0\delta\hat{\Psi}+\frac{2G_1}{n}\left[|\psi_0|^2\delta\hat{\Psi}+\psi_0^*\delta\hat{\Psi}\psi_0+\delta\hat{\Psi}^\dagger\psi_0\psi_0\right]\\&+\frac{2G_2}{n}\left[\psi_0^*\hat{\sigma}_z\psi_0\hat{\sigma}_z\delta\hat{\Psi}+\psi_0^*\hat{\sigma}_z\delta\hat{\Psi}\hat{\sigma}_z\psi_0+\delta\hat{\Psi}^\dagger\hat{\sigma}_z\psi_0\hat{\sigma}_z\psi_0\right]\end{aligned}\tag{4.209}$$

We substitute Eq. (4.200) into Eq. (4.209) and equal the coefficients of the same $\hat{b}$ operator. This results into:

$$\begin{aligned}(\mu+E_{\vec{k_0}+\vec{k},l})\vec{f}_{\vec{k_0}+\vec{k},l}(\vec{k},\vec{r})&=\hat{H}_0\vec{f}_{\vec{k_0}+\vec{k},l}(\vec{k},\vec{r})+\frac{2G_1}{n}\left[\left|\vec{\psi}_0\right|^2\vec{f}_{\vec{k_0}+\vec{k},l}(\vec{k},\vec{r})\right.\\&\left.+\vec{\psi}_0^\dagger\vec{f}_{\vec{k_0}+\vec{k},l}(\vec{k},\vec{r})\vec{\psi}_0+\vec{g}^{\tau}_{\vec{k_0}+\vec{k},l}(\vec{k},\vec{r})\vec{\psi}_0\vec{\psi}_0\right]\\&+\frac{2G_2}{n}\left[\vec{\psi}_0^*\hat{\sigma}_z\vec{\psi}_0\hat{\sigma}_z\vec{f}_{\vec{k_0}+\vec{k},l}(\vec{k},\vec{r})+\vec{\psi}_0^\dagger\hat{\sigma}_z\vec{f}_{\vec{k_0}+\vec{k},l}(\vec{k},\vec{r})\hat{\sigma}_z\vec{\psi}_0\right.\\&\left.+\vec{g}^{\tau}_{\vec{k_0}+\vec{k},l}(\vec{k},\vec{r})\hat{\sigma}_z\vec{\psi}_0\hat{\sigma}_z\vec{\psi}_0\right]\end{aligned}\tag{4.210}$$

$$\begin{aligned}(\mu-E_{\vec{k_0}+\vec{k},l})\vec{g}^*_{\vec{k_0}+\vec{k},l}(\vec{k},\vec{r})&=\hat{H}_0\vec{g}^*_{\vec{k_0}+\vec{k},l}(\vec{k},\vec{r})+\frac{2G_1}{n}\left[\left|\vec{\psi}_0\right|^2\vec{g}^*_{\vec{k_0}+\vec{k},l}(\vec{k},\vec{r})\right.\\&\left.+\vec{\psi}_0^\dagger\vec{g}^*_{\vec{k_0}+\vec{k},l}(\vec{k},\vec{r})\vec{\psi}_0+\vec{f}^\dagger_{\vec{k_0}+\vec{k},l}(\vec{k},\vec{r})\vec{\psi}_0\vec{\psi}_0\right]\\&+\frac{2G_2}{n}\left[\vec{\psi}_0^*\hat{\sigma}_z\vec{\psi}_0\hat{\sigma}_z\vec{g}^*_{\vec{k_0}+\vec{k},l}(\vec{k},\vec{r})+\vec{\psi}_0^\dagger\hat{\sigma}_z\vec{g}^*_{\vec{k_0}+\vec{k},l}(\vec{k},\vec{r})\hat{\sigma}_z\vec{\psi}_0\right.\\&\left.+\vec{f}^\dagger_{\vec{k_0}+\vec{k},l}(\vec{k},\vec{r})\hat{\sigma}_z\vec{\psi}_0\hat{\sigma}_z\vec{\psi}_0\right]\end{aligned}\tag{4.211}$$

$$\begin{aligned}(\mu-E_{\vec{k_0}-\vec{k},l})\vec{f}^*_{\vec{k_0}-\vec{k},l}(\vec{k},\vec{r})&=\hat{H}_0\vec{f}^*_{\vec{k_0}-\vec{k},l}(\vec{k},\vec{r})+\frac{2G_1}{n}\left[\left|\vec{\psi}_0\right|^2\vec{f}^*_{\vec{k_0}-\vec{k},l}(\vec{k},\vec{r})\right.\\&\left.+\vec{\psi}_0^\dagger\vec{f}^*_{\vec{k_0}-\vec{k},l}(\vec{k},\vec{r})\vec{\psi}_0+\vec{g}^\dagger_{\vec{k_0}-\vec{k},l}(\vec{k},\vec{r})\vec{\psi}_0\vec{\psi}_0\right]\\&+\frac{2G_2}{n}\left[\vec{\psi}_0^*\hat{\sigma}_z\vec{\psi}_0\hat{\sigma}_z\vec{f}^*_{\vec{k_0}-\vec{k},l}(\vec{k},\vec{r})+\vec{\psi}_0^\dagger\hat{\sigma}_z\vec{f}^*_{\vec{k_0}-\vec{k},l}(\vec{k},\vec{r})\hat{\sigma}_z\vec{\psi}_0\right.\\&\left.+\vec{g}^\dagger_{\vec{k_0}-\vec{k},l}(\vec{k},\vec{r})\hat{\sigma}_z\vec{\psi}_0\hat{\sigma}_z\vec{\psi}_0\right]\end{aligned}\tag{4.212}$$

$$\begin{aligned}(\mu+E_{\vec{k_0}-\vec{k},l})\vec{g}_{\vec{k_0}-\vec{k},l}(\vec{k},\vec{r})&=\hat{H}_0\vec{g}_{\vec{k_0}-\vec{k},l}(\vec{k},\vec{r})+\frac{2G_1}{n}\left[\left|\vec{\psi}_0\right|^2\vec{g}_{\vec{k_0}-\vec{k},l}(\vec{k},\vec{r})\right.\\&\left.+\vec{\psi}_0^\dagger\vec{g}_{\vec{k_0}-\vec{k},l}(\vec{k},\vec{r})\vec{\psi}_0+\vec{f}^{\tau}_{\vec{k_0}-\vec{k},l}(\vec{k},\vec{r})\vec{\psi}_0\vec{\psi}_0\right]\\&+\frac{2G_2}{n}\left[\vec{\psi}_0^*\hat{\sigma}_z\vec{\psi}_0\hat{\sigma}_z\vec{g}_{\vec{k_0}-\vec{k},l}(\vec{k},\vec{r})+\vec{\psi}_0^\dagger\hat{\sigma}_z\vec{g}_{\vec{k_0}-\vec{k},l}(\vec{k},\vec{r})\hat{\sigma}_z\vec{\psi}_0\right.\\&\left.+\vec{f}^{\tau}_{\vec{k_0}-\vec{k},l}(\vec{k},\vec{r})\hat{\sigma}_z\vec{\psi}_0\hat{\sigma}_z\vec{\psi}_0\right]\end{aligned}\tag{4.213}$$

As in the previous Section, we only need to diagonalize Eqs. (4.210) and (4.211), as Eqs. (4.212) (4.213) are equivalent to Eqs. (4.210) (4.211) under the change $E_{\vec{k_0}+\vec{k},l}\rightarrow$

$-E_{\vec{k}_0-\vec{k},l}$. We can then rewrite Eqs. (4.210) (4.211) in the form

$$
\begin{aligned}
(\mu + E_{\vec{k}_0+\vec{k},l})\vec{f}_{\vec{k}_0+\vec{k},l}(\vec{k},\vec{r}) &= \hat{H}_0\vec{f}_{\vec{k}_0+\vec{k},l}(\vec{k},\vec{r}) + \frac{2G_1}{n}\Big[\left|\vec{\psi}_0\right|^2\vec{f}_{\vec{k}_0+\vec{k},l}(\vec{k},\vec{r}) \\
&+\vec{\psi}_0\vec{\psi}_0^\dagger\vec{f}_{\vec{k}_0+\vec{k},l}(\vec{k},\vec{r}) + \vec{\psi}_0\vec{\psi}_0^T\vec{g}_{\vec{k}_0+\vec{k},l}(\vec{k},\vec{r})\Big] \\
&+ \frac{2G_2}{n}\Big[\vec{\psi}_0^\dagger\hat{\sigma}_z\vec{\psi}_0\hat{\sigma}_z\vec{f}_{\vec{k}_0+\vec{k},l}(\vec{k},\vec{r}) + \hat{\sigma}_z\vec{\psi}_0\vec{\psi}_0^\dagger\hat{\sigma}_z\vec{f}_{\vec{k}_0+\vec{k},l}(\vec{k},\vec{r}) \\
&+\hat{\sigma}_z\vec{\psi}_0\vec{\psi}_0^T\hat{\sigma}_z\vec{g}_{\vec{k}_0+\vec{k},l}(\vec{k},\vec{r})\Big] \qquad (4.214) \\
(\mu - E_{\vec{k}_0+\vec{k},l})\vec{g}^*_{\vec{k}_0+\vec{k},l}(\vec{k},\vec{r}) &= \hat{H}_0\vec{g}^*_{\vec{k}_0+\vec{k},l}(\vec{k},\vec{r}) + \frac{2G_1}{n}\Big[\left|\vec{\psi}_0\right|^2\vec{g}^*_{\vec{k}_0+\vec{k},l}(\vec{k},\vec{r}) \\
&+\vec{\psi}_0\vec{\psi}_0^\dagger\vec{g}^*_{\vec{k}_0+\vec{k},l}(\vec{k},\vec{r}) + \vec{\psi}_0\vec{\psi}_0^T\vec{f}^*_{\vec{k}_0+\vec{k},l}(\vec{k},\vec{r})\Big] \\
&+ \frac{2G_2}{n}\Big[\vec{\psi}_0^\dagger\hat{\sigma}_z\vec{\psi}_0\hat{\sigma}_z\vec{g}^*_{\vec{k}_0+\vec{k},l}(\vec{k},\vec{r}) + \hat{\sigma}_z\vec{\psi}_0\vec{\psi}_0^\dagger\hat{\sigma}_z\vec{g}^*_{\vec{k}_0+\vec{k},l}(\vec{k},\vec{r}) \\
&+\hat{\sigma}_z\vec{\psi}_0\vec{\psi}_0^T\hat{\sigma}_z\vec{f}^*_{\vec{k}_0+\vec{k},l}(\vec{k},\vec{r})\Big] \ . \qquad (4.215)
\end{aligned}
$$

As in Sec. 4.3.2, we have used the relations $(\vec{x}^T\vec{v})\vec{w} = (\vec{w}\vec{v}^T)\vec{x}$ and $(\vec{v}^T\vec{x})\vec{w} = (\vec{w}\vec{v}^T)\vec{x}$, with $\vec{x}, \vec{v}, \vec{w}$ vectors. We now expand $\vec{f}_{\vec{k}_0+\vec{k},l}(\vec{k},\vec{r})$ and $\vec{g}_{\vec{k}_0+\vec{k},l}(\vec{k},\vec{r})$ in terms of Bloch waves (Eqs. (4.201) to (4.203)), multiply both sides of both equations by $e^{-2in_0k_0x}$, $n_0 = -N_c, -N_c+1, ..., N_c-2, N_c-1$ and integrate over the volume V to get rid of the plane wave functions. This yields:

$$
\begin{aligned}
(\mu + E_{\vec{k}_0+\vec{k},l})\vec{f}_{\vec{k}_0+\vec{k},l,n_0} &= \hat{H}_0(\vec{k}_0 + \vec{k} + 2n_0k_0)\vec{f}_{\vec{k}_0+\vec{k},l,n_0} \\
&+ \frac{2G_1N_0}{nV}\Big[\vec{\psi}_{0,m}^\dagger\vec{\psi}_{0,m'}\vec{f}_{\vec{k}_0+\vec{k},l,n}\delta[n_0 - (n+m'-m)] \\
&+\vec{\psi}_{0,m}\vec{\psi}_{0,m'}^\dagger\vec{f}_{\vec{k}_0+\vec{k},l,n}\delta[n_0 - (n-m'+m)] \\
&+\vec{\psi}_{0,m}\vec{\psi}_{0,m'}^T\vec{g}_{\vec{k}_0+\vec{k},l,n}\delta[n_0 - (m'+m-n)]\Big] \\
&+ \frac{2G_2N_0}{nV}\Big[\vec{\psi}_{0,m}^\dagger\hat{\sigma}_z\vec{\psi}_{0,m'}\hat{\sigma}_z\vec{f}_{\vec{k}_0+\vec{k},l,n}\delta[n_0 - (n+m'-m)] \\
&+\hat{\sigma}_z\vec{\psi}_{0,m}\vec{\psi}_{0,m'}^\dagger\hat{\sigma}_z\vec{f}_{\vec{k}_0+\vec{k},l,n}\delta[n_0 - (n-m'+m)] \\
&+\hat{\sigma}_z\vec{\psi}_{0,m}\vec{\psi}_{0,m'}^T\hat{\sigma}_z\vec{g}_{\vec{k}_0+\vec{k},l,n}\delta[n_0 - (m'+m-n)]\Big] \qquad (4.216) \\
(\mu - E_{\vec{k}_0+\vec{k},l})\vec{g}^*_{\vec{k}_0+\vec{k},l,n_0} &= \hat{H}_0(\vec{k}_0 - \vec{k} + 2n_0k_0)\vec{g}^*_{\vec{k}_0+\vec{k},l,n_0} \\
&+ \frac{2G_1N_0}{nV}\Big[\vec{\psi}_{0,m}^\dagger\vec{\psi}_{0,m'}\vec{g}^*_{\vec{k}_0+\vec{k},l,n}\delta[n_0 - (n+m'-m)] \\
&+\vec{\psi}_{0,m}\vec{\psi}_{0,m'}^\dagger\vec{g}^*_{\vec{k}_0+\vec{k},l,n}\delta[n_0 - (n-m'+m)] \\
&+\vec{\psi}_{0,m}\vec{\psi}_{0,m'}^T\vec{f}^*_{\vec{k}_0+\vec{k},l,n}\delta[n_0 - (m'+m-n)]\Big]
\end{aligned}
$$

$$
\begin{aligned}
&+\frac{2G_2N_0}{nV}\Big[\vec{\psi}^{\dagger}_{0,m}\hat{\sigma}_z\vec{\psi}_{0,m'}\hat{\sigma}_z\vec{g}^{*}_{\vec{k}_0+\vec{k},l,n}\delta[n_0-(n+m'-m)]\\
&+\hat{\sigma}_z\vec{\psi}_{0,m}\vec{\psi}^{\dagger}_{0,m'}\hat{\sigma}_z\vec{g}^{*}_{\vec{k}_0+\vec{k},l,n}\delta[n_0-(n-m'+m)]\\
&+\hat{\sigma}_z\vec{\psi}_{0,m}\vec{\psi}^{\tau}_{0,m'}\hat{\sigma}_z\vec{f}^{*}_{\vec{k}_0+\vec{k},l,n}\delta[n_0-(m'+m-n)]\Big] \qquad (4.217)
\end{aligned}
$$

Since the matrix to be diagonalized is real, and the excitation spectrum energies must also be real, we assume the amplitudes $\vec{f}_{\vec{k}_0+\vec{k},l,n}$, $\vec{g}_{\vec{k}_0+\vec{k},l,n}$ to be real, i.e. $\vec{f}_{\vec{k}_0+\vec{k},l,n} = \vec{f}^{*}_{\vec{k}_0+\vec{k},l,n}$, $\vec{g}_{\vec{k}_0+\vec{k},l,n} = \vec{g}^{*}_{\vec{k}_0+\vec{k},l,n}$. We then define the vectors:

$$\vec{x}^{\tau}_{l,+} = \left(\vec{f}^{\tau}_{\vec{k}_0+\vec{k},l,-N_c},\ \dots\ ,\vec{f}^{\tau}_{\vec{k}_0+\vec{k},l,N_c-1},\vec{g}^{\tau}_{\vec{k}_0+\vec{k},l,-N_c},\ \dots\ ,\vec{g}^{\tau}_{\vec{k}_0+\vec{k},l,N_c-1}\right) \qquad (4.218)$$

$$\vec{x}^{\tau}_{l,-} = \left(\vec{f}^{\tau}_{\vec{k}_0-\vec{k},l,-N_c},\ \dots\ ,\vec{f}^{\tau}_{\vec{k}_0-\vec{k},l,N_c-1},\vec{g}^{\tau}_{\vec{k}_0-\vec{k},l,-N_c},\ \dots\ ,\vec{g}^{\tau}_{\vec{k}_0-\vec{k},l,N_c-1}\right) \qquad (4.219)$$

such that the system of equations described by Eqs. (4.216) and (4.217) can be written in matrix form. Diagonalizing this matrix system yields the eigenvalues $-E_{\vec{k}_0-\vec{k},l}$, $E_{\vec{k}_0+\vec{k},l}$ (as in Sec. 4.3.2) and the Bogoliubov amplitudes $\vec{x}_l$, for $l = 0,\ \dots\ ,8N_c-1$. The normalization condition fulfilled by the Bogoliubov amplitudes is [70]:

$$\sum_{n=-N_c}^{n=N_c-1}\vec{f}^{\tau}_{\vec{k}_0+\vec{k},l,n}\vec{f}_{k_0+\vec{k},l,n}-\left(\vec{g}^{\tau}_{\vec{k}_0+\vec{k},l,n}\vec{g}_{k_0+\vec{k},l,n}\right)=1 \qquad (4.220)$$

$$\sum_{n=-N_c}^{n=N_c-1}\vec{f}^{\tau}_{\vec{k}_0-\vec{k},l,n}\vec{f}_{k_0-\vec{k},l,n}-\left(\vec{g}^{\tau}_{\vec{k}_0-\vec{k},l,n}\vec{g}_{k_0-\vec{k},l,n}\right)=-1 \qquad (4.221)$$

As a way to check the formalism, we report in Fig. 4.3 the lowest four energy bands of the excitation spectrum in the stripe phase, in the same conditions as in Ref. [4] ($\Omega = 2$, $G_1 = 0.6$ and $G_2 = 0.16$ in our units). Only the first Brillouin Zone is displayed. As can be seen, we recover the results from Ref. [4]. Remarkably, the two lowest energy bands go to zero as k_x approaches the edges of the first Brillouin Zone. The existence of these two gapless bands reflects the two symmetries that are spontaneously broken in the stripe phase: gauge symmetry and spatial symmetry [4].

By defining the matrix:

$$M^{z}_{\vec{k}} = \left(\vec{x}_{0,+}\quad \dots\quad \vec{x}_{4N_c-1,+}\quad \vec{x}_{0,-}\quad \dots\quad \vec{x}_{4N_c-1,-}\right) \qquad (4.222)$$

that has the vectors $\vec{x}_{l,\pm}$ as columns, we can rewrite the normalization condition as:

$$M^{z,\dagger}_{\vec{k}}\tilde{I}M^{z}_{\vec{k}} = \tilde{I} \qquad (4.223)$$

$$\tilde{I}(i,j) = \delta[i-j] \qquad \tilde{I}(4N_c+i,4N_c+j) = -\delta[i-j] \qquad j = 1,2,\dots,4N_c \qquad (4.224)$$

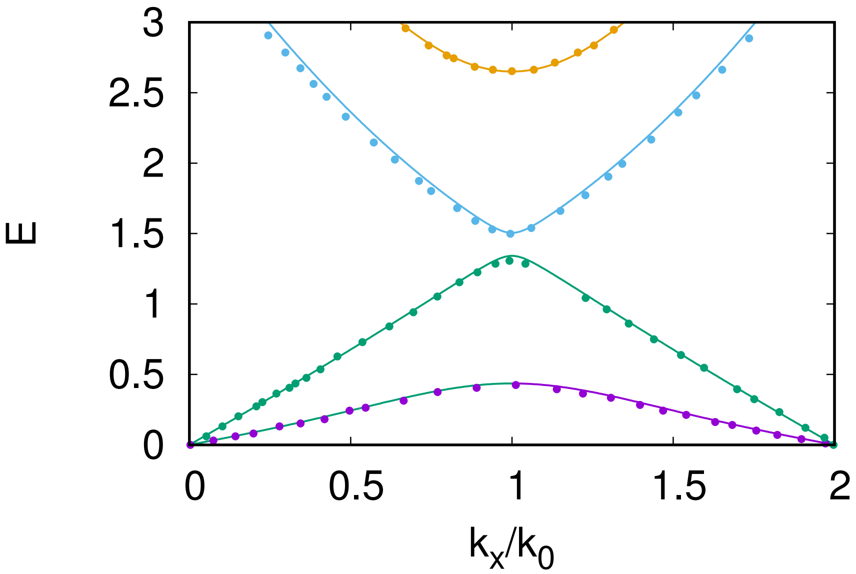

Fig. 4.3 Four lowest energy branches of the excitation spectrum in the stripe phase. We have set $\Omega = 2$, $G_1 = 0.6$ and $G_2 = 0.16$ as in Ref. [4]. Lines correspond to our results while points correspond to data from Ref. [4]. All quantities are expressed in reduced units.

We proceed now to compute the Lee-Huang-Yang energy correction of the system. Analogously to what we did in the previous Sections, we write:

$$E_{\text{g.s.}} = E_{\text{M.F.}}(N) + K_{\text{LHY}}(N_0) + \mathcal{O}\left(\delta N^2\right) \tag{4.225}$$

$$K_{\text{LHY}}(N_0) = \langle 0_b | \hat{H} - \mu \hat{N} | 0_b \rangle (N_0) - K_{\text{M.F.}}(N_0) \tag{4.226}$$

$$E_{\text{LHY}}(N) \simeq K_{\text{LHY}}(N_0) \tag{4.227}$$

$$K_{\text{M.F.}}(N_0) = E_{\text{M.F.}}(N_0) - \mu N_0 \tag{4.228}$$

with $E_{\text{M.F.}}$ given in Eq. (4.195) and the chemical potential given by

$$\begin{aligned}\mu = \frac{1}{\sum_{v\in\mathbb{Z}} \vec{\psi}^{\dagger}_{0,v}\vec{\psi}_{0,v}} \Bigg[\sum_{v\in\mathbb{Z}} \Bigg(& \frac{\hbar^2 k_0^2 (2n+1)^2}{2M} \left(\left|\psi^{+1}_{0,v}\right|^2 + \left|\psi^{-1}_{0,v}\right|^2 \right) \\ & + \frac{\hbar^2 \lambda k_0 (2n+1)}{M} \left(\left|\psi^{+1}_{0,v}\right|^2 - \left|\psi^{-1}_{0,v}\right|^2 \right) + \frac{\hbar^2\lambda^2}{2M} \left(\left|\psi^{+1}_{0,v}\right|^2 + \left|\psi^{-1}_{0,v}\right|^2 \right) - \Omega \psi^{+1}_{0,v}\psi^{-1}_{0,v} \Bigg) \\ & + \frac{2G_1 N_0}{nV} \sum_{v,w,l,q\in n\mathbb{Z}} \left(\psi^{+1}_{0,w}\psi^{+1}_{0,v} + \psi^{-1}_{0,w}\psi^{-1}_{0,v} \right) \left(\psi^{+1}_{0,l}\psi^{+1}_{0,q} + \psi^{-1}_{0,l}\psi^{-1}_{0,q} \right) \delta[v-w+l-q] \\ & + \frac{2G_2 N_0}{nV} \sum_{v,w,l,q\in n\mathbb{Z}} \left(\psi^{+1}_{0,w}\psi^{+1}_{0,v} - \psi^{-1}_{0,w}\psi^{-1}_{0,v} \right) \left(\psi^{+1}_{0,l}\psi^{+1}_{0,q} - \psi^{-1}_{0,l}\psi^{-1}_{0,q} \right) \delta[v-w+l-q] \Bigg] .\end{aligned} \tag{4.229}$$

As in the previous Section, we write:

$$\begin{aligned}
K_{\mathrm{LHY}}(N_0) &= \langle 0_b| \int d\vec{r}_1 d\vec{r}_2 \delta\hat{\Psi}^\dagger(\vec{r}_1)\left(\langle\vec{r}_1|\,\hat{H}_0\,|\vec{r}_2\rangle - \mu\delta\left(\vec{r}_2-\vec{r}_1\right)\right)\delta\hat{\Psi}(\vec{r}_2)\,|0_b\rangle \\
&+ \langle 0_b| \int d\vec{r}_1 d\vec{r}_2 \hat{\psi}_0^\dagger(\vec{r}_1)\hat{\psi}_0^\dagger(\vec{r}_2)V(\vec{r}_1,\vec{r}_2)\delta\hat{\Psi}(\vec{r}_1)\delta\hat{\Psi}(\vec{r}_2)\,|0_b\rangle \\
&+ \langle 0_b| \int d\vec{r}_1 d\vec{r}_2 \hat{\psi}_0^\dagger(\vec{r}_1)\delta\hat{\Psi}^\dagger(\vec{r}_2)V(\vec{r}_1,\vec{r}_2)\hat{\psi}_0(\vec{r}_1)\delta\hat{\Psi}(\vec{r}_2)\,|0_b\rangle \\
&+ \langle 0_b| \int d\vec{r}_1 d\vec{r}_2 \delta\hat{\Psi}^\dagger(\vec{r}_1)\hat{\psi}_0^\dagger(\vec{r}_2)V(\vec{r}_1,\vec{r}_2)\hat{\psi}_0(\vec{r}_1)\delta\hat{\Psi}(\vec{r}_2)\,|0_b\rangle \\
&= K_{\mathrm{LHY},0} + K_{\mathrm{LHY},1} + K_{\mathrm{LHY},2} + K_{\mathrm{LHY},3}\ . \qquad (4.230)
\end{aligned}$$

where $|0_b\rangle$ indicates the beyond mean field ground state, which is annihilated by all operators $\hat{b}_{\vec{k},l}$ with $\vec{k} \neq \vec{k}_0$ (ground state momentum), $l \neq 0$. We now compute each one of these terms. We do so by expanding the $\delta\hat{\Psi}$ operator using Eq. (4.200) and then, expanding the Bogoliubov amplitudes in Bloch waves using Eqs. (4.201) to (4.204). The calculation yields

$$\begin{aligned}
K_{\mathrm{LHY},0} &= \langle 0_b| \int d\vec{r}_1 d\vec{r}_2 \delta\hat{\Psi}^\dagger(\vec{r}_1)\left(\langle\vec{r}_1|\,\hat{H}_0\,|\vec{r}_2\rangle - \mu\delta\left(\vec{r}_2-\vec{r}_1\right)\right)\delta\hat{\Psi}(\vec{r}_2)\,|0_b\rangle \\
&= \langle 0_b| \int d\vec{r}_1 d\vec{r}_2 \left\{ \sum_{\substack{k_x>0,\vec{k}\in\mathrm{BZ}\\ l}} \vec{f}_{\vec{k}_0+\vec{k},l}(\vec{k},\vec{r}_1)\hat{b}_{\vec{k}_0+\vec{k},l} + \vec{f}^{*}_{\vec{k}_0-\vec{k},l}(\vec{k},\vec{r}_1)\hat{b}^\dagger_{\vec{k}_0-\vec{k},l}\right. \\
&\left. + \vec{g}_{\vec{k}_0-\vec{k},l}(\vec{k},\vec{r}_1)\hat{b}_{\vec{k}_0-\vec{k},l} + \vec{g}^{*}_{\vec{k}_0+\vec{k},l}(\vec{k},\vec{r}_1)\hat{b}^\dagger_{\vec{k}_0+\vec{k},l}\right\}^\dagger \left(\langle\vec{r}_1|\,\hat{H}_0\,|\vec{r}_2\rangle - \mu\delta\left(\vec{r}_2-\vec{r}_1\right)\right) \\
&\times \left\{ \sum_{\substack{k_x>0,\vec{k}\in\mathrm{BZ}\\ l}} \vec{f}_{\vec{k}_0+\vec{k},l}(\vec{k},\vec{r}_2)\hat{b}_{\vec{k}_0+\vec{k},l} + \vec{f}^{*}_{\vec{k}_0-\vec{k},l}(\vec{k},\vec{r}_2)\hat{b}^\dagger_{\vec{k}_0-\vec{k},l}\right. \\
&\left. + \vec{g}_{\vec{k}_0-\vec{k},l}(\vec{k},\vec{r}_2)\hat{b}_{\vec{k}_0-\vec{k},l} + \vec{g}^{*}_{\vec{k}_0+\vec{k},l}(\vec{k},\vec{r}_2)\hat{b}^\dagger_{\vec{k}_0+\vec{k},l}\right\}|0_b\rangle \\
&= \sum_{\substack{k_x>0,\vec{k}\in\mathrm{BZ}\\ l,m\\ s_1,s_2}} \left\{ f_{\vec{k}_0-\vec{k},l,m,s_1} f^{*}_{\vec{k}_0-\vec{k},l,m,s_2}\left[H_0(\vec{k}_0+\vec{k}+2m\vec{k}_0,s_1,s_2) - \delta_{s_1,s_2}\mu\right]\right. \\
&\left. + g_{\vec{k}_0+\vec{k},l,m,s_1} g^{*}_{\vec{k}_0+\vec{k},l,m,s_2}\left[H_0(\vec{k}_0-\vec{k}+2m\vec{k}_0,s_1,s_2) - \delta_{s_1,s_2}\mu\right]\right\} \\
&= \sum_{\substack{l,m\\ s_1,s_2}} \frac{V}{(2\pi)^3}\int_{\substack{k_x>0\\ \vec{k}\in\mathrm{BZ}}} d\vec{k} \left\{ f_{\vec{k}_0-\vec{k},l,m,s_1} f^{*}_{\vec{k}_0-\vec{k},l,m,s_2}\left[H_0(\vec{k}_0+\vec{k}+2m\vec{k}_0,s_1,s_2) - \delta_{s_1,s_2}\mu\right]\right. \\
&\left. + g_{\vec{k}_0+\vec{k},l,m,s_1} g^{*}_{\vec{k}_0+\vec{k},l,m,s_2}\left[H_0(\vec{k}_0-\vec{k}+2m\vec{k}_0,s_1,s_2) - \delta_{s_1,s_2}\mu\right]\right\} \qquad (4.231)
\end{aligned}$$

where l is the band index, m is the Brillouin Zone index, and $\{s_1,\ s_2\}$ indicate the components of the $\vec{f}$ and $\vec{g}$ vectors in the $\hat{\sigma}_z$ representation. Again, $H_0(\vec{k},s_1,s_2)$ corresponds to $\langle s_1|\,H_0(\vec{k})\,|s_2\rangle$, i.e. the matrix element of the one-body Hamiltonian of

Eq. (4.57) in the momentum and spin-z representation. The rest of the contributions can be obtained analogously to $K_{\mathrm{LHY},0}$. They yield:

$$\begin{aligned}
K_{\mathrm{LHY},1} &= \langle 0_b| \int d\vec{r}_1 d\vec{r}_2 \hat{\psi}_0^\dagger(\vec{r}_1)\hat{\psi}_0^\dagger(\vec{r}_2) V(\vec{r}_1,\vec{r}_2)\delta\hat{\Psi}(\vec{r}_1)\delta\hat{\Psi}(\vec{r}_2)\,|0_b\rangle \\
&= \frac{4\pi\hbar^2}{M}\langle 0_b| \int d\vec{r}\hat{\psi}_0^\dagger(\vec{r})\hat{\psi}_0^\dagger(\vec{r}) \left[\sum_{s_1,s_2} a_{s_1,s_2}\,|s_1,s_2\rangle\,\langle s_1,s_2|\right]\delta\hat{\Psi}(\vec{r})\delta\hat{\Psi}(\vec{r})\,|0_b\rangle \\
&= \frac{4\pi\hbar^2}{M}\langle 0_b| \int d\vec{r}\hat{\psi}_0^\dagger(\vec{r})\hat{\psi}_0^\dagger(\vec{r}) \left[\sum_{s_1,s_2} a_{s_1,s_2}\,|s_1,s_2\rangle\,\langle s_1,s_2|\right] \\
&\times \Bigg\{ \sum_{\substack{k_x>0,\vec{k}\in\mathrm{BZ}\\ l}} \vec{f}_{\vec{k_0}+\vec{k},l}(\vec{k},\vec{r})\hat{b}_{\vec{k_0}+\vec{k},l} + \vec{f}^{*}_{\vec{k_0}-\vec{k},l}(\vec{k},\vec{r})\hat{b}^\dagger_{\vec{k_0}-\vec{k},l} \\
&+ \vec{g}_{\vec{k_0}-\vec{k},l}(\vec{k},\vec{r})\hat{b}_{\vec{k_0}-\vec{k},l} + \vec{g}^{*}_{\vec{k_0}+\vec{k},l}(\vec{k},\vec{r})\hat{b}^\dagger_{\vec{k_0}+\vec{k},l}\Bigg\} \\
&\times \Bigg\{ \sum_{\substack{k_x>0,\vec{k}\in\mathrm{BZ}\\ l}} \vec{f}_{\vec{k_0}+\vec{k},l}(\vec{k},\vec{r})\hat{b}_{\vec{k_0}+\vec{k},l} + \vec{f}^{*}_{\vec{k_0}-\vec{k},l}(\vec{k},\vec{r})\hat{b}^\dagger_{\vec{k_0}-\vec{k},l} \\
&+ \vec{g}_{\vec{k_0}-\vec{k},l}(\vec{k},\vec{r})\hat{b}_{\vec{k_0}-\vec{k},l} + \vec{g}^{*}_{\vec{k_0}+\vec{k},l}(\vec{k},\vec{r})\hat{b}^\dagger_{\vec{k_0}+\vec{k},l}\Bigg\}\,|0_b\rangle \\
&= \frac{4\pi\hbar^2}{M}\sum_{\substack{k_x>0,\vec{k}\in\mathrm{BZ}\\ l}} \int d\vec{r}\hat{\psi}_0^\dagger(\vec{r})\hat{\psi}_0^\dagger(\vec{r}) \left[\sum_{s_1,s_2} a_{s_1,s_2}\,|s_1,s_2\rangle\,\langle s_1,s_2|\right] \\
&\times \left(\vec{g}^{*}_{\vec{k_0}+\vec{k},l}(\vec{k},\vec{r})\vec{f}_{\vec{k_0}+\vec{k},l}(\vec{k},\vec{r}) + \vec{f}^{*}_{\vec{k_0}-\vec{k},l}(\vec{k},\vec{r})\vec{g}_{\vec{k_0}-\vec{k},l}(\vec{k},\vec{r})\right) \\
&= \frac{4\pi\hbar^2 n_0}{M}\sum_{\substack{k_x>0,\vec{k}\in\mathrm{BZ}\\ l\\ n_1,n_2,n_3,n_4}} \Bigg\{ \vec{\psi}^\dagger_{0,n_1}\vec{\psi}^\dagger_{0,n_2}\left[\sum_{s_1,s_2} a_{s_1,s_2}\,|s_1,s_2\rangle\,\langle s_1,s_2|\right] \\
&\times \left(\vec{g}^{*}_{\vec{k_0}+\vec{k},l,n_3}\vec{f}_{\vec{k_0}+\vec{k},l,n_4} + \vec{f}^{*}_{\vec{k_0}-\vec{k},l,n_3}\vec{g}_{\vec{k_0}-\vec{k},l,n_4}\right)\delta[n_3+n_4-n_1-n_2]\Bigg\} \\
&= \frac{4\pi\hbar^2 n_0}{M}\sum_{\substack{k_x>0,\vec{k}\in\mathrm{BZ}\\ l\\ n_1,n_2,n_3,n_4}}\sum_{s_1,s_2} \Bigg\{ \psi^{*}_{0,n_1,s_1}\psi^{*}_{0,n_2,s_2}a_{s_1,s_2}\Big(g^{*}_{\vec{k_0}+\vec{k},l,n_3,s_1}f_{\vec{k_0}+\vec{k},l,n_4,s_2} \\
&+ f^{*}_{\vec{k_0}-\vec{k},l,n_3,s_1}g_{\vec{k_0}-\vec{k},l,n_4,s_2}\Big)\delta[n_3+n_4-n_1-n_2]\Bigg\}
\end{aligned}$$

$$
\begin{aligned}
&= \frac{4\pi\hbar^2 n_0}{M}\frac{V}{(2\pi)^3}\sum_{\substack{l\\ n_1,n_2,n_3,n_4\\ s_1,s_2}}\int_{k_x>0,\vec{k}\in\mathrm{BZ}} d\vec{k}\left\{\psi^*_{0,n_1,s_1}\psi^*_{0,n_2,s_2}a_{s_1,s_2}\right.\\
&\left.\times\left(g^*_{\vec{k}_0+\vec{k},l,n_3,s_1}f_{\vec{k}_0+\vec{k},l,n_4,s_2}+f^*_{\vec{k}_0-\vec{k},l,n_3,s_1}g_{\vec{k}_0-\vec{k},l,n_4,s_2}\right)\delta[n_3+n_4-n_1-n_2]\right\} \qquad (4.232)
\end{aligned}
$$

$$
\begin{aligned}
K_{\mathrm{LHY},2} &= \frac{4\pi\hbar^2 n_0}{M}\frac{V}{(2\pi)^3}\sum_{\substack{l\\ n_1,n_2,n_3,n_4\\ s_1,s_2}}\int_{k_x>0,\vec{k}\in\mathrm{BZ}} d\vec{k}\left\{\psi^*_{0,n_1,s_1}\psi_{0,n_2,s_1}a_{s_1,s_2}\right.\\
&\left.\times\left(g_{\vec{k}_0+\vec{k},l,n_3,s_2}g^*_{\vec{k}_0+\vec{k},l,n_4,s_2}+f^*_{\vec{k}_0-\vec{k},l,n_3,s_2}f_{\vec{k}_0-\vec{k},l,n_4,s_2}\right)\delta[-n_3+n_4-n_1+n_2]\right\}
\end{aligned}
\qquad (4.233)
$$

$$
\begin{aligned}
K_{\mathrm{LHY},3} &= \frac{4\pi\hbar^2 n_0}{M}\frac{V}{(2\pi)^3}\sum_{\substack{l\\ n_1,n_2,n_3,n_4\\ s_1,s_2}}\int_{k_x>0,\vec{k}\in\mathrm{BZ}} d\vec{k}\left\{\psi^*_{0,n_1,s_1}\psi_{0,n_2,s_2}a_{s_1,s_2}\right.\\
&\left.\times\left(g_{\vec{k}_0+\vec{k},l,n_3,s_1}g^*_{\vec{k}_0+\vec{k},l,n_4,s_2}+f^*_{\vec{k}_0-\vec{k},l,n_3,s_1}f_{\vec{k}_0-\vec{k},l,n_4,s_2}\right)\delta[-n_3+n_4-n_1+n_2]\right\}
\end{aligned}
\qquad (4.234)
$$

Collecting these results, we see that K_{LHY}/N_0 is given by:

$$
\begin{aligned}
K_{\mathrm{LHY}}/N_0 = \sum_{\substack{l,m\\ s_1,s_2}}\frac{1}{(2\pi)^3 n_0}\int_{\substack{k_x>0\\ \vec{k}\in\mathrm{BZ}}} d\vec{k}&\left\{f_{\vec{k}_0-\vec{k},l,m,s_1}f^*_{\vec{k}_0-\vec{k},l,m,s_2}\left[H_0(\vec{k}_0+\vec{k}+2m\vec{k}_0,s_1,s_2)-\delta_{s_1,s_2}\mu\right]\right.\\
&\left.+g_{\vec{k}_0+\vec{k},l,m,s_1}g^*_{\vec{k}_0+\vec{k},l,m,s_2}\left[H_0(\vec{k}_0-\vec{k}+2m\vec{k}_0,s_1,s_2)-\delta_{s_1,s_2}\mu\right]\right\}\\
&+\frac{4\pi\hbar^2}{M}\frac{1}{(2\pi)^3}\sum_{\substack{l\\ n_1,n_2,n_3,n_4\\ s_1,s_2}}\int_{k_x>0,\vec{k}\in\mathrm{BZ}} d\vec{k}\left\{\psi^*_{0,n_1,s_1}\psi^*_{0,n_2,s_2}a_{s_1,s_2}\right.\\
&\times\left(g^*_{\vec{k}_0+\vec{k},l,n_3,s_1}f_{\vec{k}_0+\vec{k},l,n_4,s_2}+f^*_{\vec{k}_0-\vec{k},l,n_3,s_1}g_{\vec{k}_0-\vec{k},l,n_4,s_2}\right)\delta[n_3+n_4-n_1-n_2]\\
&+\psi^*_{0,n_1,s_1}\psi_{0,n_2,s_1}a_{s_1,s_2}\left(g_{\vec{k}_0+\vec{k},l,n_3,s_2}g^*_{\vec{k}_0+\vec{k},l,n_4,s_2}+f^*_{\vec{k}_0-\vec{k},l,n_3,s_2}f_{\vec{k}_0-\vec{k},l,n_4,s_2}\right)\\
&\times\delta[-n_3+n_4-n_1+n_2]+\psi^*_{0,n_1,s_1}\psi_{0,n_2,s_2}a_{s_1,s_2}\\
&\left.\times\left(g_{\vec{k}_0+\vec{k},l,n_3,s_1}g^*_{\vec{k}_0+\vec{k},l,n_4,s_2}+f^*_{\vec{k}_0-\vec{k},l,n_3,s_1}f_{\vec{k}_0-\vec{k},l,n_4,s_2}\right)\delta[-n_3+n_4-n_1+n_2]\right\}\,.\\
&\simeq E_{\mathrm{LHY}}/N
\end{aligned}
\qquad (4.235)
$$

We define the integrals:

$$
\begin{aligned}
I_2 = \frac{4\pi\hbar^2}{(2\pi)^3 M} & \sum_{\substack{l \\ n_1,n_2,n_3,n_4 \\ s_1,s_2}} \int_{\substack{0<k_x<k_0 \\ 0<k_y,k_z<\infty}} d\vec{k}\, \Big\{ \psi^*_{0,n_1,s_1}\psi^*_{0,n_2,s_2} a_{s_1,s_2} \\
\times & \left(g^*_{\vec{k_0}+\vec{k},l,n_3,s_1} f_{\vec{k_0}+\vec{k},l,n_4,s_2} + f^*_{\vec{k_0}-\vec{k},l,n_3,s_1} g_{\vec{k_0}-\vec{k},l,n_4,s_2} \right) \delta[n_3+n_4-n_1-n_2] \Big\}
\end{aligned}
\tag{4.236}
$$

$$
\begin{aligned}
I_3 = \frac{4\pi\hbar^2}{(2\pi)^3 M} & \sum_{\substack{l \\ n_1,n_2,n_3,n_4 \\ s_1,s_2}} \int_{\substack{0<k_x<k_0 \\ 0<k_y,k_z<\infty}} d\vec{k} \psi^*_{0,n_1,s_1}\psi_{0,n_2,s_1} a_{s_1,s_2} \\
\times & \left(g_{\vec{k_0}+\vec{k},l,n_3,s_2} g^*_{\vec{k_0}+\vec{k},l,n_4,s_2} + f^*_{\vec{k_0}-\vec{k},l,n_3,s_2} f_{\vec{k_0}-\vec{k},l,n_4,s_2} \right) \delta[-n_3+n_4-n_1+n_2] \\
+ & \psi^*_{0,n_1,s_1}\psi_{0,n_2,s_2} a_{s_1,s_2} \left(g_{\vec{k_0}+\vec{k},l,n_3,s_1} g^*_{\vec{k_0}+\vec{k},l,n_4,s_2} + f^*_{\vec{k_0}-\vec{k},l,n_3,s_1} f_{\vec{k_0}-\vec{k},l,n_4,s_2} \right) \delta[-n_3+n_4-n_1+n_2]
\end{aligned}
\tag{4.237}
$$

which are particular contributions to K_{LHY}/N_0, as can be seen in Eq. (4.235). As in the plane wave and single-minimum phases, the integrals in Eq. (4.235) diverge, and must be properly regularized. However, before discussing the regularization procedure, we shall comment on some technical aspects regarding the computation of these integrals. The integration region in Eq. (4.235) is $k_\perp = \sqrt{k_y^2 + k_z^2} \in [0, \infty)$, $0 < k_x < k_0$, with k_0 the ground state momentum. The sum indexes $\{l, n_1, n_2, n_3, n_4\}$ range from $-\infty$, $+\infty$. In practice, we introduce cut-off values in both operations and restrict the calculation to $0 < k_\perp = \sqrt{k_y^2 + k_z^2} < k_{\perp,\max}$ and $-N_c < l, n_1, n_2, n_3, n_4 < N_c - 1$. The integration volume is then $V_I = \pi k^2_{\perp,\max} \times 4N_c k_0$, a cylinder of radius $k_{\perp,\max}$ in the $\{k_y, k_z\}$ plane and height $4N_c k_0$ in the k_x axis, centered at the origin. We define N_x and $N_\perp$ as the number of points in the x and radial axes, respectively. Looking at Eq. (4.235), one notices that the integral scales as $\mathcal{O}\left(N_x N_\perp N_c^4\right)$, while typically, $N_x \sim \mathcal{O}\left(10^2\right)$, $N_\perp \sim \mathcal{O}\left(10^3\right)$ and the calculation becomes too expensive in computational time. In order to make it feasible, we introduce two approximations. The first one involves the number of momentum components of the condensate wave function (i.e. indexes n_1 and n_2 in Eq. (4.235)). According to Ref. [70] and to our Simulated Annealing calculations, the absolute value of the Bloch wave amplitudes in the condensate wave function decreases very rapidly with the momentum index n. We thus truncate the sum and denote by $N_{c,0}$ the number of momentum components of the condensate wave function included in the computation of the LHY integral, and fix its value. In this way, the LHY integral scales as $\mathcal{O}\left(N_x N_\perp N_{c,0}^2 N_c^2\right)$, with the integration volume remaining unchanged. In practice, no significant changes are seen in the results when $N_{c,0} > 5$, so we set $N_{c,0} = 5$.

The computational cost can be furtherly reduced when a second approximation is introduced. It can be checked numerically that, as $k_\perp$ and N_c increase, the integral I_2 is dominated by the contributions from the $f_{\vec{k}_0+\vec{k},l,l,\pm 1}$ and $g_{\vec{k}_0-\vec{k},l,l,\pm 1}$ terms. Therefore, we retain only the two most dominant terms for every value of l to the integral instead of performing the whole sum over n_3 and n_4. Additionally, we retain only the two first momentum modes of the condensate state when computing the integral I_3, since we have checked that these are also the dominant contributions. These approximations reduce the scaling of the computational cost of the LHY integral on N_c up to $\text{Max}\left\{\mathcal{O}\Big(N_x N_\perp N_c N_{c,0}^2\Big),\ \mathcal{O}\Big(N_x N_\perp N_c^2\Big)\right\}$, which, in practical terms, is a significant reduction with respect to $\mathcal{O}\Big(N_x N_\perp N_{c,0}^2 N_c^2\Big)$. We show in Fig. 4.4 the marginal integrand of Eq. 4.235 after integrating over the x-axis and performing the sums, for the exact case with $N_c = 9$, and the approximated case with $N_c = 9$, $N_{c,0} = 5$. As it can be seen from the Figure, both curves are in excellent agreement.

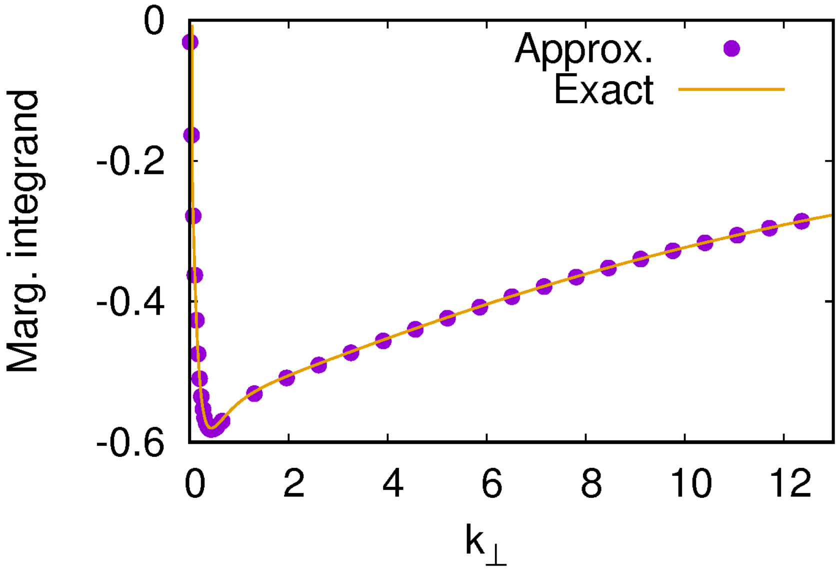

Fig. 4.4 Exact ($N_c = 9$) and approximated ($N_c = 9$, $N_{c,0} = 5$) marginal integrands of the unregularized LHY energy per particle for $\Omega = 2.8$, $a_{+1,+1} = a_{-1,-1} = 0.641982$, $\gamma = (a_{+1,+1} - a_{+1,-1})/(a_{+1,+1} + a_{+1,-1}) = 0.4$, $n = 3.7 \times 10^{-3}$, $N_x = 200$, $N_\perp = 2000$.

Next we proceed to discuss the regularization of E_{LHY}/N. We define $\epsilon_{\text{LHY}}(V_I)$ as the integral of Eq. (4.235) over a finite integration volume V_I. As mentioned previously, the LHY integral for a Raman SOC stripe system is ultraviolet divergent (i.e. $\lim_{V_I \to \infty} \epsilon_{\text{LHY}}(V_I) = \infty$), and must be regularized. To identify the diverging behavior, we compute $\epsilon_{\text{LHY}}(V_I)$ over increasingly larger cylindrical volumes. These volumes are defined as $V_I^{(i)} = \pi (k_{\perp,\max}^{(i)})^2 \times 4 N_c^{(i)} k_0$, with $k_{\perp,\max}^{(i)} = 2 N_c^{(i)} k_0$, $N_c^{(i)} \in \mathbb{N}$. We find that $\epsilon_{\text{LHY}}(V_I)$ can be fitted to

$$f_{\eta,I_0}(V_I) = \int_{V_I} d\vec{k}\ \eta/k^2 + I_0 = I_\eta(V_I) + I_0 \tag{4.238}$$

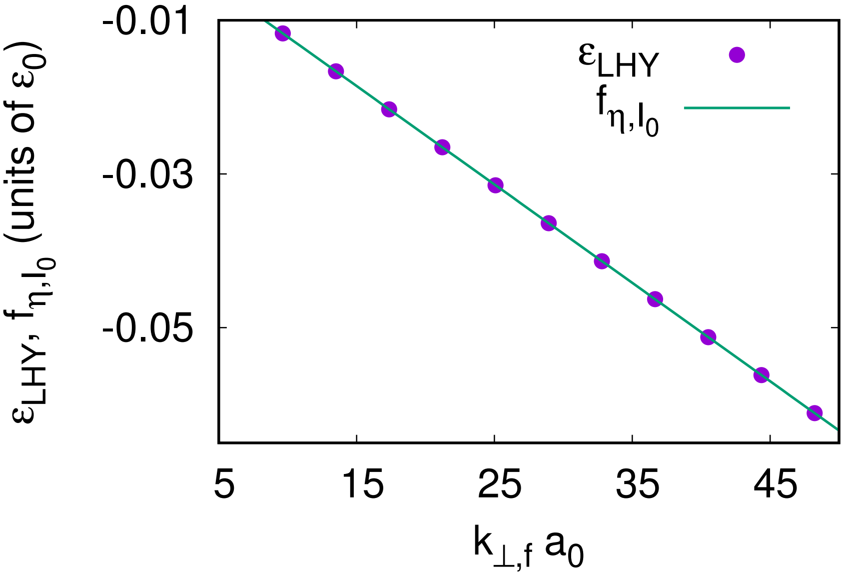

Fig. 4.5 ϵ_{LHY} (blue dots) and f_{η,I_0} (green line) computed for different integration volumes V_I, with $V_I = \pi k_{\perp,\mathrm{f}}^2 \times 2k_{\perp,\mathrm{f}}$, a cylinder of radius $k_{\perp,\mathrm{f}}$ and height $2k_{\perp,\mathrm{f}}$, with $k_{\perp,\mathrm{f}} = 2N_c k_0$, $N_c \in [5, 25]$. Other parameters are $\Omega = 1.0$, $a_{+1,+1} = a_{-1,-1} = 0.2$, $\gamma = -21$, $n = 3.11 \times 10^{-3}$, $N_x = 300$, $N_\perp = 3000$.

with η and I_0 fitting parameters, $k^2 = k_x^2 + k_y^2 + k_z^2$, and $I_\eta(V_I)$ given by:

$$I_\eta(V_I) = 8\pi\eta N_c k_0 \left(\frac{\pi}{4} + \frac{\log 2}{2}\right) \tag{4.239}$$

with $\log 2 = 0.6931$. We show $\epsilon_{\mathrm{LHY}}(V_I)$ and $f_{\eta,I_0}(V_I)$ as a function of the integration volume in Fig. 4.5. Therefore, the quantity $\lim_{V_I\to\infty} \epsilon_{\mathrm{LHY}}(V_I) - I_\eta(V_I)$ is finite. Thus, the LHY energy per particle can be computed as

$$E_{\mathrm{LHY}}/N = \lim_{V_I\to\infty} \left[\epsilon_{\mathrm{LHY}}(V_I) - I_\eta(V_I)\right] + I_\eta^{\mathrm{reg.}} \ , \tag{4.240}$$

with I_η^{reg} the regularized $I_\eta(\infty)$ value, which we obtain applying Dimensional Regularization [72, 73]. As mentioned in Sec. 4.2.1, the regularized integral of a polynomial vanishes [72], which implies $I_\eta^{\mathrm{reg}}(V_I = \infty) = 0$. Thus, the regularized LHY integral is given by:

$$E_{\mathrm{LHY}}/N = \lim_{V_I\to\infty} \left[\epsilon_{\mathrm{LHY}}(V_I) - I_\eta(V_I)\right] = I_0 \tag{4.241}$$

Ideally, the regularized LHY integral should be computed for $N_c \to \infty$, $N_x \to \infty$, $N_\perp \to \infty$. However, in practice, the values N_c, N_x and $N_\perp$ used in the calculations are finite. In order to approach the asymptotic limit, the regularized LHY integral is computed for different values $N_c \in [n_{c,0}, n_{c,1}]$ and for different number of points,

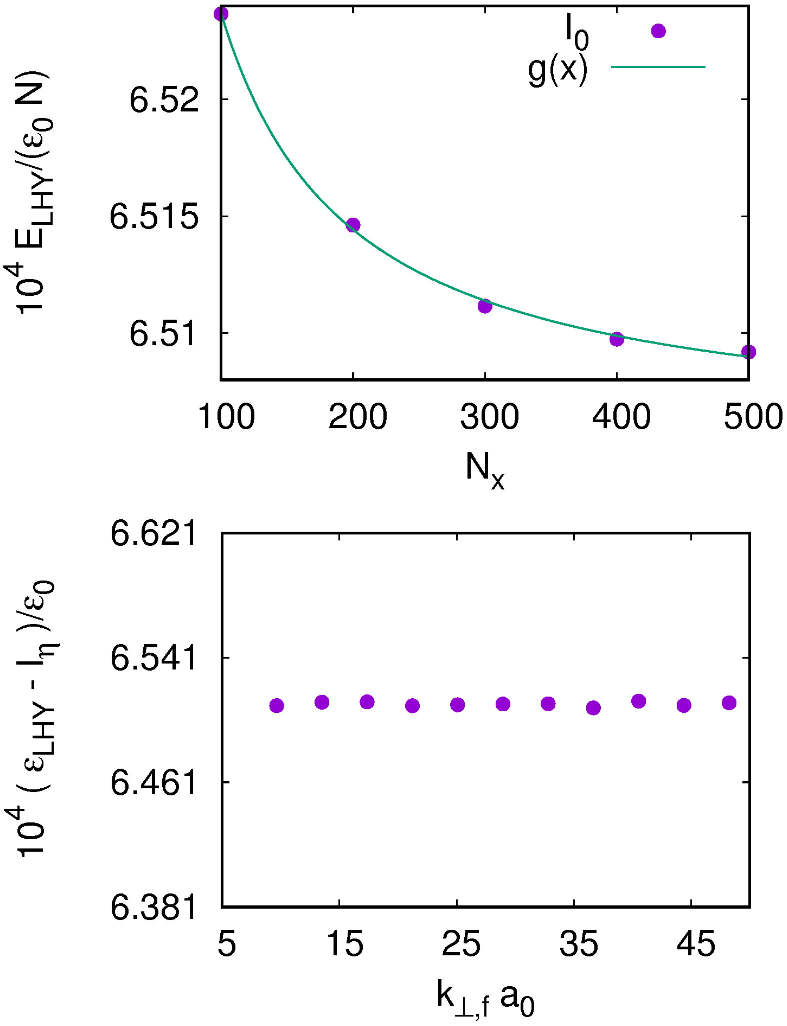

Fig. 4.6 Upper plot: $I_0(N_x)$ vs N_x. Lower plot: $\epsilon_{\mathrm{LHY}}(V_I) - I_\eta(V_I)$ computed for different integration volumes V_I, with $V_I = \pi k_{\perp,\mathrm{f}}^2 \times 2k_{\perp,\mathrm{f}}$, a cylinder of radius $k_{\perp,\mathrm{f}}$ and height $2k_{\perp,\mathrm{f}}$. Other parameters are: $\Omega = 1.0$, $a_{+1,+1} = a_{-1,-1} = 0.2$, $\gamma = -21$, $n = 3.11 \times 10^{-3}$.

$N_x \in [n_{x,0}, n_{x,1}]$, with $N_\perp = 10N_x$. For each value of N_c, the cylindrical integration volume is $V_I = \pi(2N_c k_0)^2 \times 4N_c k_0$. For each fixed number of points, the fitting of $\epsilon_{\mathrm{LHY}}(V_I)$ using the function in Eq. (4.238) is carried out, resulting in a function $I_0(N_x)$. We then extrapolate $I_0(N_x)$ to $N_x \to \infty$ using a function of the form $g(N_x) = a + b/N_x^l$ and take the extrapolation, $I_0(N_x \to \infty)$, as the final result. The shape of the function $g(N_x)$ has been chosen by inspection, as it seems suitable to perform the extrapolation in the tested cases. The range of N_c is chosen such that the quantity $\epsilon_{\mathrm{LHY}}(V_I) - I_\eta(V_I)$ does not depend on N_c, meaning that the asymptotic limit has been reached. We show in Fig. 4.6, $I_0(N_x)$ as a function of the number of points N_x for $\Omega = 1.0$, $a_{+1,+1} = a_{-1,-1} = 0.2$, $\gamma = -21$, $n = 3.11 \times 10^{-3}$, and the quantity $\epsilon_{\mathrm{LHY}}(V_I) - I_\eta(V_I)$ as a function of the number of modes N_c, for $N_x = 300$. As it can be seen from the

Figure, $\epsilon_{\mathrm{LHY}}(V_I) - I_\eta(V_I)$ shows no significant dependence on N_c. The extrapolation of $I_0(N_x)$ to $N_x \to \infty$ yields the final result $E_{\mathrm{LHY}}/N = I_0(N_x \to \infty) = 6.505 \times 10^{-4}$. In practice, one can just perform the calculations for two values of N_c and one for N_x such that $I(N_x) \simeq I(N_x \to \infty)$. As an example, setting $N_c = 5, 7$ and $N_x = 600$ one obtains $E_{\mathrm{LHY}}/N = I_0(N_x = 600) = 6.494 \times 10^{-4} \simeq I_0(N_x \to \infty)$

We can also compute other physical quantities apart from the ground state energy, as we did in Sec. 4.3.2, like the static structure factor $S(\vec{k})$, the spin static structure factor $S_\sigma(\vec{k})$ and the condensate fraction, f_c. We proceed to compute these observables. Again, we focus on the k_x dependence of $S(\vec{k})$ and $S_\sigma(\vec{k})$. The static structure factor is defined in Eq. (4.176). The elements $s_{l,\vec{k}}(q_x)$ can be written in terms of the field operator as:

$$\begin{aligned} s_{l,\vec{k}}(q_x) &= \frac{1}{\sqrt{N}} \langle 0_b| \int d\vec{r} \hat{\Psi}^\dagger(\vec{r}) e^{iq_x x} \hat{\Psi}(\vec{r}) \, |l\rangle_{\vec{k}} \\ &= \frac{1}{\sqrt{N}} \langle 0_b| \int d\vec{r} \hat{\psi}_0^\dagger(\vec{r}) e^{iq_x x} \hat{\psi}_0(\vec{r}) \, |l\rangle_{\vec{k}} + \frac{1}{\sqrt{N}} \langle 0_b| \int d\vec{r} \delta\hat{\Psi}^\dagger(\vec{r}) e^{iq_x x} \hat{\psi}_0(\vec{r}) \, |l\rangle_{\vec{k}} \\ &+ \frac{1}{\sqrt{N}} \langle 0_b| \int d\vec{r} \hat{\psi}_0^\dagger(\vec{r}) e^{iq_x x} \delta\hat{\Psi}(\vec{r}) \, |l\rangle_{\vec{k}} + \frac{1}{\sqrt{N}} \langle 0_b| \int d\vec{r} \delta\hat{\Psi}^\dagger(\vec{r}) e^{iq_x x} \delta\hat{\Psi}(\vec{r}) \, |l\rangle_{\vec{k}} \end{aligned} \tag{4.242}$$

As for the plane wave and single minimum cases, we focus on the terms which yield a non-trivial dependence on q_x in the static structure factor, with $0 < q_x < 2k_0$, corresponding to the first Brillouin Zone. These are:

$$\begin{aligned} s_{l,\vec{k}}(q_x)\Big|_{\vec{k} \neq \vec{k}_0} &= \frac{1}{\sqrt{N}} \langle 0_b| \int d\vec{r} \delta\hat{\Psi}^\dagger(\vec{r}) e^{iq_x x} \hat{\psi}_0(\vec{r}) \, |l\rangle_{\vec{k}} + \frac{1}{\sqrt{N}} \langle 0_b| \int d\vec{r} \hat{\psi}_0^\dagger(\vec{r}) e^{iq_x x} \delta\hat{\Psi}(\vec{r}) \, |l\rangle_{\vec{k}} \\ &= s_{l,\vec{k},1}(q_x) + s_{l,\vec{k},2}(q_x) \; . \end{aligned} \tag{4.243}$$

We then compute each contribution separately. We start by setting $\vec{k} = \vec{k}_0 + \vec{k}'$, $k'_x > 0$, with $0 < k_x < 2k_0$, i.e., $\vec{k}$ in the first Brillouin Zone. Then:

$$\begin{aligned} s^{(+)}_{l,\vec{k},1}(q_x) &= \frac{1}{\sqrt{N}} \langle 0_b| \int d\vec{r} \delta\hat{\Psi}^\dagger(\vec{r}) e^{iq_x x} \hat{\psi}_0(\vec{r}) \hat{b}^\dagger_{\vec{k}_0+\vec{k}',l} \, |0\rangle_b \\ &= \frac{1}{V} \sum_{m,n} \int d\vec{r} \vec{g}^{\mathcal{T}}_{\vec{k}_0+\vec{k}',l,n} e^{i(-\vec{k}_0+\vec{k}'-2nk_0x)\vec{r}} e^{iq_x x} \vec{\psi}_{0,m} e^{i(\vec{k}_0+2mk_0x)\vec{r}} \\ &= \sum_{n,m} \vec{g}^{\mathcal{T}}_{\vec{k}_0+\vec{k}',l,n} \vec{\psi}_{0,m} \delta[\vec{k}' + q_x\vec{u}_x + 2(m-n)k_0\vec{u}_x] \end{aligned} \tag{4.244}$$

with $\vec{u}_x$ the unitary vector along the x-axis. In this expression, the only non-vanishing contributions are:

$$s^{(+)}_{l,\vec{k},1}(q_x) = \sum_n \vec{g}^{\mathcal{T}}_{\vec{k}_0+\vec{k}',l,n+1} \vec{\psi}_{0,n} \delta[\vec{k}' + q_x\vec{u}_x - 2k_0\vec{u}_x] \; , \tag{4.245}$$

and by setting $\vec{k} = \vec{k}_0 - \vec{k}'$, $k'_x > 0$ we obtain

$$\begin{aligned} s^{(-)}_{l,\vec{k},1}(q_x) &= \frac{1}{\sqrt{N}} \langle 0_b| \int d\vec{r} \delta \hat{\Psi}^\dagger(\vec{r}) e^{iq_x x} \hat{\psi}_0(\vec{r}) \hat{b}^\dagger_{\vec{k}_0-\vec{k}',l} |0\rangle_b \\ &= \frac{1}{V} \sum_{m,n} \int d\vec{r} \vec{f}^{\tau}_{\vec{k}_0-\vec{k}',l,n} e^{-i(\vec{k}_0+\vec{k}'-2nk_0 x)\vec{r}} e^{iq_x x} \vec{\psi}_{0,m} e^{i\vec{k}_0\vec{r}+2imk_0 x} \\ &= \sum_{m,n} \vec{f}^{\tau}_{\vec{k}_0-\vec{k}',l,n} \vec{\psi}_{0,m} \delta[-\vec{k}' + q_x + 2(m-n)k_0 \vec{u}_x] \end{aligned} \tag{4.246}$$

The surviving contributions are

$$s^{(-)}_{l,\vec{k},1}(q_x) = \sum_n \vec{f}^{\tau}_{\vec{k}_0-\vec{k}',l,n} \vec{\psi}_{0,n} \delta[-\vec{k}' + q_x] \ , \tag{4.247}$$

and similarly

$$s^{(+)}_{l,\vec{k},2}(q_x) = \sum_n \vec{\psi}^\dagger_{0,n+1} \vec{f}_{\vec{k}_0+\vec{k}',l,n} \delta[\vec{k}' + q_x \vec{u}_x - 2k_0 \vec{u}_x] \tag{4.248}$$

$$s^{(-)}_{l,\vec{k},2}(q_x) = \sum_n \vec{\psi}^\dagger_{0,n} \vec{g}_{\vec{k}_0-\vec{k}',l,n} \delta[-\vec{k}' + q_x \vec{u}_x] \ . \tag{4.249}$$

In this way we obtain the complete expression of the static structure factor

$$S(q_x) = \sum_{l,k'_x>0} \left| s^{(+)}_{l,\vec{k},1}(q_x) + s^{(+)}_{l,\vec{k},2}(q_x) \right|^2 + \left| s^{(-)}_{l,\vec{k},1}(q_x) + s^{(-)}_{l,\vec{k},2}(q_x) \right|^2 \ . \tag{4.250}$$

Analogously, we can obtain the spin static structure factor $S_\sigma(\vec{k})$, defined in Eq. (4.185), which is given by

$$S_\sigma(q_x) = \sum_{l,k'_x>0} \left| s^{(+),\sigma}_{l,\vec{k},1}(q_x) + s^{(+),\sigma}_{l,\vec{k},2}(q_x) \right|^2 + \left| s^{(-),\sigma}_{l,\vec{k},1}(q_x) + s^{(-),\sigma}_{l,\vec{k},2}(q_x) \right|^2 \tag{4.251}$$

with:

$$s^{(+),\sigma}_{l,\vec{k},1}(q_x) = \sum_n \vec{g}^{\tau}_{\vec{k}_0+\vec{k}',l,n+1} \sigma_z \vec{\psi}_{0,n} \delta[\vec{k}' + q_x \vec{u}_x - 2k_0 \vec{u}_x] \tag{4.252}$$

$$s^{(-),\sigma}_{l,\vec{k},1}(q_x) = \sum_n \vec{f}^{\tau}_{\vec{k}_0-\vec{k}',l,n} \sigma_z \vec{\psi}_{0,n} \delta[-\vec{k}' + q_x] \tag{4.253}$$

$$s^{(+),\sigma}_{l,\vec{k},2}(q_x) = \sum_n \vec{\psi}^\dagger_{0,n+1} \sigma_z \vec{f}_{\vec{k}_0+\vec{k}',l,n} \delta[\vec{k}' + q_x \vec{u}_x - 2k_0 \vec{u}_x] \tag{4.254}$$

$$s^{(-),\sigma}_{l,\vec{k},2}(q_x) = \sum_n \vec{\psi}^\dagger_{0,n} \sigma_z \vec{g}_{\vec{k}_0-\vec{k}',l,n} \delta[-\vec{k}' + q_x \vec{u}_x] \tag{4.255}$$

We report in Fig. 4.7 the static structure factor and $S_l(q_x)$ for $l = 0,\ 1$ (i.e. the contribution to the static structure factor from each band of the excitation spectrum) for $l = 0,\ 1$ (the first and second bands, respectively)) in the same conditions as in Ref. [4] in order to benchmark our calculations. From the Figure, we see that we

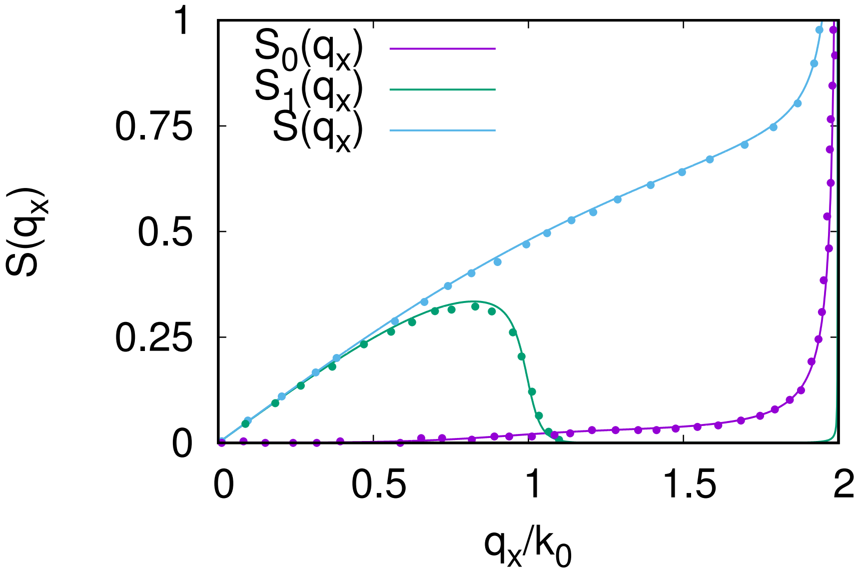

Fig. 4.7 Total static structure factor (blue line) and first and second band contributions to $S(q_x)$ (purple and green lines) as a function of q_x. We have set $\Omega = 2$, $G_1 = 0.6$ and $G_2 = 0.16$, which corresponds to the parameters of Ref. [4] expressed in our units. Lines correspond to our results while points correspond to data from Ref. [4]. All quantities are expressed in reduced units.

successfully recover the results in the reference. The static structure factor diverges as $q_x \to 2k_0$, which reflects the breaking of continuous translational symmetry in the stripe phase. Moreover, we notice that the main contribution to the static structure factor at low momentum comes from the second band. This reveals that the second band is of density nature [4], i.e. experiments where density excitations are produced will bring the system to a state in the second band.

We show in Fig. 4.8 the spin static structure factor and the contributions to this quantity arising from the first and second bands of the excitation spectrum (analogously to the static structure factor). Again, parameters are chosen to be equal to the ones from Ref. [4] in our units. Remarkably, the first band shows a higher contribution at low momentum to the spin static structure factor with respect to the second band. This indicates that the first band is of spin nature [4].

The density and spin nature of each band is a property that depends on the interatomic scattering lengths. By leaving $g_{+1,+1}$ unchanged and decreasing $g_{+1,-1}$, we see how, at low momenta, the contribution to the static structure factor coming from the first band increases, while the contribution coming from the second band decreases. The opposite effect is present for the spin static structure factor. We showcase this in Fig. 4.9. Remarkably, we have found numerically that the value of $g_{+1,-1}$ for which both bands are of spin and density nature simultaneously (i.e. they contribute equally

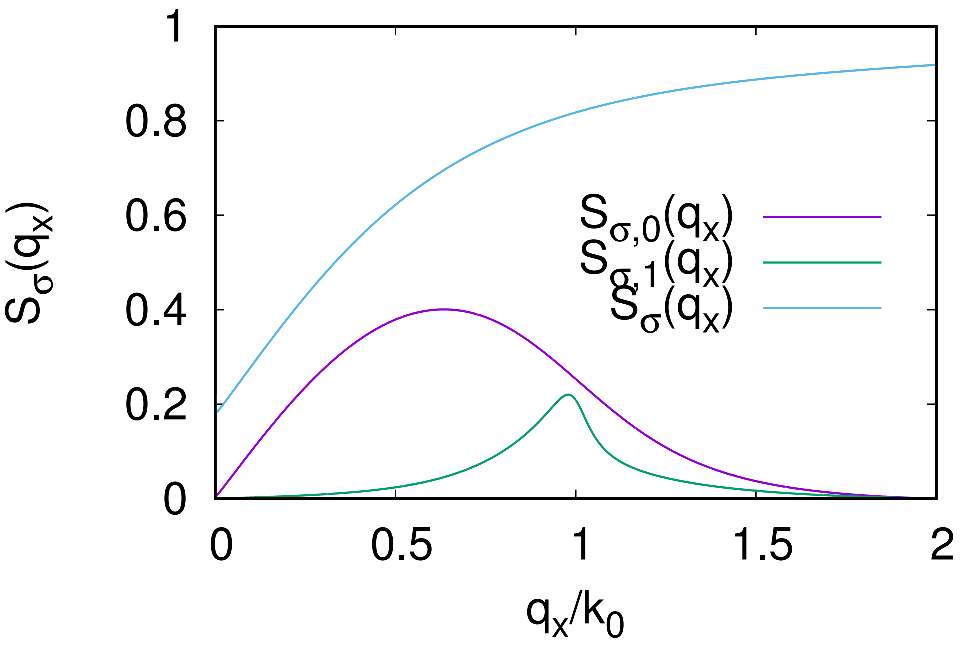

Fig. 4.8 Total spin static structure factor (blue line) and first and second band contributions to $S_\sigma(q_x)$ (purple and green lines) as a function of q_x. We have set $\Omega = 2$, $G_1 = 0.6$ and $G_2 = 0.16$ as in Ref. [4]. All quantities are expressed in reduced units.

to both the static structure factor and the spin static structure factor at low momenta) corresponds to the $g_{+1,-1}$ that makes the effective inter-species interaction between dressed spins, $g_{+1',-1'}$, vanish. As shown in Chapter 2, $g_{+1',-1'}$ is given by:

$$g_{+1',-1'} \simeq g_{+1,-1} + 4g_{+1,+1}\left(\frac{\Omega}{8\epsilon_0}\right)^2 \tag{4.256}$$

Therefore, the value $g^{\text{hybrid}}_{+1,-1}$ for which both bands are simultaneously of spin and density nature is approximately given by:

$$g^{\text{hybrid}}_{+1,-1} \simeq -4g_{+1,+1}\left(\frac{\Omega}{8\epsilon_0}\right)^2 \tag{4.257}$$

In order to validate this statement, we show in Fig. 4.10 a comparison between the values of $ng^{\text{hybrid}}_{+1,-1}$ obtained numerically and those obtained from Eq. (4.257). As we can see from the Figure, there is good agreement between analytical and numerical results. It must be remarked that $g^{\text{hybrid}}_{+1,-1} > -g_{+1,+1}$, so this effect is always present for attractive inter-atomic interactions that do not lead the mean field state to collapse, which happens for $g_{+1,-1} = -g_{+1,+1} = -g_{-1,-1}$ (see Sec. 4.4).

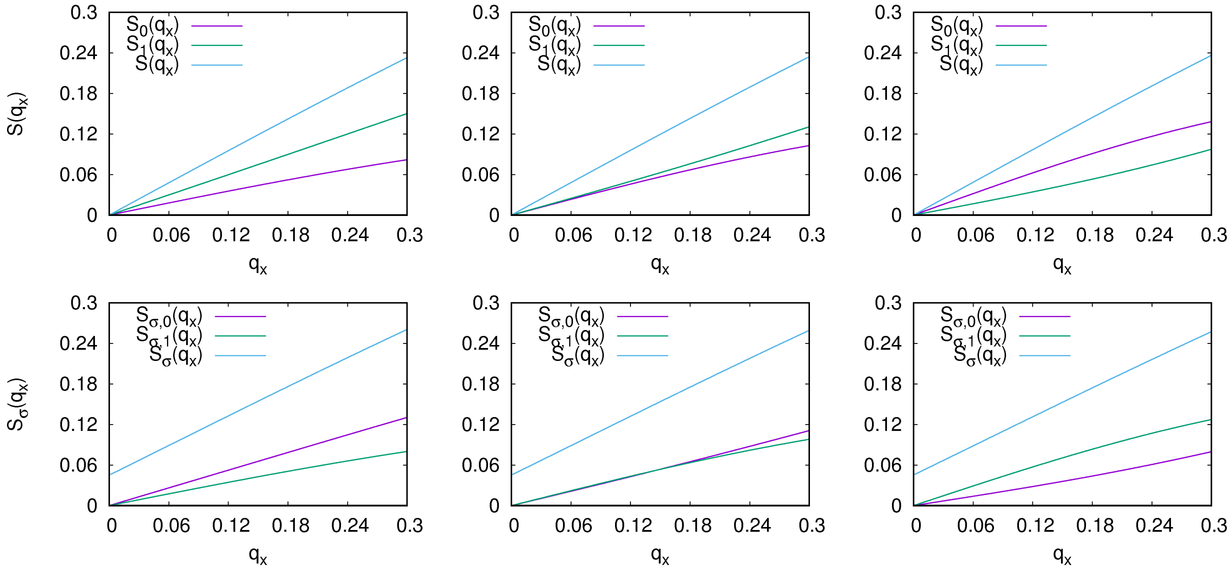

Fig. 4.9 Total static structure factor (upper plots, blue line) and first and second band contributions to $S(q_x)$ (purple and green lines) as a function of q_x. The lower plots correspond to the spin static structure factor. We have set $\Omega = 1.0$ and $ng_{+1,+1} = ng_{-1,-1} = 1.52$. The left plots correspond to $ng_{+1,-1} = -0.072$, the center plots to $ng_{+1,-1} = -0.096$ and the right plots to $ng_{+1,-1} = -0.12$. All quantities are expressed in reduced units.

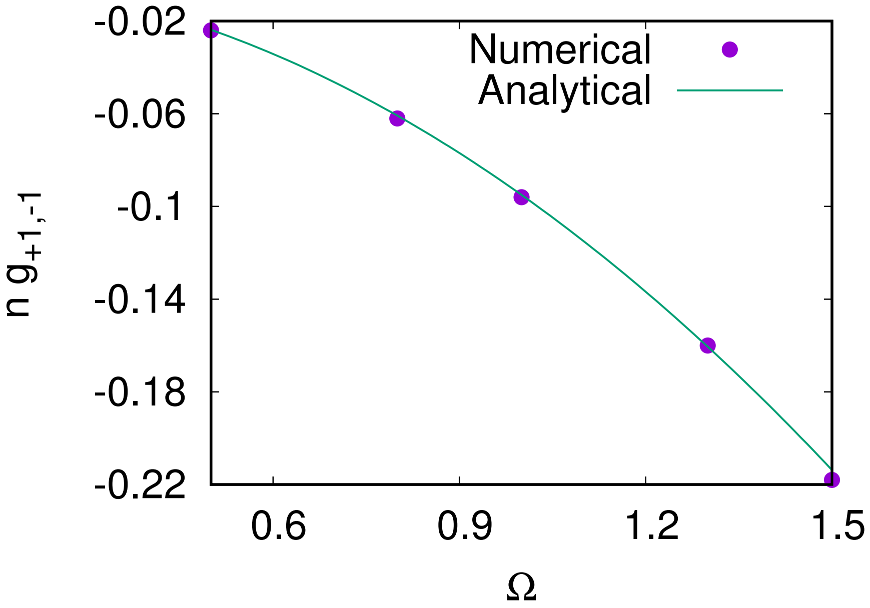

Fig. 4.10 Comparison between results of $ng^{\text{hybrid}}_{+1,-1}$ obtained numerically (points) and from Eq. (4.257) (line) for $ng^{\text{hybrid}}_{+1,-1} = 1.52$. All quantities are expressed in reduced units.

Finally, we briefly address the computation of the condensate fraction. Analogously to Sec. 4.3.2, it can be computed as:

$$f_c = \frac{1}{N} \langle 0_b| \int d\vec{r}_1 \delta\hat{\Psi}^\dagger(\vec{r}_1)\delta\hat{\Psi}(\vec{r}_1) |0_b\rangle \ , \tag{4.258}$$

which can be written as:

$$f_c = \sum_{\substack{l,m \\ s_1}} \frac{1}{(2\pi)^3 n} \int_{\substack{k_x>0 \\ \vec{k}\in\mathrm{BZ}}} d\vec{k} \left\{ f_{\vec{k}_0-\vec{k},l,m,s_1} f^*_{\vec{k}_0-\vec{k},l,m,s_1} + g_{\vec{k}_0+\vec{k},l,m,s_1} g^*_{\vec{k}_0+\vec{k},l,m,s_1} \right\} \ . \tag{4.259}$$

This expression can be used to obtain f_c once the Bogoliubov amplitudes have been obtained during the evaluation of the LHY energy.

4.4 Application: supersolid striped droplets in a Raman SOC system.

In this Section we apply the previous formalism to compute the LHY energy correction for a system under Raman SOC with attractive inter-spin interactions in the stripe phase. It must be remarked that published experimental results regarding Raman SOC feature repulsive inter and intra-spin interactions. These systems can be accurately described with the mean field approximation [60], at least for *gas parameters* up to $na^3_{+1,+1} \sim 10^{-4}$ [48]. Nevertheless, state of the art experiments currently under development, which do feature attractive inter-spin interactions, are pursuing the observation of the effect played by quantum fluctuations in these systems.

We are interested in characterizing the role played by quantum fluctuations in a mean field state with attractive enough inter-spin interactions that lead to a collapse. It is a well known result from unstable Bose-Bose mixtures without SOC that the LHY energy correction stabilizes the collapse predicted by mean field theory, resulting on a system that behaves as a liquid [35]. In particular, a finite size system admits a droplet-like solution, whose profile can be obtained by solving the extended Gross-Pitaevskii equation. These droplets represent an exotic state of matter with liquid properties at very low densities. In this Section, we evaluate the LHY energy correction for a system under Raman SOC in the stripe phase that is unstable at the mean field level, in order to determine whether quantum fluctuations stabilize the system or not, and also the properties of the system in case it is stable.

4.4.1 Stability of a system in the mean field regime

We first discuss the stability criteria in the mean field regime. Let $E(T, V, N)$ be the mean field energy of a system. We set $T = 0$ (as usual in ultracold atom systems) and consider a fixed number of particles. Therefore:

$$dE = \left.\frac{\partial E}{\partial V}\right|_N dV = -PdV \tag{4.260}$$

A system is mechanically stable if:

$$\left.\frac{\partial^2 E}{\partial V^2}\right|_N > 0 \rightarrow -\left.\frac{\partial P}{\partial V}\right|_N > 0 \tag{4.261}$$

which is equivalent to ask for the pressure of the system to decrease if the volume increases. The condition of mechanical stability can be rewritten in terms of the energy per volume and the density as:

$$\begin{aligned}\left.\frac{\partial^2 E}{\partial V^2}\right|_N &= \left.\frac{\partial}{\partial V}\left[\frac{\partial\left(E/V \times V\right)}{\partial V}\right]\right|_N = \left.\frac{\partial}{\partial V}\left[V\frac{\partial\left(E/V\right)}{\partial V} + E/V\right]\right|_N \\ &= \left.\frac{\partial}{\partial V}\left[\frac{\partial\left(E/V\right)}{\partial n}\left(-\frac{N}{V}\right) + E/V\right]\right|_N \\ &= \left.\frac{\partial}{\partial V}\left[\frac{\partial\left(E/V\right)}{\partial n}\left(-\frac{N}{V}\right)\right]\right|_N + \frac{\partial\left(E/V\right)}{\partial n}\left(-\frac{N}{V^2}\right) \\ &= \frac{N^2}{V^3}\frac{\partial^2 E/V}{\partial n^2}\end{aligned} \tag{4.262}$$

Thus, defining $\epsilon = \frac{E}{N}$, the mechanical stability condition can be expressed as:

$$\frac{\partial^2\left(n\epsilon\right)}{\partial n^2} > 0 \tag{4.263}$$

If the number of particles is not held constant, we should write

$$dE = \left.\frac{\partial E}{\partial V}\right|_N dV + \left.\frac{\partial E}{\partial N}\right|_V dN = -PdV + \mu dN \tag{4.264}$$

with μ the chemical potential. In this case, stability with respect to the number of particles must be consider together with mechanical stability. Thus, we have to impose

$$\begin{aligned}\left.\frac{\partial^2 E}{\partial N^2}\right|_V > 0 \rightarrow \left.\frac{\partial}{\partial N}\frac{\partial E}{\partial N}\right|_V > 0 \rightarrow \left.\frac{1}{V}\frac{\partial}{\partial n}\frac{\partial E/V}{\partial n}\right|_V > 0 \\ \rightarrow \frac{\partial^2\left(n\epsilon\right)}{\partial n^2} > 0\end{aligned} \tag{4.265}$$

Therefore, the condition in Eq. (4.263) guarantees both mechanical and concentration stability. Notice that this is a mathematical condition that involves a quantity that only depends explicitly on the density, $n\epsilon$, and its derivatives with respect to n.

In the case of a non-SOC system with spin-dependent scattering lengths fulfilling $a_{+1,+1} = a_{-1,-1} > a_{+1,-1} = a_{+1,-1}$, the mean field energy per particle is given by:

$$\epsilon = \frac{4\pi\hbar^2 n}{M}\left(\frac{a_{+1,+1} + a_{+1,-1}}{4}\right) \tag{4.266}$$

Thus, the stability condition reduces to:

$$\frac{\partial^2 (n\epsilon)}{\partial n^2} > 0 \to \frac{8\pi\hbar^2}{M}\left(\frac{a_{+1,+1} + a_{+1,-1}}{4}\right) > 0 \to a_{+1,+1} > -a_{+1,-1} \tag{4.267}$$

This condition can be written as

$$G_1 > 0 \tag{4.268}$$

with G_1 defined in Eq. (4.127). This stability condition is the same that is found in the case of Bose-Bose mixtures with equal masses and inter-species interactions [35].

We move on now to the computation of the stability condition for a Raman SOC system in the stripe phase. The mean field energy, in reduced units, is given by: [25]

$$\epsilon = G_1 - \frac{\Omega^2}{8\left(2 + G_1\right)} \tag{4.269}$$

This expression corresponds to Eq. (4.195) when considering only the $v = -1,\ 0$ in the sum. Now we define $g_1 = G_1/n$. The stability condition is given by:

$$\begin{aligned}\frac{\partial^2 (n\epsilon)}{\partial n^2} &= \frac{\partial}{\partial n}\left[2ng_1 - \frac{\Omega^2}{8}\left(\frac{2 + ng_1 - ng_1}{\left(2 + ng_1\right)^2}\right)\right] \\ &= 2g_1 - \frac{\Omega^2}{4}\left(\frac{-2g_1}{\left(2 + ng_1\right)^3}\right) \\ &= 2g_1 + 2g_1\frac{1}{\left(2 + ng_1\right)}\left(\frac{\Omega^2}{4\left(2 + ng_1\right)^2}\right) > 0\end{aligned} \tag{4.270}$$

The momentum in the stripe phase within the mean field approximation is given by: [25]

$$k_{\text{stripe}} = \sqrt{1 - \frac{\Omega^2}{4\left(2 + ng_1\right)^2}} \tag{4.271}$$

Therefore, we can write:

$$\frac{\partial^2 (n\epsilon)}{\partial n^2} = g_1\left\{2 + \frac{2}{\left(2 + ng_1\right)}\left(1 - k_{\text{stripe}}^2\right)\right\} > 0 \tag{4.272}$$

Assuming now $g_1 > 0$, the stability condition becomes

$$\frac{2}{(2+ng_1)}\left(1-k_{\mathrm{stripe}}^2\right) > -2 \ . \tag{4.273}$$

Since $k_{\mathrm{stripe}} < 1$ (see Eq. (4.271)), the condition is fulfilled $\forall g_1 > 0$. However, if we set $g_1 < 0$, the condition becomes:

$$\frac{2}{(2+ng_1)}\left(1-k_{\mathrm{stripe}}^2\right) < -2 \tag{4.274}$$

This stability condition is violated $\forall g_1 < 0$ that fulfill $2 > |ng_1|$ with $g_1 < 0$ in reduced units. This second condition is always fulfilled in the calculations performed in this Section. Therefore, for the purposes of this work, the mean field state is unstable if $g_1 < 0$, $2 > |ng_1|$.

4.4.2 The role of quantum fluctuations: phase diagram of the stabilized system

In this Section, we study the effect of quantum fluctuations on a Raman SOC system in the stripe phase with $a_{+1,+1} = a_{-1,-1}$, $a_{+1,-1} = a_{-1,+1} = -1.1a_{+1,+1}$. The choice for the ratios between the different scattering lengths guarantees that we do not depart excessively from the mean field stability condition. Under these circumstances, $G_1 < 0$, which results in the system being unstable in the mean field regime. However, the LHY energy is positive and stabilizes the collapsing mean field state. This is similar to the result obtained for unstable Bose-Bose mixtures without SOC [35], although remarkable differences exist between the two cases, as detailed below.

The phase diagram of the stabilized system, as a function of Ω and $a_{+1,+1} > 0$, for $\gamma = -21$ (i.e. $a_{+1,-1} = -1.1a_{+1,+1}$) is shown in Fig. 4.11. The phase diagram includes beyond mean field effects, with the ground state being the phase of minimum energy. Error bars account for the numerical error associated to the finite number of Brillouin Zones and integration points considered in the calculations. As it can be seen from the Figure, depending on the value of the Raman coupling Ω and the scattering lengths, the homogeneous system can be either a liquid ($n^{(0)} \neq 0$ with $n^{(0)}$ the density where E/N is minimum) or a gas (for which $\frac{\mathrm{d}E/N}{\mathrm{d}n} > 0 \ \forall \ n$). This is an effect entirely induced by the presence of the SOC interaction, since for unstable Bose-Bose mixtures without SOC the stabilization of the collapse by the LHY energy always brings the homogeneous system to a liquid state [35]. In order to determine if the system is in a liquid or in a gas state, we compute E/N for different densities for fixed $\{\Omega, a_{+1,+1}\}$. Typically, $n \in [3.78 \times 10^{-4}, 4.93 \times 10^{-3}]$, although this range is extended in some cases up to $n \simeq 0.1$. We show in Fig. 4.12 an example of the mean field and total energies per particle as a function of the density for both the liquid and the gas phases.

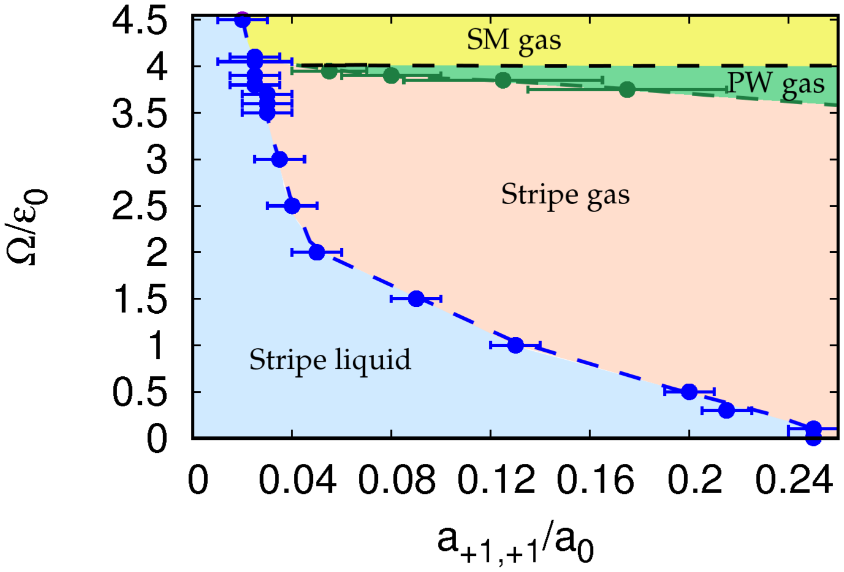

Fig. 4.11 Phase diagram of the Raman SOC system stabilized by quantum fluctuations in the stripe phase. All quantities are reported in reduced units.

Fig. 4.11 indicates that increasing the Raman coupling leads to a lower interval of scattering lengths where the system is in the stripe liquid phase. As a consequence, for fixed $a_{+1,+1}$, increasing Ω leads to a decrease in $n^{(0)}$, leading to a less correlated liquid. In much the same way, increasing $a_{+1,+1}$ with $\gamma = -21$ and keeping Ω constant drives the system from a liquid state to a gas, i.e., the equilibrium density $n^{(0)}$ shifts to lower values until $n^{(0)} = 0$, with the *gas parameter*, $n^{(0)}a^3_{+1,+1}$, also decreasing. Remarkably, this behavior is not seen in ultradilute non-SOC Bose-Bose mixtures, where multiplying all the scattering lengths by a constant leaves $n^{(0)}a^3_{+1,+1}$ invariant [35].

As it can be seen in Fig. 4.11, other phases arise as the ground state of the system for high enough values of Ω. The plane wave phase is energetically favorable for $\Omega \gtrsim 3.8$, $a_{+1,+1} \gtrsim 0.1$, $n > 3.78 \times 10^{-4}$ (although the single minimum phase may have lower energy for high enough densities), while the single minimum phase is the ground state of the system for $\Omega > 4$, $a_{+1,+1} \gtrsim 0.03$, $n > 3.78 \times 10^{-4}$. Remarkably, the plane wave and single minimum phases arise only as a gas, while the stripe liquid is present as the ground state of the system for all values of Ω if $a_{+1,+1} \lesssim 0.025$. This differs from the results obtained for fully repulsive interactions, for which the single minimum phase is the ground state of the system for $\Omega > 4$ both at the mean field level [60] and when correlations are introduced [48].

The phase diagram of Fig. 4.11 has been computed fixing $a_{+1,-1} = -1.1a_{+1,+1}$. However, due to the mean field instability present for $a_{+1,-1} < -a_{+1,+1}$, the LHY correction yields clearly unphysical imaginary contributions to the energy, since the excitation spectrum becomes imaginary at low momenta. In order to avoid that, and

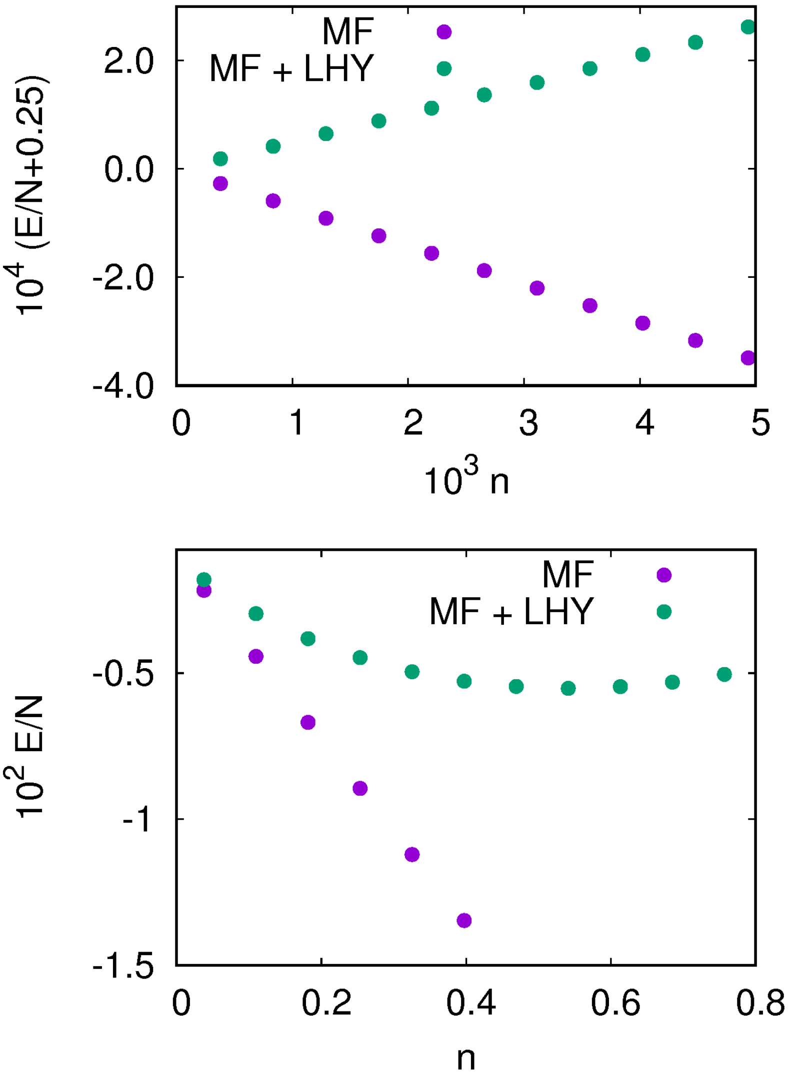

Fig. 4.12 Rescaled mean field and total energy per particle terms for: $\Omega = 2$, $a_{+1,+1} = 0.1$, $a_{+1,-1} = -0.11$ (top) and $\Omega = 0.125$, $a_{+1,+1} = 0.05$, $a_{+1,-1} = -0.055$ (bottom).

as usually done in the non-SOC case, we evaluate the LHY correction for $a_{+1,-1} = -a_{+1,+1}$, i.e., in the limit of the mean field stability, while the mean field energy terms are computed for $a_{+1,-1} < -a_{+1,+1}$. The changes in the phase diagram when $E_{\mathrm{LHY}}(a_{+1,-1} = -a_{+1,+1})$ is used instead of $\mathrm{Re}\{E_{\mathrm{LHY}}(a_{+1,-1} = -1.1a_{+1,+1})\}$ are included in the error bars.

As it happens in ultradilute non-SOC Bose-Bose mixtures, a finite size system in the liquid stripe phase can form a droplet. However, in the SOC case, the droplets show a striped pattern along the x direction, defined by $\hat{P}_x$ in $\hat{W}^{\mathrm{SOC}}$ (see Eq. (4.2)). Since Raman SOC stripes are known to be supersolid [4, 49, 48], the resulting striped droplets represent a novel quantum state of matter that mixes the self-bound character of liquids, the spatial periodicity present in solids, and a superfluid behavior. To obtain the ground state of the finite system, we solve the extended Gross-Pitaevskii equation

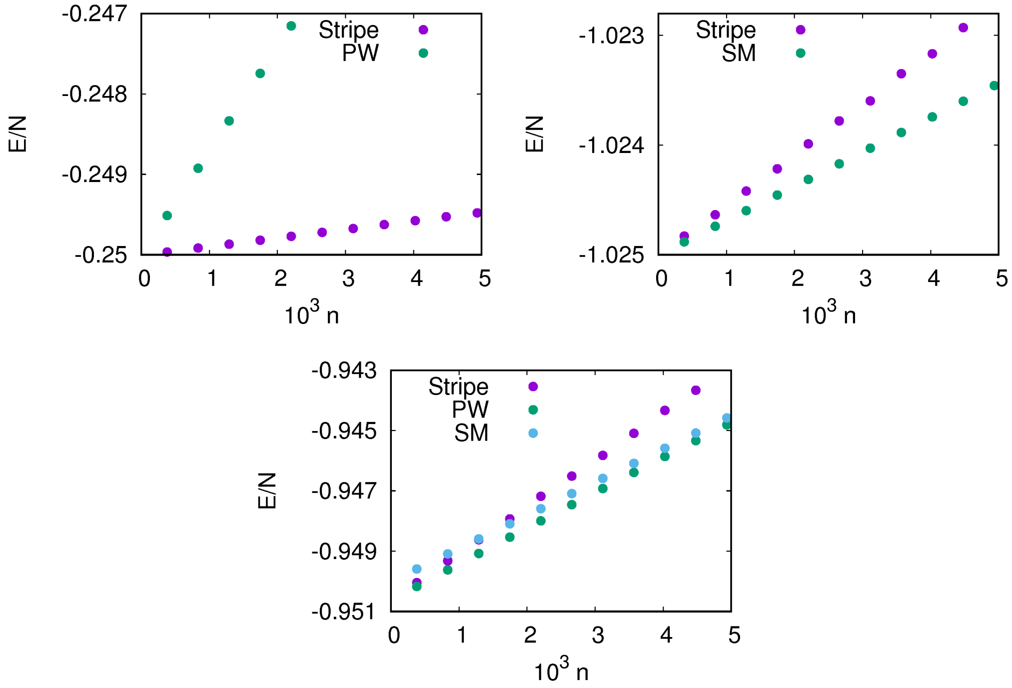

Fig. 4.13 Beyond mean field energies per particle for the indicated phases in the plots. The parameters are: $\Omega = 2$, $a_{+1,+1} = 0.125$, $a_{+1,-1} = -0.1375$ (top left), $\Omega = 4.05$, $a_{+1,+1} = 0.125$, $a_{+1,-1} = -0.1375$ (top right) and $\Omega = 3.9$, $a_{+1,+1} = 0.225$, $a_{+1,-1} = -0.2475$ (bottom)

(eGPE). To this end, we build a density-dependent energy functional by fitting the obtained LHY energy correction for different densities n. The chosen functional form is:

$$\left[E_{\mathrm{LHY}}/N\right](n) = bn + an^{3/2} \ , \tag{4.275}$$

with a and b two fitting parameters, which consistently reproduces our data in the range of densities spanned in this Section. We show in Table 4.1 the fitting parameters of the aforementioned model in two different density regimes for $\Omega = 0.125$, $a_{+1,+1} = 0.1$, $a_{+1,-1} = -0.11$. We compare the results for this model with another functional form of the type $\left[E_{\mathrm{LHY}}/N\right](n) = cn^{m}$, with c and m fitting parameters. Notice how the parameters of the first functional form show more consistency over the different density regimes than those of the second model. Further discussion of the parametrization of the LHY energy through a phenomenological functional is provided below. In order to obtain the eGPE, we minimize the energy functional

$$E(\Psi, \Psi^{\dagger}) = \int d\vec{r} \left(\epsilon_{\mathrm{MF}}(\Psi, \Psi^{\dagger}) + V_{\mathrm{osc}}(\vec{r})|\Psi|^2 + \epsilon_{\mathrm{LHY}}(\Psi, \Psi^{\dagger}) \right) \tag{4.276}$$

replacing $n \to \Psi^{\dagger}\Psi$ in the ϵ_{LHY} term. Here, ϵ_{MF} and ϵ_{LHY} are the mean field and Lee-Huang-Yang energy densities of the infinite system, respectively, and Ψ is the spinor wave function. The harmonic oscillator potential, $V_{\text{osc}}(\vec{r}) = \omega^2 r^2$ in reduced units, is added to keep the system finite.

Solving directly the eGPE is technically involved for some values of the system size because of the presence of two very different length scales: on one hand, the period of the stripes, which for values of $\Omega \leq 1$ is of order $L_s \sim \mathcal{O}(1)$ and, on the other, the radius of the droplet, which is generally much larger. Nevertheless, results for a set of parameters, for which the problem is well conditioned numerically, show that the ground-state wave function of the system obtained from the eGPE can be well approximated by

$$\Psi^{+1}(\vec{r}) = \Psi^{-1}(\vec{r}) \simeq f_{\text{stripe}}(x) f_{\text{droplet}}(r) \;, \tag{4.277}$$

with errors on the momentum of the stripes of at most 5%. Here, $f_{\text{stripe}}(x) \simeq \sqrt{\frac{V}{N_0}}\psi_0^{\pm 1}(\vec{r})$, a dimensionless factor which equals Eq. (4.192) multiplied by $\sqrt{\frac{V}{N_0}}$ and considering only the $n = -1$ and $n = 0$ terms in the sum. This is equivalent to taking the mean field ansatz of Ref. [60] divided by $\sqrt{n}$. The function $f_{\text{droplet}}(r)$ depends only on $r = |\vec{r}|$, with $\vec{r}$ the position vector in three dimensions. We present in Fig. 4.14 the comparison between the marginal probability density along the x-axis of the exact solution of the eGPE and the solution obtained with the approximation in Eq. (4.277) for a given set of parameters. As we can see from the Figure, the solution profiles are similar, although there is a shift in momentum of about 5%.

In order to efficiently compute $f_{\text{droplet}}(r)$., we apply a further approximation: we solve the eGPE obtained from the functional

$$\tilde{E}(\Psi, \Psi^\dagger) = \int d\vec{r} \left(\tilde{\epsilon}_{\text{MF}}(\Psi, \Psi^\dagger) + V_{\text{osc}}(\vec{r})|\Psi|^2 + \epsilon_{\text{LHY, SOC}}(\Psi, \Psi^\dagger) \right) \;. \tag{4.278}$$

Here, $\tilde{\epsilon}_{\text{MF}}$ is the mean field energy density obtained in the absence of SOC, while $\epsilon_{\text{LHY, SOC}}$ is the LHY energy density obtained from the full SOC calculation. Notice that the resulting eGPE can be solved efficiently with a moderate number of points as the problem only depends on $r = |\vec{r}|$, and thus the resulting eGPE is one-dimensional. We show in Fig. 4.15 the comparison between the marginal probability density along the x-axis of the solution featuring the approximation in Eq. (4.277) and of $f_{\text{droplet}}(r)$ obtained from the eGPE of the functional of Eq. (4.278).

	$n \in [7.56 \times 10^{-4}, 9.87 \times 10^{-3}]$	$n \in [0.109, 0.548]$
a	0.413 ± 0.037	0.401 ± 0.006
b	0.033 ± 0.003	0.044 ± 0.003
c	0.22 ± 0.02	0.439 ± 0.002
m	1.24 ± 0.02	1.419 ± 0.006

Table 4.1 Results for the fitting parameters of $[E_{\text{LHY}}/N](n) = bn + an^{3/2}$ and $[E_{\text{LHY}}/N](n) = cn^m$ for two different density regimes. All quantities are reported in reduced units.

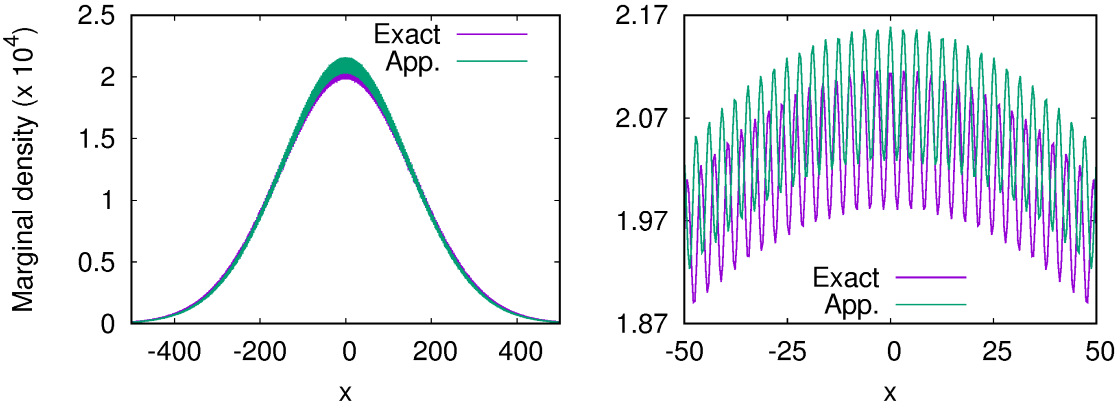

Fig. 4.14 Marginal probability densities along the x-axis of the solution of the exact eGPE vs the approximation of Eq. (4.277) for $\Omega = 0.125$, $a_{+1,+1} = 0.15$, $a_{+1,-1} = -0.165$, $N = 10^4$, $\omega = 1.97 \times 10^{-5}$. The right plot corresponds to a zoomed region of the left plot. All quantities are reported in reduced units.

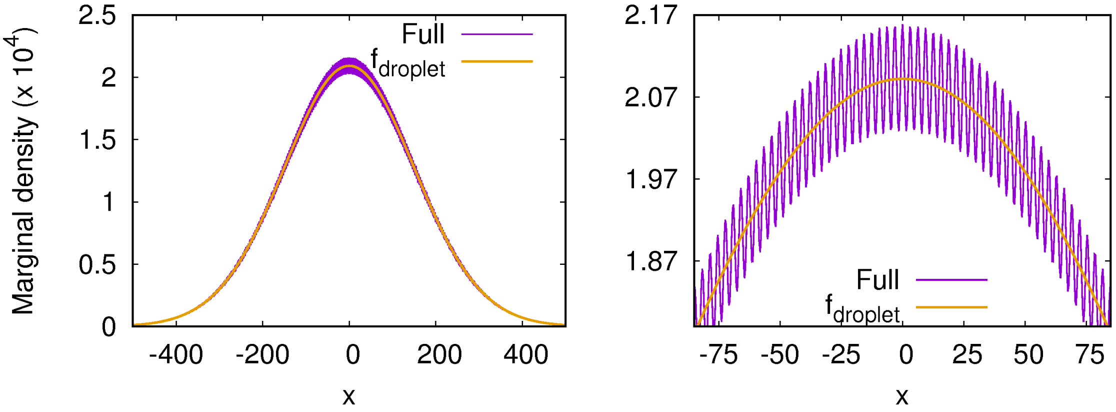

Fig. 4.15 Marginal probability densities along the x-axis of the solution featuring the approximation in Eq. (4.277) (purple line) and of $f_{\text{droplet}}(r)$ obtained from the eGPE of the functional of Eq. (4.278) (orange line) for $\Omega = 0.125$, $a_{+1,+1} = 0.15$, $a_{+1,-1} = -0.165$, $N = 10^4$, $\omega = 1.97 \times 10^{-5}$. The right plot corresponds to a zoomed region of the left plot. All quantities are reported in reduced units.

There is a minimum particle number required for a system to present a stable self-bound ground state in the form of a droplet. This is known as the critical number, N_{crit}. We determine N_{crit} by solving the eGPE for different strengths of the trapping potential and comparing the solution obtained to the ground-state wave function of the harmonic oscillator. For $N \geq N_{\text{crit}}$, changing the trapping strength leaves the solution of the eGPE unaffected. We show in Fig. 4.16 the normalized wave function, obtained under the aforementioned approximations, along the x-axis corresponding to a case where a stable droplet is formed, with parameters $\Omega = 0.5$, $a_{+1,+1} = 0.12$, $\gamma = -21$, $N = 1.4 \times 10^5$. The trapping strengths are $\omega_1 = 4.93 \times 10^{-6}$ and $\omega_2 = 2.77 \times 10^{-6}$. We only show the $+1$ spinor component, since it is equal to the -1 component.

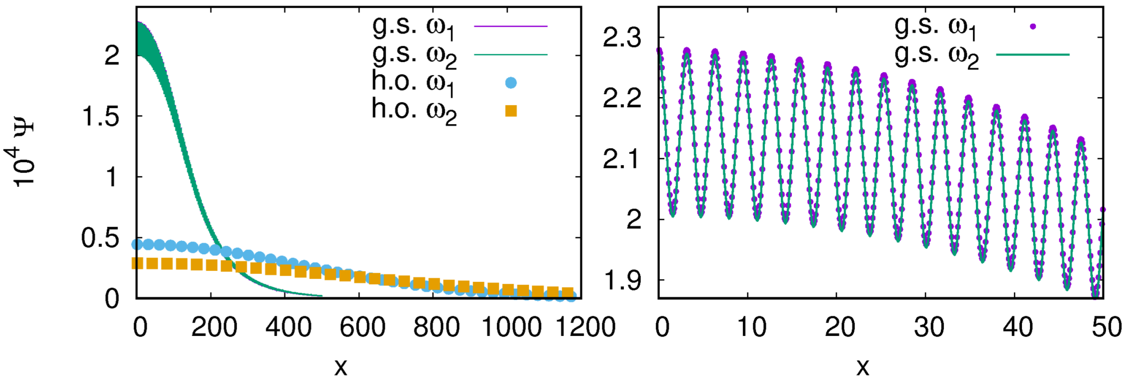

Fig. 4.16 Left panel: normalized wave function of the droplet along the x-axis for $\Omega = 0.5$, $a_{+1,+1} = 0.12$, $\gamma = -21$, $N = 1.4 \times 10^5$ with $\omega_1 = 4.93 \times 10^{-6}$ (green line). The profile corresponding to the same N, $a_{+1,+1}$, γ, Ω values but for $\omega_2 = 2.77 \times 10^{-6}$ is indistinguishable from the one reported in the left panel. The harmonic oscillator ground-state solution for both values of ω is shown as squares and circles. Right panel: magnified view of the two droplet wave functions at small x. Only $x > 0$ values are displayed since the profile is symmetric in the x-axis.

We report in Fig. 4.17, the critical number as a function of $a_{+1,+1}$ for $\Omega = 0.125, 0.5, 1.0$ and $\gamma = -21$ ($a_{+1,-1} = -1.1a_{+1,+1}$). Errorbars account for the numerical inaccuracies associated to both the finite number of Brillouin Zones being integrated and the number of points used in the computation of E_{LHY}, and also for the difference in the results obtained when employing either $E_{\text{LHY}}(a_{+1,-1} = -a_{+1,+1})$ or $\text{Re}\{E_{\text{LHY}}(a_{+1,-1} = -1.1a_{+1,+1})\}$. As can be seen from the Figure, the critical number increases with both Ω and the scattering lengths, consistently with the results shown in Fig. 4.11. Remarkably, the critical numbers obtained are reachable in current experimental setups, opening the possibility to observe and measure quantum properties of striped droplets. For the sake of comparison, previous experiments with SOC systems have been carried out with $N \sim 1.8 \times 10^5$ [1] and $N \sim 10^5$ [2] particles. Another interesting quantity regarding the number of particles in a droplet is the saturation number, N_s. If $N > N_s$, $f_{\text{droplet}}(r)$ shows a plateau at a range of positions $r \in [0, r_{\text{max.}}]$ with $r_{\text{max.}}$ increasing as N increases. For $\Omega = 0.125$, the saturation number in all cases is of $\mathcal{O}\left(10^6\right)$ or higher, which makes it challenging to be observed. We report in Fig. 4.18, $\sqrt{N} f_{\text{droplet}}(r) / \sqrt{\int d\vec{r}\ 2 f^2_{\text{droplet}}(r)}$ for different numbers of particles. The factor 2 in the denominator accounts for the fact that the wave function is a spinor with equal up and down components. As we can see from the Figure, a plateau on $f_{\text{droplet}}(r)$ starts to be noticeable for $N \simeq 2 \times 10^6$.

Despite the evaluation of E_{LHY} for SOC systems presented in this work is quite more involved than in non-SOC systems, the resulting observed dependence on the system parameters is smooth enough to allow for a simple functional form approximation. In this way, we report an approximated density functional for $E_{\text{LHY}}(a_{+1,-1} = -a_{+1,+1})$ in

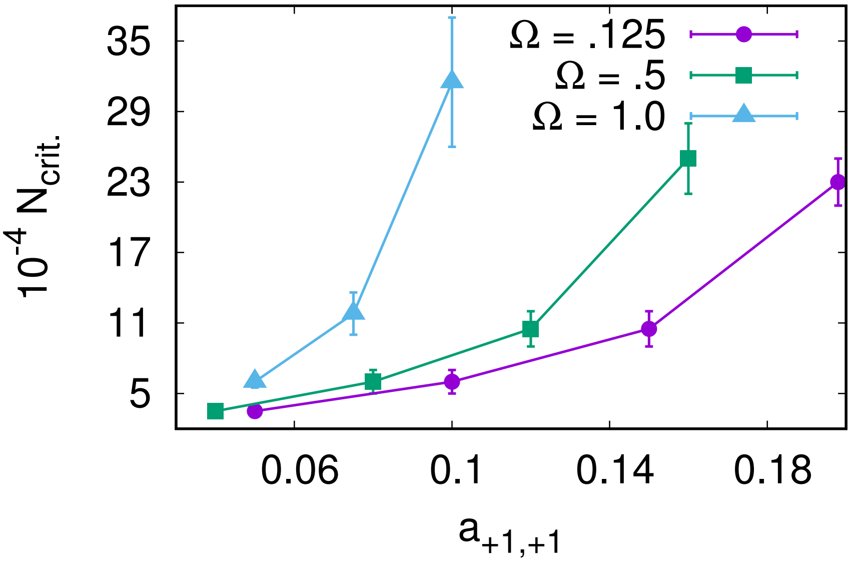

Fig. 4.17 Critical number as a function of the scattering length $a_{+1,+1}$ for $a_{+1,-1} = -1.1a_{+1,+1}$ and for different values of Ω. Lines are a guide to the eye.

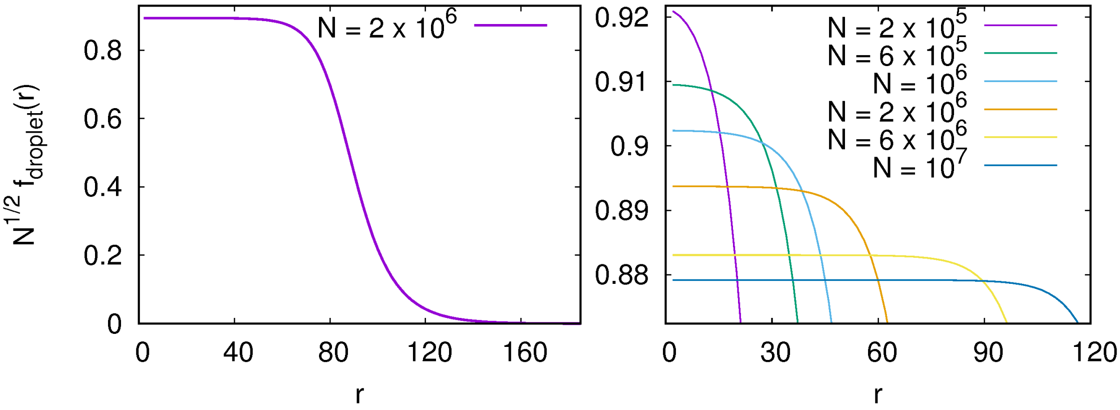

Fig. 4.18 $\sqrt{N} f_{\text{droplet}}(r)/\sqrt{\int d\vec{r} f^2_{\text{droplet}}(r)}$ for $N = 2 \times 10^6$, $\Omega = 0.125$, $a_{+1,+1} = 0.05, a_{+1,-1} = -0.055$, $\omega = 2.77 \times 10^{-6}$ (left plot). Same quantity for different numbers of particles (right plot). All quantities are reported in reduced units.

the stripe phase. This functional depends on $a_{+1,+1}$, n and Ω, and has been obtained by fitting the LHY energies in different density regimes. It is given by

$$E_{\text{LHY}}/N\bigg|_{\substack{a_{+1,-1}= \\ -a_{+1,+1}}} \simeq (A + B\Omega^2)na^2_{+1,+1} + C\sqrt{n^3 a^5_{+1,+1}} \tag{4.279}$$

with $A = 1.89 \pm 0.04$, $B = 2.17 \pm 0.03$ and $C = 37 \pm 2$ in dimensionless form. The above expression reproduces the obtained LHY energies with errors between 1% and 10% for $0 < \Omega < 3$, $0 < n \lesssim 0.1$, $0 < a_{+1,+1} < 0.225$, although the limiting value of the density can be increased further for scattering lengths $a_{+1,+1} \lesssim 0.05$, keeping the error of the functional approximation within the mentioned boundaries.

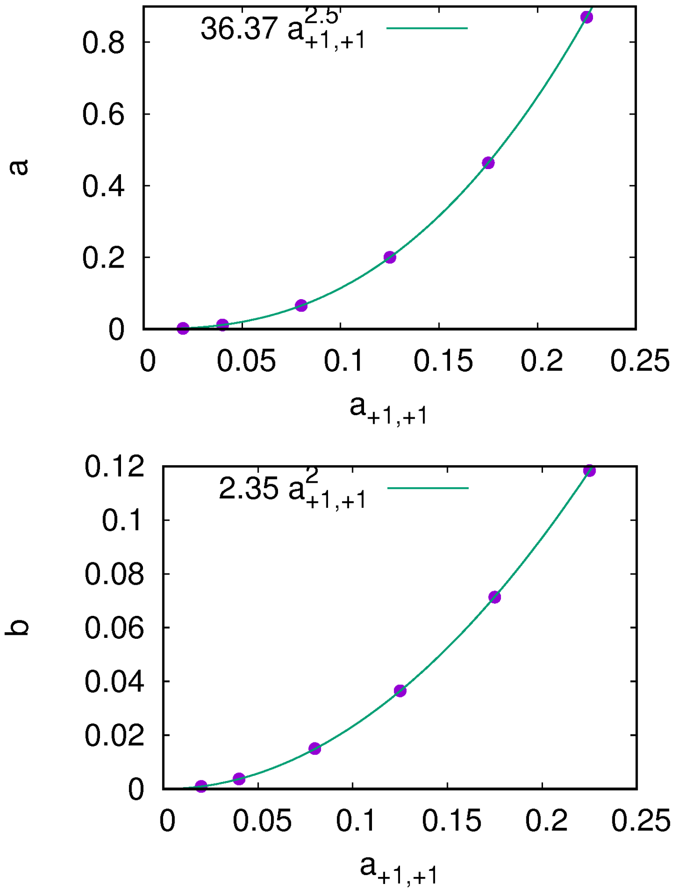

Fig. 4.19 Dependence of the terms a and b from Eq. (4.275) for $a_{+1,+1} = -a_{+1,-1}$. The value of Ω is $\Omega = 1.0$ (top plot) and $\Omega = 0.5$ (bottom plot). All quantities are reported in reduced units.

The form of the functional in Eq. (4.279) can be understood by looking at the properties of the system. The first important remark is that the power series of E_{LHY}/N must be of the form $\sum_\alpha n^\alpha a_{+1,+1}^{\alpha+1} f_\alpha$, i.e., there must be a difference of one between the powers in the density and the scattering length. This can be seen from Eq. (4.235), since the whole LHY integral is a function of $na_{+1,+1}$ divided by a factor n. Here, f_α is a factor that gives the sum dimensions of energy. We show in Fig. 4.19 the terms a and b of Eq. (4.275), obtained through the fitting of the LHY energies to the functional in Eq. (4.275), with respect to $a_{+1,+1}$ for fixed Ω. As can be seen from the Figure, the type of dependence on $a_{+1,+1}$ matches the aforementioned condition of the exponent: b scales as $a_{+1,+1}^2$ while a scales as $a_{+1,+1}^{2.5}$. The second remark is that a linear dependence with respect to n is clearly seen at low densities for some values of Ω, $a_{+1,+1}$, as it can be seen from Fig. 4.12, which justifies the linear contribution on the density. The third remark is that the term $\propto \sqrt{n^3 a_{+1,+1}^5}$ is introduced in analogy to the non-SOC case [35], and also due to the apparent consistency in the fitting shown in Table 4.1 in two different density regimes.

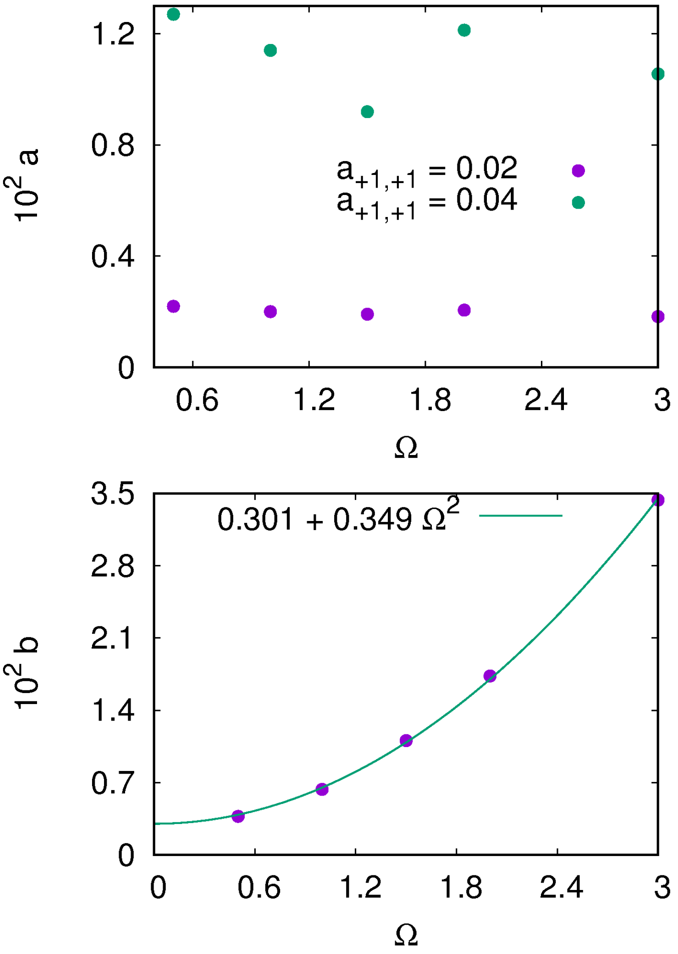

Fig. 4.20 Dependence of the terms a and b from Eq. (4.275) for $a_{+1,+1} = -a_{+1,-1}$. In the bottom plot, $a_{+1,+1} = 0.04$. All quantities are reported in reduced units.

In order to get the dependence with respect to Ω, we compute the terms a and b Eq. (4.275) for different values of Ω and fixed $a_{+1,+1}$. We show the results in Fig. 4.20. As it can be seen, the term b shows a quadratic dependence with Ω. The term a is taken as a constant, computing the average over Ω. We show in Fig. 4.21, the comparison between the numerically obtained LHY energies and the LHY energy obtained from the functional in Eq. (4.279) for two cases not used in the fitting process: $\Omega = 0.125$, $a_{+1,+1} = 0.15$ and $\Omega = 3.0$, $a_{+1,+1} = 0.175$. As we can see from the Figure, the phenomenological functional is able to reproduce accurately the numerical results. Therefore, one can just take this functional as an input for the eGPE and use it to obtain information about the system without the need of going through the full calculation of the LHY energy. However, this is only the case for $a_{+1,+1} = a_{-1,-1}$,

$a_{+1,-1} = -a_{+1,+1}$. Any variation of these conditions requires the computation of a new functional.

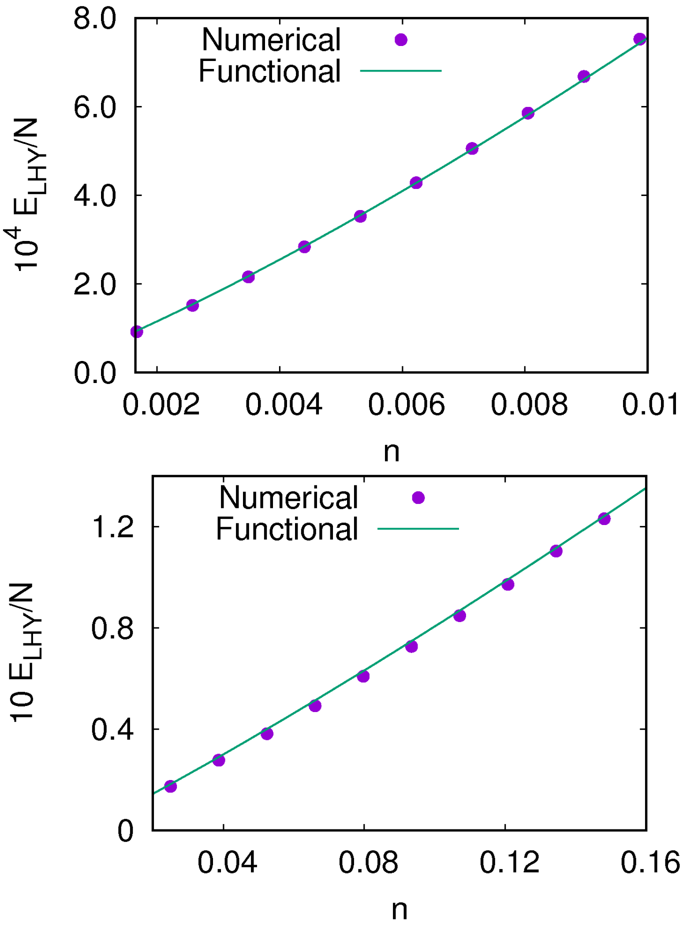

Fig. 4.21 Rescaled LHY energies per particle obtained through the full numerical calculation and the phenomenological functional of Eq. (4.279) for $a_{+1,-1} = -a_{+1,+1}$. The upper plot corresponds to $\Omega = 0.125$, $a_{+1,+1} = 0.15$ while the lower plot corresponds to $\Omega = 3.0$, $a_{+1,+1} = 0.175$. All quantities are reported in reduced units.

Regarding the potential experimental observation of the ultradilute, supersolid striped droplets, we have performed calculations of the liquid equation of state and the critical number for droplet formation for parameters close to the experimental conditions of Refs. [1], [2], $\Omega^{(1,2)} = 0.313$, $a^{(1)}_{+1,+1} \simeq 0.025$ for the case close to Ref. [2], and $a^{(2)}_{+1,+1} = 0.0146$ for the case close to Ref. [1]. The densities are $n^{(1)} = 5.82$ and $n^{(2)} \simeq 50.2$, with all quantities expressed in reduced units. However, we have set $\gamma = -21$ to enable the formation of droplets, unlike the scattering lengths employed in both experiments, which are positive and thus make the formation of droplets not possible. Remarkably, both experimental systems lay within the stripe liquid region of the diagram of Fig. 4.11, which implies that an interaction with an attractive enough inter-spin component should lead to the formation of supersolid striped droplets.

Moreover, the minimum of the energy per particle is located at a density close to the one employed in both experiments, with $n^{(1)}_{\mathrm{min}} = 7.1 \pm 1.5$ and $n^{(2)}_{\mathrm{min}} = 40 \pm 10$. Regarding the critical number, it lays below particle numbers employed in both experiments, since $N^{(1)} = 10^5$, $N^{(2)} = 1.8 \times 10^5$, while we find $N^{(1)}_{\mathrm{crit.}} = 22500 \pm 2500$ and $N^{(2)}_{\mathrm{crit.}} = 17500 \pm 2500$. For the particle numbers used in the experiments, the droplets have a central density of $n^{(1)}_{\mathrm{cent.}} \simeq 7.9$, $n^{(2)}_{\mathrm{cent.}} \simeq 42.9$. Although our calculations are restricted to the case $a_{+1,+1} = a_{-1,-1}$, $a_{+1,-1} = -1.1a_{+1,+1}$, both experiments lay far from the liquid-gas transition of Fig. 4.11 in terms of both Ω and $a_{+1,+1}$. Therefore, we do not expect the modification of any of the conditions considered in this work regarding the scattering lengths to disable droplet formation under the experimental parameters of Refs. [1], [2].

Chapter 5

Spin Orbital Angular Coupling

5.1 Introduction to Spin Orbital Angular Coupling

The synthetic elaboration of Spin Orbital Angular Coupling (SOAC) was first achieved in 2018 [49]. This type of SOC interaction involves the coupling between a spin degree of freedom and an angular momentum component, unlike the rest of types of SOC that have been studied in this Thesis. Because of that, SOAC lays closer to the original meaning of "spin-orbit coupling" in atomic physics, where the orbital angular momentum of an atom is coupled to the electron's spin. Similarly to the experimental set-up where Raman SOC was first implemented, two hyperfine states of a ^{87}Rb atom are treated as pseudospin states, for which the SOC is synthetically engineered. However, in order to induce SOAC between the pseudospins, a pair of laser beams with different orbital angular momentum must be employed. For this purpose, one of the beams utilized is of the Laguerre-Gaussian type which carries non-zero angular momentum, while the other is a Raman beam without angular momentum. In this way, the relative winding phase of the photons is transmitted to the ^{87}Rb during the Raman transition, which involves angular momentum transfer, in contrast to the linear momentum transfered in the Raman SOC scheme. The pair of Laguerre-Gaussian beams are of the form [5]

$$E_j(\vec{r}) = \sqrt{2I_{j0}}\exp\left[-il_j\phi\right]\left(\frac{\rho}{w}\right)^{|l_j|}\exp\left[-\rho^2/w^2 + ikz\right] \;\; j = 1, 2 \tag{5.1}$$

with $\vec{r} = (\rho,\ \phi,\ z)$, w is the beam waist and I_{j0} is the intensity of the beam. Notice the factor $\exp\left[-il_j\phi\right]$ in Eq. (5.1), which reflects the non-zero angular momentum carried by the beam. As mentioned previously, these beams couple two hyperfine states of the ^{87}Rb atom, giving rise to an effective spin-1/2 Hamiltonian, given by [5]

$$\hat{\mathcal{H}}_0 = \begin{pmatrix} -\frac{\hbar^2}{2m}\nabla^2 & 0 \\ 0 & -\frac{\hbar^2}{2m}\nabla^2 \end{pmatrix} + \begin{pmatrix} \frac{1}{2}m\omega^2 r^2 & 0 \\ 0 & \frac{1}{2}m\omega^2 r^2 \end{pmatrix} + \begin{pmatrix} \frac{\delta}{2} & 0 \\ 0 & -\frac{\delta}{2} \end{pmatrix}$$
$$+ \Omega_R \left(\frac{\rho}{w}\right)^{|l_1|+|l_2|} \exp\left[-2(\rho^2/w^2)\right] \begin{pmatrix} 0 & \exp\left[-i(l_1-l_2)\phi\right] \\ \exp\left[i(l_1-l_2)\phi\right] & 0 \end{pmatrix} \quad (5.2)$$

with Ω_R is the Raman coupling strength, ω is the strength of the harmonic trap, δ is the two-photon detuning, l_1 and l_2 is the orbital angular momentum carried by the two beams, respectively. The application of a unitary transformation given by the matrix

$$U = \begin{pmatrix} \exp\left[-il\phi\right] & 0 \\ 0 & \exp\left[il\phi\right] \end{pmatrix} \quad (5.3)$$

makes it possible to write the Hamiltonian as [5]

$$\hat{H}_0 = \frac{\hat{P}^2}{2m} + \frac{1}{2}m\omega^2 r^2 + \frac{\delta}{2}\hat{\sigma}_z + \Omega_R \left(\frac{\rho}{w}\right)^{|l_1|+|l_2|} \exp\left(-2\rho^2/w^2\right)\hat{\sigma}_x - \frac{l\hbar}{m\rho^2}\hat{L}_z\hat{\sigma}_z + \frac{(l\hbar)^2}{2m\rho^2}\,, \quad (5.4)$$

where $l = (l_1 - l_2)/2$, with $|l|$ the total angular momentum of the system. In this Section, we employ the values of Ref. [5], which correspond to $l_1 = 0$, $l_2 = 2$, $l = -1$. In contrast to the one-body Raman SOC Hamiltonian from Chapter 2, the SOC depends on $\hat{L}_z\hat{\sigma}_z$ rather than $\hat{p}_x\hat{\sigma}_z$. Remarkably, the Raman coupling term presents a spatial dependence, absent in the SOC Hamiltonians previously presented.

The physics of the system at the single-particle level are somewhat similar to the Raman SOC system. Notice that the Hamiltonian in Eq. (5.4) commutes with $\hat{L}_z$ and therefore its eigenstates have definite z-angular momentum, with $l_z = -1, 0, 1$ as $|l| = 1$. This is analogous to the Raman SOC case, where the eigenstates of the one-body Hamiltonian have definite linear momentum. From Eq. (5.4),we can infer that the energy dispersion (energy vs z-orbital angular momentum) features a double minima for $\delta = 0$ at low enough Ω_R, since the Hamiltonian is invariant under the transformation $l_z \to -l_z$, $\sigma_z \to -\sigma_z$. This degeneracy is broken if $\delta \neq 0$, as it is the case with Raman SOC, with the $l_z = 1$ state being the non-degenerate ground state if $\delta > 0$, $\Omega_R < \Omega_{R,\text{lim}}$ and the $l_z = -1$ state being the non-degenerate ground state if $\delta < 0$, $\Omega_R < \Omega_{R,\text{lim}}$ [5]. For $\Omega_R > \Omega_{R,\text{lim}}$, the ground state of the single particle system has $l_z = 0$. Remarkably, a first order phase transition takes place with respect to Ω_R for fixed $\delta \neq 0$ due to the discrete nature of the z-angular momentum ($l_z = \pm 1 \leftrightarrow l_z = 0$ in the ground state). Such effect is not present in the single-particle Raman SOC system, for which the momentum changes continuously without degeneracy because $\delta \neq 0$. The aforementioned states constitute the phase diagram of the system, which is reported in Fig. 5.1. The polarization $\langle\hat{\sigma}_z\rangle$ is a good variable to characterize the different phases. The $l_z = 0$ phase has $\langle\hat{\sigma}_z\rangle \simeq 0$ while the $l_z = \pm 1$ phases show a non-zero polarization $\langle\hat{\sigma}_z\rangle = \mp s_{z,0} \neq 0$, with $s_{z,0} > 0$ [5].

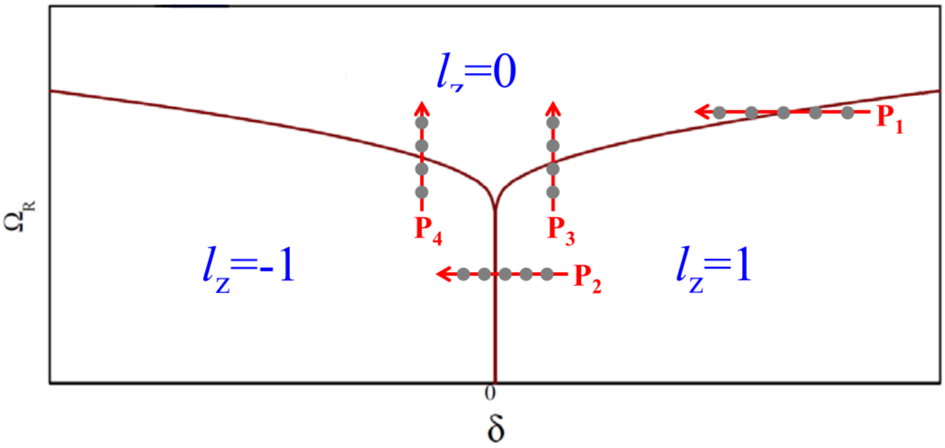

Fig. 5.1 Phase diagram of the system described by the one-body Hamiltonian in Eq. (5.4) (re-printed from Ref. [5]).

We present in this Chapter our results regarding SOAC. In Sec. 5.2, we follow the steps of Ref. [5] to derive a simplified Gross-Pitaevskii equation featuring Spin Orbital Angular Coupling. In Sec. 5.3, we discuss the extension of the phase diagram presented in Ref. [5] to a regime where inter-atomic correlations are increased with respect to the mean field level. We discuss how to rescale the experimental system of Ref. [5] in order to do so by means of the DTDMC method presented in Chapter 3.

5.2 Spin Orbital Angular Coupling in the dilute regime: the one-dimensional Gross-Pitaevskii equation

The introduction of interactions at the mean field level leaves the phase diagram of the system practically unchanged with respect to the single particle picture [5]. However, properties such as the polarization are significantly modified, as we show in this Section. In order to obtain the ground state of the system in the mean field regime, we must solve the Gross-Pitaevskii equation. In principle, this is a three-dimensional equation which must be discretized in position space, while imaginary time evolution must be applied for each spatial point. Therefore, the number of operations needed to successfully implement imaginary time propagation is of $\mathcal{O}(N_t N_x N_y N_z)$, where N_t is the number of imaginary time steps, and N_x, N_y and N_z are the number of discretization points in the x, y and z axes of the grid, respectively. This can be demanding from the perspective of the computational cost. One must, therefore, take advantage of all the symmetries of the Hamiltonian in order to obtain an approximated Gross-Pitaevskii equation of lower dimensionality, such that the computational cost is reduced. The approximations that must be applied are presented in the supplementary material of Ref. [5]. Here, we present a more detailed derivation following the steps of the Reference. We start with the imaginary time Gross-Pitaevskii equation, which, for a SOAC system, it takes the form

$$
\begin{aligned}
-\frac{\partial \psi_{+1}(\vec{r})}{\partial \tau} &= -\frac{\hbar^2}{2m}\nabla^2\psi_{+1} + \frac{1}{2}m\omega^2 r^2 \psi_{+1}(\vec{r}) + \Omega(\rho)\psi_{-1}(\vec{r}) + \frac{\delta}{2}\psi_{+1}(\vec{r}) \\
&\quad + i\frac{l\hbar^2}{m\rho^2}\left(x\frac{\partial \psi_{+1}}{\partial y} - y\frac{\partial \psi_{+1}}{\partial x}\right) + \frac{l^2\hbar^2}{2m\rho^2}\psi_{+1}(\vec{r}) + Ng_{+1,+1}\left|\psi_{+1}(\vec{r})\right|^2\psi_{+1}(\vec{r}) \\
&\quad + Ng_{+1,-1}\left|\psi_{-1}(\vec{r})\right|^2\psi_{+1}(\vec{r}) \qquad (5.5) \\
-\frac{\partial \psi_{-1}(\vec{r})}{\partial \tau} &= -\frac{\hbar^2}{2m}\nabla^2\psi_{-1} + \frac{1}{2}m\omega^2 r^2 \psi_{-1}(\vec{r}) + \Omega(\rho)\psi_{+1}(\vec{r}) - \frac{\delta}{2}\psi_{-1}(\vec{r}) \\
&\quad - i\frac{l\hbar^2}{m\rho^2}\left(x\frac{\partial \psi_{-1}}{\partial y} - y\frac{\partial \psi_{-1}}{\partial x}\right) + \frac{l^2\hbar^2}{2m\rho^2}\psi_{-1}(\vec{r}) + Ng_{-1,-1}\left|\psi_{-1}(\vec{r})\right|^2\psi_{-1}(\vec{r}) \\
&\quad + Ng_{+1,-1}\left|\psi_{+1}(\vec{r})\right|^2\psi_{-1}(\vec{r}) \qquad (5.6)
\end{aligned}
$$

where, analogously to Chapter 2, the inter-atomic interaction is represented by a contact potential proportional to the spin-dependent scattering lengths $a_{\pm 1,\pm 1}$, with $a_{+1,-1} = a_{-1,+1}$. Through this Section, the ±1 subindexes in $\psi_{\pm 1}$ indicate the spinor components of the wave function. Eqs. (5.5) and (5.6) can be expressed in a compact form as:

$$
\begin{aligned}
-\frac{\partial \psi_{\pm 1}}{\partial \tau} &= -\frac{\hbar^2}{2m}\nabla^2\psi_{\pm 1} + \frac{1}{2}m\omega^2 r^2 \psi_{\pm 1} + \Omega(\rho)\psi_{\mp 1} \pm \frac{\delta}{2}\psi_{\pm 1} \\
&\quad \pm i\frac{l\hbar^2}{m\rho^2}\left(x\frac{\partial \psi_{\pm 1}}{\partial y} - y\frac{\partial \psi_{\pm 1}}{\partial x}\right) + \frac{l^2\hbar^2}{2m\rho^2}\psi_{\pm 1} + Ng_{\pm 1,\pm 1}\left|\psi_{\pm 1}\right|^2\psi_{\pm 1} \\
&\quad + Ng_{\pm 1,\mp 1}\left|\psi_{\mp 1}\right|^2\psi_{\pm 1}\ . \qquad (5.7)
\end{aligned}
$$

Notice that the only potential that depends explicitly on the z coordinate is the harmonic oscillator. Therefore, the mean field ground state is approximated by [5]:

$$
\psi_{\pm 1}(\vec{r}) \simeq \psi^{\mathrm{2D}}_{\pm 1}(x,y)\frac{\exp\left(-z^2/(2b^2)\right)}{\pi^{1/4}b^{1/2}} \qquad (5.8)
$$

Here b is the width of the atomic cloud along the z axis, measured experimentally (although in the rescaled system that we study in the next Section, b is considered a variational parameter). We now multiply both sides of Eqs. (5.5) and (5.6) by $\frac{\exp\left(-z^2/(2b^2)\right)}{\pi^{1/4}b^{1/2}}$ and integrate over z. This yields a system of two equations for $\psi_{\pm 1}(x,y)$, effectively reducing the dimensionality of the system. Eq. (5.7) becomes:

$$\begin{aligned}
-\frac{\partial\psi^{2\mathrm{D}}_{\pm1}}{\partial\tau} &= -\frac{\hbar^2}{2m}\nabla^2_{2\mathrm{D}}\psi^{2\mathrm{D}}_{\pm1} + \frac{1}{2}m\omega^2\rho^2\psi^{2\mathrm{D}}_{\pm1} + \Omega(\rho)\psi^{2\mathrm{D}}_{\mp1} \pm \frac{\delta}{2}\psi^{2\mathrm{D}}_{\pm1} \\
&\pm i\frac{l\hbar^2}{m\rho^2}\left(x\frac{\partial\psi^{2\mathrm{D}}_{\pm1}}{\partial y} - y\frac{\partial\psi^{2\mathrm{D}}_{\pm1}}{\partial x}\right) + \frac{l^2\hbar^2}{2m\rho^2}\psi^{2\mathrm{D}}_{\pm1} \\
&+ \frac{N}{\pi b^2}\left(\int_{-\infty}^{\infty} dz\ e^{-2z^2/b^2}\right)\left(g_{\pm1,\pm1}\left|\psi^{2\mathrm{D}}_{\pm1}\right|^2\psi^{2\mathrm{D}}_{\pm1} + g_{\pm1,\mp1}\left|\psi^{2\mathrm{D}}_{\mp1}\right|^2\psi^{2\mathrm{D}}_{\pm1}\right) \\
&- \frac{\hbar^2}{2mb\sqrt{\pi}}\left(\int_{-\infty}^{\infty} dz\ e^{-z^2/(2b^2)}\frac{\mathrm{d}^2e^{-z^2/(2b^2)}}{\mathrm{d}z^2}\right)\psi^{2\mathrm{D}}_{\pm1} \\
&+ \frac{1}{2b\sqrt{\pi}}m\omega^2\left(\int_{-\infty}^{\infty} dz\ z^2e^{-z^2/b^2}\right)\psi^{2\mathrm{D}}_{\pm1} \qquad (5.9)
\end{aligned}$$

where

$$\int_{-\infty}^{\infty} dz\ e^{-2z^2/b^2} = b\sqrt{\frac{\pi}{2}} \qquad (5.10)$$

$$\int_{-\infty}^{\infty} dz\ z^2e^{-z^2/b^2} = \frac{\pi^{1/2}b^3}{2} \qquad (5.11)$$

$$\int_{-\infty}^{\infty} dz\ e^{-z^2/(2b^2)}\frac{\mathrm{d}^2e^{-z^2/(2b^2)}}{\mathrm{d}z^2} = -\frac{\sqrt{\pi}}{2b}\ . \qquad (5.12)$$

Thus, Eq. (5.9) becomes:

$$\begin{aligned}
-\frac{\partial\psi^{2\mathrm{D}}_{\pm1}}{\partial\tau} &= -\frac{\hbar^2}{2m}\nabla^2_{2\mathrm{D}}\psi^{2\mathrm{D}}_{\pm1} + \frac{1}{2}m\omega^2\rho^2\psi^{2\mathrm{D}}_{\pm1} + \Omega(\rho)\psi^{2\mathrm{D}}_{\mp1} \pm \frac{\delta}{2}\psi^{2\mathrm{D}}_{\pm1} \\
&\pm i\frac{l\hbar^2}{m\rho^2}\left(x\frac{\partial\psi^{2\mathrm{D}}_{\pm1}}{\partial y} - y\frac{\partial\psi^{2\mathrm{D}}_{\pm1}}{\partial x}\right) + \frac{l^2\hbar^2}{2m\rho^2}\psi^{2\mathrm{D}}_{\pm1} \\
&+ \frac{N}{\sqrt{2\pi}b}\left(g_{\pm1,\pm1}\left|\psi^{2\mathrm{D}}_{\pm1}\right|^2\psi^{2\mathrm{D}}_{\pm1} + g_{\pm1,\mp1}\left|\psi^{2\mathrm{D}}_{\mp1}\right|^2\psi^{2\mathrm{D}}_{\pm1}\right) \\
&+ \left(\frac{\hbar^2}{4mb^2} + \frac{b^2}{4}m\omega^2\right)\psi^{2\mathrm{D}}_{\pm1} \qquad (5.13)
\end{aligned}$$

Eq. (5.13) can be understood as an effective 2D GPE with effective interaction strengths $g_{s_1,s_2}/\sqrt{2\pi}b$ and a chemical potential shifted by the constant term $\frac{\hbar^2}{4mb^2} + \frac{b^2}{4}m\omega^2$. In order to furtherly reduce the dimensionality of the problem, we make another approximation. Following Ref. [5], we focus on wave functions of the form:

$$\psi^{2\mathrm{D}}_{\pm1}(\rho,\phi) = \psi^{1\mathrm{D}}_{\pm1}(\rho)\frac{\exp\left(il_z\phi\right)}{\sqrt{2\pi}} \qquad (5.14)$$

with $\{\rho,\phi\}$ the polar coordinates the x-y plane. A wave function of this type describes the main phases present in the phase diagram of Ref. [5]. These phases are analogous to the plane wave and single minimum phases of the Raman SOC system described in previous Chapters, in the sense that they correspond to single z-angular momentum component functions with $l_z = -1,\ 0$ and $+1$, much like the plane wave and single minimum phases correspond to single linear momentum states.

In order to obtain a one-dimensional GPE for $\psi^{\mathrm{1D}}_{\pm1}(\rho)$ we multiply Eq. (5.13) by $e^{il_z\phi}/\sqrt{2\pi}$ and integrate over ϕ, yielding

$$\begin{aligned}-\frac{\partial\psi^{\mathrm{1D}}_{\pm1}}{\partial\tau} &= -\frac{\hbar^2}{2m}\left(\frac{\partial^2\psi^{\mathrm{1D}}_{\pm1}}{\partial\rho^2}+\frac{1}{\rho}\frac{\partial\psi^{\mathrm{1D}}_{\pm1}}{\partial\rho}\right)+\frac{\hbar^2 l_z^2}{2m\rho^2}\psi^{\mathrm{1D}}_{\pm1}+\frac{1}{2}m\omega^2\rho^2\psi^{\mathrm{1D}}_{\pm1}+\Omega(\rho)\psi^{\mathrm{1D}}_{\mp1}\pm\frac{\delta}{2}\psi^{\mathrm{1D}}_{\pm1}\\ &\mp\frac{l l_z\hbar^2}{m\rho^2}\psi^{\mathrm{1D}}_{\pm1}+\frac{l^2\hbar^2}{2m\rho^2}\psi^{\mathrm{1D}}_{\pm1}+\frac{N}{(2\pi)^{3/2}\,b}\left(g_{\pm1,\pm1}\left|\psi^{\mathrm{1D}}_{\pm1}\right|^2\psi^{\mathrm{1D}}_{\pm1}+g_{\pm1,\mp1}\left|\psi^{\mathrm{1D}}_{\mp1}\right|^2\psi^{\mathrm{1D}}_{\pm1}\right)\\ &+\left(\frac{\hbar^2}{4mb^2}+\frac{b^2}{4}m\omega^2\right)\psi^{\mathrm{1D}}_{\pm1}\end{aligned} \tag{5.15}$$

Solving Eq. (5.15) leads to the wave function of the system. One can elaborate the phase diagram of the mean field system by computing the energy of the $l_z = -1,\ 0$ and $+1$ phases as a function of Ω_R and δ and checking which phase provides the lowest energy. The phase diagram is reported in Fig. 5.2 [5]. The phase diagram of the non-interacting system (shown in Fig. 5.1) is only slightly modified by interactions at the mean field level [5]. However, other quantities such as the polarization are significantly modified. We present in Fig. 5.3 the average value of the spin z operator, $\hat{\sigma}_z$ for $\Omega_R = 2.269$, $\delta \in [-0.01\ ,0.01]$ (transition P_2 in Ref. [5], see Fig. 5.1) and $\Omega_R \in [83.21\ ,291.235]$, $\delta = 0.129$ (transition P_3 in Ref. [5], see Fig. 5.1) for both the non-interacting problem and the solution of the GPE. We also include the experimental points. Notice how the inclusion of interactions yields points that lay closer to the experimental values. The discrepancy between GPE results and the experiment is claimed to be caused by finite temperature effects [5].

A wave function of the form described in Eq. (5.14) can not describe a stripe state presenting density modulations with respect to the angle ϕ. Such state does actually correspond to the ground state of the SOAC system over a tiny region of the phase diagram presented in Fig. 5.2 [5, 76]. However, due to the low contrast between different spin channels of the inter-atomic interactions of ^{87}Rb, stripes are not visible experimentally, and they only span a tiny region of the phase diagram. Recently, a study on the contrast and visibility of the stripes in terms of the parameters of the Hamiltonian has been carried out [77], yielding a set of parameters that enable their potential experimental observation. We build the stripe wave function as:

$$\psi^{\text{stripe, 2D}}_{\pm1}(\rho,\phi,l_z) = \frac{1}{\sqrt{2}}\left(\psi^{\mathrm{1D}}_{\pm1}(\rho,l_z)\frac{\exp\left(il_z\phi\right)}{\sqrt{2\pi}}+\psi^{\mathrm{1D}}_{\pm1}(\rho,-l_z)\frac{\exp\left(-il_z\phi\right)}{\sqrt{2\pi}}\right) \tag{5.16}$$

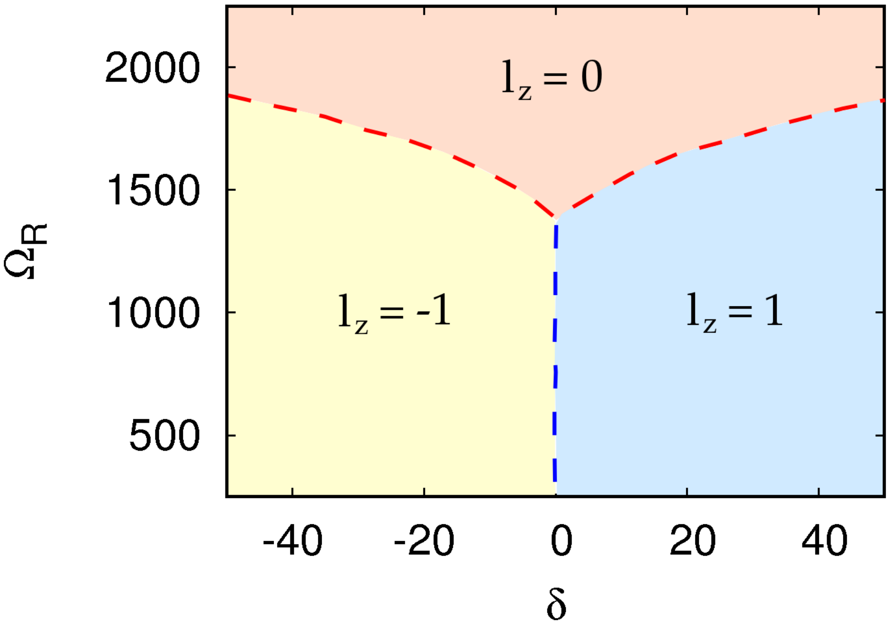

Fig. 5.2 Phase diagram of the experimental system of Ref. [5] (re-printed), where quantities are expressed in units of $\hbar\omega$.

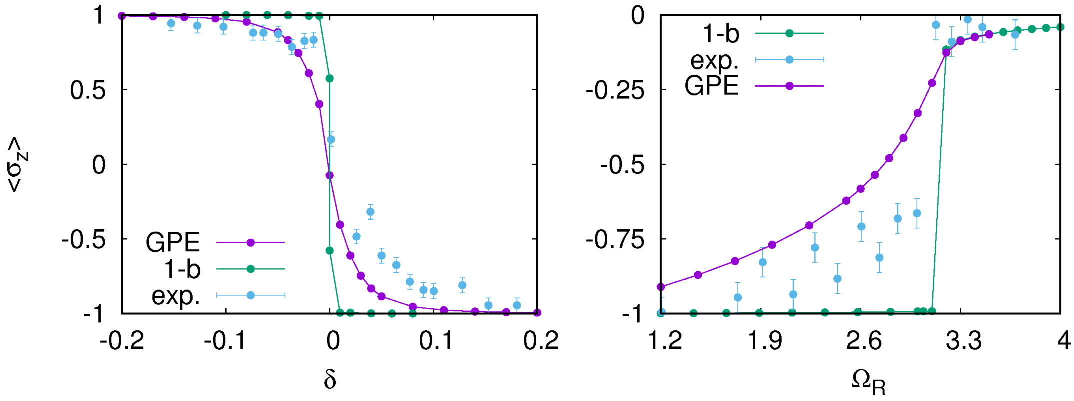

Fig. 5.3 Polarization of the SOAC system for the transitions labeled as P_2 ($\Omega_R = 2.269$, $\delta \in [-0.01\ ,0.01]$, see Fig. 5.1, left plot) and P_3 ($\Omega_R \in [1.2\ ,4]$, $\delta = 0.0258$, see Fig. 5.1, right plot) in Ref. [5]. Purple points correspond to the solution of the GPE equation, green points correspond to the non-interacting problem and blue points correspond to the experimental data of Ref. [5]. The parameters are $N = 1.2 \times 10^5$, $a_{+1,+1} = 0.1301$, $a_{+1,-1} = a_{-1,+1} = a_{-1,-1} = 0.1295$, $w = 1.626 \times 10^3$ and $b = 101.825$. All quantities are reported in reduced units, with the characteristic energy and length scales given by $\epsilon_0 = 500\hbar\omega$ and $a_0 = \sqrt{\frac{\hbar^2}{2m\epsilon_0}}$, respectively.

We do so in analogy to the Raman SOC case. The squared modulus of the wave function is given by:

$$\left|\psi_{\pm1}^{\text{stripe, 2D}}\right|^2 = \frac{1}{4\pi}\left[(\psi_{\pm1}^{\text{1D}}(\rho,l_z))^2 + \psi_{\pm1}^{\text{1D}}(\rho,-l_z))^2 + 2\psi_{\pm1}^{\text{1D}}(\rho,l_z)\psi_{\pm1}^{\text{1D}}(\rho,-l_z)\cos(2l_z\phi)\right] \tag{5.17}$$

As it can be seen from Eq. (5.17), the probability density of the wave function of Eq. (5.16) shows sinusoidal modulations along the ϕ axis. Hence, the stripe phase on a system under SOAC presents density modulations along the polar angle unlike in Raman SOC systems, where modulations go along the x-axis. Remarkably, the period of the stripe modulation is related to the z-angular momentum quantum number. Thus, in principle, it could be modified experimentally by changing the orbital angular momentum carried by the Laguerre-Gaussian beam. We now insert the functional form of Eq. (5.16) into Eq. (5.13), which yields:

$$\begin{aligned}
&-\frac{\partial}{\partial\tau}\left[\frac{1}{\sqrt{2}}\left(\psi^{\text{1D}}_{\pm1}(\rho,l_z)\frac{e^{il_z\phi}}{\sqrt{2\pi}}+\psi^{\text{1D}}_{\pm1}(\rho,-l_z)\frac{e^{-il_z\phi}}{\sqrt{2\pi}}\right)\right]=\\
&-\frac{\hbar^2}{2m\sqrt{2}}\left(\frac{\partial^2\psi^{\text{1D}}_{\pm1}(l_z)}{\partial\rho^2}\frac{e^{il_z\phi}}{\sqrt{2\pi}}+\frac{\partial^2\psi^{\text{1D}}_{\pm1}(-l_z)}{\partial\rho^2}\frac{e^{-il_z\phi}}{\sqrt{2\pi}}+\frac{1}{\rho}\frac{\partial\psi^{\text{1D}}_{\pm1}(l_z)}{\partial\rho}\frac{e^{il_z\phi}}{\sqrt{2\pi}}+\frac{1}{\rho}\frac{\partial\psi^{\text{1D}}_{\pm1}(-l_z)}{\partial\rho}\frac{e^{-il_z\phi}}{\sqrt{2\pi}}\right.\\
&\left.-\frac{1}{\rho^2}l_z^2\psi^{\text{1D}}_{\pm1}(\rho,l_z)\frac{e^{il_z\phi}}{\sqrt{2\pi}}-\frac{1}{\rho^2}l_z^2\psi^{\text{1D}}_{\pm1}(\rho,-l_z)\frac{e^{-il_z\phi}}{\sqrt{2\pi}}\right)+\frac{1}{\sqrt{2}}\left(\psi^{\text{1D}}_{\pm1}(\rho,l_z)\frac{e^{il_z\phi}}{\sqrt{2\pi}}+\psi^{\text{1D}}_{\pm1}(\rho,-l_z)\frac{e^{-il_z\phi}}{\sqrt{2\pi}}\right)\\
&\times\left(\frac{1}{2}m\omega^2\rho^2\pm\frac{\delta}{2}+\frac{l^2\hbar^2}{2m\rho^2}+\frac{\hbar^2}{4mb^2}+\frac{b^2}{4}m\omega^2\right)\\
&+\frac{1}{\sqrt{2}}\left(\mp\frac{ll_z\hbar^2}{m\rho^2}\psi^{\text{1D}}_{\pm1}(\rho,l_z)\frac{e^{il_z\phi}}{\sqrt{2\pi}}+\pm\frac{ll_z\hbar^2}{m\rho^2}\psi^{\text{1D}}_{\pm1}(\rho,-l_z)\frac{e^{-il_z\phi}}{\sqrt{2\pi}}\right)\\
&+\Omega(\rho)\frac{1}{\sqrt{2}}\left(\psi^{\text{1D}}_{\mp1}(\rho,l_z)\frac{e^{il_z\phi}}{\sqrt{2\pi}}+\psi^{\text{1D}}_{\mp1}(\rho,-l_z)\frac{e^{-il_z\phi}}{\sqrt{2\pi}}\right)\\
&+\frac{N}{2(2\pi)^{3/2}b}\frac{1}{\sqrt{2}}\left(\psi^{\text{1D}}_{\pm1}(\rho,l_z)\frac{e^{il_z\phi}}{\sqrt{2\pi}}+\psi^{\text{1D}}_{\pm1}(\rho,-l_z)\frac{e^{-il_z\phi}}{\sqrt{2\pi}}\right)\\
&\times\left[g_{\pm1,\pm1}\left(\left(\psi^{\text{1D}}_{\pm1}(\rho,l_z)\right)^2+\left(\psi^{\text{1D}}_{\pm1}(\rho,-l_z)\right)^2+\psi^{\text{1D}}_{\pm1}(\rho,l_z)\psi^{\text{1D}}_{\pm1}(\rho,-l_z)\left(e^{2il_z\phi}+e^{-2il_z\phi}\right)\right)\right.\\
&\left.+g_{\pm1,\mp1}\left(\left(\psi^{\text{1D}}_{\mp1}(\rho,l_z)\right)^2+\left(\psi^{\text{1D}}_{\mp1}(\rho,-l_z)\right)^2+\psi^{\text{1D}}_{\mp1}(\rho,l_z)\psi^{\text{1D}}_{\mp1}(\rho,-l_z)\left(e^{2il_z\phi}+e^{-2il_z\phi}\right)\right]
\end{aligned}\tag{5.18}$$

We now multiply Eq. (5.18) by $e^{\pm il_z\phi}/\sqrt{2\pi}$ and integrate along the ϕ axis in order to obtain a set of equations for $\psi^{\text{1D}}_{\pm1}(\rho,l_z)$ and $\psi^{\text{1D}}_{\pm1}(\rho,-l_z)$. However, due to the presence of the interaction, we can multiply Eq. (5.18) by $e^{\pm3il_z\phi}/\sqrt{2\pi}$ and integrate over ϕ to get

$$\psi^{\text{1D}}_{\pm1}(\rho,l_z)\left[g_{\pm1,\pm1}\psi^{\text{1D}}_{\pm1}(\rho,l_z)\psi^{\text{1D}}_{\pm1}(\rho,-l_z)+g_{\pm1,\mp1}\psi^{\text{1D}}_{\mp1}(\rho,l_z)\psi^{\text{1D}}_{\mp1}(\rho,-l_z)\right]=0\tag{5.19}$$

$$\psi^{\text{1D}}_{\pm1}(\rho,-l_z)\left[g_{\pm1,\pm1}\psi^{\text{1D}}_{\pm1}(\rho,l_z)\psi^{\text{1D}}_{\pm1}(\rho,-l_z)+g_{\pm1,\mp1}\psi^{\text{1D}}_{\mp1}(\rho,l_z)\psi^{\text{1D}}_{\mp1}(\rho,-l_z)\right]=0\tag{5.20}$$

If $\psi^{\rm 1D}_{\pm 1}(\rho, l_z) \neq 0$ and $\psi^{\rm 1D}_{\pm 1}(\rho, -l_z) \neq 0$, we should impose:

$$g_{+1,+1}\psi^{\rm 1D}_{+1}(\rho, l_z)\psi^{\rm 1D}_{+1}(\rho, -l_z) + g_{+1,-1}\psi^{\rm 1D}_{-1}(\rho, l_z)\psi^{\rm 1D}_{-1}(\rho, -l_z) = 0 \tag{5.21}$$

$$g_{-1,-1}\psi^{\rm 1D}_{-1}(\rho, l_z)\psi^{\rm 1D}_{-1}(\rho, -l_z) + g_{+1,-1}\psi^{\rm 1D}_{+1}(\rho, l_z)\psi^{\rm 1D}_{+1}(\rho, -l_z) = 0 \tag{5.22}$$

which implies:

$$\frac{g_{+1,-1}}{g_{+1,+1}}\psi^{\rm 1D}_{-1}(\rho, l_z)\psi^{\rm 1D}_{-1}(\rho, -l_z) = \frac{g_{-1,-1}}{g_{+1,-1}}\psi^{\rm 1D}_{-1}(\rho, l_z)\psi^{\rm 1D}_{-1}(\rho, -l_z) \tag{5.23}$$

If $\psi^{\rm 1D}_{-1}(\rho, l_z) \neq 0$, $\psi^{\rm 1D}_{-1}(\rho, -l_z) \neq 0$, then:

$$\frac{g_{+1,-1}}{g_{+1,+1}} = \frac{g_{-1,-1}}{g_{+1,-1}} \tag{5.24}$$

In general, for arbitrary $g_{+1,+1}$, $g_{-1,-1}$, $g_{+1,-1}$, this condition is not fulfilled. This is because the ansatz in Eq. (5.16) is not compatible with the ground state solution of the system at the mean field level in the stripe phase. This is analogous to what happens in a Raman SOC system, where the stripe ground state is a linear combination of an infinite number of linear momentum states (as stated in Chapter 4), instead of a linear combination of $\pm k_0$ momentum states, being $2k_0$ the period of the stripes. However, as stated in Ref. [25], a simple linear combination of only the $\pm k_0$ states turns out to be an excellent approximation to the stripe ground state under Raman SOC. Therefore, and in analogy to that case, we take the wave function in Eq. (5.16) as our approximation to the mean field ground state of the SOAC system in the stripe phase, thus neglecting the contributions in Eq. (5.18) proportional to $e^{\pm 3 i l_z \phi}/\sqrt{2\pi}$. Still, one must note that, in order to find the exact ground state, we should use an ansatz of the form:

$$\psi^{\text{stripe, 2D}}_{\pm 1}(\rho, \phi, l_z) = \sum_{n=-\infty}^{\infty} \psi^{\rm 1D}_{\pm 1}(\rho, n, l_z) \exp\left(i n l_z \phi\right) \tag{5.25}$$

which constitutes a combination of an infinite number of angular momentum states, just like the stripe wave function of the aforementioned Raman SOC system contains a superposition of an infinite number of linear momentum states. Considering only

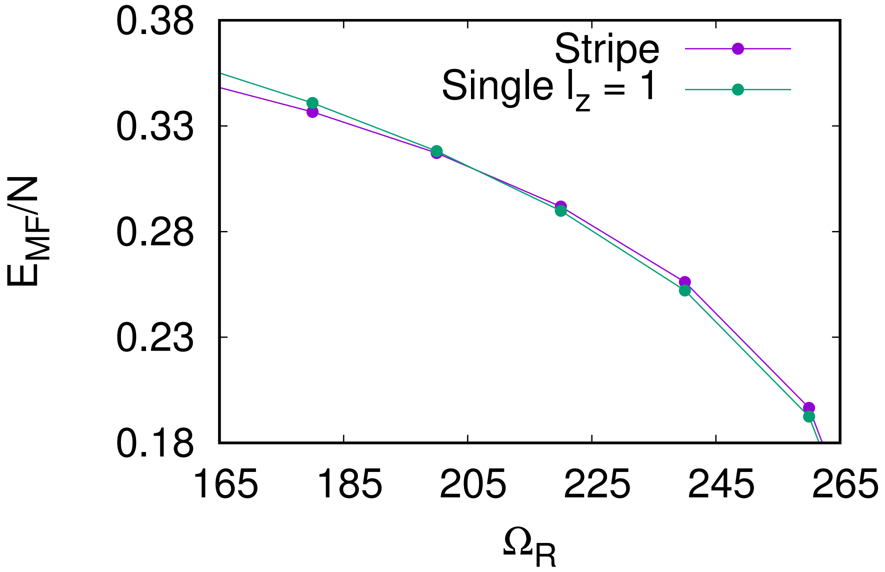

Fig. 5.4 Mean field energies per particle for the stripe phase (purple points) and for the single z-angular momentum state (green points) for $N = 60$, $\delta = 0$, $w = 162.2$, $a_{+1,+1} = 0.1301$, $\gamma = 0.4$, $l_z = 1$, $l = -1$. b is optimized variationally, which leads to $b = 3.78$. Lines are a guide to the eye. All quantities are expressed in reduced units, with the characteristic energy and length scales given by $\epsilon_0 = 5\hbar\omega$ and $a_0 = \sqrt{\frac{\hbar^2}{2m\epsilon_0}}$, respectively.

the $\pm l_z$, the equations for $\psi^{\mathrm{1D}}_{\pm1}(\rho, l_z)$ and $\psi^{\mathrm{1D}}_{\pm1}(\rho, -l_z)$ are:

$$\begin{aligned}
&-\frac{\partial\psi^{\mathrm{1D}}_{\pm1}(\rho,l_z)}{\partial\tau} = -\frac{\hbar^2}{2m}\left(\frac{\partial^2\psi^{\mathrm{1D}}_{\pm1}(l_z)}{\partial\rho^2} + \frac{1}{\rho}\frac{\partial\psi^{\mathrm{1D}}_{\pm1}(l_z)}{\partial\rho} - \frac{l_z^2}{\rho^2}\psi^{\mathrm{1D}}_{\pm1}(\rho,l_z)\right)\\
&+\left(\frac{1}{2}m\omega^2\rho^2 \pm \frac{\delta}{2} \mp \frac{l l_z\hbar^2}{m\rho^2} + \frac{l^2\hbar^2}{2m\rho^2} + \frac{\hbar^2}{4mb^2} + \frac{b^2}{4}m\omega^2\right)\psi^{\mathrm{1D}}_{\pm1}(\rho,l_z) + \Omega(\rho)\psi^{\mathrm{1D}}_{\mp1}(\rho,l_z)\\
&+\frac{N}{2(2\pi)^{3/2}b}\left[g_{\pm1,\pm1}\left(\left(\psi^{\mathrm{1D}}_{\pm1}(\rho,l_z)\right)^2\psi^{\mathrm{1D}}_{\pm1}(\rho,l_z) + 2\left(\psi^{\mathrm{1D}}_{\pm1}(\rho,-l_z)\right)^2\psi^{\mathrm{1D}}_{\pm1}(\rho,l_z)\right)\right.\\
&+g_{\pm1,\mp1}\left(\left(\psi^{\mathrm{1D}}_{\mp1}(\rho,l_z)\right)^2\psi^{\mathrm{1D}}_{\pm1}(\rho,l_z) + \left(\psi^{\mathrm{1D}}_{\mp1}(\rho,-l_z)\right)^2\psi^{\mathrm{1D}}_{\pm1}(\rho,l_z)\right.\\
&\left.\left.+\psi^{\mathrm{1D}}_{\mp1}(\rho,l_z)\psi^{\mathrm{1D}}_{\mp1}(\rho,-l_z)\psi^{\mathrm{1D}}_{\pm1}(\rho,-l_z)\right)\right]
\end{aligned}\tag{5.26}$$

$$\begin{aligned}
&-\frac{\partial\psi^{\mathrm{1D}}_{\pm1}(\rho,-l_z)}{\partial\tau} = -\frac{\hbar^2}{2m}\left(\frac{\partial^2\psi^{\mathrm{1D}}_{\pm1}(-l_z)}{\partial\rho^2} + \frac{1}{\rho}\frac{\partial\psi^{\mathrm{1D}}_{\pm1}(-l_z)}{\partial\rho} - \frac{l_z^2}{\rho^2}\psi^{\mathrm{1D}}_{\pm1}(\rho,-l_z)\right)\\
&+\left(\frac{1}{2}m\omega^2\rho^2 \pm \frac{\delta}{2} \pm \frac{l l_z\hbar^2}{m\rho^2} + \frac{l^2\hbar^2}{2m\rho^2} + \frac{\hbar^2}{4mb^2} + \frac{b^2}{4}m\omega^2\right)\psi^{\mathrm{1D}}_{\pm1}(\rho,-l_z) + \Omega(\rho)\psi^{\mathrm{1D}}_{\mp1}(\rho,-l_z)\\
&+\frac{N}{2(2\pi)^{3/2}b}\left[g_{\pm1,\pm1}\left(\left(\psi^{\mathrm{1D}}_{\pm1}(\rho,-l_z)\right)^2\psi^{\mathrm{1D}}_{\pm1}(\rho,-l_z) + 2\left(\psi^{\mathrm{1D}}_{\pm1}(\rho,l_z)\right)^2\psi^{\mathrm{1D}}_{\pm1}(\rho,-l_z)\right)\right.\\
&+g_{\pm1,\mp1}\left(\left(\psi^{\mathrm{1D}}_{\mp1}(\rho,-l_z)\right)^2\psi^{\mathrm{1D}}_{\pm1}(\rho,-l_z) + \left(\psi^{\mathrm{1D}}_{\mp1}(\rho,l_z)\right)^2\psi^{\mathrm{1D}}_{\pm1}(\rho,-l_z)\right.\\
&\left.\left.+\psi^{\mathrm{1D}}_{\mp1}(\rho,-l_z)\psi^{\mathrm{1D}}_{\mp1}(\rho,l_z)\psi^{\mathrm{1D}}_{\pm1}(\rho,l_z)\right)\right]
\end{aligned}\tag{5.27}$$

This forms to a set of four one-dimensional coupled equations that can be solved through imaginary time propagation. Doing so yields to the approximated ground state of the system in the stripe phase. By setting $g_{+1,+1} = g_{-1,-1} \neq g_{+1,-1}$ and $\gamma = (g_{+1,+1} - g_{+1,-1})/(g_{+1,+1} + g_{+1,-1}) = 0.4$ we can see that the stripe phase is energetically favourable with respect to single z-angular momentum states for a given density dependent range of values of Ω_R, thus suggesting that, as in the Raman SOC case, an increase in the contrast of the spin-dependent inter-atomic interactions leads to a stripe ground state. We show in Fig. 5.4 the mean field energies per particle for both a single z-angular momentum state with $l_z = 1$ and the stripe state for $N = 60$, $\delta = 0$, $w = 162.2$, $a_{+1,+1} = 0.1301$, $\gamma = 0.4$, $l_z = 1$, $l = -1$. As can be seen from the Figure, the stripe phase is energetically favourable for $\Omega_R \lesssim 220$, while the single angular momentum state corresponds to the ground state of the system for $\Omega_R \gtrsim 220$. The energy of the single momentum state with $l_z = 0$ is not shown because it is larger than the plotted energies in the displayed regime for Ω_R.

We show in Fig. 5.5 the marginal probability density on the x-y plane for both the single angular momentum phase and the stripe phase. Notice that. while both the $+1$ and -1 spinor components of the single angular momentum wave function are isotropic, this is not the case in the stripe phase, since the sinusoidal dependence of the probability density with respect to ϕ (see Eq. (5.17)) induces anisotropy.

5.3 Spin Orbital Angular Coupling and Diffusion Monte Carlo

The DMC methods presented in Chapter 3 can also be employed to study a system under SOAC. Since, in general, one has to deal with two-body spin-dependent interactions, the results presented in this Section have been obtained with the DTDMC method (see Chapter 3). While DMC algorithms account for inter-atomic correlations beyond the mean field level, there exist limitations in terms of the number of particles. An exceedingly large number of particles can lead to very large computation time scales. Because of this, it is not possible to directly simulate the experimental system of Ref. [5] with DMC, which has $N = 1.2 \times 10^5$ particles. Therefore, rescaling the system is a must. We introduce a rescaling scheme in Sec. 5.3.1. Afterwards, we present in Sec. 5.3.2 the results for the phase diagram of the rescaled system, both for the inter-atomic interaction parameters of Ref. [5], for which the stripe phase is irrelevant, and for an interaction with non-zero contrast between the different spin channels, which favors the stripe phase. We compare DMC and GPE results as the *gas parameter* of the system increases in order to determine the effect of inter-atomic correlations in the phase diagram.

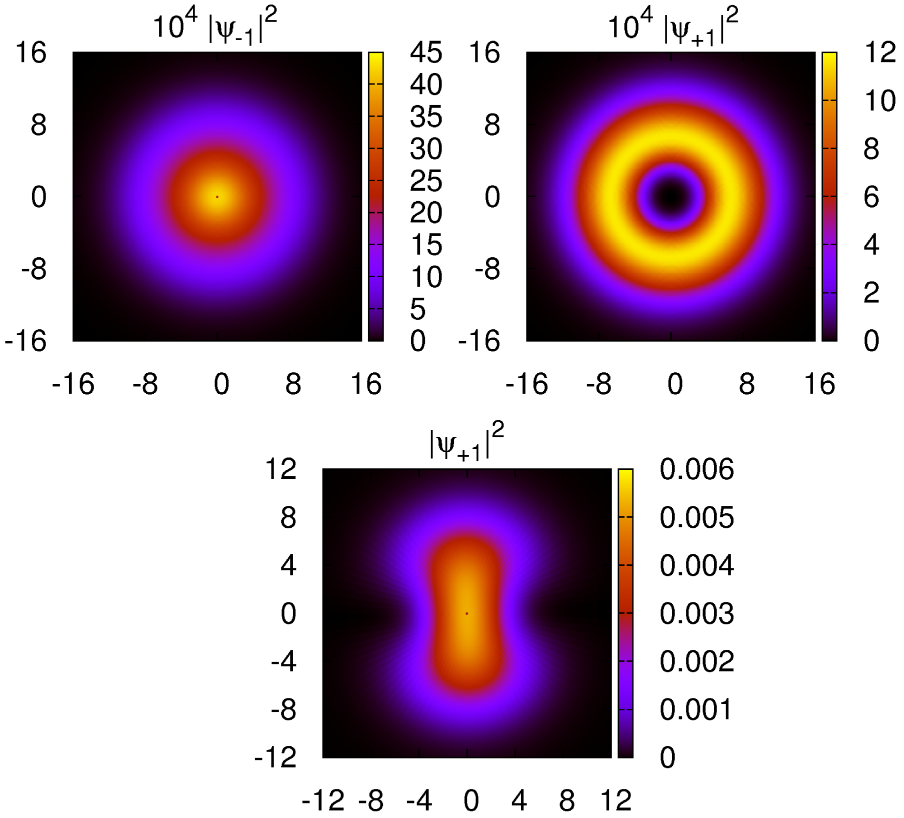

Fig. 5.5 Marginal probability densities in the x-y plane for the stripe phase (lower plot) and for the single z-angular momentum state (upper plots). Only the $+1$ component is reported for the stripe phase since it equals the -1 component. The parameters are $\Omega = 180$ (stripe phase), $\Omega = 240$ (single angular momentum phase), $N = 60$, $\delta = 0$, $w = 162.2$, $a_{+1,+1} = 0.1301$, $\gamma = 0.4$, $l_z = 1$, $l = -1$. b is optimized variationally, which leads to $b = 3.78$. All quantities are expressed in reduced units, with the characteristic energy and length scales given by $\epsilon_0 = 5\hbar\omega$ and $a_0 = \sqrt{\frac{\hbar^2}{2m\epsilon_0}}$, respectively.

5.3.1 The rescaled system

In order to rescale the experimental system, we impose the condition:

$$\frac{N}{a_0^3} = 2\frac{N^{(r)}}{(a_0^{(r)})^3} \tag{5.28}$$

where $N = 1.2 \times 10^5$ and $a_0 = \sqrt{\frac{\hbar}{m\omega}}$, $\omega = 2\pi \times 77.5$Hz corresponds to the experimental system of Ref. [5]. In this way, we rescale the number of particles together with one of the relevant size scales of the system, the harmonic oscillator length. The scaling law in Eq. 5.28 enables us to work with a feasible number of particles while preserving the conditions of diluteness of the experiment of Ref. [5], as discussed below. In this Section, we refer to the parameters of the rescaled system with the superindex $^{(r)}$. We set $N^{(r)} = 60$, which implies:

$$\omega^{(r)} = \omega \left(\frac{N}{2N^{(r)}} \right)^{2/3} = 100\omega \tag{5.29}$$

We also impose:

$$\frac{w}{a_0} = \frac{w^{(r)}}{a_0^{(r)}} \tag{5.30}$$

We can recover the qualitative behaviour of $\langle \hat{\sigma}_z \rangle$ with respect to δ and ω in a rescaled region of the phase diagram of the rescaled system, as shown in Fig. 5.6. For the rescaled system, $\Omega^{(r)} = 116.5\Omega^{\text{plot}}$, $\delta^{(r)} = 18\delta^{\text{plot}}$ for the P_2 transition (see Fig. 5.1) and $\Omega^{(r)} = 83.21\Omega^{\text{plot}}$, $\delta^{(r)} = 5\delta^{\text{plot}}$ for the P_3 transition (see Fig. 5.1). It must be remarked that if the proposed rescaling was flawless, the ratio between the quantities $\Omega^{(r)}$ and $\delta^{(r)}$ of the rescaled system and those from the plots would be constant across all transitions, including P_2 and P_3. Thus, we emphasize that the rescaling procedure leads to a system qualitatively approximated to the original one.

The rescaled system preserves the diluteness of the experimental system, which we measure through the *gas parameter*, that we define as $x_g = \text{Max}(n) a^3_{+1,+1}$, with Max($n$) the maximum value of the density. For instance, for $\Omega = 2.26$, $\delta \in [-0.05, 0.05]$ in the experimental system we have $x_g \simeq 1.5 \times 10^{-5}$ while for $\Omega = 264.33$, $\delta \in [-0.9, 0.9]$ in the rescaled system we have $x_g \simeq 4 \times 10^{-5}$. Notice that, since we are working with a harmonically trapped system, the density is not constant, hence to compute x_g we use the maximum value of the density.

5.3.2 The phase diagram of the rescaled system: DMC and GPE results

5.3.2.1 ^{87}Rb interactions: single angular momentum states

We first focus on the case with inter-atomic scattering lengths given by $a_{+1,+1} = 0.1301$, $a_{+1,-1} = a_{-1,+1} = a_{-1,-1} = 0.1295$ expressed in reduced units, which corresponds to the experimental system of Ref. [5]. The GPE phase diagram of the rescaled system is presented in Fig. 5.7. As we can see from the Figure, the diagram qualitatively resembles the phase diagram of the aforementioned experimental system, reported in Fig. 5.2.

We have performed DTDMC calculations at several points of the phase diagram near the $l_z = 1 \leftrightarrow l_z = 0$ transition, as shown in Table 5.1. We can see that the DMC energies per particle are very close to the GPE ones and thus one recovers the transition line predicted by the GPE. This is not surprising, since the system lays in the dilute regime, where inter-atomic correlations do not affect very much the physics of the system.

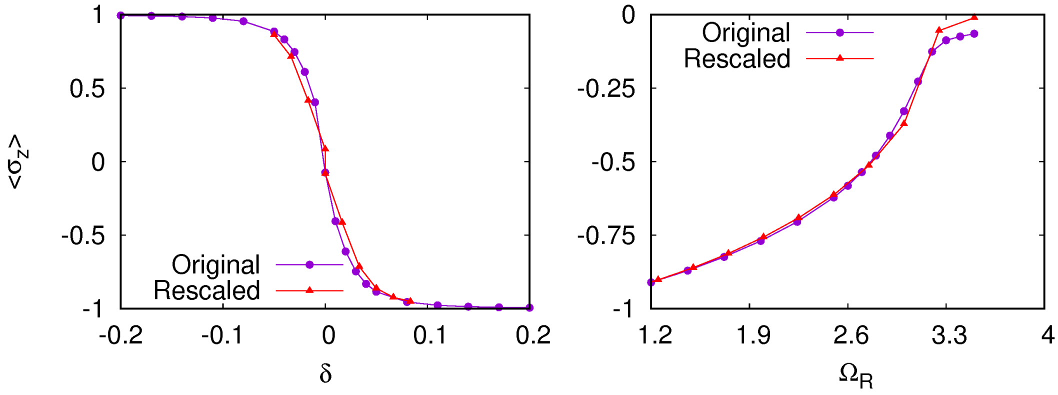

Fig. 5.6 Polarization of the SOAC system for the transitions labeled as P_2 (see Fig. 5.1) (left plot) and P_3 (see Fig. 5.1) (right plot) in Ref. [5]. Purple and red points correspond to the solution of the GPE equation for the experimental and the rescaled systems respectively. The parameters of the experimental system are given in Fig. 5.3, while in the rescaled system we have $N^{(r)} = 60$, $a^{(r)}_{+1,+1} = 0.1301$, $a^{(r)}_{+1,-1} = a^{(r)}_{-1,+1} = a^{(r)}_{-1,-1} = 0.1295$, $w^{(r)} = 162.6$ and $b^{(r)} = 10.182$. All quantities are reported in reduced units, with the characteristic energy and length scales given by $\epsilon_0 = 500\hbar\omega = 5\omega^{(r)}$ and $a_0 = \sqrt{\frac{\hbar^2}{2m\epsilon_0}}$, respectively, with ω the harmonic oscillator frequency of the experimental system. For the rescaled system, $\Omega^{(r)} = 116.5\Omega^{\mathrm{plot}} = 264.33$, $\delta^{(r)} = 18\delta^{\mathrm{plot}}$ for transition P_2 and $\Omega^{(r)} = 83.21\Omega^{\mathrm{plot}}$, $\delta^{(r)} = 5\delta^{\mathrm{plot}} = 0.129$ for transition P_3.

	$\delta = 0.05$		$\delta = 0.894$		$\delta = 2.974$	
	$\Omega_R = 245$	$\Omega_R = 255$	$\Omega_R = 285$	$\Omega_R = 295$	$\Omega_R = 315$	$\Omega_R = 325$
GPE $l_z = 1$	0.2357	0.2068	-0.09954	-0.2672	-1.0734	-1.3908
DMC $l_z = 1$	0.2344	0.2060	-0.1017	-0.2677	-1.3908	-1.3913
GPE $l_z = 0$	0.2388	0.2050	-0.07099	-0.2686	-0.9931	-1.3914
DMC $l_z = 0$	0.2377	0.2042	-0.0712	-0.2691	-1.3914	-1.3919

Table 5.1 Energy per particle for several points of the phase diagram of the rescaled system. All DMC errors are $\leq 5 \times 10^{-4}$. The parameters are the same as in Fig. 5.7.

In order to evaluate the effect of inter-atomic correlations, we increase the gas parameter by raising the scattering lengths, and compare DMC and GPE results, again for points of the phase diagram near the $l_z = 1 \leftrightarrow l_z = 0$ transition. We show the results in Table 5.2. Remarkably, despite the increase in the gas parameter, DMC calculations reveal that the transition line is mostly unchanged. Also, GPE results still lay close to DMC, even for scattering lengths a factor a hundred larger than those in the experiment of Ref. [5]. This suggests that the scattering lengths should be furtherly increased in order for inter-atomic correlations to have an impact on the physics of the system.

Finally, we discuss the case with inter-atomic scattering lengths given by $a_{+1,+1} = a_{-1,-1} = 0.1301$, $\gamma = 0.4$, and $\delta = 0$, expressed in reduced units, which is a configuration that favors the stripe phase. Here, $\gamma = (a_{+1,+1} - a_{+1,-1})/(a_{+1,+1} + a_{+1,-1})$, as in the

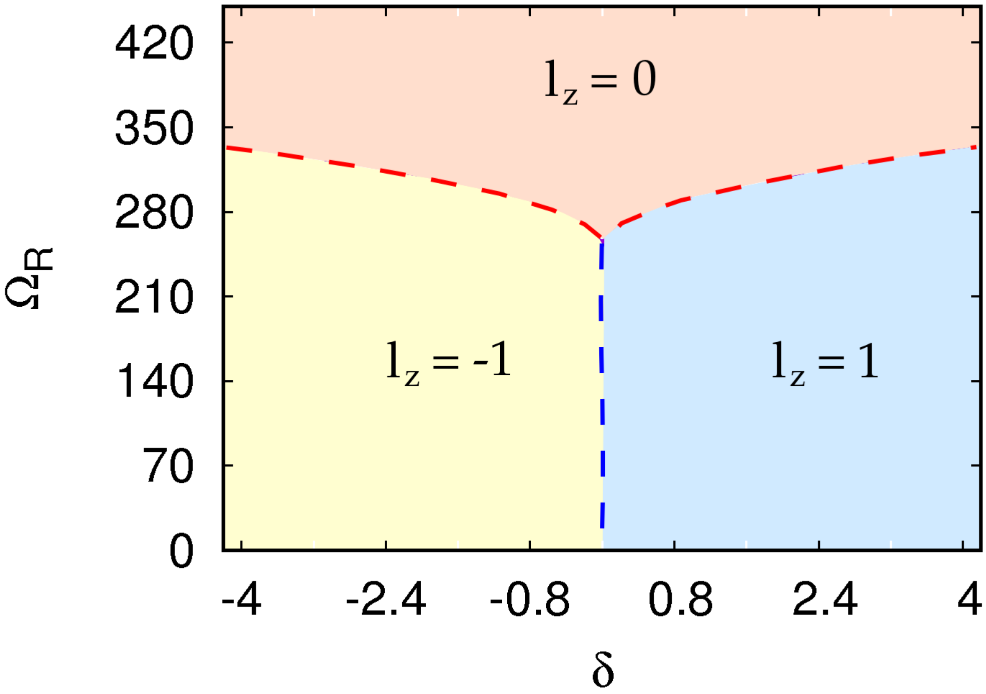

Fig. 5.7 Phase diagram of the rescaled system at the mean field level. The parameters are $N^{(r)} = 60$, $a^{(r)}_{+1,+1} = 0.1301$, $a^{(r)}_{+1,-1} = a^{(r)}_{-1,+1} = a^{(r)}_{-1,-1} = 0.1295$ and $w^{(r)} = 162.6$. $b^{(r)}$ is optimized variationally, which leads to $b^{(r)} = 3.16$. All quantities are reported in reduced units, with the characteristic energy and length scales given by $\epsilon_0 = 5\hbar\omega^{(r)} = 500\hbar\omega$ and $a_0 = \sqrt{\frac{\hbar^2}{2m\epsilon_0}}$, respectively.

previous Chapters. We have already shown in Fig. 5.4 that the asymmetry present in the spin channels leads to a stripe ground state for $\Omega_R \lesssim 220$. This is confirmed by DMC simulations, as shown in Table 5.3. Again, DMC results lay close to GPE results. And again, we furtherly increase the scattering lengths of the system in order to check if GPE results depart from DMC, thus shifting the transition value of Ω_R. Results are shown in Table 5.4. This time, scattering lengths are increased up to $a'_{s_1,s_2} = 10000^{1/3} a_{s_1,s_2}$. As a result, we see a significant departure between the DMC and the GPE results, meaning that the system lays in a regime where inter-atomic correlations are relevant. Notice how the transition between the stripe and the single angular momentum phase has shifted to lower values of Ω_R: while $\Omega_{R,\text{ GPE, trans}} \simeq 67$, DMC calculations yield $\Omega_{R,\text{ DMC, trans}} \simeq 55$, leading to a reduced domain of Ω_R where the stripe phase is favored. Remarkably, this situation is the opposite to what one finds in a Raman SOC system, where inter-atomic correlations enhance the domain of the stripe phase on the phase diagram (see Chapter 3).

	$a'_{s_1,s_2} = 100^{1/3} a_{s_1,s_2}$ ($x_g \sim 10^{-3}$)		$a'_{s_1,s_2} = 1000^{1/3} a_{s_1,s_2}$ ($x_g \sim 10^{-2}$)			
	$\delta = 0.894$		$\delta = 0.802$		$\delta = 2.914$	
	$\Omega_R = 285$	$\Omega_R = 295$	$\Omega_R = 285$	$\Omega_R = 295$	$\Omega_R = 315$	$\Omega_R = 325$
GPE $l_z = 1$	-0.05752	-0.2455	-0.02016	-0.2137	-0.9540	-1.3409
DMC $l_z = 1$	-0.0572	-0.2460	-0.0173	-0.2132	-0.9454	-1.3440
GPE $l_z = 0$	-0.04830	-0.2464	-0.01470	-0.2151	-0.9404	-1.3415
DMC $l_z = 0$	-0.0485	-0.2475	-0.0127	-0.2146	-0.9430	-1.3445

Table 5.2 Energy per particle for several points of the phase diagram of the rescaled system for increased scattering lengths. All DMC errors are of the same order as the last figure included in the results. The parameters are the same as in Fig. 5.7. $b^{(r)}$ is optimized variationally via the GPE, which leads to $b^{(r)} = 3.44$ for $a'_{s_1,s_2} = 100^{1/3} a_{s_1,s_2}$ and $b^{(r)} = 4.08$ for $a'_{s_1,s_2} = 1000^{1/3} a_{s_1,s_2}$.

	$\delta = 0$	
	$\Omega_R = 200$	$\Omega_R = 220$
GPE $l_z = 1$	0.3180	0.2898
DMC $l_z = 1$	0.3160	0.2871
GPE Stripe	0.3172	0.2198
DMC Stripe	0.3149	0.2885

Table 5.3 Energy per particle for the single angular momentum and stripe phases in the rescaled system. All DMC errors are of the same order as the last figure included in the results. The parameters are the same as in Fig. 5.7, except for $b^{(r)}$ and the scattering lengths, whose value is specified in the text. $b^{(r)}$ is optimized variationally via the GPE, which leads to $b^{(r)} = 3.78$.

	$a'_{s_1,s_2} = 10000^{1/3} a_{s_1,s_2}$			
	$\delta = 0$			
	$\Omega_R = 55$	$\Omega_R = 60$	$\Omega_R = 66$	$\Omega_R = 72$
GPE $l_z = 0$			0.9549	0.9428
DMC $l_z = 0$	1.355 ± 0.005	1.346 ± 0.002	1.331 ± 0.003	1.316 ± 0.002
GPE Stripe			0.9502	0.9440
DMC Stripe	1.359 ± 0.004	1.353 ± 0.004	1.340 ± 0.004	1.330 ± 0.002

Table 5.4 Energy per particle for the single angular momentum ($l_z = 0$) and stripe phases in the rescaled system for increased scattering lengths. All DMC errors are of the same order as the last figure included in the results. The parameters are the same as in Fig. 5.7, except for $b^{(r)}$ and the scattering lengths, for which $a'_{s_1,s_2} = 10000^{1/3} a_{s_1,s_2}$, with the values a_{s_1,s_2} specified in the text. The $b^{(r)}$ parameter is optimized variationally, which leads to $b^{(r)} = 6$ for the GPE stripe phase, $b^{(r)} = 5.25$ for the GPE single angular momentum $l_z = 0$ and $b^{(r)} = 3.4$ for the DMC calculations.

Chapter 6

Conclusions

In this Thesis we have presented two approaches to calculate ground state properties of quantum many-body systems with Spin Orbit Coupling (SOC) interactions. On one hand, we have presented the formalism and application of two Diffusion Monte Carlo (DMC) methods able to deal with this kind of system. These methods have been used to study systems under Raman SOC and Spin Orbital Angular Coupling (SOAC). On the other hand, we have followed the Bogoliubov formalism to perform beyond mean field calculations of Raman SOC systems at the beyond mean field level for all the stripe, plane wave and single minimum phases.

In what follows, we summarize the main results of this Thesis.

6.1 Diffusion Monte Carlo methods for Spin Orbit Coupling interactions

In Chapter 3, we have developed the formalism of two Diffusion Monte Carlo methods able to sample Spin Orbit Coupling potentials. We have derived the propagator for SOC Hamiltonians and discussed its implementation in the context of the DMC formalism. These two methods are the Discrete Spin T-moves DMC (DTDMC), which corresponds to an adaptation to discrete spins of the method presented in Ref. [19], and the Spin Integrated DMC (SIDMC), a completely original method developed in this Thesis. The DTDMC algorithm resorts to two approximations: the fixed phase and the effective Hamiltonian approximations, which implies that the energy obtained with this method corresponds to an upper bound to the fixed phase energy, which in turn is an upper bound to the exact ground state energy. We have shown how to bypass the effective Hamiltonian approximation via the SIDMC method by propagating the spin integrated wave function in imaginary time. We have shown that the energy obtained with the SIDMC method corresponds to the fixed phase energy of the system, although this method is not able to deal with spin-dependent two-body interactions. For both methods, we have provided schemes detailing their implementation. We have also reported numerical tests involving the computation of the energy in one-body, two-body, diluted many-body and strongly correlated many-body systems, with successful comparisons with the energies obtained using other approaches, like the exact integration of the Schrödinger equation, or the Gross-Pitaevskii equation.

6.2 The phase diagram of a Raman SOC many-body system: supersolid stripes enhanced by correlations

In Chapter 3 we also present results for the phase diagram of a many-body Raman SOC system featuring spin-dependent two-body interactions. The diagram is obtained with the DTDMC method. We extend the previously reported phase diagram, computed at the mean field level [25], to the strongly correlated regime. Remarkably, we observe that, even at low *gas parameters*, $na^3_{+1,+1} \sim 10^{-4}$, with n the density and $a_{+1,+1}$ the up-up scattering length, the extension of the region of the stripe phase in the diagram is enhanced with respect to mean field calculations. This enhancement becomes more pronounced the higher the gas parameter, where correlations are more relevant. Therefore, we conclude that inter-atomic correlations enhance the stripe phase. We also characterize the superfluidity of the stripes with the Monte Carlo method and obtain a non-zero superfluid fraction in the direction across the density modulations. Thus, this shows the stripes to be superfluid, in agreement with results obtained in mean field, phase twist calculations [49] and in beyond mean field calculations [4]. We have characterized how the superfluid fraction changes with the Raman coupling. We have also computed other observables of the system, such as the static structure factor, which reflects the periodicity of the stripe phase, the two-body pair correlation function, and the one-body density matrix.

6.3 The Lee-Huang-Yang energy correction in a Raman SOC system in the stripe phase

In Chapter 4 we present the Bogoliubov-de Gennes formalism leading to the calculation of the LHY energy correction for a Raman SOC system in the stripe phase, which has not been derived before. We discuss in detail the technical aspects of the calculation, since it is numerically challenging. We have presented the necessary approximations in order to significantly reduce the computational cost of the calculations, which mainly involve retaining specific contributions to the LHY energy. We have also illustrated the application of Dimensional Regularization to the problem, in order to successfully regularize the divergent LHY integral and produce physically meaningful results. Finally, we have analyzed the dependence of the LHY energy on the number of Brillouin Zones and discretization points employed in the calculations.

6.4 Supersolid striped droplets in a Raman SOC system

We have also characterized in Chapter 4 the role played by quantum fluctuations in a Raman SOC system in the stripe phase with attractive inter-spin interactions, which is aimed to be realized in current state of the art experiments. We have shown that, if the attractive component is negative enough, the system collapses at the mean field level. However, we have reported that quantum fluctuations (the LHY energy correction) stabilize the system, leading to either a stripe gas or a stripe liquid, depending on the values of the parameters of the Hamiltonian. We have quantitatively characterized the phase diagram of the stabilized system in the stripe phase. By solving the extended Gross-Pitaevskii equation, we have also shown that, in the stripe liquid phase, the finite system presents a droplet-like ground state for a high enough number of particles. Remarkably, these droplet states feature density modulations induced by SOC, which implies that they represent a state of matter that combines the self-bound character of a liquid, density modulations reminiscent of solids, and superfluidity, since the stripes induced by Raman SOC have been proved to be superfluid [4, 48, 49]. We have quantitatively characterized the critical number of particles for self-binding as a function of the Raman coupling and the scattering lengths, and we have also provided an analytical energy functional (obtained through the fit of numerical results) in order to ease the evaluation of the LHY energy.

6.5 Evaluation of the effect of correlations in a Spin Orbital Angular Coupled system

In Chapter 5, we first review the mean field formalism for a system with Spin Orbital Angular Coupling. We present in detail the derivation of the effective one-dimensional Gross Pitaevskii equation (addressed originally in Ref. [5]). We also present the extension of this formalism to the stripe phase. We report a proposal for the rescaling of the experimental system of Ref. [5], as a way to allow its study through DMC. We evaluate the transition boundaries between the different single momentum phases with the GPE and DMC for different values of the interaction scattering lengths, finding little discrepancies in the regime of parameters considered. We follow the same approach for a SOAC system with non-negligible contrast between different spin channels, which has not yet been realized in experiments, but that supports a striped ground state. Analogously to the results seen for the rescaled experimental system of Ref. [5], little discrepancies between DMC and GPE results are seen for the regime of parameters considered. This differs from the results reported for Raman SOC systems, for which, even at low gas parameters, important differences between DMC and GPE results regarding the phase diagram of the system are observed.

References

[1] Y.-J. Lin, K. Jiménez-García, and I. B. Spielman, Nature **471**, 83 (2011).

[2] J.-R. Li, J. Lee, W. Huang, S. Burchesky, B. Shteynas, F. Ç. Top, A. O. Jamison, and W. Ketterle, Nature **543**, 91 (2017).

[3] W. Zheng, Z.-Q. Yu, X. Cui, and H. Zhai, Journal of Physics B: Atomic, Molecular and Optical Physics **46**, 134007 (2013).

[4] Y. Li, G. I. Martone, L. P. Pitaevskii, and S. Stringari, Phys. Rev. Lett. **110**, 235302 (2013).

[5] D. Zhang, T. Gao, P. Zou, L. Kong, R. Li, X. Shen, X.-L. Chen, S.-G. Peng, M. Zhan, H. Pu, and K. Jiang, Phys. Rev. Lett. **122**, 110402 (2019).

[6] M. H. Anderson, J. R. Ensher, M. R. Matthews, C. E. Wieman, and E. A. Cornell, Science **269**, 198 (1995), https://science.sciencemag.org/content/269/5221/198.full.pdf .

[7] K. B. Davis, M. O. Mewes, M. R. Andrews, N. J. van Druten, D. S. Durfee, D. M. Kurn, and W. Ketterle, Phys. Rev. Lett. **75**, 3969 (1995).

[8] A. Einstein, Sitzungsberg. Preuss. Akad. Wiss., Phys. Math. K , 3 (1925).

[9] L. Chomaz, S. Baier, D. Petter, M. J. Mark, F. Wächtler, L. Santos, and F. Ferlaino, Phys. Rev. X **6**, 041039 (2016).

[10] H. Kadau, M. Schmitt, M. Wenzel, C. Wink, T. Maier, I. Ferrier-Barbut, and T. Pfau, Nature **530**, 194 (2016).

[11] S. Inouye, M. R. Andrews, J. Stenger, H.-J. Miesner, D. M. Stamper-Kurn, and W. Ketterle, Nature **392**, 151 (1998).

[12] M. Z. Hasan and C. L. Kane, Rev. Mod. Phys. **82**, 3045 (2010).

[13] J. Radić, A. Di Ciolo, K. Sun, and V. Galitski, Phys. Rev. Lett. **109**, 085303 (2012).

[14] W. S. Cole, S. Zhang, A. Paramekanti, and N. Trivedi, Phys. Rev. Lett. **109**, 085302 (2012).

[15] Z. Cai, X. Zhou, and C. Wu, Phys. Rev. A **85**, 061605 (2012).

[16] M. Sato and Y. Ando, Reports on Progress in Physics **80**, 076501 (2017).

[17] J. D. Sau, R. M. Lutchyn, S. Tewari, and S. Das Sarma, Phys. Rev. Lett. **104**, 040502 (2010).

[18] I. Žutić, J. Fabian, and S. Das Sarma, Rev. Mod. Phys. **76**, 323 (2004).

[19] C. A. Melton, M. C. Bennett, and L. Mitas, The Journal of Chemical Physics **144**, 244113 (2016).

[20] X.-J. Liu, M. F. Borunda, X. Liu, and J. Sinova, Phys. Rev. Lett. **102**, 046402 (2009).

[21] V. Galitski and I. B. Spielman, Nature **494**, 49 (2013).

[22] Y. A. Bychkov and E. I. Rashba, Journal of Physics C: Solid State Physics **17**, 6039 (1984).

[23] G. Dresselhaus, Phys. Rev. **100**, 580 (1955).

[24] S. Ashhab and A. J. Leggett, Phys. Rev. A **68**, 063612 (2003).

[25] Y. Li, G. I. Martone, and S. Stringari, in *Annual Review of Cold Atoms and Molecules*, Chap. CHAPTER 5, pp. 201–250.

[26] C. Hamner, Y. Zhang, M. A. Khamehchi, M. J. Davis, and P. Engels, Phys. Rev. Lett. **114**, 070401 (2015).

[27] T. M. Bersano, J. Hou, S. Mossman, V. Gokhroo, X.-W. Luo, K. Sun, C. Zhang, and P. Engels, Phys. Rev. A **99**, 051602 (2019).

[28] L. W. Cheuk, A. T. Sommer, Z. Hadzibabic, T. Yefsah, W. S. Bakr, and M. W. Zwierlein, Phys. Rev. Lett. **109**, 095302 (2012).

[29] P. Wang, Z.-Q. Yu, Z. Fu, J. Miao, L. Huang, S. Chai, H. Zhai, and J. Zhang, Phys. Rev. Lett. **109**, 095301 (2012).

[30] S. Kolkowitz, S. L. Bromley, T. Bothwell, M. L. Wall, G. E. Marti, A. P. Koller, X. Zhang, A. M. Rey, and J. Ye, Nature **542**, 66 (2017).

[31] B. Song, C. He, S. Zhang, E. Hajiyev, W. Huang, X.-J. Liu, and G.-B. Jo, Phys. Rev. A **94**, 061604 (2016).

[32] L. F. Livi, G. Cappellini, M. Diem, L. Franchi, C. Clivati, M. Frittelli, F. Levi, D. Calonico, J. Catani, M. Inguscio, and L. Fallani, Phys. Rev. Lett. **117**, 220401 (2016).

[33] N. Q. Burdick, Y. Tang, and B. L. Lev, Phys. Rev. X **6**, 031022 (2016).

[34] S. Giorgini, J. Boronat, and J. Casulleras, Phys. Rev. A **60**, 5129 (1999).

[35] D. S. Petrov, Phys. Rev. Lett. **115**, 155302 (2015).

[36] V. Cikojević, L. V. c. v. Markić, G. E. Astrakharchik, and J. Boronat, Phys. Rev. A **99**, 023618 (2019).

[37] C. R. Cabrera, L. Tanzi, J. Sanz, B. Naylor, P. Thomas, P. Cheiney, and L. Tarruell, Science **359**, 301 (2018), https://science.sciencemag.org/content/359/6373/301.full.pdf .

[38] G. Semeghini, G. Ferioli, L. Masi, C. Mazzinghi, L. Wolswijk, F. Minardi, M. Modugno, G. Modugno, M. Inguscio, and M. Fattori, Phys. Rev. Lett. **120**, 235301 (2018).

[39] J. Sánchez-Baena, J. Boronat, and F. Mazzanti, (2020), arXiv:2007.04196 [cond-mat.quant-gas] .

[40] G. Ortiz, D. M. Ceperley, and R. M. Martin, Phys. Rev. Lett. **71**, 2777 (1993).

[41] C. A. Melton, M. Zhu, S. Guo, A. Ambrosetti, F. Pederiva, and L. Mitas, Phys. Rev. A **93**, 042502 (2016).

[42] A. Ambrosetti, F. Pederiva, and E. Lipparini, Phys. Rev. B **83**, 155301 (2011).

[43] A. Ambrosetti, P. L. Silvestrelli, F. Pederiva, L. Mitas, and F. Toigo, Phys. Rev. A **91**, 053622 (2015).

[44] M. Casula, S. Moroni, S. Sorella, and C. Filippi, The Journal of Chemical Physics **132**, 154113 (2010).

[45] D. F. B. ten Haaf, H. J. M. van Bemmel, J. M. J. van Leeuwen, W. van Saarloos, and D. M. Ceperley, Phys. Rev. B **51**, 13039 (1995).

[46] A. Macia, D. Hufnagl, F. Mazzanti, J. Boronat, and R. E. Zillich, Phys. Rev. Lett. **109**, 235307 (2012).

[47] R. Bombin, J. Boronat, and F. Mazzanti, Phys. Rev. Lett. **119**, 250402 (2017).

[48] J. Sánchez-Baena, J. Boronat, and F. Mazzanti, Phys. Rev. A **101**, 043602 (2020).

[49] H.-R. Chen, K.-Y. Lin, P.-K. Chen, N.-C. Chiu, J.-B. Wang, C.-A. Chen, P.-P. Huang, S.-K. Yip, Y. Kawaguchi, and Y.-J. Lin, Phys. Rev. Lett. **121**, 113204 (2018).

[50] L. Zhang and X.-J. Liu, "Review article: Spin-orbit coupling and topological phases for ultracold atoms," (2018) pp. 1–87.

[51] N. Goldman, G. Juzeliūnas, P. Öhberg, and I. B. Spielman, Reports on Progress in Physics **77**, 126401 (2014).

[52] Z. Wu, L. Zhang, W. Sun, X.-T. Xu, B.-Z. Wang, S.-C. Ji, Y. Deng, S. Chen, X.-J. Liu, and J.-W. Pan, Science **354**, 83 (2016).

[53] J. Ruseckas, G. Juzeliūnas, P. Öhberg, and M. Fleischhauer, Phys. Rev. Lett. **95**, 010404 (2005).

[54] J. Dalibard, F. Gerbier, G. Juzeliūnas, and P. Öhberg, Rev. Mod. Phys. **83**, 1523 (2011).

[55] A. M. Dudarev, R. B. Diener, I. Carusotto, and Q. Niu, Phys. Rev. Lett. **92**, 153005 (2004).

[56] A. Jacob, P. Öhberg, G. Juzeliūnas, and L. Santos, Applied Physics B **89**, 439 (2007).

[57] B. M. Anderson, G. Juzeliūnas, V. M. Galitski, and I. B. Spielman, Phys. Rev. Lett. **108**, 235301 (2012).

[58] B. M. Anderson, I. B. Spielman, and G. Juzeliūnas, Phys. Rev. Lett. **111**, 125301 (2013).

[59] L. Huang, Z. Meng, P. Wang, P. Peng, S.-L. Zhang, L. Chen, D. Li, Q. Zhou, and J. Zhang, Nature Physics **12**, 540 (2016).

[60] Y. Li, L. P. Pitaevskii, and S. Stringari, Phys. Rev. Lett. **108**, 225301 (2012).

[61] G. I. Martone, Y. Li, L. P. Pitaevskii, and S. Stringari, Phys. Rev. A **86**, 063621 (2012).

[62] Y.-C. Zhang, Z.-Q. Yu, T. K. Ng, S. Zhang, L. Pitaevskii, and S. Stringari, Phys. Rev. A **94**, 033635 (2016).

[63] X.-L. Chen, J. Wang, Y. Li, X.-J. Liu, and H. Hu, Phys. Rev. A **98**, 013614 (2018).

[64] R. Guardiola, in *Monte Carlo Techniques in the Many Body Problem, in First International Course on Condensed Matter* (WORLD SCIENTIFIC, 1988).

[65] G. Bhanot, Reports on Progress in Physics **51**, 429 (1988).

[66] P. Zhang, L. Zhang, and Y. Deng, Phys. Rev. A **86**, 053608 (2012).

[67] S. Zhang, N. Kawashima, J. Carlson, and J. E. Gubernatis, Phys. Rev. Lett. **74**, 1500 (1995).

[68] Y.-C. Zhang, Z.-Q. Yu, T. K. Ng, S. Zhang, L. Pitaevskii, and S. Stringari, Phys. Rev. A **94**, 033635 (2016).

[69] R. K. Pathria, *Statistical mechanics, by R. K. Pathria*, [1st ed.] ed. (Pergamon Press Oxford, New York, 1972) pp. xiii, 527 p.

[70] G. I. Martone and G. V. Shlyapnikov, Journal of Experimental and Theoretical Physics **127**, 865 (2018).

[71] A. L. Fetter and J. D. Walecka, *Quantum Theory of Many-Particle Systems* (McGraw-Hill, Boston, 1971).

[72] L. Salasnich and F. Toigo, Physics Reports **640**, 1 (2016).

[73] G. Leibbrandt, Rev. Mod. Phys. **47**, 849 (1975).

[74] L. Salasnich, Applied Sciences **8**, 1998 (2018).

[75] J. R. Harland and P. Salamon, Nuclear Physics B - Proceedings Supplements **5**, 109 (1988).

[76] C. Qu, K. Sun, and C. Zhang, Phys. Rev. A **91**, 053630 (2015).

[77] N.-C. Chiu, Y. Kawaguchi, S.-K. Yip, and Y.-J. Lin, arXiv:2005.12007 .